

MID-MIOCENE MAGMATISM IN THE OWYHEE MOUNTAINS, ID: ORIGIN AND
PETROGENESIS OF VOLCANIC ROCKS IN THE SILVER CITY DISTRICT

by

ZACHARY EUGENE LEVI HASTEN

B.S., San Diego State University, 2010

A THESIS

submitted in partial fulfillment of the requirements for the degree

MASTER OF SCIENCE

Department of Geology
College of Arts and Sciences

KANSAS STATE UNIVERSITY
Manhattan, Kansas

2012

Approved by:

Major Professor
Matthew E. Brueseke

Abstract

Previous studies of the northern Great Basin have indicated that mid-Miocene epithermal gold and silver ore deposits distributed regionally are temporally related to the magmatic activity associated with the onset of widespread extension and the Yellowstone hotspot (Saunders and Crowe, 1996; Kamenov et al., 2007). This study is focused on the volcanic rocks and ore deposits from the Silver City district (SCD), ID to address the petrogenesis and magmatic evolution that was influential in forming local precious metal deposits. The goal is to understand the tectonomagmatic conditions that contributed to the petrogenesis of the volcanic suite in the Silver City district, which can be used to provide details on the relationship between coeval mid-Miocene magmatism and mineralization across the northern Great Basin and Oregon Plateau. In order to better constrain the magmatic evolution of the SCD and potential sources of the precious metals, we have undertaken detailed sampling of local crust and mid-Miocene volcanic units to constrain their physical, geochemical, isotopic, and geochronological characteristics, as well as provide constraints on the petrogenesis of the mid-Miocene volcanic package. Prior studies of the local volcanism have yielded K-Ar and $^{40}\text{Ar}/^{39}\text{Ar}$ ages of ~16.6 to 14 Ma (Bonnichsen, 1983), while others have dated adularia from one SCD mineral vein and obtained $^{40}\text{Ar}/^{39}\text{Ar}$ ages of between 15.6 and 16.3 Ma (Hames et al., 2009; and Aseto et al., 2011). Field observations are consistent with earlier work (Lindgren, 1900; Asher, 1968; Pansze, 1975; Halsor et al., 1988; Bonnichsen and Godchaux, 2006; Camp and Ross, 2009) and reveal a sequence of basalt consisting of regionally prevalent Steens Basalt that pre-dated precious metal mineralization. Some of the basalt appears to have been erupted locally, based on the presence of mafic dikes and thick pyroclastic deposits similar to other regional mid-Miocene magmatic systems. Stratigraphically overlying this lower basalt suite is a complex package of rhyolite flows and domes, thin silicic pyroclastic units, additional basaltic lava flows, intermediate lava flows, and mafic/silicic shallow intrusives. Geochemical analysis indicates that the basaltic and basaltic andesite lava flows are locally erupted flows of Steens Basalt while the intermediate and silicic volcanism in SCD can be classified into nine distinct units including two andesites, one dacite, four rhyolites and two rhyolite tuffaceous units. Geochemical modeling suggest that the intermediate and silicic magmas were formed by a combination of open system processes,

including low pressure partial melting and assimilation of mid to upper crustal granitoid basement rock, and magma mixing between silicic and basaltic endmembers. The formation of silicic volcanism in the SCD is similar to other regional mid-Miocene silicic volcanic systems (e.g. Santa Rosa-Calico volcanic field and Jarbidge Rhyolite). Based on new $^{40}\text{Ar}/^{39}\text{Ar}$ geochronology of both volcanic units and epithermally emplaced mineralization, SCD volcanism appears to have erupted over a relatively short amount of time that overlaps with local epithermal Au-Ag mineralization.

Table of Contents

List of Figures	vii
List of Tables	x
Acknowledgements.....	xi
Chapter 1 - Introduction.....	1
Introduction.....	1
Regional Geology	2
Local Geology.....	3
Chapter 2 - Methods.....	9
Field Methods	9
Rock Powder Preparation	11
Petrography.....	11
Major and Trace Element Geochemistry	12
Select Trace and Rare Earth Element Geochemistry	13
Radiogenic Isotope Analysis	13
Oxygen Isotope Analysis	14
⁴⁰ Ar/ ³⁹ Ar Geochronology.....	15
Chapter 3 - Field Relationships.....	16
Chapter 4 - Petrography	51
Granitoid basement.....	52
Basalt	54
Andesite	56
Hayden Peak and quartz latite	58
Glass Mountain dacite and rhyolite	60
Silver City rhyolite.....	62
Tuffaceous units.....	64
Chapter 5 - Geochemistry	66
Geochemical Classification	66
Granitoid Geochemistry.....	74

Regional Steens Basalt Geochemistry	74
Volcanic Major Element Geochemistry	75
Basalt and intermediate	75
Dacite and rhyolite	75
Trace Element Geochemistry.....	82
Basalt and intermediate.....	82
Dacite and rhyolite	82
Rare Earth Element Geochemistry	95
Basalt and andesite.....	95
Dacite and rhyolite	95
Radiogenic Isotope Geology.....	102
Chapter 6 - Oxygen Isotopes.....	108
Chapter 7 - Geochronology.....	110
Chapter 8 - Geochemical and Isotopic Constraints on Magma Production.....	111
Trace Element Modeling	111
Isotope Modeling	135
Chapter 9 - Regional Comparison.....	138
Chapter 10 - Results.....	143
Physical Characteristics	143
Petrography.....	143
Trace Element and Radiogenic Isotope Modeling.....	144
Oxygen Isotope	145
Geochronology.....	146
Regional Comparison	146
Chapter 11 - Summary	147
Chapter 12 - Suggested Future Work.....	149
References.....	150
Appendix A - Sample Locations and Petrographic Descriptions	157
Appendix B - Geochemistry	190
Appendix C - Radiogenic Isotope Data	205
Appendix D - Oxygen Isotope Results	210

Appendix E - Geochronology 211

List of Figures

Figure 1.1: Regional map.....	7
Figure 1.2: Geologic map	8
Figure 3.1: Aerial image of local geography	21
Figure 3.2: Potosti Ridge stratigraphy	23
Figure 3.3: Tennessee Mountain stratigraphy.....	25
Figure 3.4: Florida Mountain stratigraphy.....	27
Figure 3.5: Silver City granite range.....	29
Figure 3.6: War Eagle Mountain	30
Figure 3.7: Silver City granite outcrop	31
Figure 3.8: Metamorphic outcrop	32
Figure 3.9: Metamorphic rocks.....	33
Figure 3.10: Ore bearing quartz vein	34
Figure 3.11: Steens Basalt.....	35
Figure 3.12: Andesitic shallow intrusive	36
Figure 3.13: Hayden Peak and quartz latites	37
Figure 3.14: Hayden Peak.....	38
Figure 3.15: Hayden Peak latite.....	39
Figure 3.16: Vitrophyre on Hayden Peak	40
Figure 3.17: Glass Mountain.....	41
Figure 3.18: Glass Mountain dacite eruptive center	42
Figure 3.19: Ash flow tuff	43
Figure 3.20: Ruby City intrusive	44
Figure 3.21: Glass Mountain rhyolite	45
Figure 3.22: Tuff of Flint Creek	46
Figure 3.23: Silver City contact	47
Figure 3.24: Sawpit Peak eruptive center	48
Figure 3.25: Silver City eruptive center.....	49
Figure 3.26: Potosi Ridge outcrop	50

Figure 4.1: Granitoid petrography	52
Figure 4.2: IUGS granitoid classification	52
Figure 4.3: Basalt petrography.....	54
Figure 4.4: Andesite petrography	56
Figure 4.5: Hayden Peak and quartz latite petrography.....	58
Figure 4.6: Glass Mountain dacite and rhyolite petrography	60
Figure 4.7: Silver City rhyolite petrography.....	62
Figure 4.8: Tuffaceous unit petrography	64
Figure 5.1: Total Alkali diagram	69
Figure 5.2: Mafic classification diagrams.....	70
Figure 5.3: Alumina saturation diagram	71
Figure 5.4: Granitoid classification diagrams.....	72
Figure 5.5: Frost classification diagrams	73
Figure 5.6: Mafic and Intermediate Harker diagrams.....	76
Figure 5.7: Silicic Harker diagrams	78
Figure 5.8: Complete Harker diagrams.....	80
Figure 5.9: Mafic trace element diagrams	85
Figure 5.10: MORB normalized spider diagram of Silver City district mafic samples.	87
Figure 5.11: Silicic trace element diagrams.....	88
Figure 5.12: Trace element diagrams.....	90
Figure 5.13: Zr trace element diagrams	92
Figure 5.14: Upper continental crust normalized trace element diagrams	94
Figure 5.15: Chondrite normalized rare earth element diagrams	97
Figure 5.16: REE vs. Zr Harker diagrams	98
Figure 5.17: Upper continental crust normalized rare earth element diagrams.....	100
Figure 5.18: Chondrite normalized rare earth element diagrams	101
Figure 5.19: Pb isotope diagrams.....	104
Figure 5.20: Pb isotope diagrams.....	105
Figure 5.21: Sr and Nd isotope diagrams.....	106
Figure 5.22: Silver City district Sr and Nd diagrams.....	107
Figure 6.1: Oxygen isotopes	109

Figure 8.1: Andesite type 1 AFC trends	122
Figure 8.2: Andesite type 1 AFC comparison	123
Figure 8.3: Hayden Peak latite AFC trends	124
Figure 8.4: Hayden Peak latite AFC comparison	125
Figure 8.5: Quartz latite FC comparison.....	126
Figure 8.6: Granite classification diagrams	127
Figure 8.7: Silver City rhyolite AFC trends.....	128
Figure 8.8: Silver City rhyolite AFC comparison.....	129
Figure 8.9: Andesite type 2 mixing trends.....	130
Figure 8.10: Andesite type 2 mixing comparison.....	131
Figure 8.11: Glass Mountain dacite and rhyolite mixing trends.....	132
Figure 8.12: Glass Mountain dacite mixing comparison	133
Figure 8.13: Glass Mountain rhyolite mixing comparison	134
Figure 8.14: Andesite type 1 isotope modeling	136
Figure 8.15: Hayden Peak latite and Silver City rhyolite isotope modeling	137
Figure 9.1: Steens Basalt comparison.....	140
Figure 9.2: Regional silicic comparison	141

List of Tables

Table 1.1: Unit names and abbreviations for volcanic units found in SCD	5
Table 2.1: Unit correlation to previous work.....	10
Table 8.1: Representative Unit Geochemistry	112
Table 8.2: AFC modeling results	118
Table 8.3: Fractional crystallization and mixing modeling results	120
Table B.1: Raw major element geochemistry	191
Table B.2: Trace element geochemistry	195
Table B.3: Trace element geochemistry (continued).....	199
Table B.4: Rare earth element geochemistry	203
Table C.1: Radiogenic isotope geochemistry	209
Table D.1: Oxygen isotope data.....	210

Acknowledgements

I would like to thank Dr. Matthew Brueseke for providing me with the opportunity to work on this research project. As well as providing continuous support, insight, and encouragement. I would like to thank the National Science Foundation for the generous funding of my research project as well as funding through the EiDRoP GK-12 Fellowship. I would like to thank collaborators Dr. James Saunders and Dr. Willis Hames of Auburn University, and Dr. Peter Larson of Washington State University for their contributions to this project. Also Dr. Vic Camp for providing me with exceptional teaching and preparation for research work, as well as, unpublished data for use in this research. Dr. Elisabeth Widom and Dave Kuentz of Miami University, and Dr. Richard Conery and Laureen Wagoner of Washington State University for assistance with geochemical analysis. I also thank Dr. Saugata Datta and Dr. Sambhudas Chaudhuri for serving on my committee, Dr. George Clark for making sure the department was supportive of graduate research and providing funding for conference travel, and Lori Page-Willyard for keeping the department running smoothly. All of the current and former graduate students that I encountered during my time at Kansas State for making this an enjoyable and rewarding time, specifically Jeff Calliccoat for providing a place to stay and insight during my initial visit; Andy Neal for getting me accustomed to life in Manhattan, Derek Ohl and Randi Isham for keeping my office full of laughs; and Robinson Barker for being a great officemate and sounding board. Finally I would like to thank my family for their support, most importantly my fiancée Tanya and my daughter April for always believing in me and for providing me with limitless motivation.

Chapter 1 - Introduction

Introduction

Widespread mid-Miocene bimodal volcanism common throughout much of the northern Great Basin and Oregon Plateau is associated with the initiation of the Yellowstone hotspot and collapse of the Nevadaplano and is recorded in the Owyhee Mountains of southwestern Idaho. The extensive volcanism began with the initial eruption of the Steens Basalt and the Columbia River Flood Basalt Group around 16.7 Ma (Camp et al., 2003; Brueseke et al., 2007; Camp et al., in press). Contemporaneous with the substantial mafic eruptions and extension, was abundant silicic volcanism. While some of the mid-Miocene silicic volcanism has been studied in depth (Santa Rosa-Calico volcanic field by Brueseke and Hart, 2008; Jarbidge Rhyolite by Callicoa, 2010; northwestern NV volcanism; Coble and Mahood, 2012), other areas, like the Owyhee Mountains in southwestern Idaho, have been largely overlooked in detailed studies and in the regional context. In addition to the regionally extensive flood basalts and silicic volcanism, the northern Great Basin contains abundant precious metal deposits. The precious metal deposits commonly occur as shallowly emplaced epithermal deposits. In order to address the relationship between magmatism and mineralization research was conducted in and around the Silver City mining district (SCD) near Silver City, ID.

The previous broadly identified mid-Miocene volcanic units in SCD are the older “lower basalt” and the younger Silver City rhyolite that both overlie a late Cretaceous age granitoid batholith (Lindgren, 1900; Asher, 1968; Ekren et al., 1981; Bonnicksen, 1983; Halsor et al., 1988; Cupp, 1989 and Bonnicksen and Godchaux, 2006) and metamorphic roof pendants (Piper and Laney, 1926; Bennett, 1976; Ekren et al., 1982; Kolb et al., 2011). Previous studies in the Owyhee Mountain and Silver City district have provided adequate mapping results, however, detailed chemical analysis, eruptive history and petrogenetic interpretations are lacking. Field evidence points towards a magmatic system with multiple local eruptive centers throughout SCD and a multi-stage formation of the intermediate and silicic volcanic units.

During both the mid 19th century and late 20th century, the SCD was a major producer of gold and silver ore using both vein and open pit mining techniques and the type locality for epithermal mineral deposits (Lindgren, 1900). Despite the extensive mining and exploration of

the area, the origin of the precious metals and the relationship to local volcanic activity has not been well established. Furthermore, recent work suggests a link between shallow epithermal ore-forming processes and coeval, spatially coincident mafic magmatism (Hedenquist and Lowenstern, 1994). Saunders and Crowe (1996) presented evidence that both the onset of bimodal volcanism and the associated epithermal ore deposits across the northern Great Basin are related to the emergence of the Yellowstone hotspot. Subsequent work indicates that the regional flood basalt magmas were the likely origin of the precious metals found throughout the northern Great Basin (Kamenov et al., 2007; Saunders et al., 2008; Hames et al., 2009).

The purpose of this research is to better determine the timing and petrogenetic evolution of the mid-Miocene SCD volcanism using field and petrographic relationships, major and trace element geochemistry, isotope geochemistry, and geochemical modeling. This research also addresses the similarities of the SCD volcanism to other regional mid-Miocene volcanic systems where published geochemical data exists.

Regional Geology

The Pacific Northwest region of the United States was a focal point for extensive volcanism during the mid-Miocene. Prior to 19 Ma, the activity in the region was largely subduction zone related calc-alkaline volcanism, which includes the formation of the Mesozoic Idaho Batholith (Taubeneck, 1977; Carlson and Hart, 1987; Norman and Leeman, 1989). Figure 1.1 illustrates the major geologic events that shaped the region in the mid-Miocene. One of the most significant Cenozoic magmatic phenomena in the region are the voluminous Columbia River and Steens flood basalt eruptions, which were sourced from N-NW trending dike swarms that formed contemporaneously with the emergence of the Yellowstone hotspot beginning around 16.7 Ma (Camp and Ross, 2004; Brueseke & Hart, 2008). The Owyhee Mountains and Silver City in particular are located in a geologically complex region that marks the intersection of the Oregon Plateau, the northern Great Basin and the Snake River Plain. Although the majority of the Columbia River basalt province is contained to Columbia Plateau to the north, stratigraphically overlapping Steens Basalt lava flows are present in the northern Great Basin and Oregon Plateau (Brueseke et al., 2007; Camp et al., in press).

The majority of the Columbia River/Steens Flood Basalt volcanism occurred throughout the northern Great Basin and Oregon Plateau between 16.6 - 15.0 Ma (Camp and Ross, 2004). Contemporaneous with the basaltic volcanism, widespread silicic volcanism was also active across the northern Great Basin and Oregon Plateau. The silicic volcanics appear as numerous eruptive centers across the region such as the Santa Rosa-Calico volcanic field, the Jarbidge Rhyolite, McDermitt volcanic field and several eruptive loci across the Oregon High Lava Plains (Jordan et al., 2004; Brueseke et al., 2007; Brueseke & Hart, 2008; Starkel et al., 2009; Callicoa, 2010; Coble and Mahood, 2012). After 14.0 Ma, volcanism migrated away from the northern Great Basin/ Oregon Plateau area of southwestern Idaho. Two volcanic provinces have developed across the High Lava Plains (HLP) and the central/eastern Snake River Plain. The northwestward migration of volcanism across the HLP formed as a dominantly bimodal package of basalt and rhyolite eruptions that get progressively younger to the northwest culminating with the latest eruption approximately 1,300 years ago (Sherrod et al., 1997; and Jordan et al., 2004). Volcanism across the central and eastern Snake River Plain is associated with the emergence and subsequent track of the Yellowstone hotspot. Volcanism in the central Snake River Plain began with the formation of the Bruneau-Jarbidge volcanic field 12.7 Ma. The volcanic fields get progressively younger including the ~10 Ma Twin Falls and Picabo volcanic fields, the ~6.7 - 4 Ma Heise volcanic field and the present day Yellowstone volcanic field that initiated at ~2.2 Ma. (Christiansen et al., 2002; and Bonnicksen et al., 2008).

In addition to the bimodal volcanism, the northern Great Basin and Oregon Plateau underwent contemporaneous periods of bonanza style gold and silver epithermal mineralization. The precious metal mineralization is evident in many prosperous mining district such as the Jarbidge, Midas, Ivanhoe, and National districts (John, 2001; Wallace, 2003; and Saunders et al., 2008). While a large portion of the mineralization occurred in north-central Nevada, there are also epithermal systems in the Owyhee Mountains, specifically in the Silver City district (Lindgren, 1900; and Saunders et al., 2008).

Local Geology

Previous work indicates that the Silver City district is not as structurally and stratigraphically complex as other portions of the northern Great Basin and Oregon Plateau

(Asher, 1968; Pansze, 1975) and as a result, it provides an ideal location to understand the relationship between flood basalt volcanism, silicic magma formation, and precious metal emplacement. There are large Cenozoic volcanic packages in the Owyhee area including the Challis volcanics to the south (Norman, 1991; Ekren et al., 1982) and the Salmon Creek Volcanics to the north (Norman, 1987) that do not appear in the SCD. The oldest exposed rocks in the Silver City district are small outcrops of metamorphic rocks of an unknown age that are present in near the mining town of Flint and present in larger outcrops south of the SCD, near South Mountain (Piper and Laney, 1926; Bennett, 1976; Ekren et al., 1982; Kolb et al., 2011). The metamorphic rocks occur as probable roof pendants that are found in and on top of a granitoid basement that underlies the SCD (Bennett, 1976). The granitoids are approximately 66 - 62 Ma biotite-muscovite granodiorites and quartz monzonites that are known as the Silver City Granite and are part of the Idaho batholith (Bonnichsen, 1983, Benford et al., 2010; Kolb et al., 2011). Overlying the granitoids are 16.6 - 16 Ma basalt flows that have been classified as locally erupted members of the Steens/Imnaha flood basalts (Camp and Ross, 2009), but reinterpreted here as all Steens Basalt based on chemical characteristics. Evidence of local basaltic eruptive centers are identified as feeder dikes that culminate in basal basalt flows, as well as a near vent flow/spatter package located at Black Warrior (W.K. Hart, personal communication). Above the “lower basalt,” are packages of rhyolite flows (Silver City rhyolite), ash-flow tuffs, silicic domes and shallow intrusive bodies (Asher, 1968). In addition to the silicic units, these younger volcanic deposits include latite and a younger suite of basalt (Asher, 1968). A generalized geologic map of the SCD is shown in Figure 1.2.

The upper more varied suite was likely deposited between 16.4 - 14 Ma (Ekren et al., 1981; Bonnichsen, 1983; Bonnichsen and Godchaux, 2006) and new $^{40}\text{Ar}/^{39}\text{Ar}$ geochronology from Silver City rhyolite lava flows indicated they erupted at 15.9 Ma (Aseto, 2012). While the physical characteristics of mafic and silicic units are somewhat defined, the overall eruptive and petrogenetic history of the SCD is not well constrained. The presence of multiple shallow intrusives and extrusive domes in the Silver City district indicate that the silicic volcanism may be sourced from numerous loci and may represent a multi-stage magmatic development with differing magma chamber evolutions. Additionally, this study works to further identify physically and chemically distinct units within the Silver City rhyolite unit. This study has identified six physically and chemically distinct silicic units within the larger Silver City rhyolite

body. This study has identified seven silicic units the quartz latite, Hayden Peak latite, Glass Mountain dacite, Glass Mountain rhyolite, Silver City rhyolite, and one tuffaceous unit (tuff of Flint Creek). While other workers have subdivided the Silver City rhyolite and separated out the rhyolite of the Millsite variation (Ekren et al., 1982; and Bonnicksen, 1983; Cupp, 1989), this study did not find sufficient physical or chemical differences to warrant a separate classification. However, this study did subdivide chemically distinct latitic units from the broader Silver City rhyolite group as previously defined. The mid-Miocene volcanic units identified in this study are summarized in Table 1.1. Table 2.1 illustrates the unit divisions designated in this thesis and how they compare to those defined by previous workers.

Table 1.1: Unit names and abbreviations for volcanic units found in SCD

Unit	Abbreviation
Silver City rhyolite	Tsc
Glass Mountain rhyolite	Tgmr
Glass Mountain dacite	Tgmd
tuff of Flint Creek	Ttfc
quartz latite	Tql
Hayden Peak latite	Thpl
Cold Springs tuff	Tcst
andesite type 2	Ta ₂
andesite type 1	Ta ₁
Steens Basalt	Tsb

Aside from the recent ages of Aseto (2012), the timing of the silicic volcanism in SCD is not well constrained. Field relationships indicate multiple eruptive centers in the district and contemporaneous emplacement of the distinct silicic units. Based on field relationships, discussed later, the Hayden Peak latite and quartz latites appear to be associated with the initial

phase of silicic volcanism, while the Glass Mountain units, Silver City rhyolite and tuff of Flint Creek followed. Some of the units also appear to be areally confined, such as the tuff of Flint Creek and the Hayden Peak latite and one unit, the Cold Springs tuff, represents a distal deposit which erupted from a coeval, but different volcanic center (e.g. Santa Rosa-Calico volcanic field; Brueseke and Hart, 2008).

Packages of north-northwest trending normal faults have been previously identified and mapped (Piper and Laney, 1926; Asher, 1968; Pansze, 1975; Ekren et al., 1981). The faults are typically high angle and produce only slight northeast dip displacement (Bonnichsen, 1983). Further fault mapping was not performed as part of this research. The mid-Miocene volcanic dikes that are exposed in SCD follow the same north-northwest trend and some of the local eruptive centers are located in the immediate vicinity of mapped faults. The faults in the SCD maintain the same N20° - 25°W trend as the large-scale regional trends associated with other mid-Miocene fault/dike occurrences (flood basalt dike swarms/northern Nevada rift).

Similarly to other areas in and adjacent to the northern Great Basin, the SCD is host to abundant mid-Miocene gold and silver epithermal mineralization as identified by Lindgren (1900). Where emplaced as quartz and mineral veins, the veins follow a similar north-northwest trend that is exhibited by the contemporaneous local volcanics and faulting. The precious metal mineralization is hosted in the granitic batholith and basaltic units as epithermal veins made up of quartz adularia and calcite with electrum and Ag-selenides/sulfides/sulfosalt ore deposits (Aseto, 2012). Mineralization in the younger Silver City rhyolite is highly disseminated along micro-fractures and the lava flows' inherent porosity. The epithermal mineralization has caused intense alteration in some areas, most notably in the rhyolites near Florida and DeLamar Mountains. (Piper and Laney, 1926; Halsor et al., 1988; Cupp, 1989; Bonnichsen, 1983; this study). The SCD was an active mining district in the mid to late 19th century, as well as the late 20th and early 21st centuries, with the recent open pit mining of Florida and DeLamar Mountains and operations underway by Silver Falcon Mining Inc. Recent dating of the precious metal mineralization compliments this work and indicates that the epithermal mineralization system was active between 16.3 - 15.6 Ma and the majority of deposits formed at 15.7 Ma (Hames et al., 2009; Aseto et al., 2011).

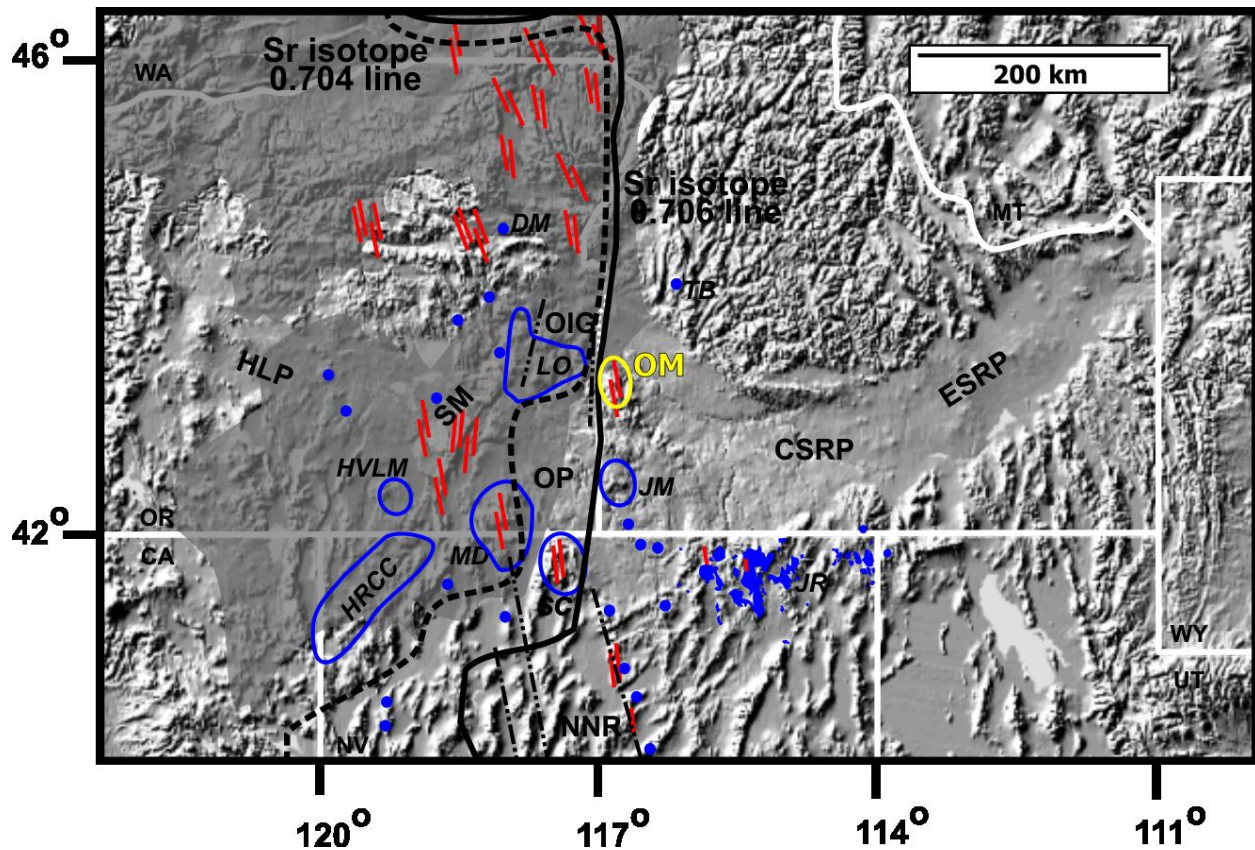


Figure 1.1: Regional map

Shaded relief map of the Pacific Northwest of the United States after Brueseke and Hart (2008). The study area is indicated by the yellow oval designating the location of the Owyhee Mountains (OM). The range of the regionally extensive Columbia River and Steens flood basalts are indicated by the dark gray shaded regions, while the blue areas indicate the location and extent of mid-Miocene rhyolite deposits and volcanic fields. The red lines indicate dike swarms/eruptive loci. $^{87}\text{Sr}/^{86}\text{Sr}$ isopleths indicate the boundaries of the Precambrian continental craton to the east (0.706), and the Mesozoic accreted terranes to the west (0.704) and the transitional lithosphere that lies in between. The black dashed lines indicate the limits of the Oregon-Idaho Graben and northern Nevada rift mid-Miocene extensional systems.

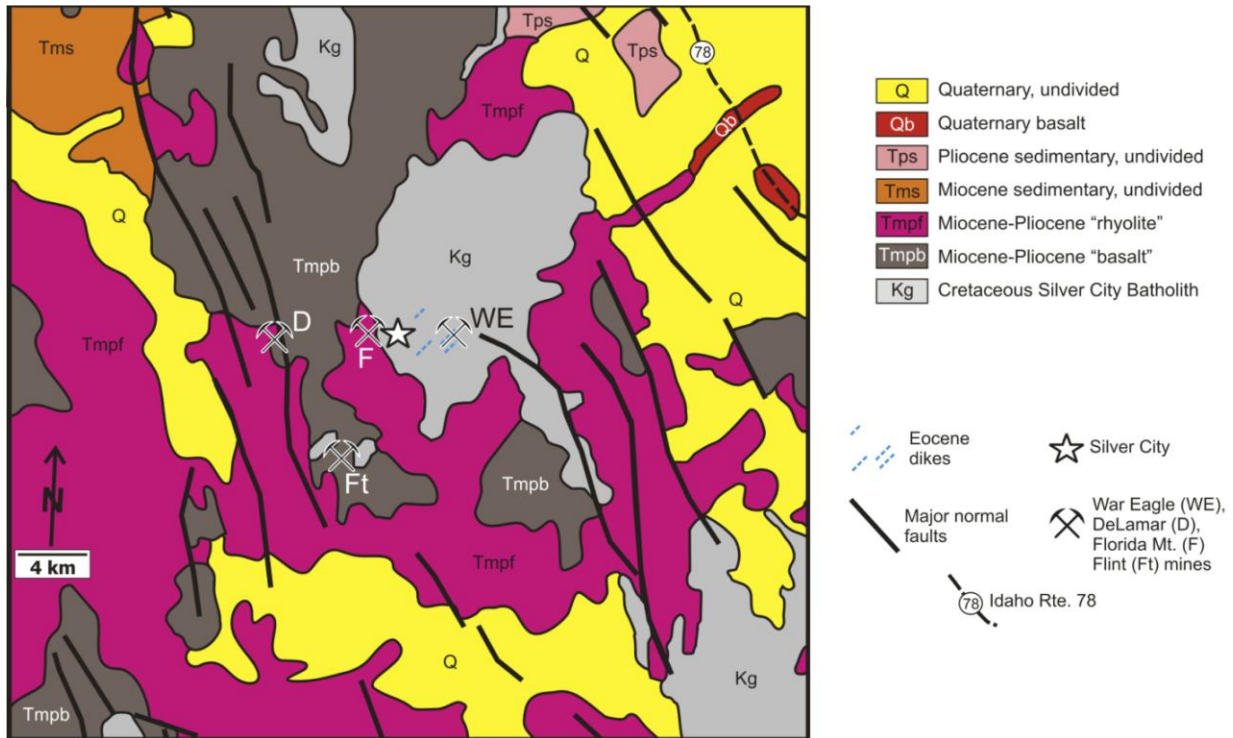


Figure 1.2: Geologic map

Generalized geologic map from the Silver City district with locations of major producing mines and identified faults. Map unit Tmpb is the occurrence of the “Lower Basalt”, the map unit Tmpf is identified as the Silver City rhyolite. Many of the shallow intrusive bodies mimic the NW trend seen in the localized faulting. Work for this project is focused in the vicinity of War Eagle Mountain (Silver City district).

Chapter 2 - Methods

Field Methods

Samples were collected from the field over the course of four summers between 2007 and 2011. Sampling areas were determined based on previous mapping of the region including Asher (1968); Pansze (1975); Ekren et al. (1981); Bonnichsen (1983); Halsor et al. (1988); and Bonnichsen and Godchaux (2006). Samples were collected from areas that would maximize stratigraphic relationships among units, sample diversity, and areal coverage and were mainly accessed by foot. While many of the rocks in this area have undergone hydrothermal alteration, care was taken to collect the freshest possible samples from outcrops. Altered rinds and material was chipped off with a rock hammer to expose fresh surfaces before collecting. Some samples have undergone silicification as a result of the epithermal mineralization in the immediate vicinity of the rocks. Samples of these materials were collected and silicification was noted in the sample descriptions (Appendix A). In most cases, a larger than fist-sized sample was collected to allow for petrography and geochemistry analysis while maintaining an intact hand sample. Sample locations were recorded on a DeLorme Eartmate PN-60 handheld GPS device. All locations were recorded in Universal Transverse Mercator (UTM) coordinates and the 1927 North American Datum (NAD27). Coordinates for all collected samples are located in Appendix A.

Table 2.1: Unit correlation to previous work

This Study	Asher, 1968	Pansze, 1975	Ekren, 1982	Halsor, 1988	Bonnichsen and Godchaux, 2006
Tsb	Basalt-latite	Lower basalt	Basalt	Lower basalt	Lower basalt
Ta	Basalt-latite	Lower basalt	Basalt	Porphyritic rhyolite	Lower basalt
Tcst	Not identified	Ash flow 1	Not identified	Not identified	Not identified
Thpl	Not identified	Lower rhyolite/quartz latite	Silver City	Quartz latite	Silver City rhyolite
Tql	Basalt-latite/Welded tuff 2/Undiff. Silver City rhyolite	Quartz latite/Flow breccia	Silver City	Quartz latite	Silver City rhyolite
Ttfc	Not identified	Ash flow 2	Not identified	Not identified	Tuff of Flint Creek
Tgmd/Tgmr	Basalt-latite/quartz latite domes/Undiff. Silver City rhyolite	Upper rhyolite	Basalt	Millsite rhyolite	Latite flows/ Millsite rhyolite
Tsc	Quartz latite domes/Undiff. Silver City rhyolite	Upper rhyolite	Silver City	Banded rhyolite/Millsite rhyolite	Silver City rhyolite/Millsite rhyolite

Rock Powder Preparation

Samples collected in the field were initially processed for petrography, geochemistry, and geochronology at Kansas State University. Samples were split and crushed with a RockLabs hydraulic press fitted with tungsten carbide splitting and crushing surfaces. The large samples were initially split into smaller pieces with the splitting plates on the press. Care was taken to remove visibly altered portions of the sample during splitting. Non-fresh surfaces that could not be split off were removed using a rock/tile saw equipped with a diamond tipped blade. Small impurities were also removed with a grinding wheel mounted with silica carbide sandpaper. The split and cut samples were visually inspected, then washed in deionized water to remove any residual dust, saw marks or other contaminants and allowed to completely dry overnight. After washing and drying, the samples were then crushed using the crushing plates on the press. The samples were crushed down to a size of approximately 5 mm or smaller and collected. An approximately 20 mL random sample of the crushed material was obtained using a cone and quarter method. This material was then powdered to a grain size of approximately 70 microns using a Spex Industries shatterbox, with an alumina ceramic puck assemblage.

Petrography

Thin sections were prepared by using smaller pieces obtained during the rock-crushing portion of sample processing. The pieces used for thin sections were picked based on freshness and the appearance of being representative of the whole rock. Thin section blanks were cut on the rock saw to an approximate size of 24 x 44 mm with a thickness of approximately 13 mm and then sent to Spectrum Petrographics Inc. for thin section production. The thin sections were mounted in epoxy and cut to a thickness of 30 microns and finished with a glass slipcover. General petrographic analysis was performed on all samples while detailed petrographic analysis and point counting was performed on a select set of representative samples. Samples were selected based on geographic location and geochemical classification in order to provide an adequate representation of the various units in the SCD. Point counting was performed on a Nikon Eclipse E600 POL polarizing using the 10x objective with a 1 mm step interval. While a target of 1,000 counts was set for each thin section, the actual counts varied from 606 to 800 with

an average count of 766 per thin section. The detailed petrographic description and point counted mineral abundances can be found in Appendix A as part of the sample descriptions.

Major and Trace Element Geochemistry

Major and trace elements were analyzed for all 99 samples processed for geochemistry using a ThermoARL AdvantXP+ x-ray fluorescence spectrometer (XRF) at the GeoAnalytical Lab at Washington State University, Pullman, Washington (WSU). Rock powder samples were sent to WSU for final preparation and analysis. WSU uses a single bead and low dilution method developed in the GeoAnalytical lab (Johnson et al., 1999). Approximately 3.5 g of rock powder was combined with approximately 7.0 g of di-lithium tetraborate flux for a 2:1 flux to rock ratio. The rock and flux was then fused in graphite crucibles in a muffle furnace with temperatures near 1000 °C. The resulting beads are allowed to completely cool before being re-powdered in a Spex Industries shatterbox with a tungsten carbide puck assemblage and re-fused in the oven. After the second fusion the beads are polished on increasingly finer diamond lap wheels to create a smooth surface. The beads are washed in a sonication bath and rinsed with alcohol to prepare for analysis.

During analysis, all of the present Fe was recorded as FeO*. The raw Fe data was corrected for oxidation and FeO and Fe₂O₃ were determined based on the following equation after LeMaitre (1976):

$$\text{Oxidation Ratio: Ox} = \text{FeO}/(\text{FeO}+\text{Fe}_2\text{O}_3) = 0.93 - 0.0042(\text{SiO}_2) - 0.022(\text{Na}_2\text{O} + \text{K}_2\text{O})$$

$$\text{Fe}_2\text{O}_3 = [0.899813(\text{Ox})(\text{Fe}_2\text{O}_3^*)]/[-0.899813 - 0.100187(\text{Ox})]$$

$$\text{FeO} = (\text{Fe}_2\text{O}_3^* - \text{Fe}_2\text{O}_3)/1.111342$$

Multiple replicate samples and two continually run standards were analyzed to verify the data reproducibility. The major element weight percentages were then normalized to 100%. Major and trace element results are presented in Appendix B.

Loss on ignition (LOI) was also measured for all geochemically analyzed samples. Approximately 1.0 g of rock powder was placed in a ceramic crucible and placed into the 1000 °C muffle oven for 16 hours. The samples were cooled at room temperature slightly and then placed in airtight desiccators to completely cool before reweighing. The LOI is presented as a percentage of sample and was calculated with the formula $\text{LOI} = ((\text{Mass}_{\text{initial}} - \text{Mass}_{\text{final}}) /$

($\text{Mass}_{\text{initial}}$) * 100. The LOI results are presented as part of the major element results in Appendix B. The complete technical notes on XRF analysis including the analytical precision and accuracy can be found online at www.sees.wsu.edu/Geolab/note.html.

Select Trace and Rare Earth Element Geochemistry

A select set of 45 samples was analyzed for detailed trace and rare earth element abundances using an Agilent 7700 Inductively Coupled Plasma Mass Spectrometer (ICP-MS) at WSU. The samples were chosen to provide a representative coverage of units exposed in the Silver City district. The WSU GeoAnalytical Lab uses a combination low dilution fusion and acid dissolution for sample preparation. Approximately 2.0 g of rock powder were combined with an equal amount of di-lithium tetraborate flux for a 1:1 flux to rock ratio. The powder solution was fused in graphite crucibles in a muffle furnace with temperatures near 1000 °C. After fusing, the bead was allowed to cool and re-powdered in the shatterbox. Approximately 250 mg of powder was set aside for acid dissolution. The powder was dissolved in 2 mL HNO₃, 6 mL HF and 2 mL HClO₄ and heated to stimulate evaporation. After complete drying, the sample was rehydrated with a small amount of water and 2 mL HClO₄ and allowed to completely dry again. The dried samples were then re-dissolved in 10 mL water, 3 mL HNO₃, 5 drops of H₂O₂, and 2 drops of HF. The solutions were heated until a clear solution remained. The samples were diluted to a total weight of 60 g with de-ionized water and submitted for analysis. The complete technical notes on ICP-MS including the analytical precision and accuracy can be found online at www.sees.wsu.edu/Geolab/note.html.

Radiogenic Isotope Analysis

Fourteen samples were analyzed for the radiogenic isotopes of Sr, Nd, and Pb. The sample set includes two Steens Basalt, one olivine-rich basalt, one basaltic andesite, one andesite type 1, one Glass Mountain dacite, one Glass Mountain rhyolite, one Hayden Peak latite, one quartz latite, two Silver City rhyolite, and three Silver City granite. The samples were chosen to provide an adequate representation of the various units in the SCD. Additionally, one spiked sample and one replicate sample were analyzed to verify the accuracy of the results. The samples were analyzed on a Thermo Finnigan Triton thermal ionization mass spectrometer (TIMS) at

Miami University, Oxford, Ohio (MU). Approximately 0.1 - 0.2 g of whole rock powder was dissolved in HF-HNO₃, prior to chemical separation.

Except for Sm – Nd separation, these procedures follow Walker et al. (1989). Sm - Nd separations were performed by methods similar to Pin and Zalduegui (1997), using EiChrom Ln-Spec resin. Isotopic compositions were measured by thermal ionization mass spectrometry (TIMS) at Miami University, using a Finnigan Triton mass spectrometer. Strontium isotopic ratios were fractionation corrected using $^{86}\text{Sr}/^{88}\text{Sr} = 0.1194$. 123 measurements of the NBS 987 strontium standard gave an average of $^{87}\text{Sr}/^{86}\text{Sr} = 0.710239 \pm 0.000015$ (2 SD). Neodymium isotopic ratios were fractionation corrected using $^{143}\text{Nd}/^{146}\text{Nd} = 0.7219$. Ninety measurements of the La Jolla neodymium standard gave an average of $^{143}\text{Nd}/^{144}\text{Nd} = 0.511846 \pm 0.000007$ (2 SD).

The measured results for Pb were adjusted manually based on internal reproducibility of the standard, while the Sr and Nd were adjusted as the samples were analyzed by the analyzing software (Snyder, 2004).

The various Pb isotopic ratios had specific adjustment factors that were used to correct the measured data for the internal reproducibility of the TIMS equipment. The adjustment values, reported as % per amu difference, were as follows: $^{206}\text{Pb}/^{204}\text{Pb} = 0.100\%$; $^{207}\text{Pb}/^{204}\text{Pb} = 0.097\%$; $^{208}\text{Pb}/^{204}\text{Pb} = 0.102\%$; $^{207}\text{Pb}/^{206}\text{Pb} = 0.090\%$; and $^{208}\text{Pb}/^{206}\text{Pb} = 0.103\%$. The measured data was then adjusted accordingly using the equation: (Measured $^{206}\text{Pb}/^{204}\text{P}$) x (1.002) = Actual $^{206}\text{Pb}/^{204}\text{Pb}$.

Sr and Nd isotope ratios for all mid-Miocene volcanic rocks were age corrected back to initial ratios based on an 16.0 Ma eruption age. 16.0 Ma was also used to correct back Silver City granitoid Sr and Nd isotope ratios. In the age correction, $^{87}\text{Sr}/^{86}\text{Sr}_0 = 0.702700$ for depleted mantle and CHUR $^{143}\text{Nd}/^{144}\text{Nd}_0 = 0.512636$.

Oxygen Isotope Analysis

Fifteen rhyolite and granitoid samples were submitted for oxygen isotope analysis at WSU. The set included two Glass Mountain rhyolite, two Hayden Peak latite, one quartz latite, five Silver City rhyolite, and six Silver City granite samples. Crushed portions of rock samples were sieved to separate grains between 0.25 and 2 mm. The separated grains were then sorted under a binocular microscope. Individual quartz and feldspar crystals were picked based on

freshness. Approximately 20 mg of both quartz and feldspar grains were collected for each sample. The samples were processed using techniques outlined by Sharp (1990) and the oxygen was measured on a Finnigan Delta S Isotope Ratio Mass Spectrometer (IRMS). The oxygen isotope results are located in Appendix D.

$^{40}\text{Ar}/^{39}\text{Ar}$ Geochronology

Twenty-eight samples were submitted for $^{40}\text{Ar}/^{39}\text{Ar}$ geochronology to Auburn University (AU) and processed in their Auburn Noble Isotope Mass Analysis Laboratory (ANIMAL). Representative samples from the separate volcanic units were selected to accurately constrain the timing of volcanism in the study area. A portion of crushed material generated during the rock preparation phase was sent to AU for analysis. The mafic samples were handpicked for individual plagioclase crystals and silicic samples were handpicked for sanidine crystals at AU. Sodium cobaltinitrite staining was used to identify and separate the sanidine crystals. The samples were run as single crystals analyses. Multiple sanidine crystals were analyzed for each sample. The samples were analyzed using a 50W Synrad CO₂ infrared laser. The data collection was performed with National Instruments hardware and used an ANIMAL specific Labview program. Raw data reduction was achieved using an in-house Excel worksheet and using Isoplot (Ludwig, 2003). Results are still anticipated as of the date when this thesis was written.

Chapter 3 - Field Relationships

The SCD has been previously mapped by others as including granitoid basement overlain by a basaltic unit and topped with various rhyolitic units (Asher, 1968; Ekren et al., 1981; Bonnicksen, 1983; and Bonnicksen and Godchaux, 2006). This study used these previously published maps to identify sample areas. The samples were collected and described in the field to help determine contacts and unit relationships. Throughout the sample collecting process, multiple silicic units were identified based on physical characteristics and field relationships. An aerial image depicting local landmarks is included in Figure 3.1. Field observations noted the overlapping and inter-fingering nature of the volcanic deposits in the Silver City district. Field observations indicate contemporaneous effusive eruptions of that led to complex stratigraphic relationships. Select stratigraphic sections are presented in Figures 3.2 thru 3.4.

The oldest and lowest stratigraphic unit exposed in SCD is the underlying granitoid batholith that serves as the basement (Figures 3.5 - 3.7). This granitoid has been mapped as the Silver City Granite (SCG) and is identified as a two-mica, granite and granodiorite unit dated to approximately 66 - 62 Ma (Asher, 1968; Pansze, 1975; Bonnicksen, 1983; and Benford et al., 2010). The granitoid batholith in SCD has been correlated as a southern extension of the larger Idaho Batholith that is present throughout much of central and northern Idaho (Taubeneck, 1971; Benford et al., 2010; Kolb et al., 2011). The batholith present in Silver City has been separated from the rest of the Idaho Batholith during the formation and extension of the western Snake River Plain at ~12-10 Ma (Lindgren, 1900; Taubeneck, 1971; Ekren et al., 1982; Bonnicksen et al., 2008). There are also small exposures of quartz-biotite-muscovite schists present south of the SCD near the former mining town of Flint. The metamorphic rocks are similar to other pre-Cretaceous rocks found south of the study area near South Mountain (Piper and Laney, 1926; Bennett, 1976; Ekren et al., 1982). These metamorphic outcrops (seen in Figures 3.8 and 3.9) are found within an outcrop of granitoid and most likely represent roof pendants formed during the emplacement of the SCG (Kolb et al., 2011), thus are the oldest rocks present in the Owyhee Mountains. Subsequent exposure and erosion of the batholith led to the formation of a paleotopographic surface that would control the deposition of the mid-Miocene volcanic units. The SCG serves as the topographic high (War Eagle Mountain) on the east side of the study area

but is contained to the lower portions of the Jordan Creek valley and the ridges to the west of Silver City. The SCG is also intruded in places by younger Eocene intermediate composition dikes (Piper and Laney, 1926; and Asher, 1968). These dioritic and dacitic dikes trend northeast and are present only cutting through the SCG; they do not appear in the younger basaltic or rhyolitic units. Lava flows likely related to these dikes have been mapped southeast of the study area (Bonnichsen and Godchaux, 2006). The Eocene dikes were not studied as part of this work. The granitoid body near War Eagle Mountain is also cut by abundant precious metal-bearing quartz veins (Figure 3.10) that were formed as part of the mid-Miocene epithermal mineralization in SCD (Piper and Laney, 1926).

Overlying the SCG is a package of basalt that has not been formally named but has been mapped as the “lower basalt” (Figure 3.11). The basalt package is up to 750 m in some areas (Asher, 1968) with individual flows up to 40 m thick. This unit was deposited on the granitoid paleotopographic surface and is present throughout the study region. The basaltic unit has a probable eruptive center south of Silver City near Flint where a approximately 460 m thick sequence of mafic, pyroclastic deposits underlies the continuous lava flow package (Asher, 1968; W.K. Hart, personal communication. Map patterns of this package of lava flows indicate that they flowed north from Flint into the SCD, through topographic lows cut into the Silver City Granite prior to mid-Miocene volcanism. The basalt unit is exposed to the southeast of War Eagle Mountain and to the west and north of Jordan Creek. Additionally, in Flint and in Silver City, there are exposures of basaltic dikes that appear to terminate at the base of basaltic flows (Lindgren, 1900; and Asher, 1968). Field evidence supports the idea that the majority of the basalt was locally erupted effusively through fissures or vents with some small episodes of early explosive activity. Some of the basalt and basaltic andesites of this unit are black with a very fine grained to aphanitic matrix and typically contain plagioclase phenocrysts up to 1 cm, which resemble regionally exposed Steens Basalt (Brueseke et al., 2007). Additionally, a single basalt flow with a coarse grained matrix and abundant 1 cm plagioclase phenocrysts and also pyroxene and olivine phenocrysts is also found directly overlying the granitic basement and underlying north of Flint. Some areas of the “lower basalt” near Silver City are host to some epithermal mineral veins (e.g. the Trade Dollar mine; Bonnichsen, 1983). Early studies of the SCD have avoided designating the “lower basalt” as part of the Steens/Columbia River Basalt Group (Lindgren, 1900; Asher, 1968; Bennett and Galbraith, 1975; Pansze, 1975). However, more

recent studies have included the “lower basalt” as part of the regional flood basalt sequence as either part of the Imnaha Basalt (Bonnichsen, 1983) and Steens Basalt (Camp and Ross 2009). This research has confirmed based on whole rock chemical evidence (see Chapter 5) that the “lower basalt” lava flows are in fact locally erupted Steens Basalt.

Stratigraphically above the Steens Basalt is a complex package of intermediate and silicic eruptive units that include andesite, dacite, rhyolite, and quartz latite flows and domes, thin pyroclastic units, and shallow intrusives (Hasten et al., 2011). One group of andesites, identified as andesite type 1, is found overlying the granitoid atop War Eagle Mountain and north of Silver City near Slacks Mountain. The outcrop near Slacks Mountain (Figure 3.12) is a shallow intrusive body that has been exposed at the surface. The shallow intrusive outcrop contains vertical columnar jointing and represents one of the many local eruptive centers. These samples are black to dark gray with a very fine grained to aphanitic matrix with some large (up to 2 mm) plagioclase phenocrysts. A second group of andesites (andesite type 2) is exposed on the flanks of Tennessee Mountain overlying Glass Mountain dacite flows and underlying the quartz latite and also overlying the Hayden Peak latite flows along a ridge near the head of Jordan Creek. The second set of andesites are physically similar with black, dense, very fine grained and aphanitic matrix, however, these samples do not contain as many phenocrysts.

One 100 m exposure of the ~15.5 - 15.8 Ma Cold Springs tuff (Brueseke and Hart, 2008) is found south of Silver City along the road to Flint. This tuff overlies a package of Steens Basalt in a tilted normal fault block, thus providing age constraints on the faulting. The tuff is a slightly welded deposit with abundant 1 mm and smaller, black glassy fragments and <1mm feldspars. This unit was not found at any other location in the SCD; its physical characteristics and bulk chemistry indicate that it is a Cold Springs tuff distal fall deposit. The Cold Springs tuff is the youngest silicic unit that erupted from the mid-Miocene Santa Rosa-Calico volcanic field (Figure 1.1).

Previous workers have mapped the silicic package as the Silver City rhyolite and have made attempts to further identify smaller units within the Silver City rhyolite such as the tuff of Flint Creek, the rhyolite of the Millsite, and aphanitic and porphyritic varieties. However, there has not been a consistent agreement on the subdivisions due to the poorly understood nature of the Silver City rhyolite (Bonnichsen, 1983). As part of this study, nine intermediate and silicic units were chemically identified as distinct volcanic units. These units include two andesite units

(type 1 and type 2), the Cold Springs tuff, the Hayden Peak latite, a quartz latite unit, the tuff of Flint Creek, the Glass Mountain dacite, the Glass Mountain rhyolite, and the Silver City rhyolite. While the units are distinguishable chemically (see Chapter 5), differences in the physical and field characteristics are often difficult to discern. The physical similarities between the intermediate and silicic units has made it difficult for previous workers to find an agreement in unit classifications. Field observations confirmed the previous workers findings that the silicic volcanism occurs predominately as lava flows with additional dikes, vents and domes. The lava flows often contain basal vitrophyre that in places grades into very fine grained flows. Many samples also include flow banding, ramping and devitrification textures.

The stratigraphically lowest unit in the silicic package is the Hayden Peak latite. This is found overlying the basalt flows north of Flint and to the southeast of the study area. The Hayden Peak latite forms a ridge of mountains (Figures 3.13 and 3.14) that includes Cinnabar, Turntable, and Quicksilver Mountains and extends southeast through Toy Pass. The thickest exposure of Hayden Peak latite (550 m) occurs at near vent exposures on top of Hayden Peak (on Cinnabar Mountain) and includes ramping and basal vitrophyric flows as seen in Figures 3.15 and 3.16. The topographic high of the vent area atop Hayden Peak is the highest point in the Owhyee Mountains and has the thickest exposure of Hayden Peak latite in the SCD. This unit is not found in the central of northern portion of the study area. The Hayden Peak latite is a commonly crystal poor and light purplish gray latite with very fine grained matrix and rare plagioclase and quartz phenocrysts. The outcrops commonly show flow banding textures and weather along platy jointing. A second latite unit, the quartz latite, is physically similar to the Hayden Peak latite and can be found throughout the entire study area and is usually found overlying the lower basalt unit and is also found in contact with the Hayden Peak latite near Turntable Mountain (Figure 3.13). The quartz latite is up to 300 m thick and also crystal poor and light purplish gray with rare quartz, plagioclase and pyroxene phenocrysts. The quartz latite unit also occurs alongside outcrops of matrix supported flow breccia in some outcrops.

The third latite unit is the Glass Mountain dacite and is most easily identified north of Jordan Creek at Glass Mountain, a 100 m thick extrusive dome and outflow facies seen in Figure 3.17. The dome has been identified as an eruptive center based on the mushrooming topographic characteristics and the steeply dipping near vent layering (Figure 3.18) and local ash flow units to the east (Figure 3.19). Flows of the Glass Mountain dacite are most commonly found north of

Jordan Creek overlying the Steens Basalt. The Glass Mountain rhyolite occurs as small exposures that are found closer to Silver City in the form of the Ruby City intrusive body, a silicic intrusive and associated dikes that cut the granitoid basement along Jordan Creek (Figure 3.20). Multiple flows also overlie the quartz latite and Silver City rhyolite along Potosi Ridge (Figure 3.21).

The tuff of Flint Creek was found primarily in the area of Flint and can be found overlying portions of the basaltic lava flows and underlying the Silver City rhyolite (Figure 3.22). The tuff of Flint Creek has an average thickness of 100 m. One exposed dike intruding into Steens Basalt on the north side of Jordan Creek near DeLamar has similar chemistry to the tuff of Flint Creek and might be genetically related. No obvious source of eruption (e.g. caldera or topographic depression) has been identified. The tuff samples are highly welded with abundant lithic and flattened pumice fragments, and 1 – 2 mm plagioclase and quartz phenocrysts in a very fine grained matrix. The dike sample is white with a very fine grained matrix and similar 1 – 2 mm phenocrysts of quartz and plagioclase.

The highest stratigraphic unit in much of the SCD is the Silver City rhyolite with a thickness up to 430 m. The Silver City rhyolite is white, pink and light purplish gray with abundant flow banding and scattered sanidine and quartz phenocrysts. Some of the outcrops show devitrification textures and some areas of hydrothermal alteration related to the subsequent epithermal mineralization system. In places, this rhyolite unit overlies the granitoid basement, Steens Basalt, quartz latite and the Glass Mountain rhyolite. The Silver City rhyolite also comprises some of the larger peaks in SCD including, Sawpit Peak, Florida Mountain and DeLamar Mountain. Sawpit Peak is shown in Figure 3.23 and 3.24. Sawpit Peak overlies the granitoid basement rock while a large dome seen in Figure 3.25 cuts the quartz latite unit. The Silver City rhyolite that caps Florida and DeLamar Mountains is also host to abundant gold and silver mineralization (Figure 3.26), which is disseminated throughout the Silver City rhyolite unit in high permeability zones (e.g. upper and lower rhyolite flow margins).

Figure 3.1: Aerial image of local geography

Next page - (Top) A Google Earth image of the Silver City district with significant geographic landmarks noted. The yellow star indicates the location of Silver City and the yellow box represents the area seen in a zoomed in image of Silver City.

(Bottom) A zoomed in Google Earth image of Silver City and the immediate vicinity with local geographic landmarks noted. The blue line indicates the location of Jordan Creek.

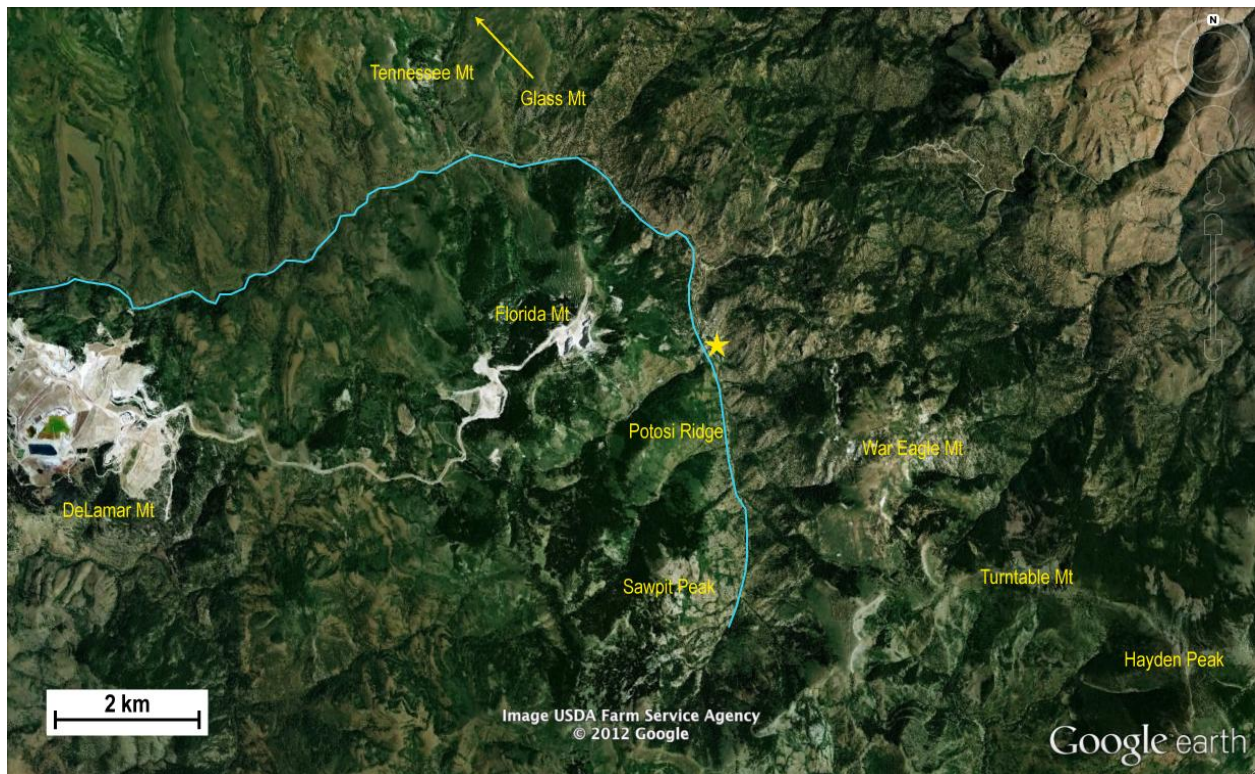
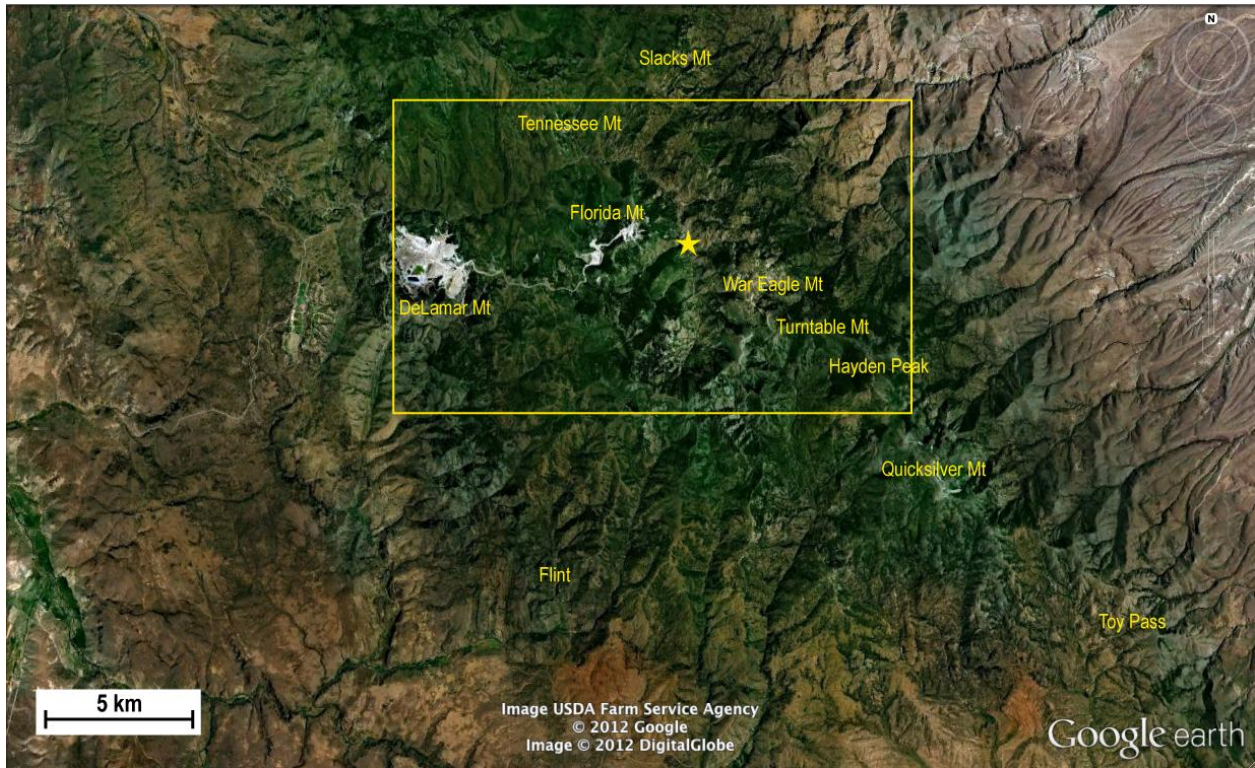


Figure 3.2: Potosti Ridge stratigraphy

Next page - Potosi Ridge is a good example of the complex stratigraphy related to the mid-Miocene volcanism. The base of the ridge is comprised of Silver City granite with multiple Steens Basalt flows deposited over the erosional paleotopography. Above the basalt are alternating deposits of Silver City rhyolite and quartz latite and Glass Mountain dacite.

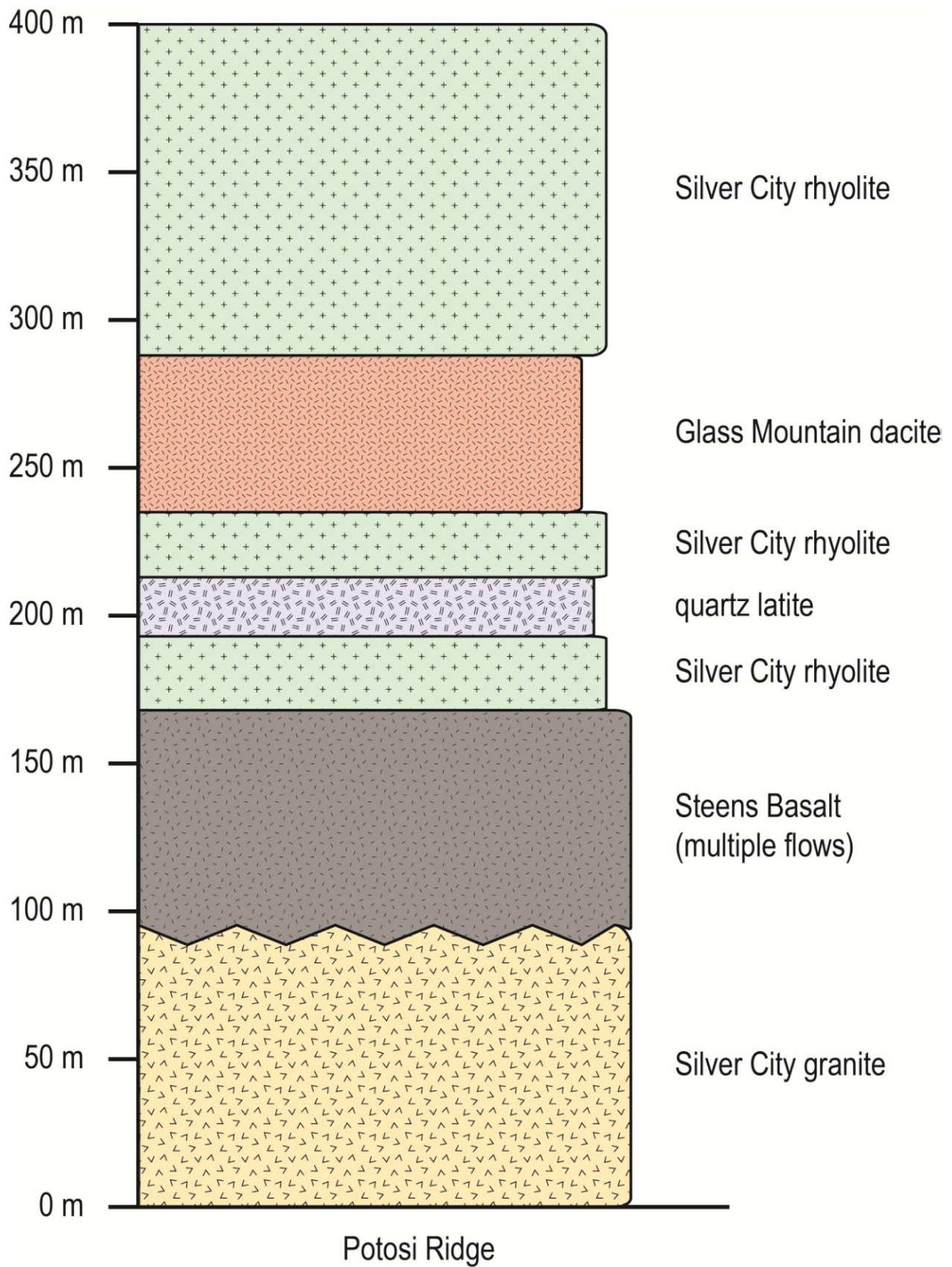


Figure 3.3: Tennessee Mountain stratigraphy

Next page - Previous workers have mapped Tennessee Mountain as a rhyolite dome with (Asher, 1968) flows of Silver City rhyolite surrounding the dome. However, field observations show the peak of Tennessee Mountain is composed of the quartz latite unit. The flanks of Tennessee Mountain are part of the andesite type 2 and Glass Mountain dacite deposits likely associated with the intrusive unit at nearby Glass Mountain.

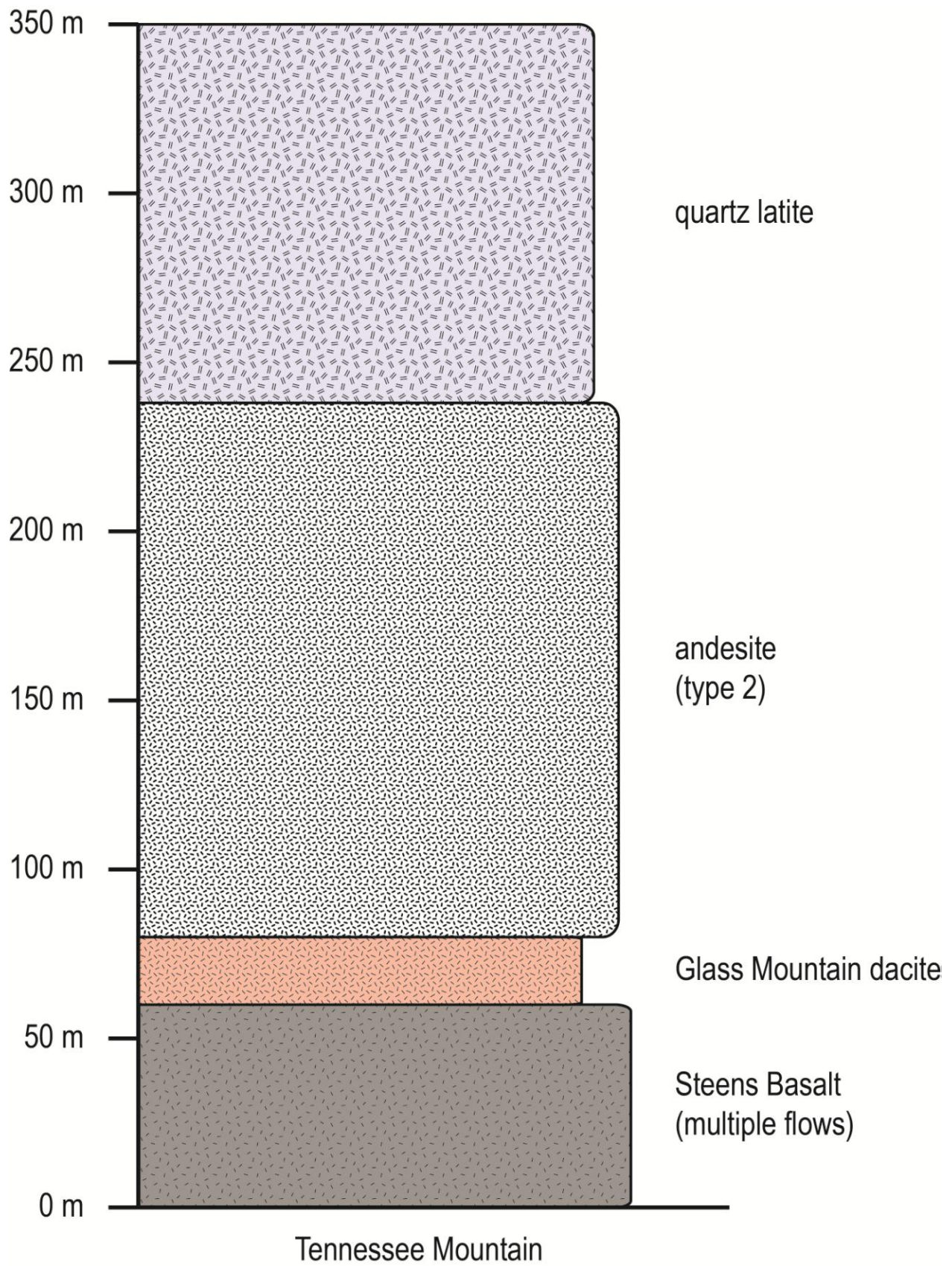
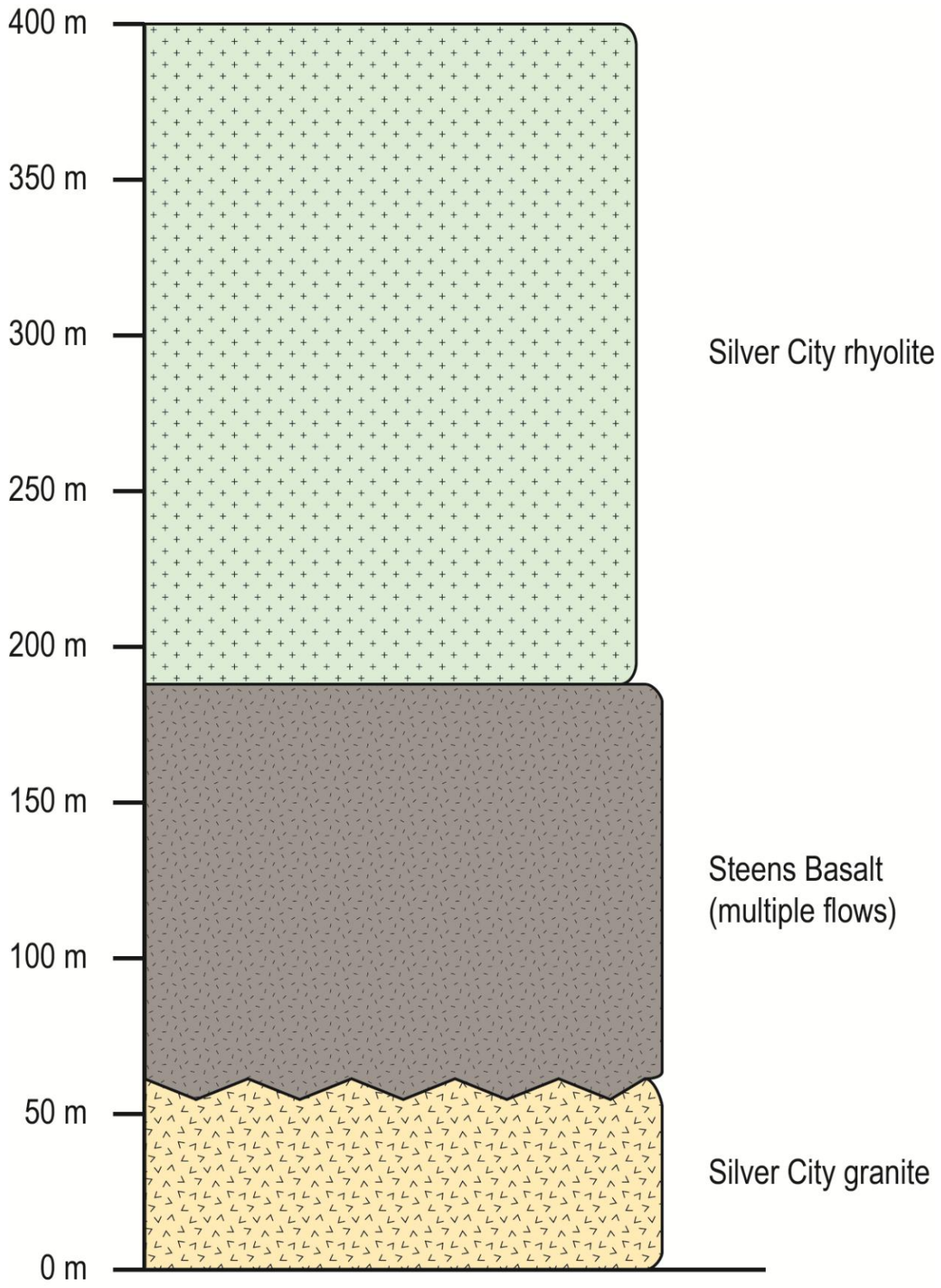


Figure 3.4: Florida Mountain stratigraphy

Next page - Stratigraphy from the east side of Florida Mountain with a flow package of Steens Basalt deposited on the Silver City granite basement. The Silver City rhyolite atop Florida Mountain is host to abundant disseminated epithermal Au and Ag mineralization.



Florida Mountain

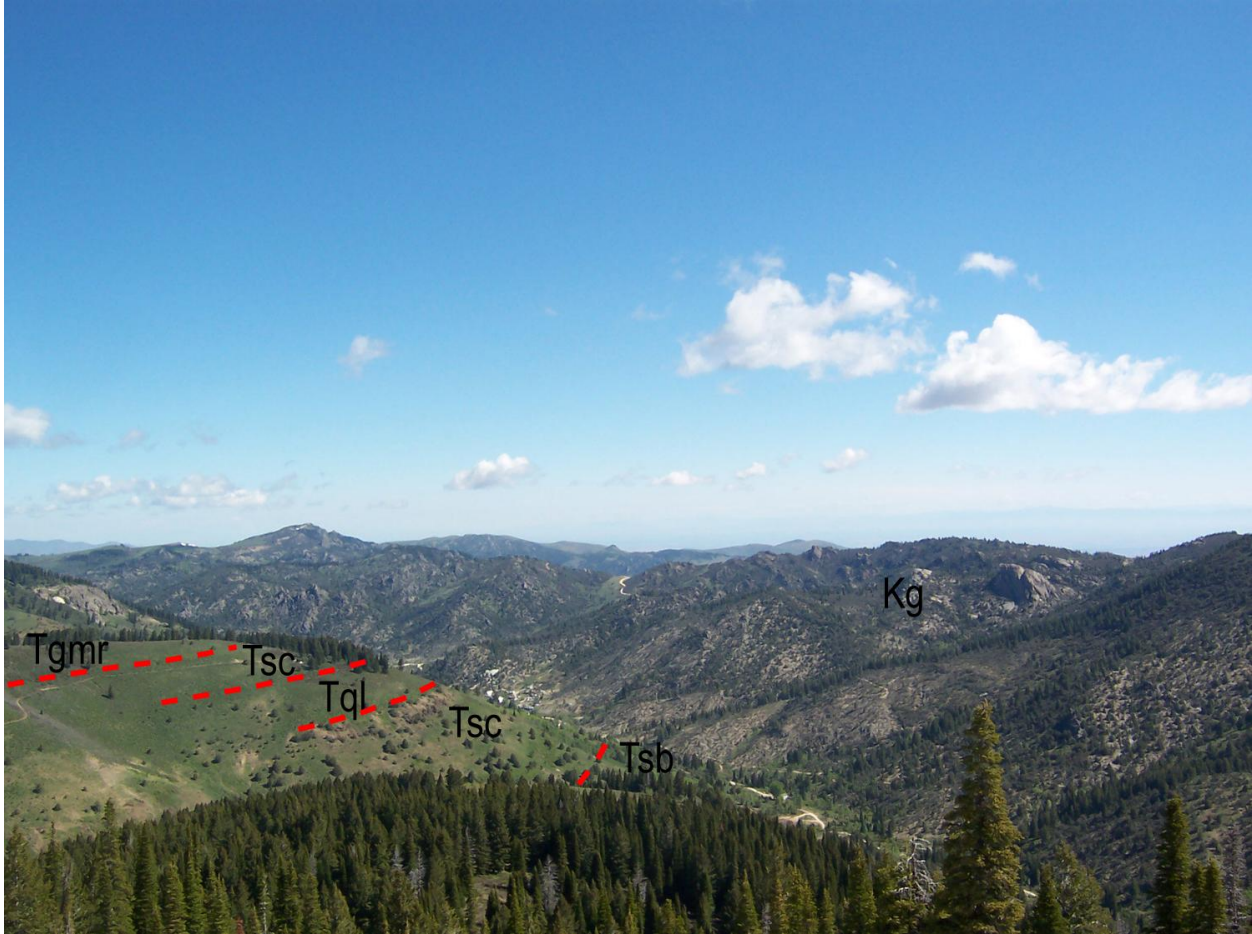


Figure 3.5: Silver City granite range

Northeast looking photo of granitoid ridge that makes up a large portion of the eastern Silver City range. The Cretaceous age batholith has been preliminarily identified as a southwestern extent of the Idaho Batholith (Taubeneck, 1971; Ekren et al., 1982; Kolb et al., 2011). Potosi ridge can be seen opposite of the granitoid ridge with interbedded Silver City rhyolite and quartz latite.

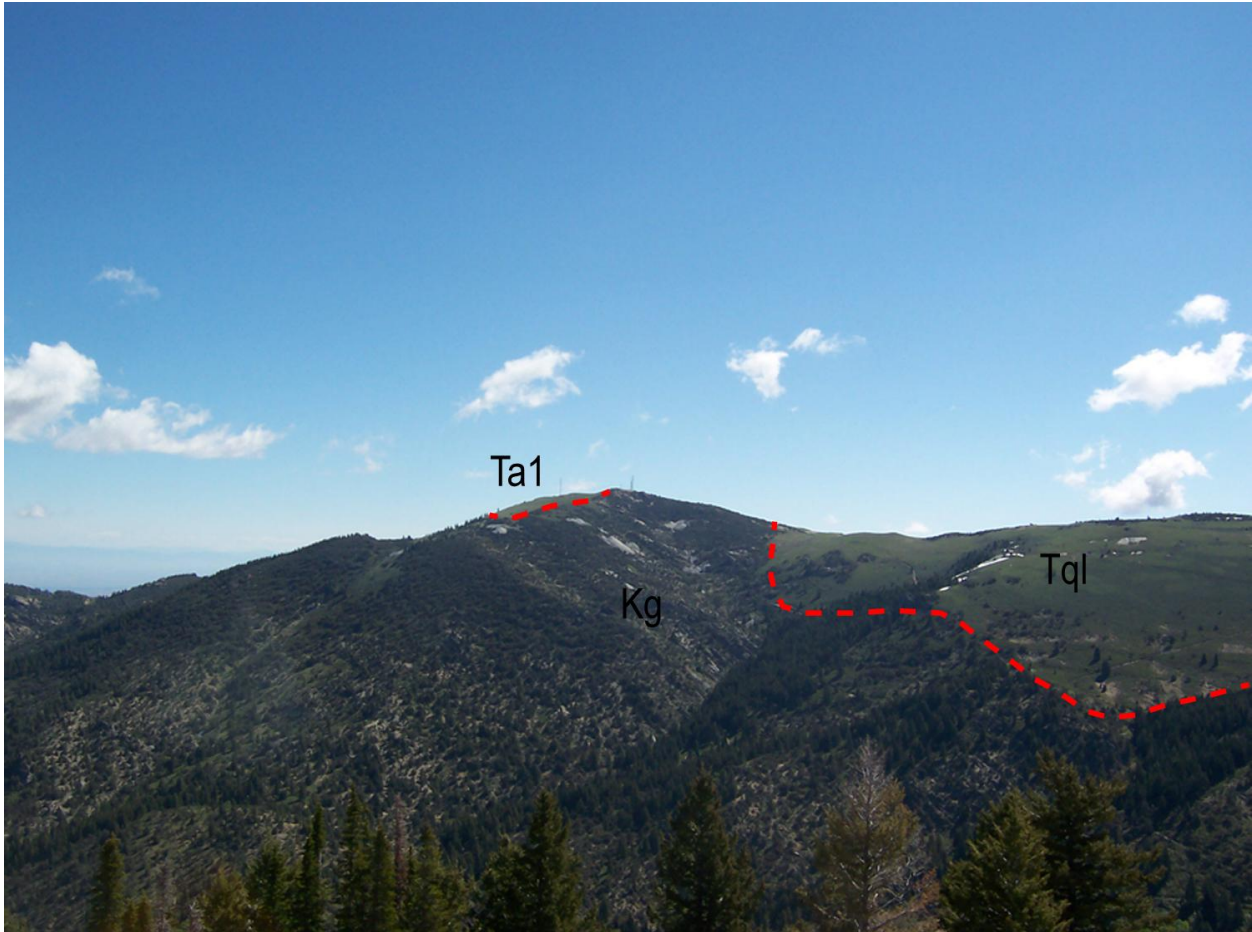


Figure 3.6: War Eagle Mountain

Photo looking east toward War Eagle Mountain, the most prominent granitic peak in SCD. War Eagle Mountain is host to countless epithermal quartz and precious metal veins that have been extensively mined since the mid 19th century. The contact between the granitoid and overlying mid-Miocene volcanic units is delineated by the dashed red line. At this location the granitoid is overlain by approximately 230 meters of quartz latite and a thin exposure of andesite type 1.



Figure 3.7: Silver City granite outcrop

Photo of granitoid outcrop near Slacks Mountain, north of Silver City.



Figure 3.8: Metamorphic outcrop

Metamorphic rocks exposed near the former mining town of Flint. The rocks are commonly quartz-biotite-muscovite schist with smaller amounts of gneiss and quartzite. This outcrop is found within a granitoid body and is most likely a localized roof pendant related to the granitoid emplacement (Kolb et al., 2011). Similar metamorphic roof pendants outcrop near South Mountain approximately 20 miles southwest of Silver City (Piper and Laney, 1926; Bennett, 1976; Ekren et al., 1982).



Figure 3.9: Metamorphic rocks

Example of two metamorphic rocks found in near Flint. The rocks range from slightly foliated gneisses (left) to strongly foliated biotite-muscovite schists (right). These pre-Cretaceous rocks are roof pendants formed during the emplacement of the Silver City batholith (Kolb et al., 2011).

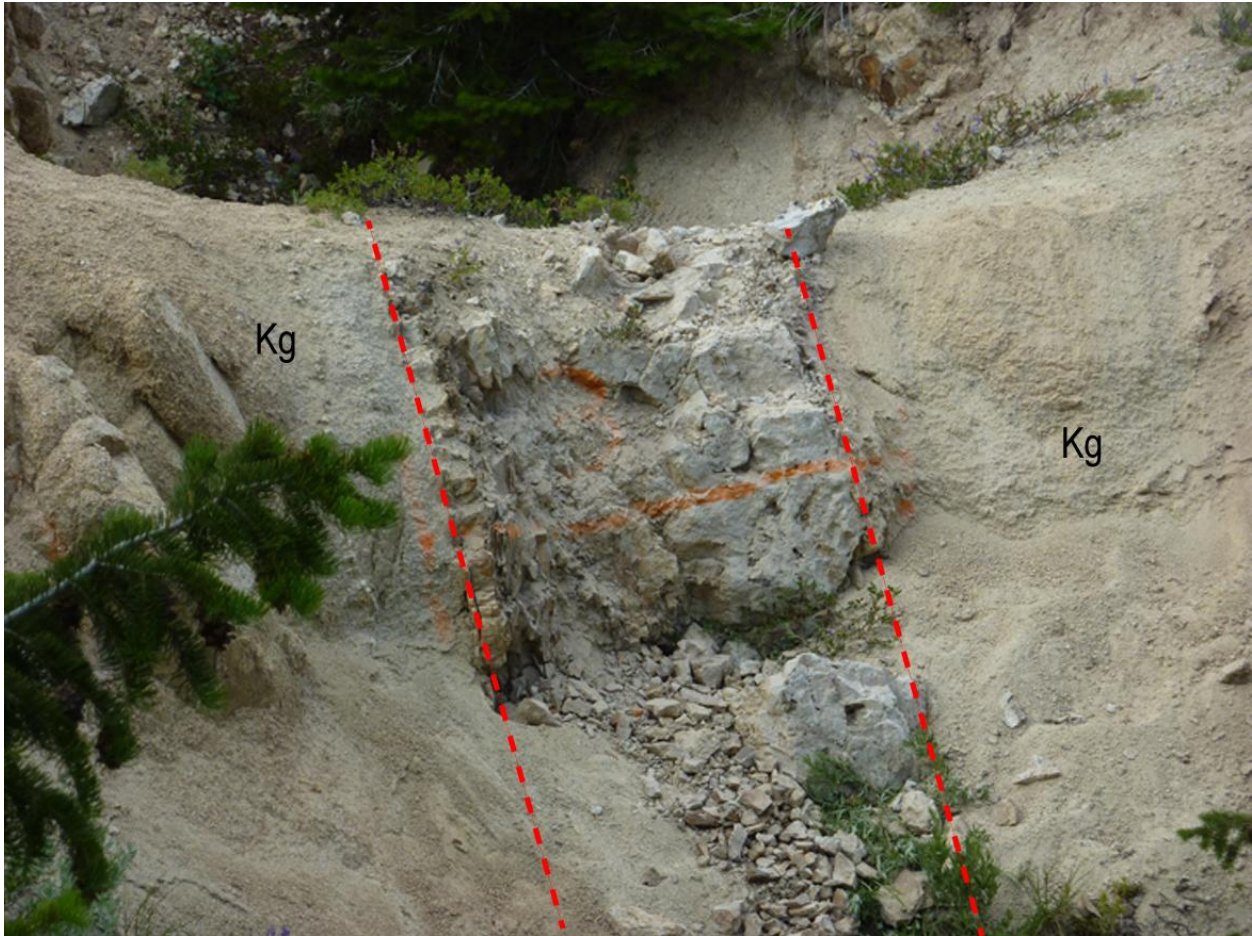


Figure 3.10: Ore bearing quartz vein

Example of the gold and silver bearing quartz epithermal veins hosted in the granitoid of War Eagle Mountain. The Oro Fino vein (pictured above) is approximately 3 feet wide at this location on the north side of War Eagle Mountain.

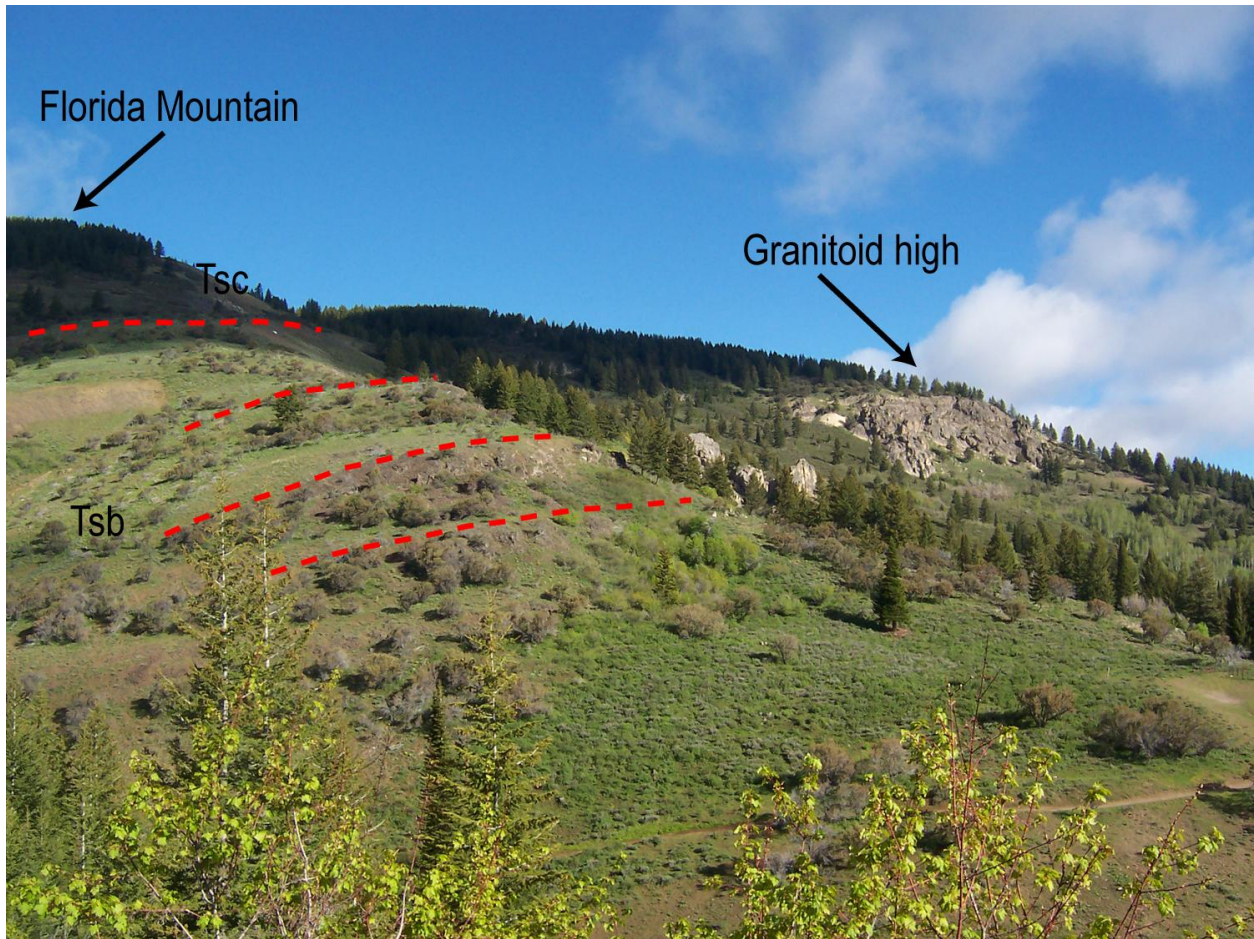


Figure 3.11: Steens Basalt

Photo looking north at a section of basalt flows on the south side of Florida Mountain. The individual flows formed identifiable benches indicated by the dashed red lines. The entire deposit of basalt shown is approximately 200 meters thick with individual flows ranging in thickness from about 20 meter to about 40 meter. The “lower basalt” was deposited on top of the granitoid basement rock and deposition was controlled by the erosional paleotopography. The basalt mostly overlies basement and appears to have flowed around/adjacent to an erosional granitoid topographic high, as seen in the background.



Figure 3.12: Andesitic shallow intrusive

The andesite type 1 shallow intrusive unit found near Slacks Mountain. The outcrop displays vertical columnar jointing and represents a possible local eruptive center.

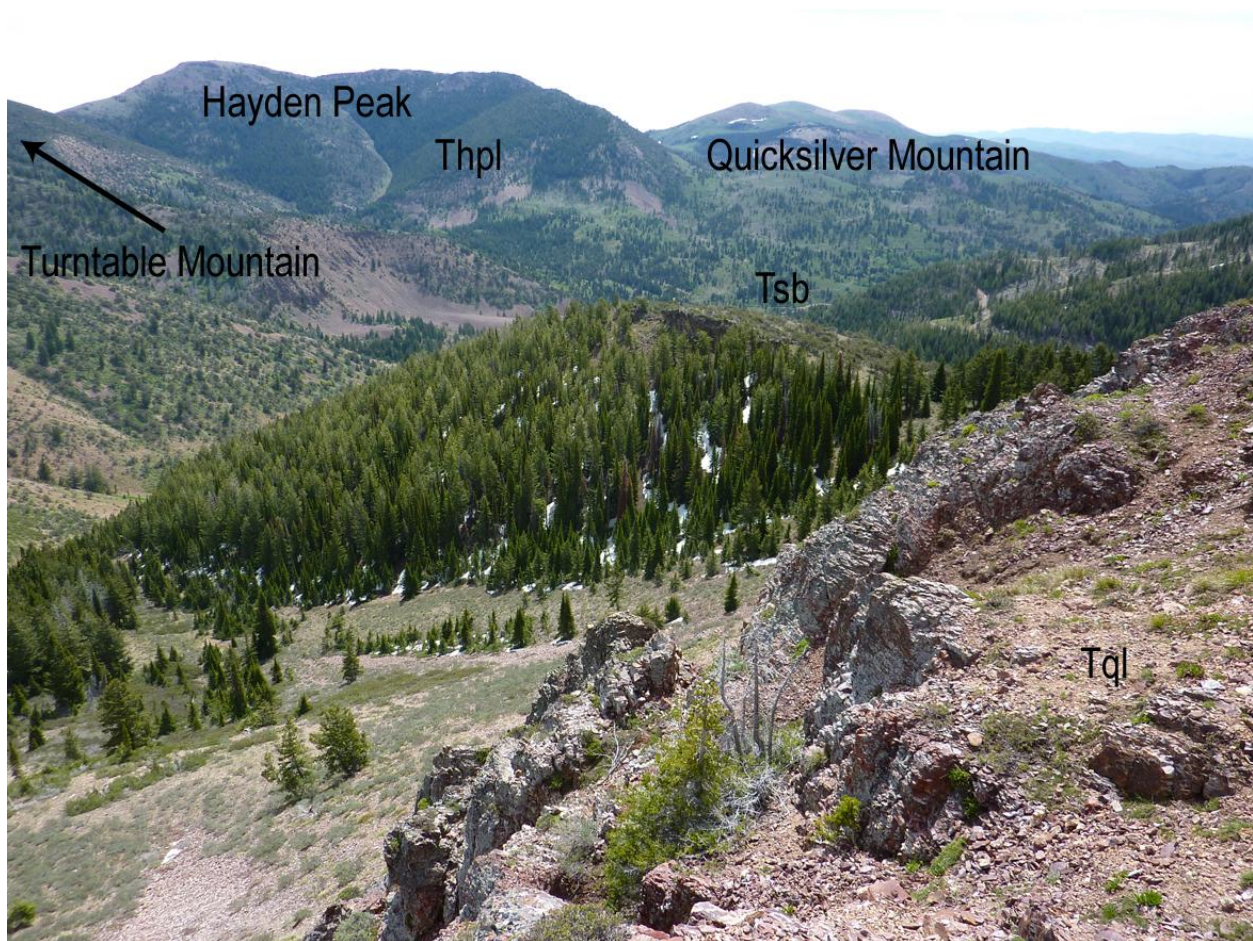


Figure 3.13: Hayden Peak and quartz latites

Photo facing east of a ridge of Hayden Peak, Turntable Mountain (not shown) and Quicksilver Mountain, composed of the Hayden Peak latite. The latite (up to 550 m thick) is deposited above the local basalt flows and extends southeast to Toy Pass (out of field of view to the right). The Hayden Peak latite is found only in the southern and southeastern portion of the study area. The photo was taken atop the quartz latite unit that is physically similar, yet chemically distinct from the Hayden Peak latite.

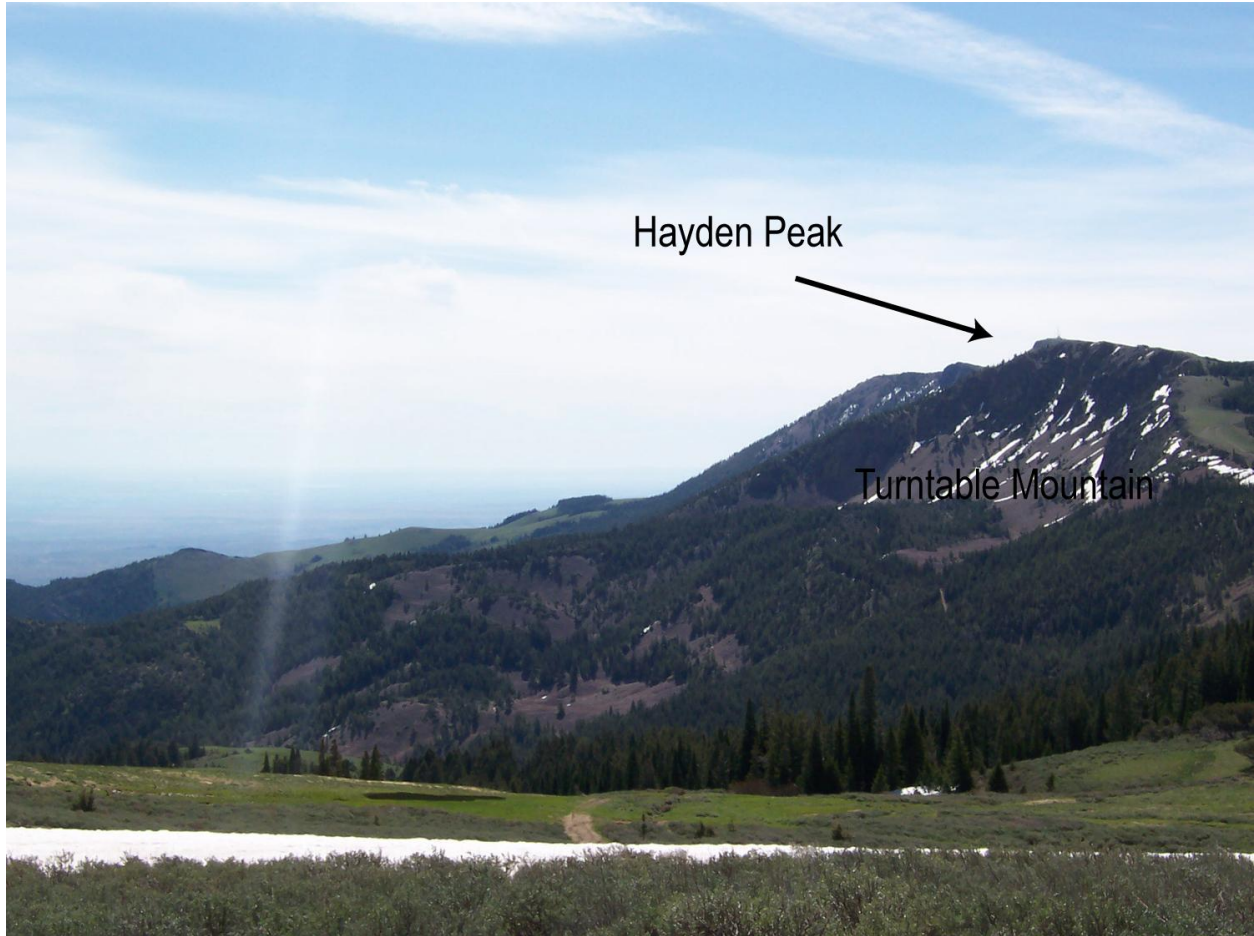


Figure 3.14: Hayden Peak

Photo from atop War Eagle Mountain looking south at Hayden Peak (in background) and Turntable Mountain.



Figure 3.15: Hayden Peak latite

Ramping and flow structures in latite flows atop Hayden Peak. Weathering along platy joints can be seen along with the ramping.



Figure 3.16: Vitrophyre on Hayden Peak

Photo showing the transitional basal vitrophyre of the upper most flow of the Hayden Peak latite.

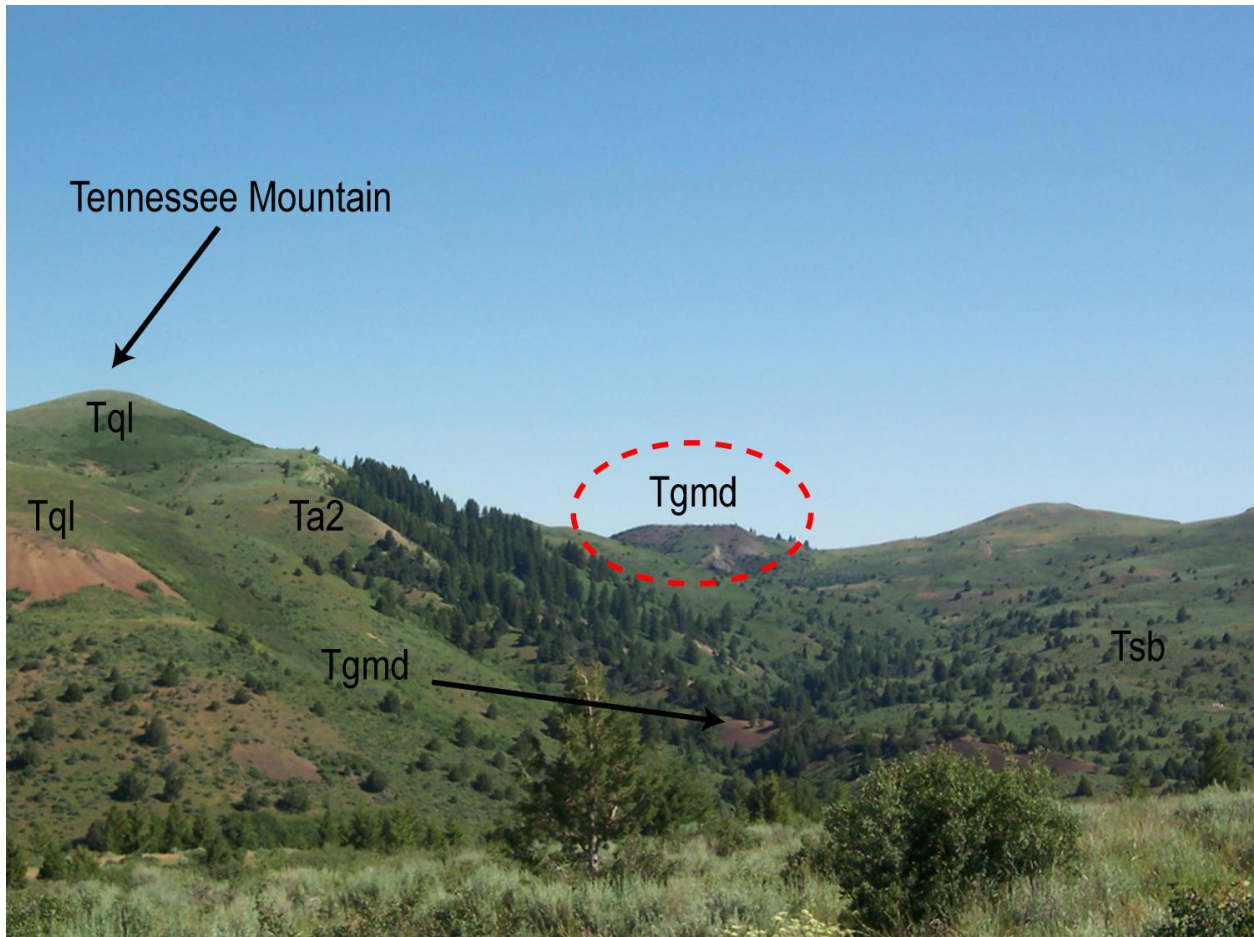


Figure 3.17: Glass Mountain

North facing photo of the Glass Mountain extrusive dome, in the red circle, north of Jordan Creek. The extrusive unit shown is emplaced onto the lower basalt. Besides the dome, flows of this dacite are also found on the south side of Tennessee Mountain and to the west near DeLamar.



Figure 3.18: Glass Mountain dacite eruptive center

Photo of ramping flow from Glass Mountain. Columnar jointing is present and radiates out from the lower portion of the photo.



Figure 3.19: Ash flow tuff

Highly welded ash flow tuff deposit near Slacks Mountain, north of Silver City. The tuff is a pyroclastic unit associated with the Glass Mountain dacite. A field book is shown for scale. The unit has columnar jointing and contains flattened and elongated pumice and rock fragments.



Figure 3.20: Ruby City intrusive

Photo of intrusive body and two parallel dikes related to the Glass Mountain rhyolite. The intrusive bodies occur south of Jordan Creek near the former location of Ruby City.



Figure 3.21: Glass Mountain rhyolite

Basal vitrophyre of Glass Mountain rhyolite from Potosi Ridge. The vitrophyre grades into and is intercalated with a basal flow breccia. The hammer is included for scale.



Figure 3.22: Tuff of Flint Creek

Outcrop of the tuff of Flint Creek exposed along road into Flint. The upper margin of the ash flow tuff unit contained abundant “apache tears” that have weathered out of the unit. A sample of the vitrophyric spheres are shown in the sample bag.

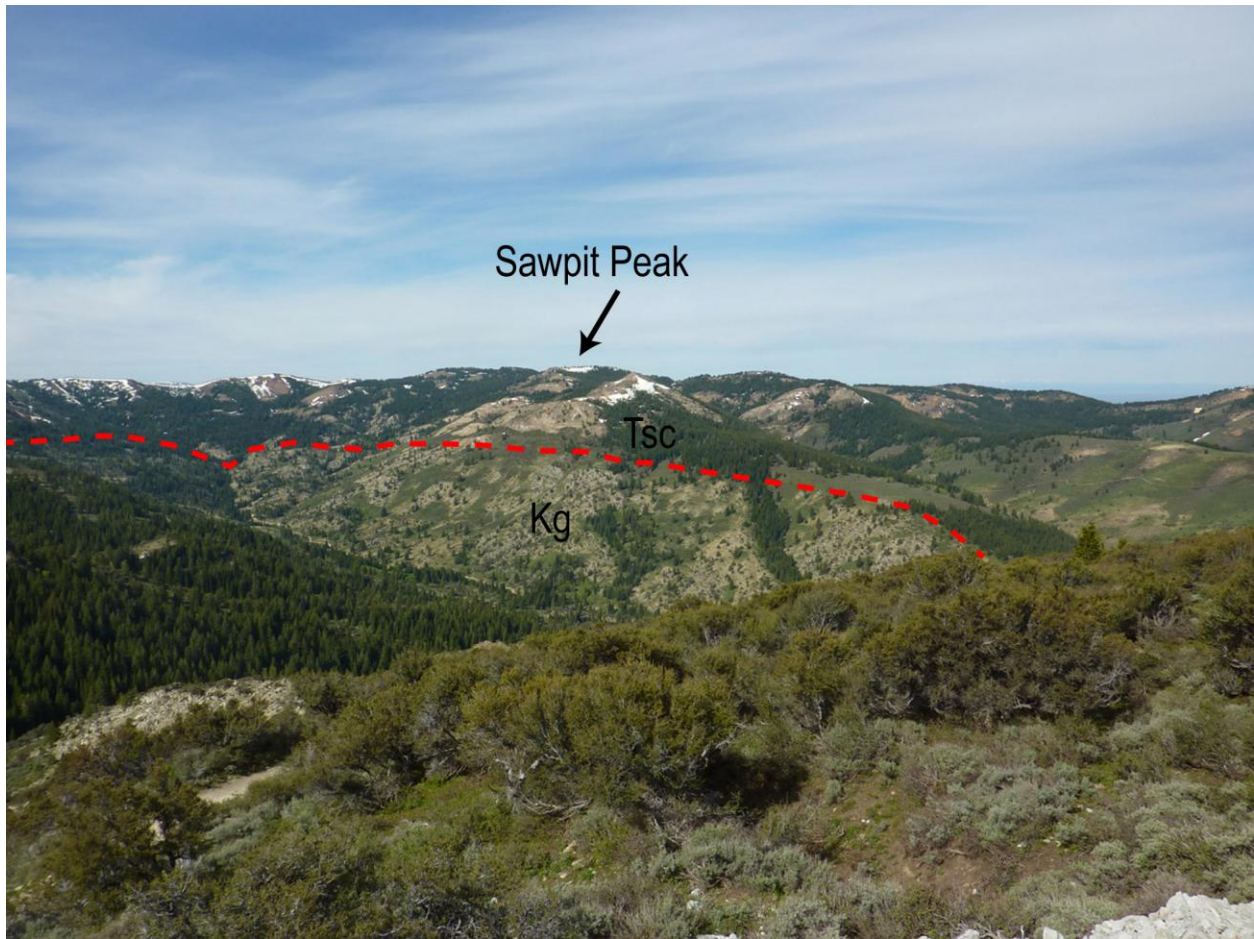


Figure 3.23: Silver City contact

Photo from War Eagle Mountain looking southwest towards Sawpit Peak. The peak is composed of 200 m of Silver City rhyolite that sits atop the granitoid basement in the valley. The red dashed line indicates the contact between the two units.



Figure 3.24: Sawpit Peak eruptive center

Photo looking north at Sawpit Peak. The Silver City rhyolite at the peak shows mushrooming flow patterns indicating the peak is a local eruptive center (e.g. rhyolite dome). The eastern edge of the dome is outlined by the dashed red line that separates the granitoid basement from the overlying Silver City rhyolite.



Figure 3.25: Silver City eruptive center

A ridge of Silver City rhyolite on the ridgecrest near the head of Jordan Creek. This ridge cuts the quartz latite unit and serves as one of the numerous local eruptive centers in SCD.



Figure 3.26: Potosi Ridge outcrop

Northwest looking photo showing the outcrop of Silver City rhyolite on top of Potosi Ridge. Florida Mountain, which is capped by the Silver City rhyolite, can be seen in the background. The rhyolite contains abundant disseminated gold and silver epithermal deposits.

Chapter 4 - Petrography

23 samples of the SCD volcanic units were analyzed for detailed thin section petrography. Representative samples were chosen from the different volcanic units to provide an adequate petrographic description of the SCD rocks. The samples include two basalts, one basaltic andesite, one andesite type 1, one olivine basalt, six Silver City rhyolites, three Hayden Peak latites, two quartz latites, three Glass Mountain dacites, one Glass Mountain rhyolite, two ash flow tuff deposits and one air fall tuff deposit. Additionally, a summary of the petrography of the granitoid basement from Kolb et al. (2011) is presented below. All of the samples, excluding the tuff deposits, were point counted to determine modal abundances. The modal abundances are included with field information and sample descriptions in Appendix A.

Granitoid basement

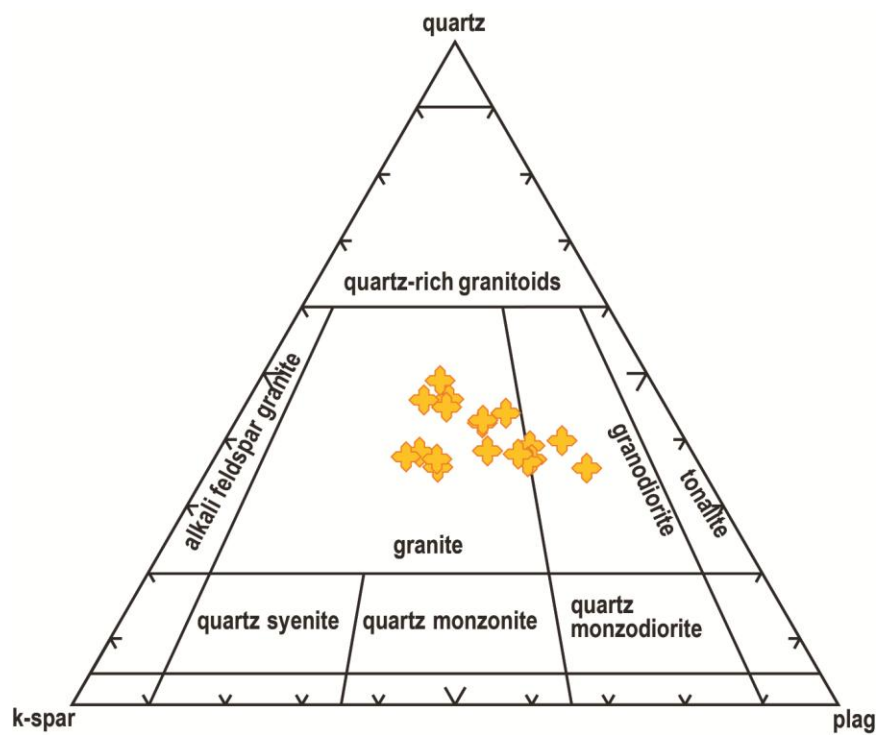
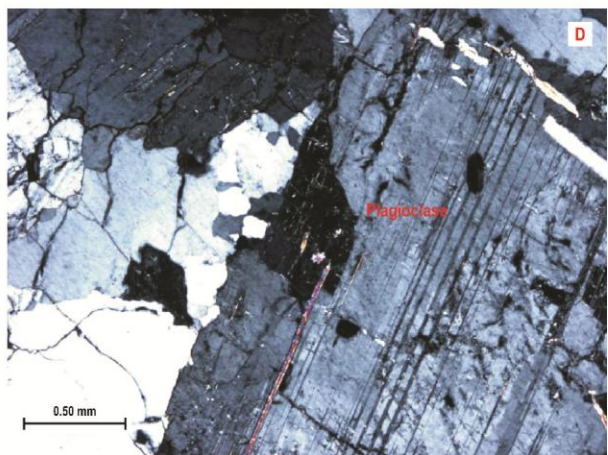
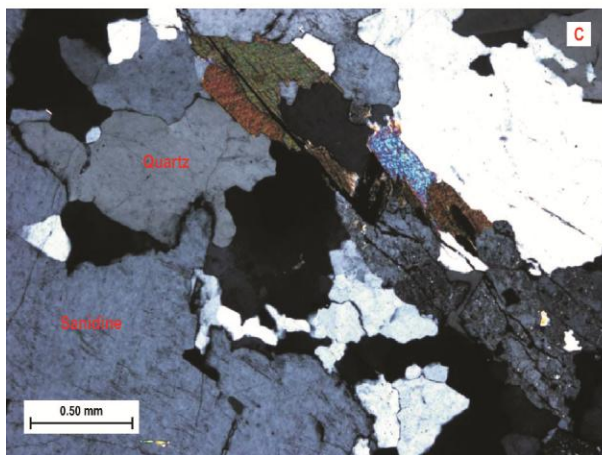
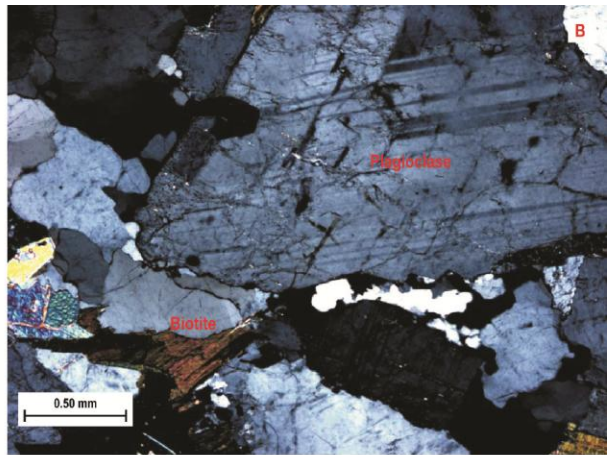
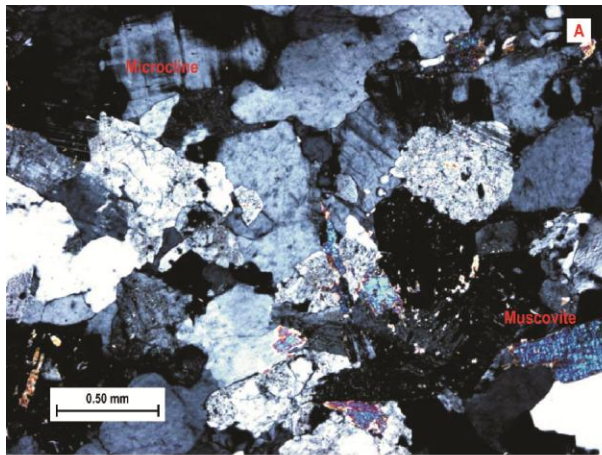
Petrography of the granitic rocks found in SCD show medium to coarse grained granites and granodiorites with predominantly anhedral, equigranular grains with larger subhedral plagioclase grains. Photomicrographs from 4 granitoid samples show an assemblage of quartz, plagioclase, K-feldspar, biotite and muscovite. The samples also include zircon and rare garnet crystals that are not pictured. Kolb et al. (2011) identified similar petrographic characteristics consistent with previous work (Asher, 1968; Pansze, 1975; Benford et al., 2010). The granitoids have average modal abundances of 36.8% quartz, 31.1% plagioclase, 24.6% K-feldspar, 3.7% biotite, 3.5% muscovite with rare (<1%) garnet and zircon. An IUGS granitoid classification diagram is shown in Figure 4.2. The samples plot as granite and granodiorite, based on thin section point counting (Kolb et al., 2011).

Figure 4.1: Granitoid petrography

Next page – (top) The granitoid samples showing A - D) anhedral plagioclase and quartz with dominated samples with interspersed microcline, sanidine, biotite, muscovite and larger twinned plagioclase grains.

Figure 4.2: IUGS granitoid classification

Next page – (bottom) Granitoid classification diagram for the Silver City granite. The samples were point counted (Kolb et al., 2011) to estimate modal abundances.

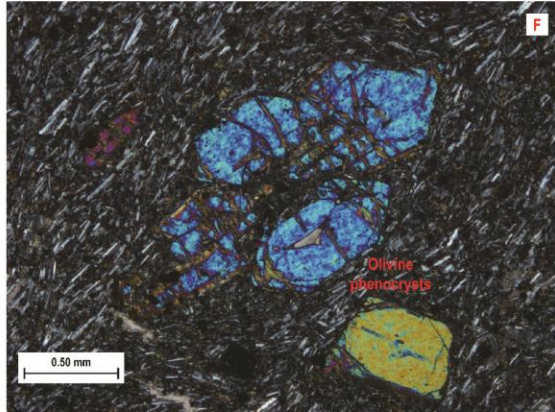
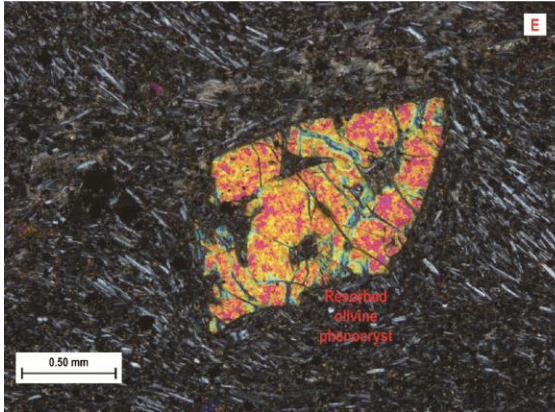
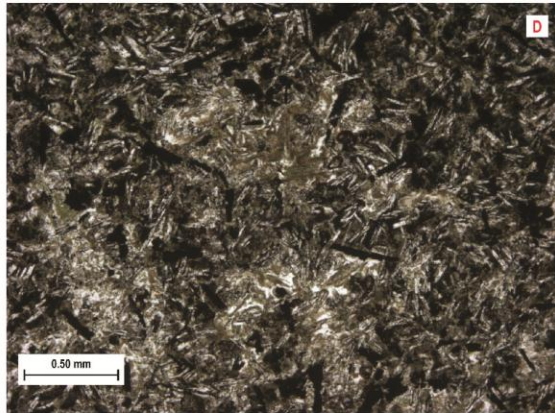
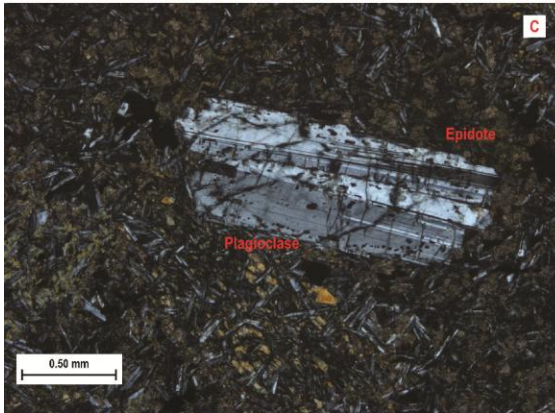
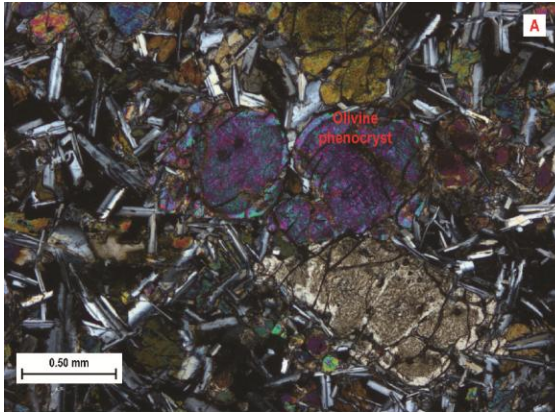


Basalt

These lava flows (MB09-13 and MB09-27) and shallow intrusive bodies contain a fine to medium grained matrix composed of plagioclase laths and iron oxides with olivine, plagioclase and clinopyroxene phenocrysts. In some instances the phenocrysts occur as glomeroporphyritic clots. The plagioclase phenocrysts are subhedral with albite twinning and some sieve and resorption textures. The olivine phenocrysts are subhedral with some interstitial clinopyroxene occurring throughout the samples. Examples of the matrix and phenocrysts can be seen in Figure 4.3. The basaltic andesite samples (MB09-5) generally have a hypocrystalline matrix with iron oxide and plagioclase laths with interstitial aphanitic groundmass. The basaltic andesites are largely void of any phenocrysts. The basaltic andesite samples have an average of 61.8% matrix, 23.0% Fe-oxide, 14.8% plagioclase and 0.4% vesicles. An olivine rich basalt sample (ZH11-4) contains a matrix of aphanitic interstitial material and flow aligned plagioclase laths and abundant 1 - 2 mm olivine phenocrysts. The olivine phenocrysts are euhedral to subhedral and have undergone slight alteration to iddingsite along fractures and rims. The aphanitic basalts contain an average of 87.1% matrix, 5.6% pyroxene, 4.2% olivine, 2.8% Fe-oxide, and 0.3% plagioclase. The phyric basalts contain 47.0% plagioclase, 28.4% clinopyroxene, 16.5% olivine and 8.1% Fe-oxide.

Figure 4.3: Basalt petrography

Next page - Photomicrographs from basalt (MB09-13) showing A) olivine and B) plagioclase phenocrysts in cross-polarized light (xpl); C) MB09-27 showing a slightly sieved plagioclase phenocryst with epidote altered matrix in xpl; D) basaltic andesite (MB09-5) with the plagioclase and iron oxide matrix in plane polarized light (ppl); E & F) olivine basalt (ZH11-4) with aligned felty plagioclase matrix with up to 2 mm skeletal olivine phenocrysts.

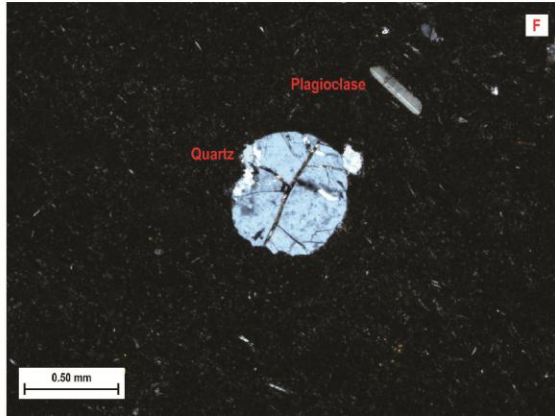
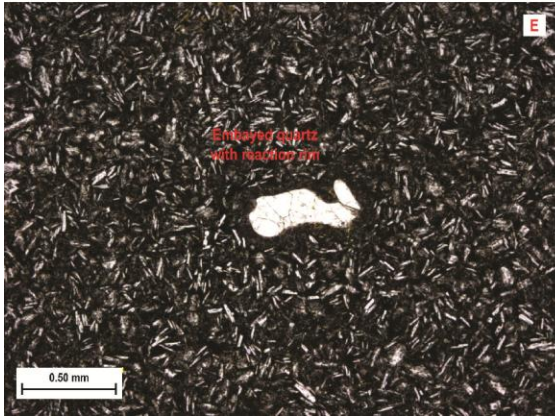
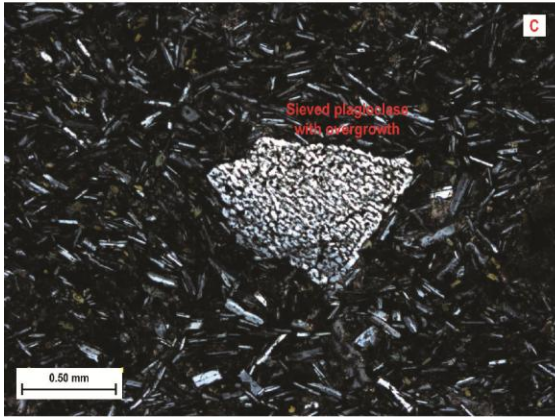
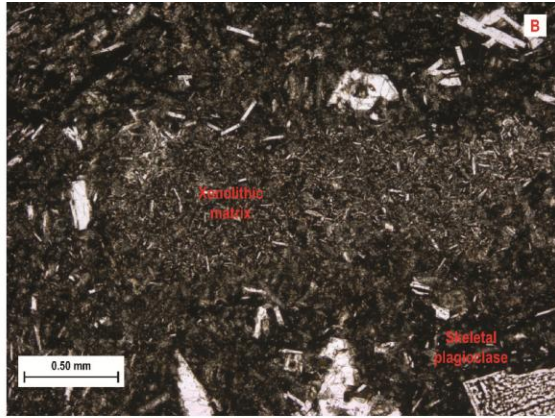
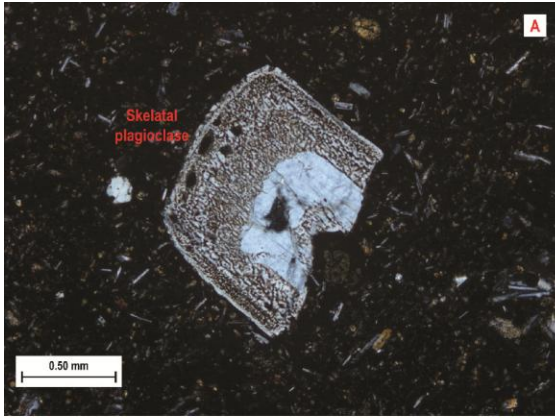


Andesite

The andesite samples typically have a very fine grained to aphanitic matrix with felty plagioclase and pyroxene micro phenocrysts. Figure 4.4 shows the andesite type 1 and type 2 samples. The type 1 samples (ZH10-40 and ZH10-20), shown in Figure 4.4a-c, have a matrix of aphanitic to vitrophyric groundmass and plagioclase laths and pyroxene microcrysts with larger up to 2 mm plagioclase phenocrysts. The samples are matrix dominated with up to 98.7% matrix and only 1.3% plagioclase phenocrysts. The larger plagioclase occurs as skeletal and sieved phenocrysts with overgrowth rims along the phenocrysts. There are also areas of entrapped xenolithic matrix that is similar to but it more crystal rich than the surrounding matrix. The type 2 andesites (Figure 4.4d-f) have similar matrix conditions with more abundant felty plagioclase micro phenocrysts. Sample ZH11-6 shows skeletal plagioclase phenocrysts with overgrowth rims, as well as, embayed quartz phenocrysts surrounded by reaction rims. Type 2 sample ZH10-25 is more aphanitic with less altered quartz and plagioclase phenocrysts.

Figure 4.4: Andesite petrography

Next page - Photomicrographs andesite type 1 with A) sample ZH10-40 showing a skeletal plagioclase phenocryst with an overgrowth rim in xpl; B) fine grained xenolith that texturally resembles a basalt/andesite; C) sample ZH10-20 with similar skeletal plagioclase with overgrowth rim phenocryst in a matrix with more abundant plagioclase laths; type 2 andesite sample ZH11-6 with plagioclase lath rich matrix and D) skeletal and overgrowth rimmed plagioclase phenocrysts; E) embayed quartz phenocrysts with reaction rims; and sample ZH10-25 with F) a more aphanitic matrix and plagioclase and quartz phenocrysts.

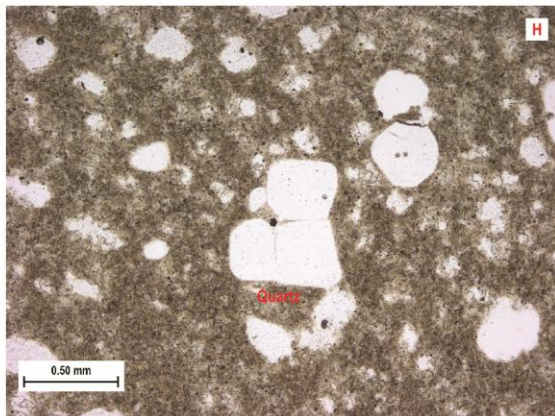
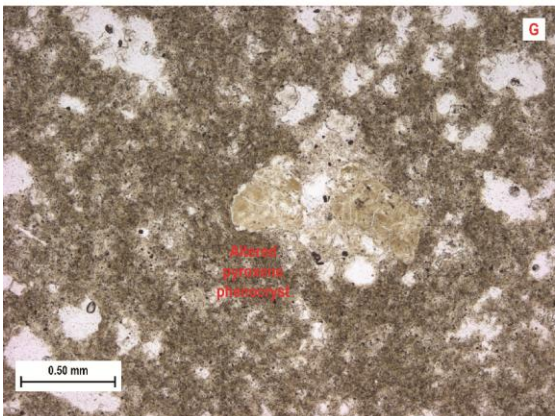
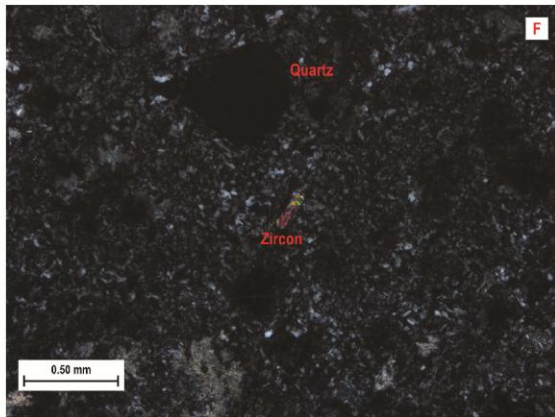
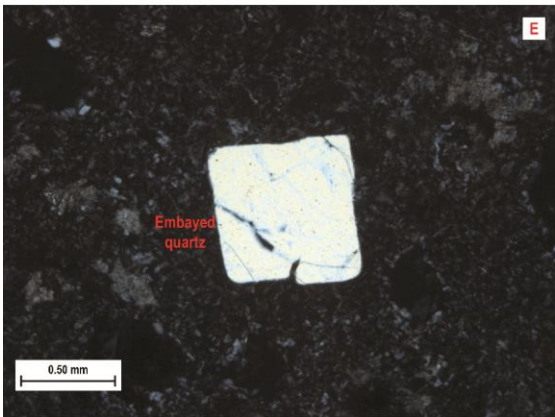
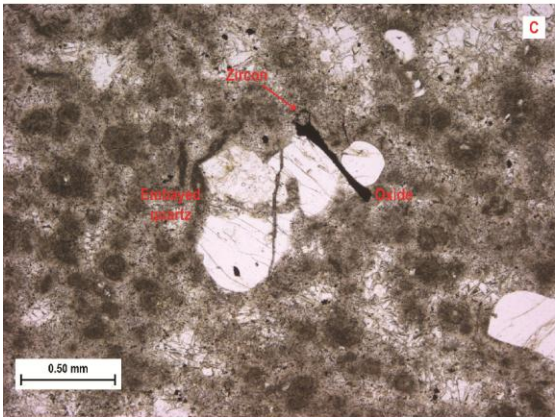
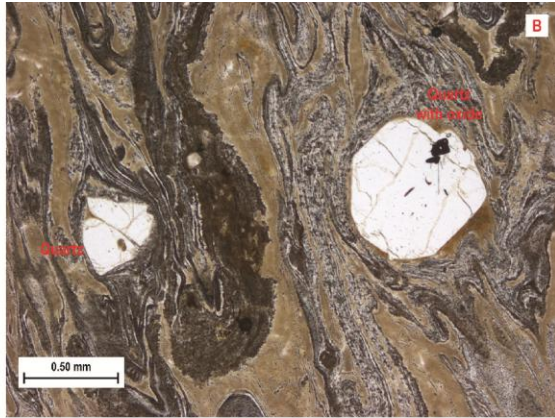
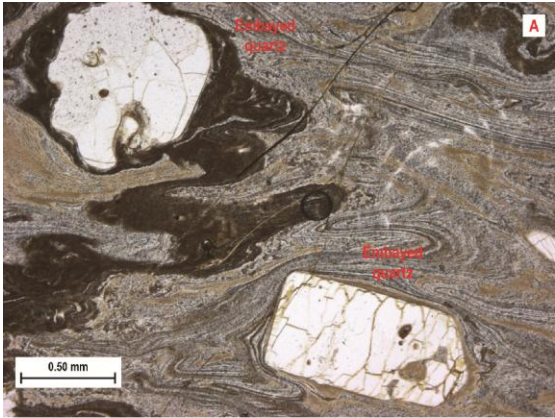


Hayden Peak and quartz latite

The Hayden Peak latite (Figure 4.5) is crystal poor with aphanitic matrix and typically less than 5 - 6% phenocrysts. Less than 1 mm quartz grains are the dominant phenocrysts with small amounts of iron oxide, zircon and plagioclase also present. The quartz grains are typically subhedral and slightly embayed. Some of the quartz grains also have spherulite rims present along the edge of the grains. Flow banding is also present in sample ZH11-2, which was taken from a basal vitrophyre at the summit of Hayden Peak as seen in Figure 3.11. The Hayden Peak latites have an average modal abundance of 90.6% matrix, 8.0% quartz, 0.7% K-feldspar, 0.3% plagioclase and 0.1% Fe-oxide. The quartz latite (Figure 4.5) is similar in thin section to the Hayden Peak latite units. The quartz latite units (ZH10-24 and ZH10-29) contain an aphanitic matrix with rare 0.5 - 1 mm quartz phenocrysts that have been embayed and altered. However, the quartz latite does not exhibit spherulite rims that are present in the Hayden Peak latite samples. The quartz latite also contains rare altered pyroxene and biotite, replaced plagioclase and rare zircon and iron oxide microcrysts. The quartz latites contain on average 97.0% matrix, 2.2% quartz and 0.8% plagioclase.

Figure 4.5: Hayden Peak and quartz latite petrography

Next page - Photomicrographs of the Hayden Peak latite (ZH11-5) showing A & B) flow banded, aphanitic matrix with embayed quartz phenocrysts up to 1 mm in ppl; C) ZH10-35 (Hayden Peak latite) with spherulitic rims on quartz phenocrysts with microcrysts of zircon and iron oxide in ppl & D) ZH11-2 (Hayden Peak latite) with spherulitic rims on quartz phenocrysts with microcrysts of iron oxide in ppl. Samples from the quartz latite unit (E-H) are shown with E) ZH10-24 with embayed 0.5 mm quartz phenocrysts in xpl; F) ZH10-24 with quartz and zircon phenocrysts in xpl; G) ZH10-29 with altered pyroxene phenocrysts in the aphanitic matrix in ppl; H) ZH10-29 with quartz phenocrysts with small iron oxide crystals in ppl.

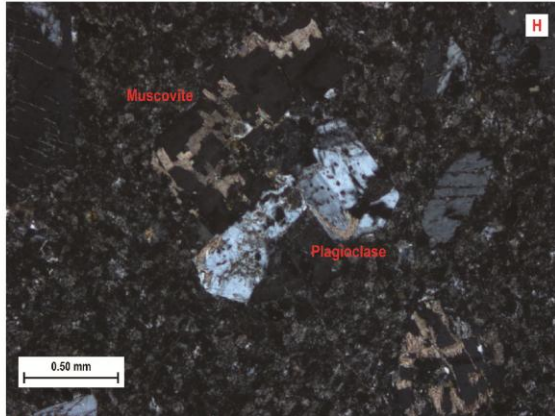
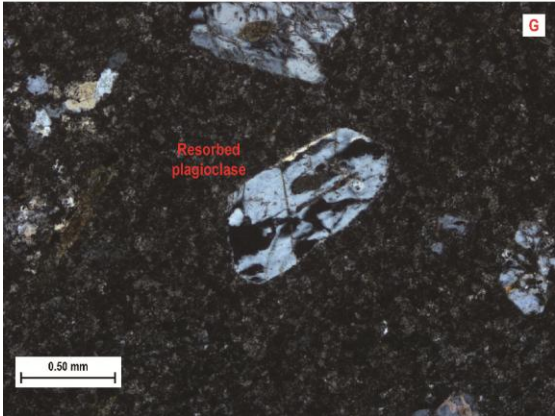
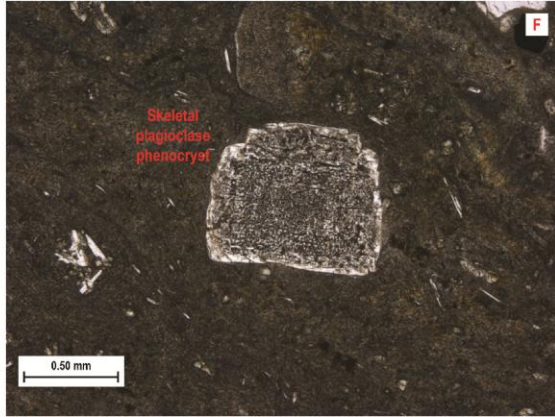
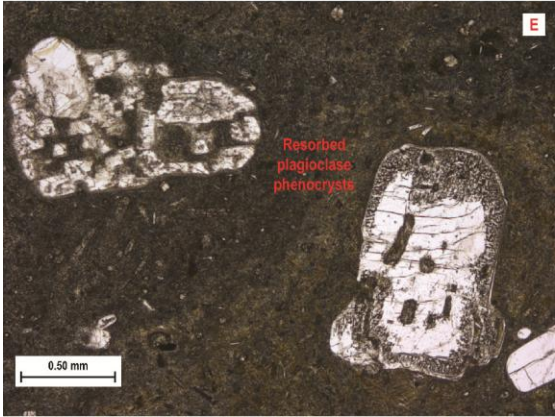
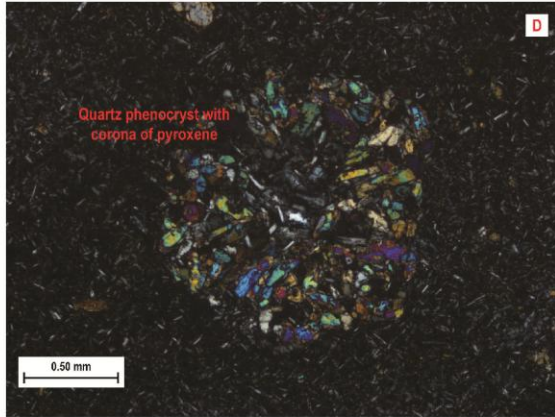
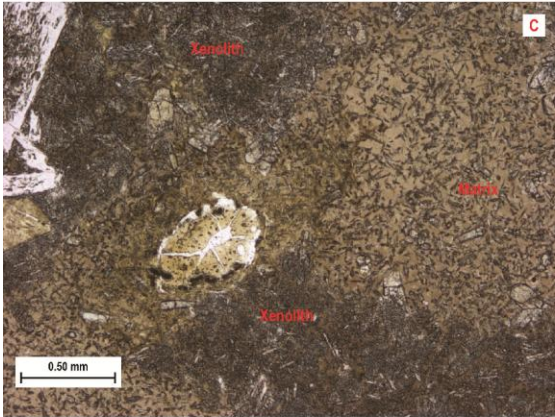
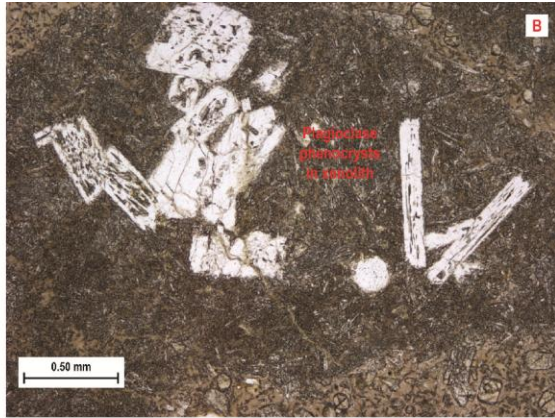
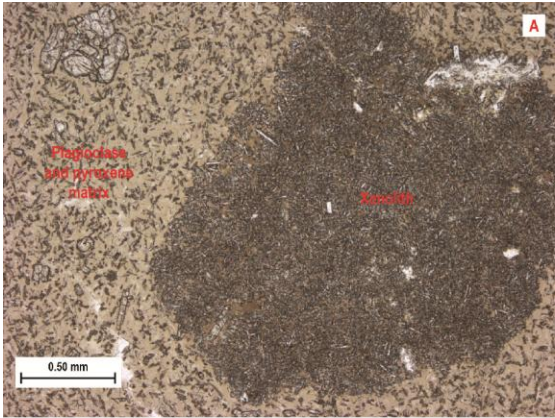


Glass Mountain dacite and rhyolite

The Glass Mountain dacite and rhyolite samples (Figure 4.6) have two different petrographic types that can be seen in thin section. The dacite samples (ZH10-22 and ZH10-33) that were observed show the presence of entrapped xenoliths that consist of a medium-grained matrix of Fe-Ti oxides and skeletal plagioclase, similar to the basalts discussed earlier. These xenoliths (or enclaves) comprise up to 20% of the samples and appear to be more mafic than latite host rock. The xenoliths are more crystal rich, with larger felty plagioclase laths and plagioclase and orthopyroxene phenocrysts. Besides the xenoliths, the samples contain an aphanitic, glassy matrix with lathy plagioclase, clinopyroxene and orthopyroxene phenocrysts. The pyroxene phenocrysts often occur as corona rims around resorbed quartz grains. The dacite samples contain on average 75.3% matrix, 10.1% plagioclase, 9.8% xenolith, 2.5% clinopyroxene, 2.0% orthopyroxene, and 0.1% quartz. One sample (ZH10-41) also contains an aphanitic to very fine-grained matrix with microphenocrysts of plagioclase and clinopyroxene. The samples contain plagioclase, quartz, and orthopyroxene phenocrysts up to 2 mm. The rhyolite sample (ZH10-43) that was analyzed for petrography contains an aphanitic matrix with up to 15% phenocrysts of 1-2 mm quartz and again, resorbed plagioclase. While this Glass Mountain rhyolite does not contain the mafic xenoliths, the plagioclase phenocrysts are often skeletal cores with overgrowth along the rims. The samples also include zircon and iron oxide microcrysts in the matrix. These average 85.1% matrix, 8.4% plagioclase, 5.0% quartz, 0.8% muscovite, 0.5% Fe-oxide, and 0.3% zircon.

Figure 4.6: Glass Mountain dacite and rhyolite petrography

Next page - Photomicrographs of the Glass Mountain dacite showing ZH10-22 with A, B, & C) entrapped xenoliths with 1 mm skeletal and sieved plagioclase phenocrysts in ppl; D) glomeroporphyritic pyroxene clot in ZH10-33 that is likely occurring a corona around a quartz xenocryst in xpl; E & F) ZH10-41 with resorbed and skeletal plagioclase phenocrysts in ppl; G & H) Glass Mountain rhyolite sample ZH10-43 with resorbed plagioclase phenocrysts with slight seriticization in xpl.

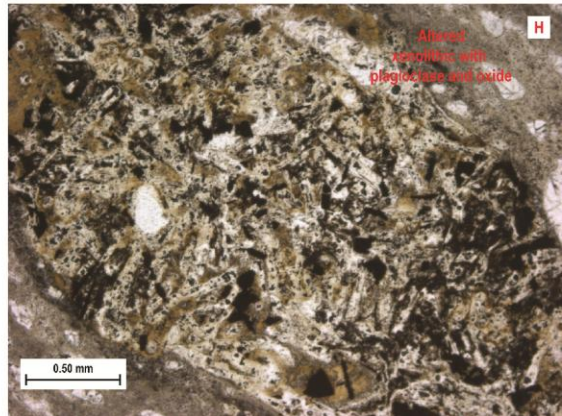
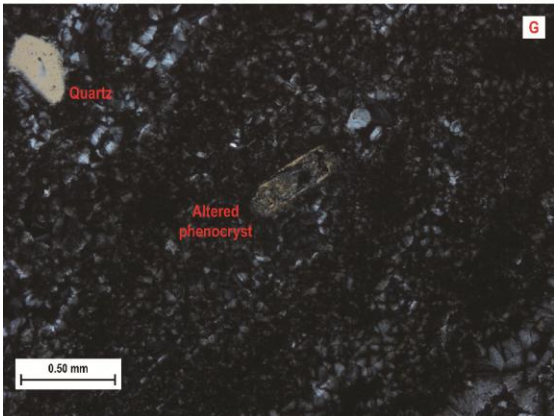
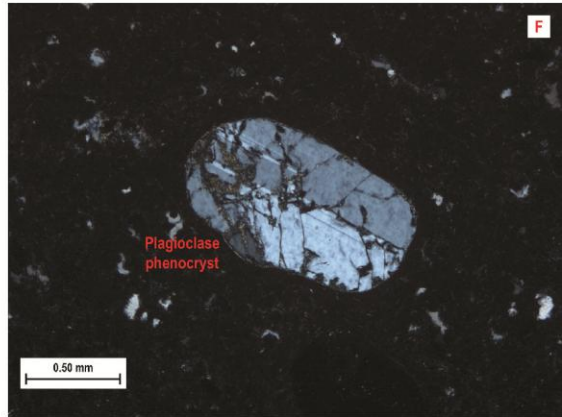
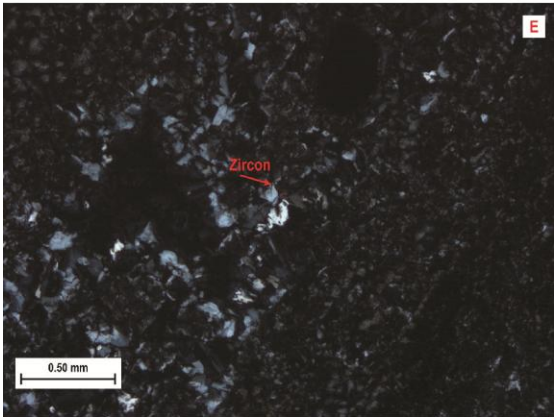
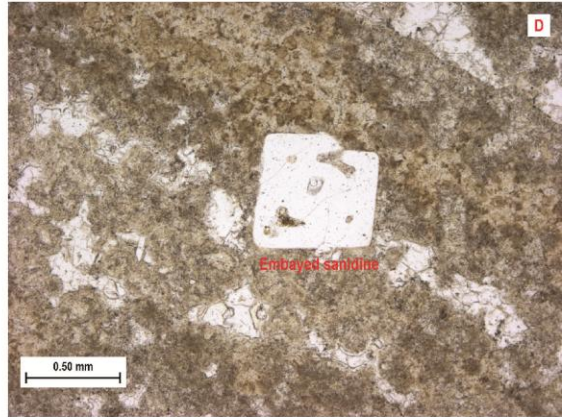
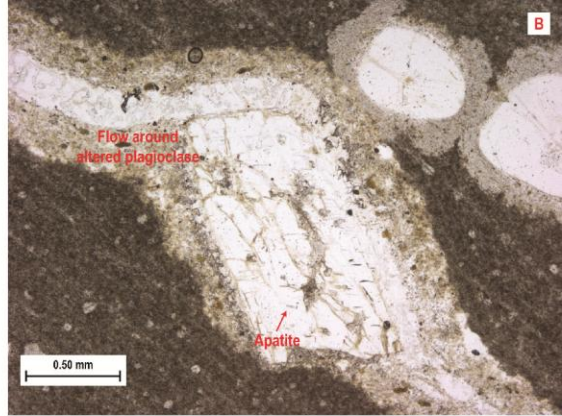


Silver City rhyolite

Silver City rhyolite (Figure 4.7) samples are crystal poor with all samples showing less than 15% phenocrysts. The Silver City latite has an aphanitic and often flow banded matrix as seen in ZH10-15 (Fig. 4.7a). The flow banding is present as alternating very fine grained and fine to medium grained layers, that likely reflects devitrification. The unit commonly contains 1 - 3 mm quartz and plagioclase phenocrysts with rarer pyroxene, biotite, iron oxide, zircon, and altered pyroxene, biotite and plagioclase phenocrysts. The quartz and plagioclase phenocrysts are subhedral with abundant embayment and resorption present. Quartz grains in ZH10-31 contain spherulitic devitrification textures round the rims. Some flows within the Silver City latite also show devitrification textures and very fine grained cristobalite in the interstitial matrix (ZH11-11). There are also small inclusions of altered fine-grained mafic xenoliths in MB09-22. Average modal abundances for the Silver City rhyolite contain 92.4% matrix, 2.9% quartz, 1.6% plagioclase, 1.7% vesicles, 1.0% altered xenoliths, 0.4% biotite, 0.1% Fe-oxide.

Figure 4.7: Silver City rhyolite petrography

Next page - Photomicrographs of the Silver City rhyolite showing A) ZH10-15 with flow banded matrix with spherulite rimmed quartz phenocryst and biotite inclusion in ppl; B) ZH10-15 with flow banded matrix around a plagioclase phenocryst along with spherulite rimmed quartz phenocrysts in ppl; C) ZH11-11 embayed sanidine phenocrysts up to 3 mm in ppl; D) ZH10-31 with embayed sanidine phenocryst in ppl; E) ZH10-31 with an example of zircon microcrysts that are found throughout unit in xpl; F) ZH10-42 with twinned and slightly altered, rounded plagioclase phenocryst in xpl; G) ZH10-31 with example of altered phenocryst of clinopyroxene in the aphanitic matrix in xpl; H) coarse grained xenolith surrounded by aphanitic matrix in MB09-22.

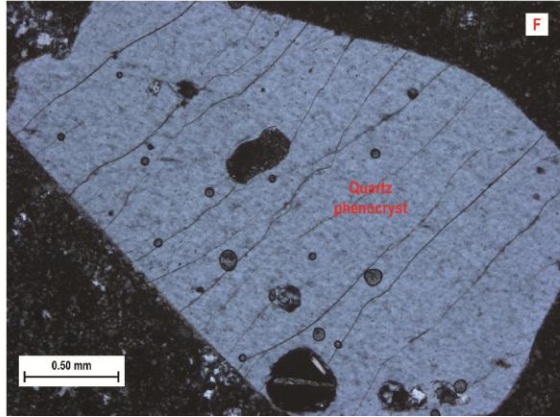
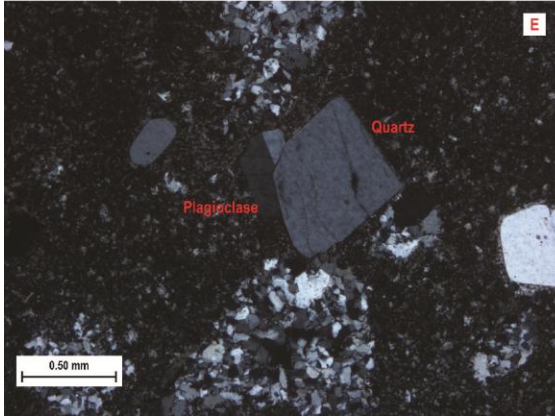
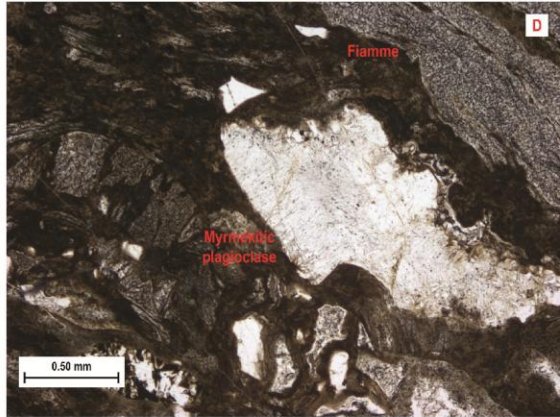
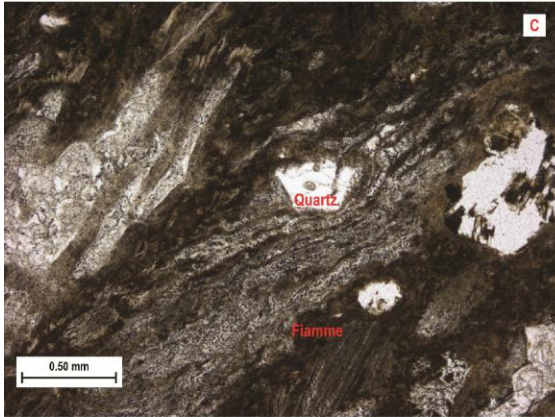


Tuffaceous units

There are two separate tuffaceous units that were found in SCD. The first appears to be a deposit of the ~15.5-15.7 Ma Cold Springs tuff (Knight et al., 2004; Brueseke and Hart, 2008) and the second, a more localized deposit of the tuff of Flint Creek (Panze, 1975). The Cold Springs tuff was identified in one sample collected (MB09-20) and contains a aphanitic to vitrophyric matrix with abundant 0.25 mm embayed subhedral quartz and larger 1 - 2 mm plagioclase phenocrysts as seen in Figure 4.8. Microcrysts also exist in the matrix. Elongated and flattened glass shards are present throughout the sample. The Cold Springs tuff sample also contains banded areas of coarser grain layers with more abundant phenocrysts, consistent with an origin as a primary ash-fall deposit. Two samples from the tuff of Flint Creek (Figure 4.8) were analyzed: one sample (MB09-16) is an ash-flow tuff deposit and the other sample (ZH11-12) is a silicic dike sample that appears to be geochemically related to the tuff deposits and a possible feeder for the tuffaceous eruption. The dike sample contains an aphanitic matrix with abundant 1 -3 mm resorbed quartz and plagioclase phenocrysts. The ash-flow tuff sample contains similar quartz and plagioclase phenocrysts with an aligned and banded fiamme up to 2 mm in an aphanitic to vitrophyric matrix.

Figure 4.8: Tuffaceous unit petrography

Next page - The Cold Springs tuff sample (MB09-20) showing A) aligned and compressed glass shards in ppl; B) slightly sieved plagioclase phenocryst in ppl. The tuff of Flint Creek (MB09-16) with C & D) a flow sample showing compressed and aligned matrix with quartz and plagioclase phenocrysts in ppl; E & F) dike (ZH11-12), with up to 3 mm quartz and plagioclase phenocrysts in xpl.



Chapter 5 - Geochemistry

Of the 120 collected samples, 99 of them were analyzed for major and trace element geochemistry using XRF. The 99 analyses include granitoid and metamorphic basement rocks as well as basaltic through silicic volcanic rocks. Care was taken to submit the freshest material for analysis. Samples that were determined to be too highly altered based on visible characteristics were not submitted for geochemical analysis. In addition to the major and trace element analysis, 45 samples were analyzed for more precise trace and rare earth element (REE) geochemistry using ICP-MS. The major element concentrations are presented as weight percent oxide (wt. %) while the trace and rare earth element concentrations are presented as parts per million (ppm). Additionally, fourteen samples were submitted for Pb, Sr, and Nd isotopic analysis using TIMS and fifteen silicic and granitoid samples were submitted for O isotopic analysis using IRMS.

Seven samples were submitted for all of the geochemical analysis (major , trace, REE, and Sr-Nd-Pb-O isotope) as well as geochronology. One sample was chosen from each of the following units: olivine rich basalt, andesite type 1, Glass Mountain dacite, Glass Mountain rhyolite, Hayden Peak latite, quartz latite, and Silver City rhyolite. The olivine rich basalt, andesite type 1, and Glass Mountain dacite samples were not submitted for O isotope analysis due to the mafic and intermediate nature of the rocks. Additionally, three granite samples were submitted for complete geochemical analysis without submission for geochronology. Complete geochemical data for all of the analyzed samples can be found in Appendices B, C, and D. Major and select trace element data for one representative sample from each unit can be found in Table 8.1.

Geochemical Classification

Analysis of major element concentrations of the Silver City district volcanics show a continual range of rock type from basalt through rhyolite. While the volcanics are dominantly basaltic and rhyolitic in composition there are also multiple intermediate flows located in Silver City district. A total alkali silica (TAS) diagram after LeBas et al. (1986) in Figure 5.1 shows the subalkaline trend and the compositional range of the Silver City district rocks. While naturally

occurring rhyolites typically fall below 78 wt. % SiO₂, some Silver City district samples above this range have undergone hydrothermal alteration associated with the precious metal deposition and have been subsequently depleted in alkalis and enriched in silica. The silicified samples that contain more than 78 wt. % SiO₂ are not included in subsequent diagrams and figures.

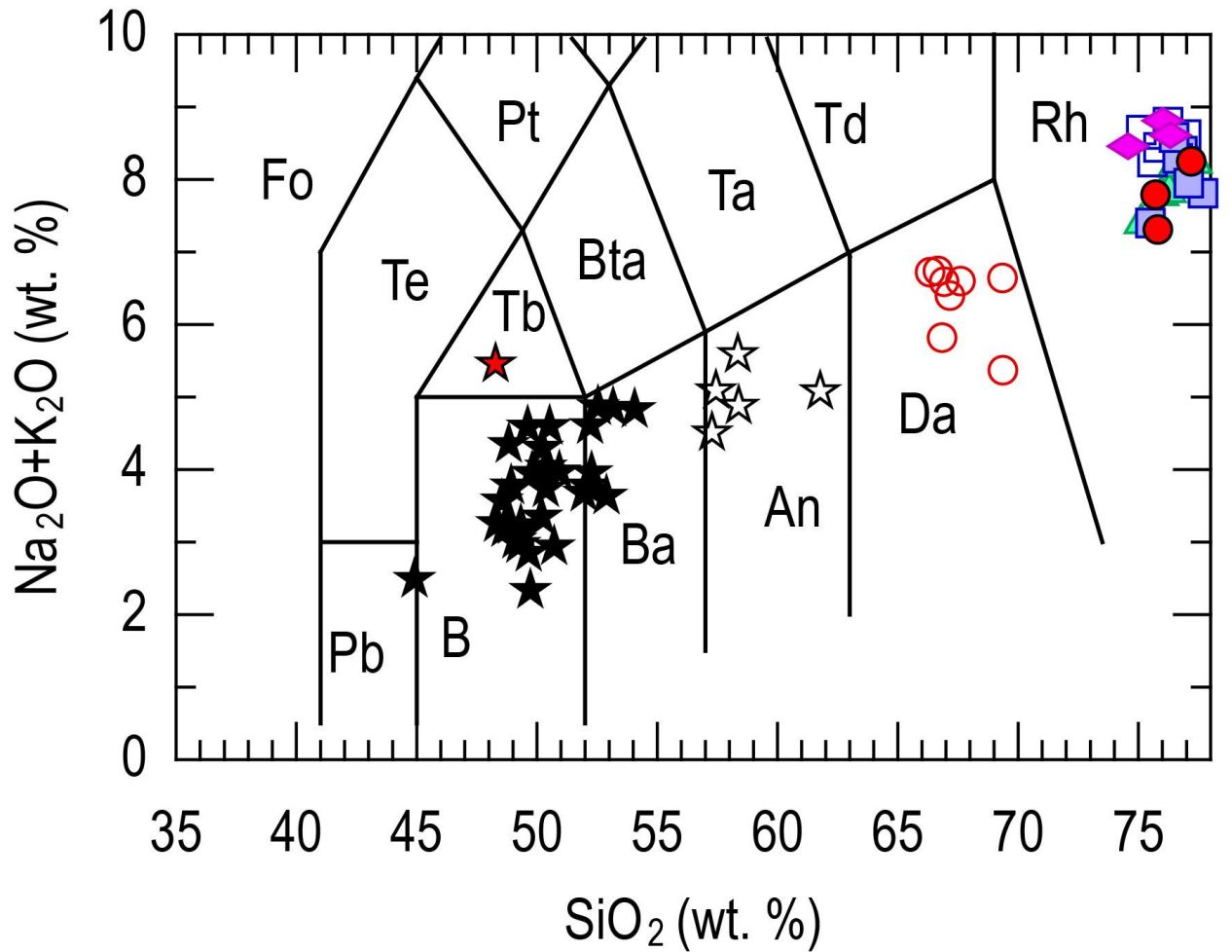
In addition to being subalkaline, the basalts and basaltic andesites in the Silver City district are tholeiitic (Figure 5.2) based on both AFM (Irvine and Baragar, 1971) and SiO₂ vs. FeO*/MgO (Miyashiro, 1974) diagrams. The more evolved andesites (type 1 and 2), however, are calc-alkaline.

All of the silicic samples (>65 wt. % SiO₂) plot as either peraluminous or metaluminous (Figure 5.3) based on Shand's alumina saturation index (ASI) (1943). The silicic samples constantly plot near an ASI of 1.0 and show a range of 0.85 - 1.25 for the unaltered silicic samples (SiO₂ < 78 wt. %) with increasing ASI as SiO₂ increases. The peraluminous nature of these samples may in part be caused by Na loss associated with the mid-Miocene hydrothermal system.

The dacite and rhyolite samples in the Silver City district plot in both the volcanic arc granite (VAG) and within plate granite (WPG) fields (Figure 5.4) according to classification of Pearce et al. (1984). The Silver City rhyolite plots as a small group within VAG field while the three latite groups and the tuff of Flint Creek all plot within the WPG field. The underlying granitoid basement also plots as VAG, consistent with the subduction-related formation of this portion of the Cretaceous Idaho Batholith (Gaschnig et al., 2011). Figure 5.4 also shows the granitoid classification scheme of Whalen et al. (1987) with the Silver City rhyolite plotting with the Silver City Batholith in the I-type field, while the Hayden Peak, Glass Mountain dacite and Glass Mountain rhyolite, and quartz latites all plot as A-type rhyolites. I-type granitoids typically occur in a VAG setting and indicate an igneous source rock such as lower crustal rocks in a subduction zone setting. A-type granitoids occur in WPG settings and are considered to occur anogenically. A-type granitoids are typically metaluminous in nature which is inconsistent with the peraluminous nature of the Silver City district latite. These conflicting classifications are further evidence of Na loss due to the active hydrothermal system.

The silicic samples can be further classified using the scheme of Frost and Frost (2011). These are mostly ferroan based on the calculation of Fe index (Fe*) using the molecular weight of oxides. Fe index ($Fe^* = FeO^*/FeO^*+MgO$) as seen in Figure 5.5. Figure 5.5 also shows the

modified alkali lime index plot and the calc-alkalic nature of the majority of the Silver City district silicics. Some of the less evolved Glass Mountain dacite samples are magnesium-rich and plots in the magnesian and calcic fields.



- ★ Steens Basalt
- ★ Olivine rich basalt
- ☆ Andesite
- Hayden Peak latite
- Quartz latite
- ▲ Silver City rhyolite
- Glass Mountain dacite
- Glass Mountain rhyolite
- ◆ Tuff units

Figure 5.1: Total Alkali diagram

Total Alkali diagram showing the compositional range of the Silver City district volcanics. Hydrothermally altered samples above 78 wt. % SiO₂ are not shown.

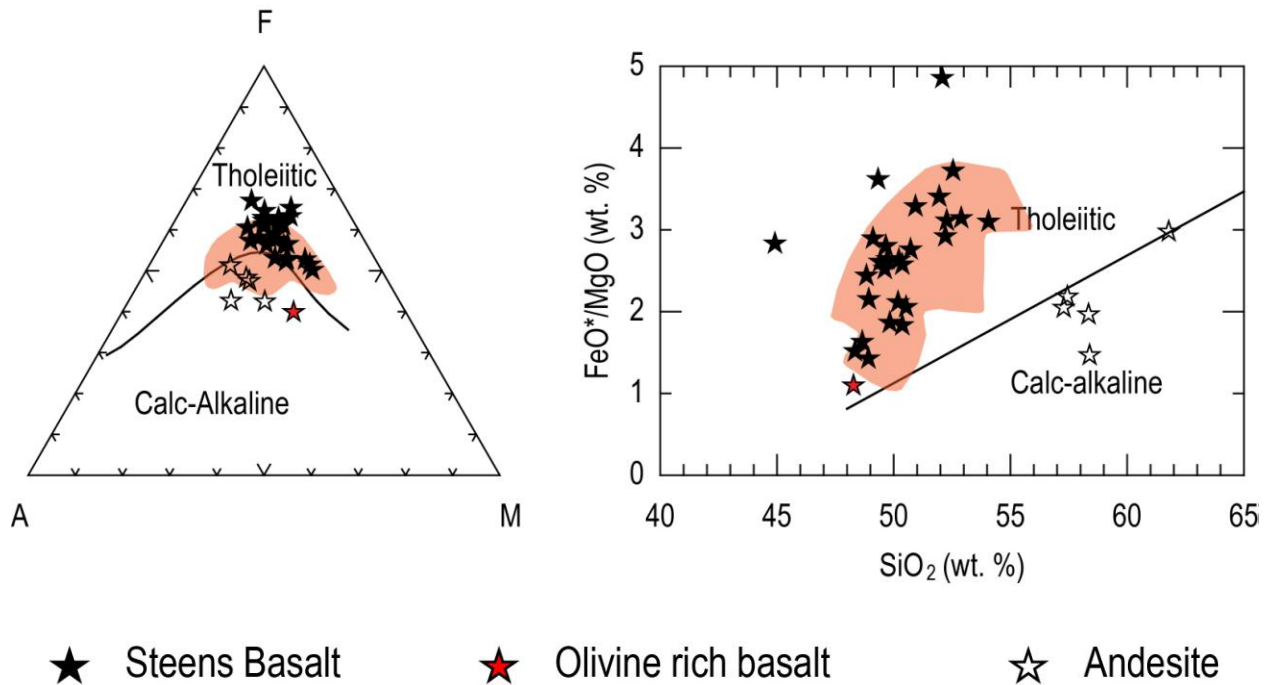
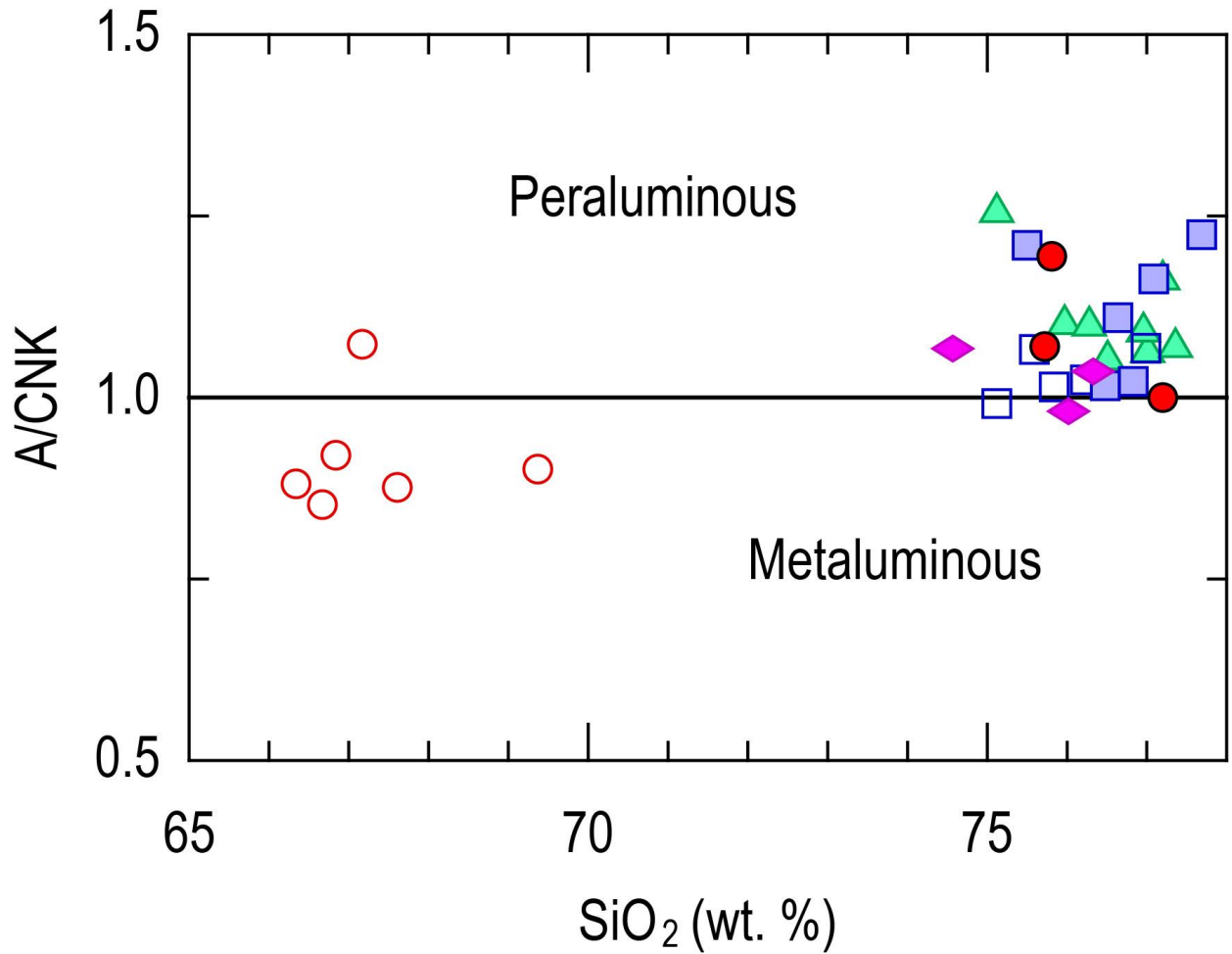


Figure 5.2: Mafic classification diagrams

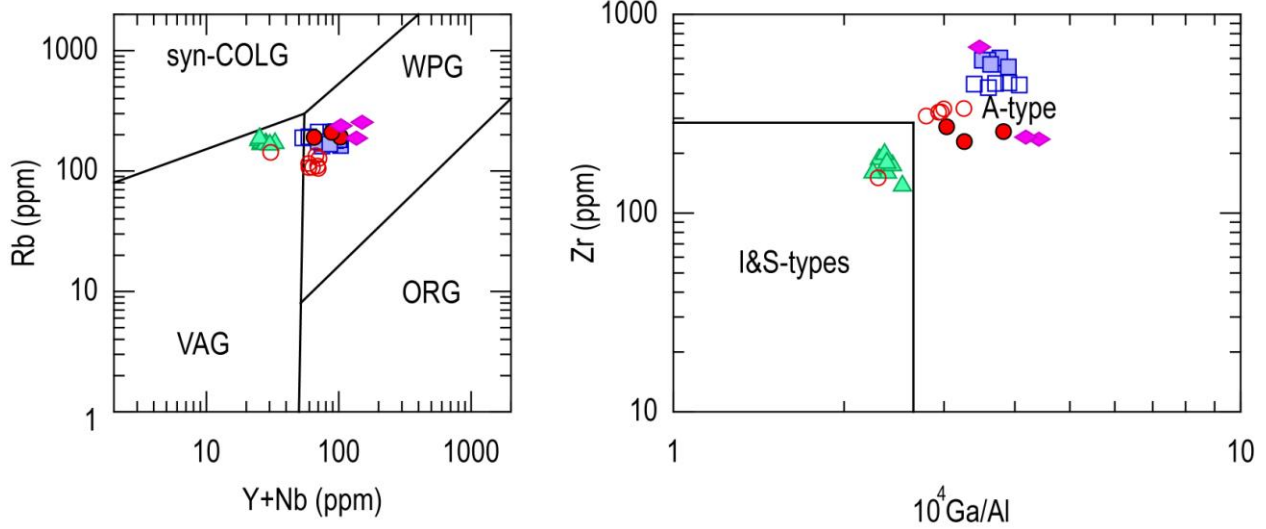
Tholeiitic classification of the Silver City district basalt, basaltic andesite and andesite of Irvine and Baragar, 1971 (left), and Miyashiro, 1974 (right). The regional Steens Basalt samples are represented by the orange field (Johnson et al., 1998).



- | | | |
|----------------------|------------------------|---------------------------|
| □ Hayden Peak latite | ▲ Silver City rhyolite | ○ Glass Mountain dacite |
| ■ Quartz latite | ◆ Tuff units | ● Glass Mountain rhyolite |

Figure 5.3: Alumina saturation diagram

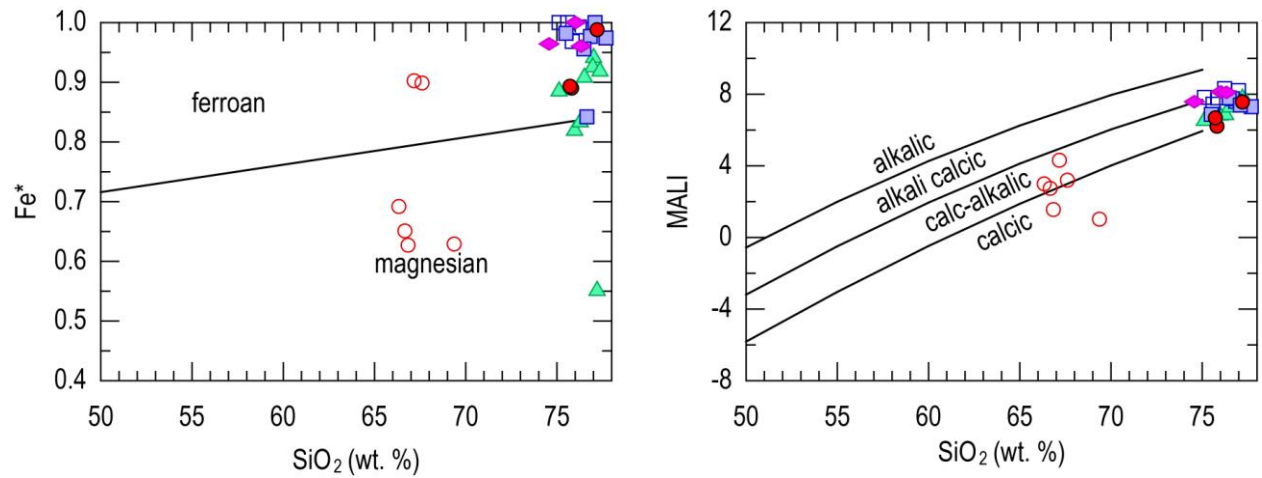
Plot of alumina saturation index showing the metaluminous and peraluminous nature of the Silver City district silicic units. The dacites plot mostly as metaluminous while the rhyolites fall into the peraluminous field.



- | | | |
|----------------------|------------------------|---------------------------|
| □ Hayden Peak latite | ▲ Silver City rhyolite | ○ Glass Mountain dacite |
| ■ Quartz latite | ◆ Tuff units | ● Glass Mountain rhyolite |

Figure 5.4: Granitoid classification diagrams

Pearce (1984) and Whalen et al. (1987) silicic classification of the Silver City district silicic samples. The Silver City rhyolite plots as volcanic-arc granites (VAG; I-type) while the latitic units plot as within-plate granites (WPG; A-Type). A single ash flow tuff of the Glass Mountain dacite plots as a volcanic arc granite.



- Hayden Peak latite ▲ Silver City rhyolite ○ Glass Mountain dacite
- Quartz latite ◆ Tuff units ● Glass Mountain rhyolite

Figure 5.5: Frost classification diagrams

Frost and Frost (2004) classification of the Silver City district silicic units. The rhyolite units plot as ferroan and calc-alkalic. Some of the dacitic samples are magnesian and calcic.

Granitoid Geochemistry

The silver city granite that underlies the mid-Miocene volcanic system has major element wt % oxide value ranges of 65.65 - 77.58% SiO₂; 0.01 - 0.66% TiO₂; 13.71 - 16.44% Al₂O₃; 0 - 0.08% FeO*; 0.02 - 1.88% MnO; 0.63 - 4.51% MgO; 2.07 - 3.94% CaO; 2.42 - 4.2% Na₂O; 0.02 - 0.19% K₂O; and 0.19 - 4.29% P₂O₅. The granitoid is ranges from dacite to rhyolite on a TAS diagram (LeBas et al., 1986) and plots as peraluminous according to the alumina saturation index (Shand, 1943). They plot primarily as magnesian and calcic on the Frost and Frost (2011) classification scheme.

The Silver City granite has trace element value ranges of 10.3 - 79.5 ppm Ba; 1.36 - 16.3 ppm Nb; 639.4 - 3048.17 ppm Nd; 55.2 - 115.37 ppm Rb; 120.2 - 565.5 ppm Sc; 32.2 - 184.8 ppm Sr; 2.24 - 13.1 ppm Zn; and 13.31 - 37.2 ppm Zr. Rare earth element range in values of 20.8 - 63.4 ppm Ce; 8.9 - 27.3 ppm Cs; 0 - 2.6 ppm Eu; 1.04 - 2.74 ppm Hf; 1.74 - 4.32 ppm La; 0.56 - 1.69 ppm Lu; 0.29 - 1.64 ppm Sm; and 0.05 - 0.24 ppm Yb. The Silver City granite plots as volcanic arc in origin (Pearce et al., 1984). They are predominately I –type with some Ga rich samples plotting as A-type (Whalen et al., 1987).

Regional Steens Basalt Geochemistry

The Steens Basalt data set of Johnson et al. (1998) was used as part of this thesis to compare the regional Steens Basalt to the local Steens Basalt eruptions found in the Silver City district. The regional Steens Basalt volcanism ranges occurs as basalt, trachybasalt, basaltic andesite and basaltic trachyandesite on LeBas et al. (1986) TAS diagrams. The samples are dominantly tholeiitic with some samples plotting as calc-alkaline. The regional Steens Basalt has major element wt % oxide value ranges of 44.81 - 56.7% SiO₂; 0.87 - 3.47% TiO₂; 13.44 - 20.95% Al₂O₃; 7.82433 - 13.992828% FeO*; 0.12 - 0.24% MnO; 2.36 - 8.94% MgO; 5.79 - 11.36% CaO; 2.33 - 4.67% Na₂O; 0.3 - 2.89% K₂O; and 0.12 - 1.29% P₂O₅. And have trace element value ranges of 77 – 1023 ppm Ba; 5.7 – 19 ppm Nb; 4 – 81 ppm Rb; 17.6 – 40 ppm Sc; 201 – 730 ppm Sr; 73 – 182 ppm Zn; and 89 – 368 ppm Zr.

Volcanic Major Element Geochemistry

Basalt and intermediate

The basalt and intermediate flow samples are mafic in composition and fall below 65 wt. % SiO₂. The Steens Basalt have a SiO₂ wt. % range of 44.9 - 54.1% while the andesite type 1 and type 2 have a wt % SiO₂ range of 57.3 - 61.8%. Figure 5.6 shows Harker diagrams of the mafic samples that show consistent arrays throughout the range of samples. FeO*, TiO₂, MnO and P₂O₅ increase with increasing SiO₂ until 52 wt. % SiO₂, and have decreasing concentrations after 52 wt % SiO₂. MgO and CaO wt% decrease with increasing SiO₂, while K₂O wt% increases with increasing SiO₂. Both Al₂O₃ and Na₂O maintain fairly consistent values with no apparent increase or decrease.

Dacite and rhyolite

The silicic (SiO₂ wt. % > 65) units have SiO₂ wt. % ranges of 75.1 – 77.0% (Hayden Peak latite); 75.5 – 77.7% (quartz latite); 66.3 - 69.4% (Glass Mountain dacite); 75.7 - 77.2% (Glass Mountain rhyolite); 75.1 - 77.4% (Silver City rhyolite); 76.0 – 76.3% (tuff of Flint Creek); and 74.6% (Cold Springs tuff sample). Figure 5.7 shows Harker diagrams for the silicic samples above 65 wt. % SiO₂. The silicic samples continuously plot in an overlapping group while the element behavior noted in the mafic samples can be seen in the silicic samples. TiO₂, FeO*, MnO, MgO, CaO, and P₂O₅ all show a continuing inverse relationship with decreasing wt. % as SiO₂ wt. % increases. K₂O shows increasing wt. % with increases in SiO₂. Na₂O shows no apparent array and maintains a constant range between 1.85 - 3.74 wt. % and Al₂O₃ maintains consistent values between 11.8 and 14.0 wt. %. Harker diagrams showing the complete range of all samples can be seen in Figure 5.8.

Figure 5.6: Mafic and Intermediate Harker diagrams

Next page - Harker diagrams of major element oxide concentrations (wt. %) for the mafic and intermediate (<65 wt. % SiO₂) samples.

★ Steens Basalt

★ Olivine rich basalt

☆ Andesite

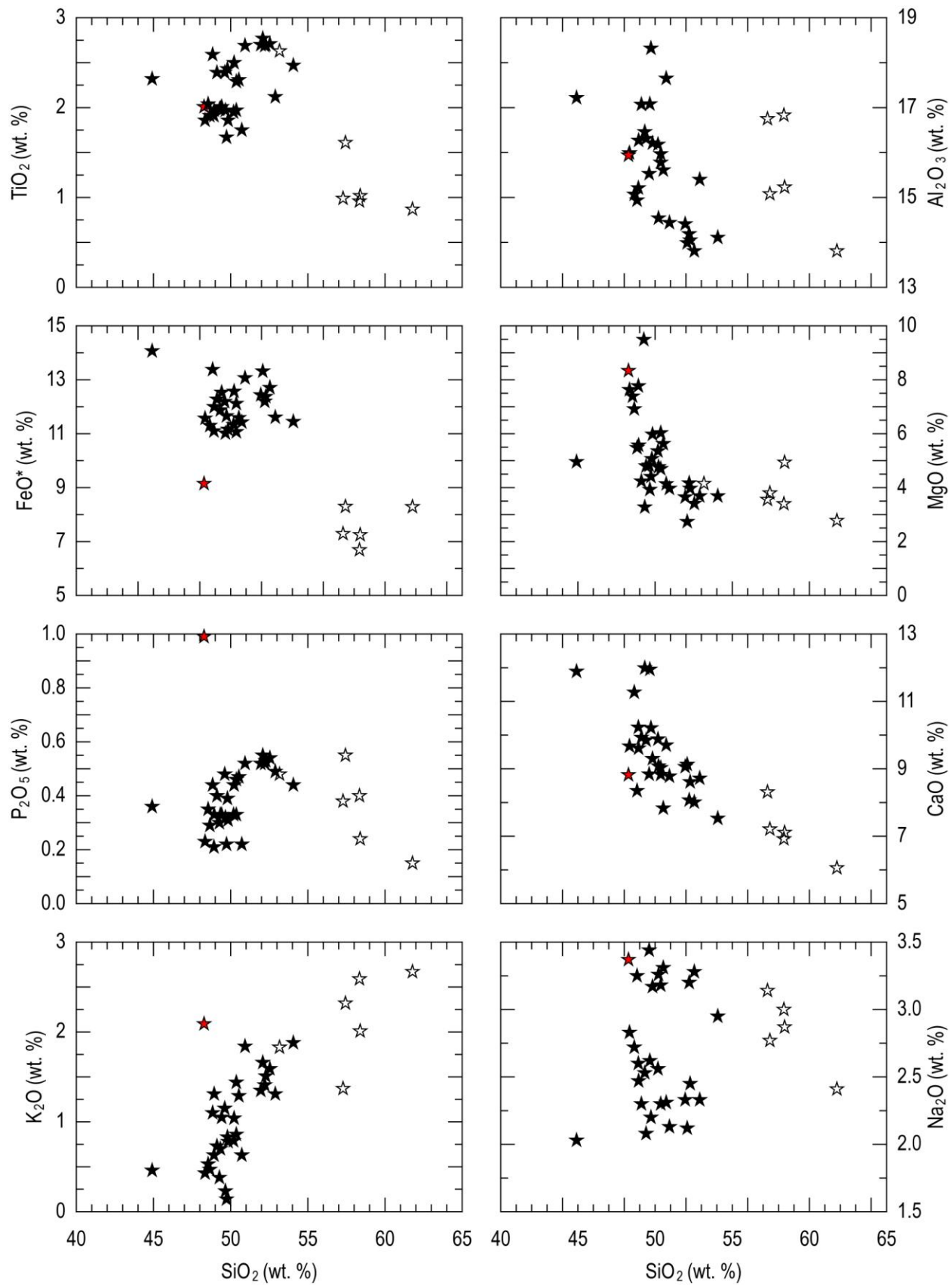


Figure 5.7: Silicic Harker diagrams

Next page - Harker diagrams of major element oxide concentrations (wt. %) for the silicic (>65 wt. % SiO₂) samples.

- | | | |
|--|--|---|
|  Hayden Peak latite |  Silver City rhyolite |  Glass Mountain dacite |
|  Quartz latite |  Tuff units |  Glass Mountain rhyolite |

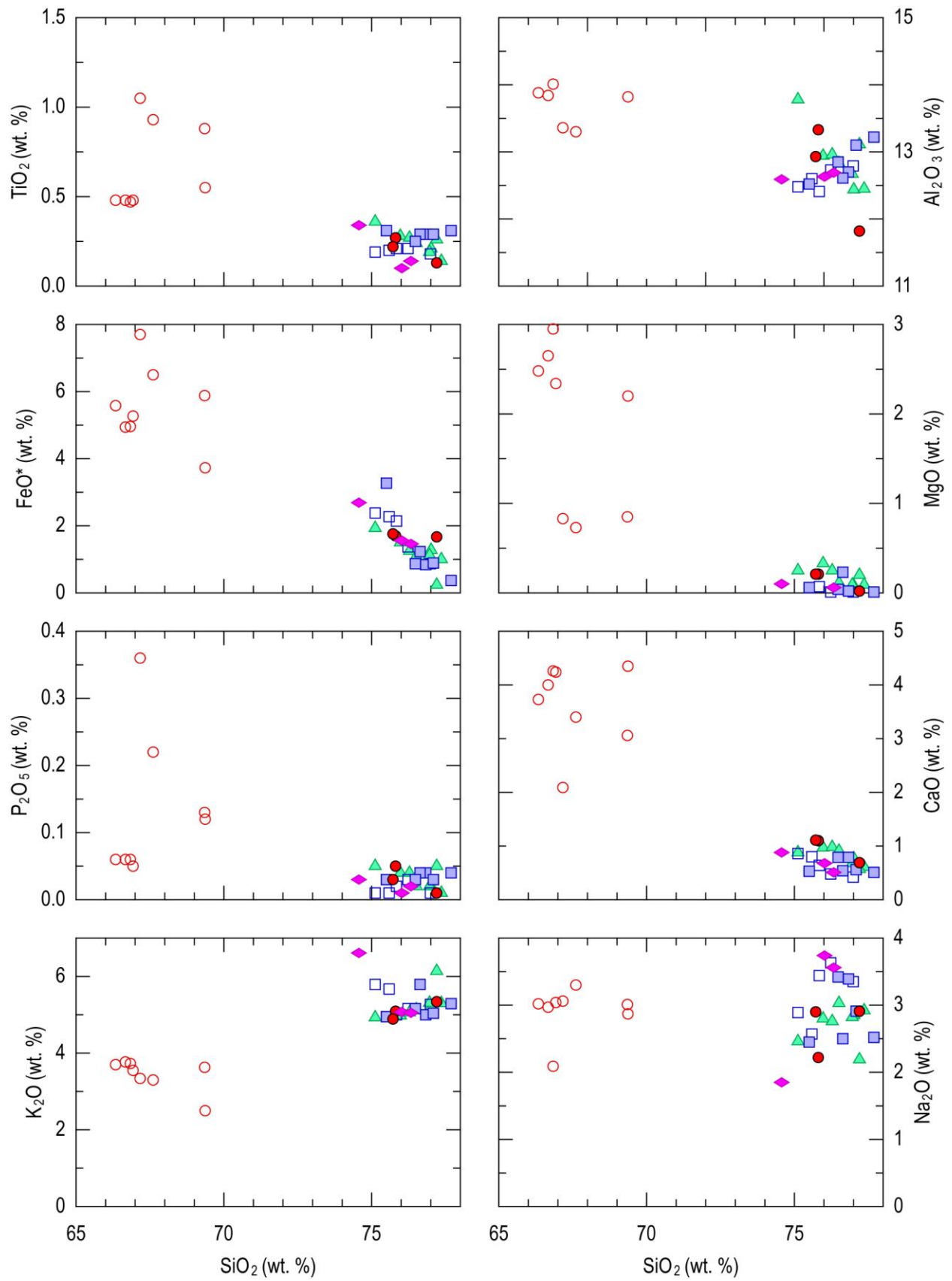
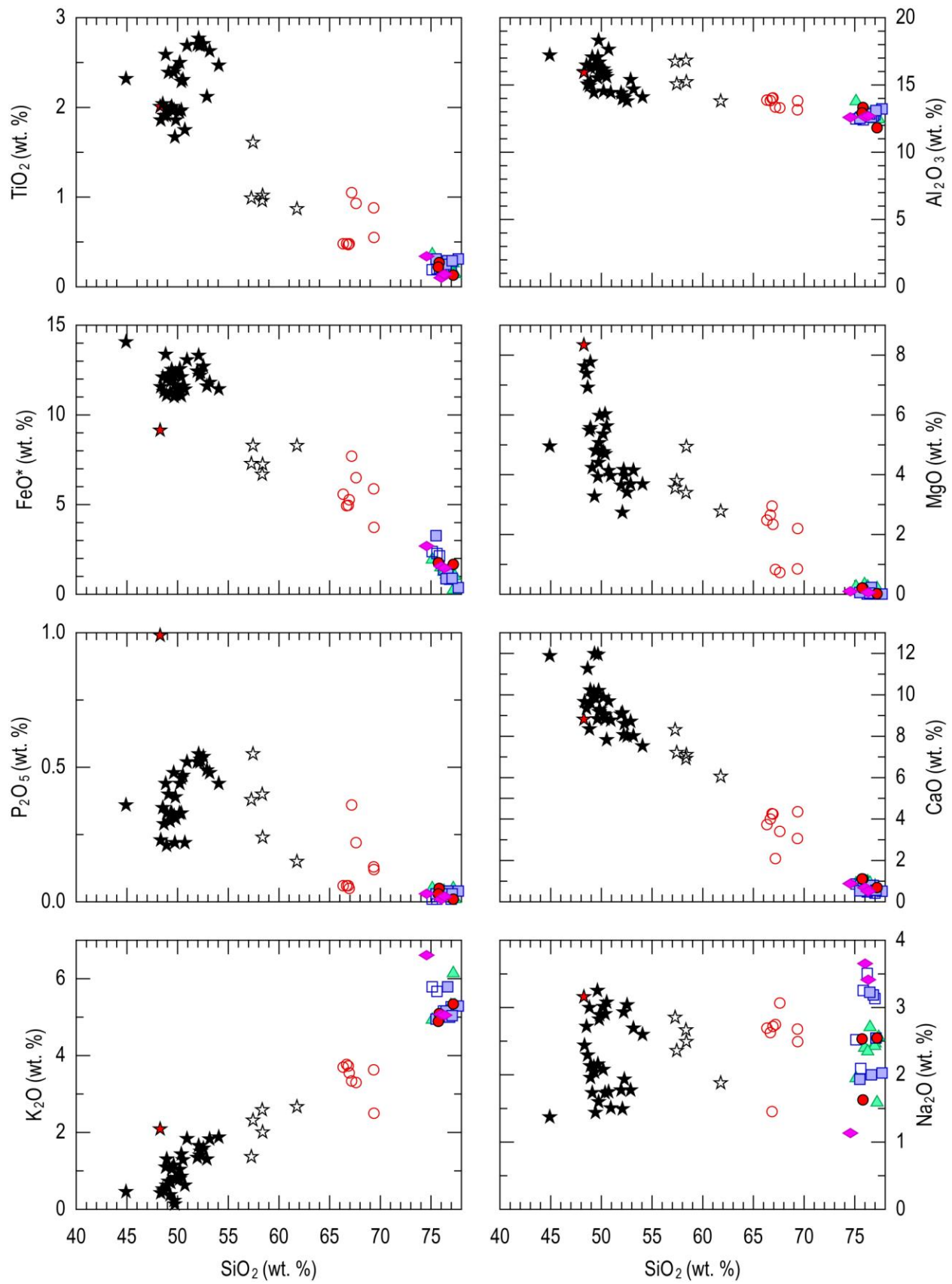


Figure 5.8: Complete Harker diagrams

Next page - Harker diagrams of major element oxide concentrations (wt. %) for all Silver City district volcanic samples.

- | | | |
|-----------------------|------------------------|---------------------------|
| ★ Steens Basalt | □ Hayden Peak latite | ○ Glass Mountain dacite |
| ★ Olivine rich basalt | □ Quartz latite | ● Glass Mountain rhyolite |
| ☆ Andesite | ▲ Silver City rhyolite | ◆ Tuff units |



Trace Element Geochemistry

Basalt and intermediate

Select trace element diagrams of the mafic volcanic samples are shown in Figure 5.9. Compatible trace elements, such as Sc, Cr, and Ni show decreasing concentrations with increasing SiO₂. Elements such as, Ba, Rb, Nb, Nd, Y, Zn, and Zr (incompatible in typical mafic magmas) all show increasing concentrations as SiO₂ increases. Sr and V do not show increasing or decreasing arrays and maintain consistent value ranges. A sample of olivine-rich basalt (ZH11-4) has elevated concentrations of Sr, Ba, and Nd.

The basalts, basaltic andesite and andesite samples in the Silver City district are normalized to MORB and plotted on a spider diagram after Pearce (1983) in Figure 5.10. The samples plot with highly enriched levels of large ion lithophile elements (LILE) and slightly enriched to depleted levels of high field strength elements (HFSE) and positive Ce anomalies. The samples demonstrate a consistent normalized trend with the exception of two samples that are depleted in K and Rb, which is likely due to hydrothermal alteration of the samples. The normalized plots overlap with the plots of Steens Basalt samples (Johnson et al., 1998) as seen in Figure 5.10 (orange field). The multi-element diagrams are consistent with the Steens Basalt designation for the Silver City district basalt and basaltic andesites.

Dacite and rhyolite

Figure 5.11 shows selected trace element concentrations of the silicic samples plotted against SiO₂. When plotted against SiO₂, samples from the separate volcanic units overlap in plots of Ni, Rb, and Sr. Plots of Cr and V show the Silver City rhyolite with slightly higher concentrations. Plots of Nd, Nb, Y, Zr, Zn show the Silver City rhyolite has lower concentrations and the Hayden Peak and quartz latite units have higher concentrations while the Glass Mountain rhyolite samples plot with intermediate values in between and often overlapping with the Silver City rhyolite and Hayden Peak and quartz latites. The Hayden Peak latites have higher Ba and Sc concentrations while the quartz latite, Glass Mountain rhyolite, and Silver City rhyolite samples overlap at lower concentrations.

The Glass Mountain dacite samples have a wider range of concentrations than the Glass Mountain rhyolite samples. Ni, Cr, V, and Sr plots show a range from higher concentrations to concentrations that overlap with the Glass Mountain rhyolite and other latite samples. Sc concentrations are higher than the other silicic volcanics while Y has overlapping concentrations with the other silicic volcanics. Zr, Nb, and Nd concentrations overlap with the Glass Mountain rhyolite and Silver City rhyolite samples. Nd plots also show concentrations overlapping with the quartz latite samples as well. The Zn concentrations are higher and overlap with the Hayden Peak and quartz latite samples.

The tuff of Flint Creek and the Cold Springs tuff samples overlap with the other Silver City district rhyolite samples in Cr and Ni concentrations have higher Nb concentrations and lower Sr concentrations. Nd concentrations also overlap with the Hayden Peak and quartz latites. The Cold Springs tuff has higher concentrations in Zr and Y, overlaps with all samples in Rb, with the quartz latite in Sc, with the Silver City rhyolite in V, with the Hayden Peak latite in Zn and with the Silver City rhyolite and Hayden Peak latite in Ba. The tuff of Flint Creek has lower Ba and higher Rb concentrations. The tuff of Flint Creek has concentrations of V and Y that overlap with the Hayden Peak and quartz latites, Zn concentrations that overlap with quartz latite, Sc concentrations that overlap with the Hayden Peak latite and Silver City rhyolite, and Zr concentrations that overlap with the Silver City rhyolite and Glass Mountain rhyolite. Complete trace element diagrams plotted against SiO₂ are shown in Figure 5.12.

While major elements often show overlap between the silicic samples, trace element plotted against Zr show very distinct chemical relationships that are used to classify the samples into individual silicic units (Figure 5.13). As seen in a plot of Zr vs. SiO₂ (Figure 5.11) the silicic samples do not overlap in Zr concentrations and therefore would be ideal for classifying the volcanic units. The silicic samples range from 137.0 to 684.5 ppm. The Silver City rhyolite samples and one Glass Mountain dacite sample fall below 200 ppm, the Glass Mountain rhyolite and tuff of Flint Creek plot between 200 and 300 ppm, the Glass Mountain dacite plots between 300 and 400 ppm, the Hayden Peak latite plots between 400 and 500 ppm, the quartz latite plots above 500 ppm and the Cold Springs tuff has 684.5 ppm Zr. In general, plots of Zn, Sc, Ba, Y, Nb, and Nd show increasing arrays with increasing Zr concentrations throughout the range of samples. While Ni, Cr, V, Rb, and Sr show fairly flat arrays with consistent concentrations from

low to high Zr. The Glass Mountain dacite samples do not always plot in the arrays with the rest of the samples and have higher Ni, Cr, V, and Sc concentrations and lower Rb concentrations.

When normalized to upper continental crust of Taylor and McLennan (1985), the various silicic samples largely follow the same pattern with slightly enriched to slightly depleted and overlapping patterns for the LILE (Figure 5.14). The Silver City rhyolite and Glass Mountain dacite are more depleted in Ta and Nb. Small differences can be seen with the HFSE as the Silver City rhyolite is slightly depleted while the latitic units are slightly enriched relative to upper continental crust. While most of the samples show a pronounced negative Sr and Ti anomalies, the Glass Mountain dacite samples only show a slight negative anomaly but they do show a depletion of Ba that is not seen in the other units. The tuff of Flint Creek and Cold Springs tuff samples have the largest negative Sr and Ba anomalies.

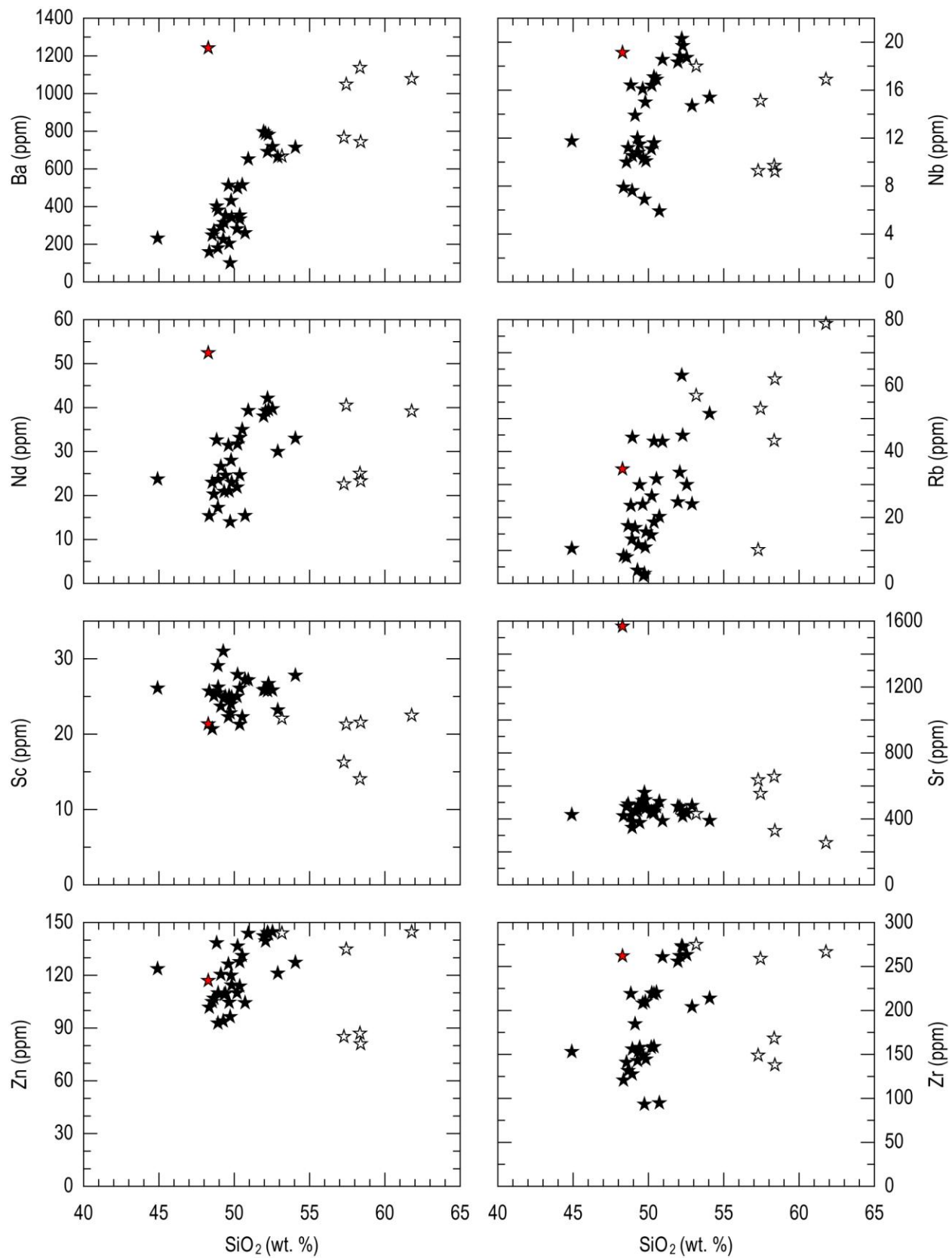
Figure 5.9: Mafic trace element diagrams

Next page - Select trace element concentrations (ppm) plotted against SiO₂ (wt. %) for mafic samples.

★ Steens Basalt

★ Olivine rich basalt

☆ Andesite



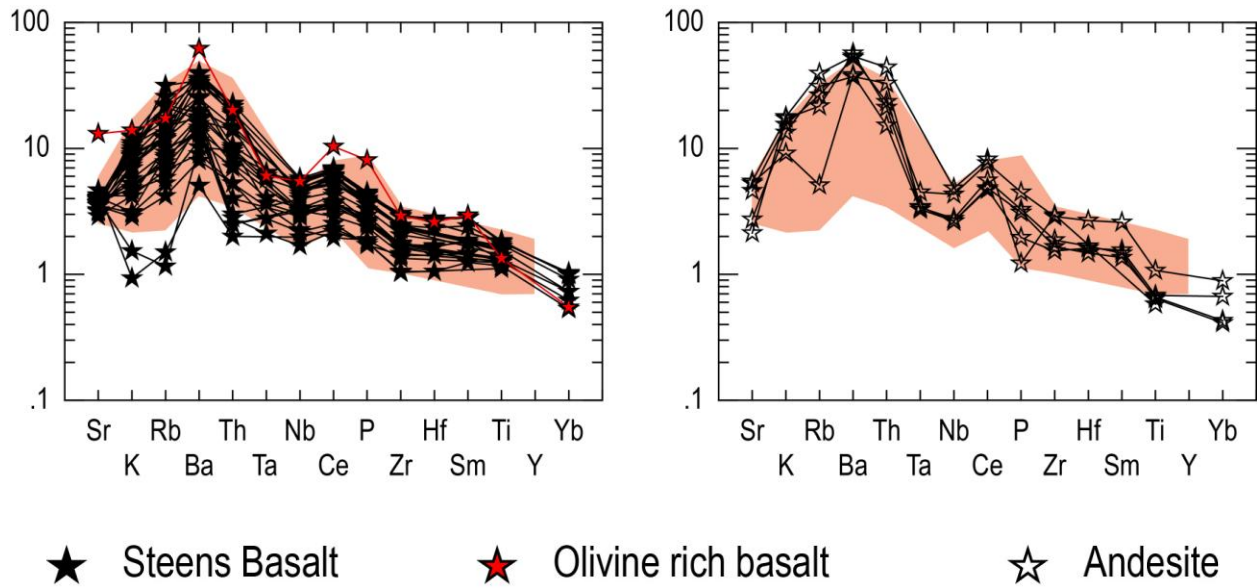


Figure 5.10: MORB normalized spider diagram of Silver City district mafic samples.

The basalt and basaltic andesite (left) and andesite (right) samples follow a consistent pattern with high enrichment of LILE and slight enrichment to slight depletion of HFSE. The Steens Basalt is represented by the orange field (Johnson et al., 1998).

Figure 5.11: Silicic trace element diagrams

Next page - Select trace element concentrations (ppm) plotted against SiO₂ (wt. %) for silicic samples.

- | | | |
|---|---|--|
| <input type="checkbox"/> Hayden Peak latite | <input type="checkbox"/> Silver City rhyolite | <input type="checkbox"/> Glass Mountain dacite |
| <input type="checkbox"/> Quartz latite | <input type="checkbox"/> Tuff units | <input type="checkbox"/> Glass Mountain rhyolite |

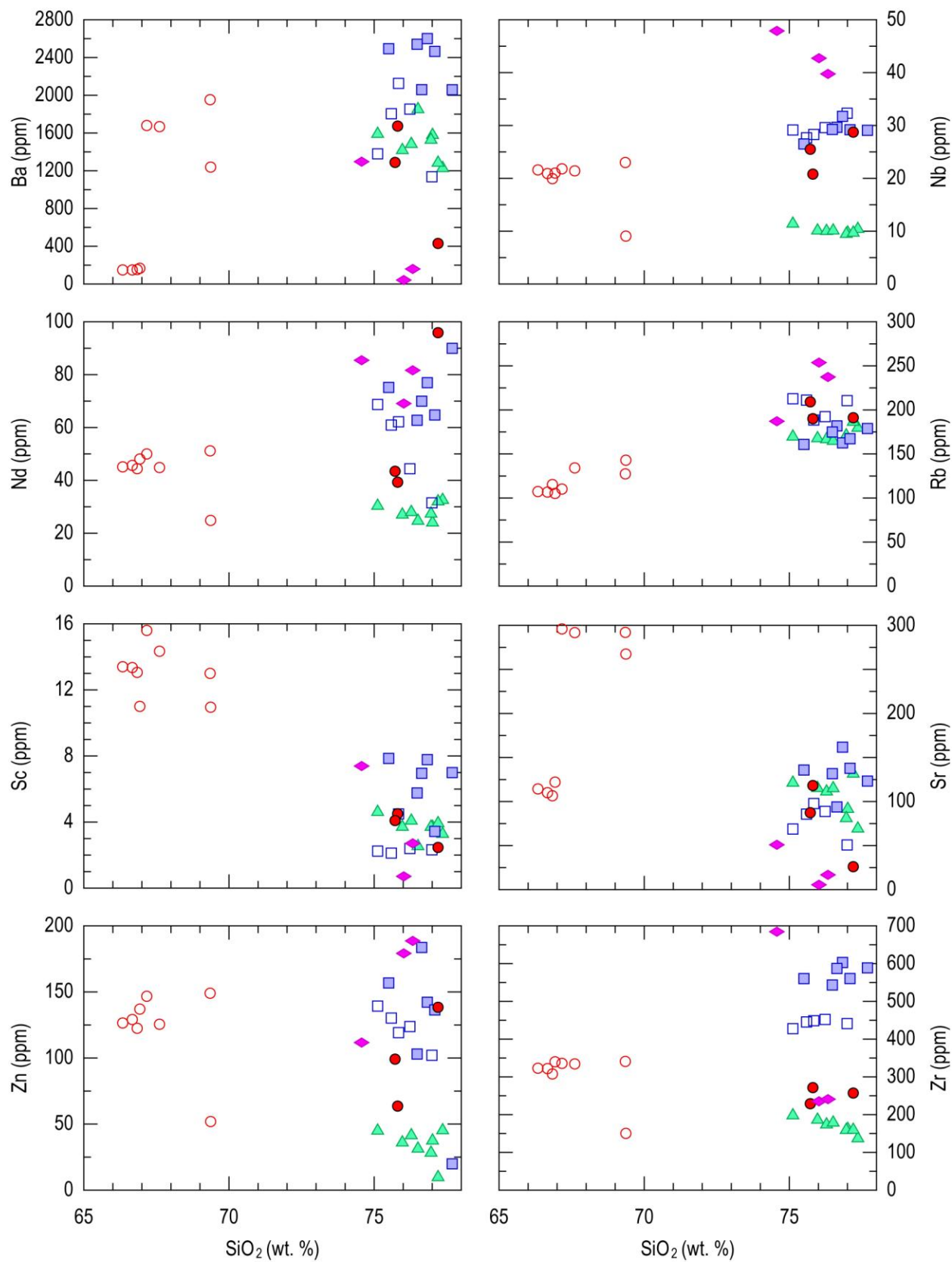


Figure 5.12: Trace element diagrams

Next page - Harker diagrams illustrating trace element (ppm) concentrations plotted against SiO₂ (wt. %).

- | | | |
|-----------------------|------------------------|---------------------------|
| ★ Steens Basalt | □ Hayden Peak latite | ○ Glass Mountain dacite |
| ★ Olivine rich basalt | □ Quartz latite | ● Glass Mountain rhyolite |
| ☆ Andesite | ▲ Silver City rhyolite | ◆ Tuff units |

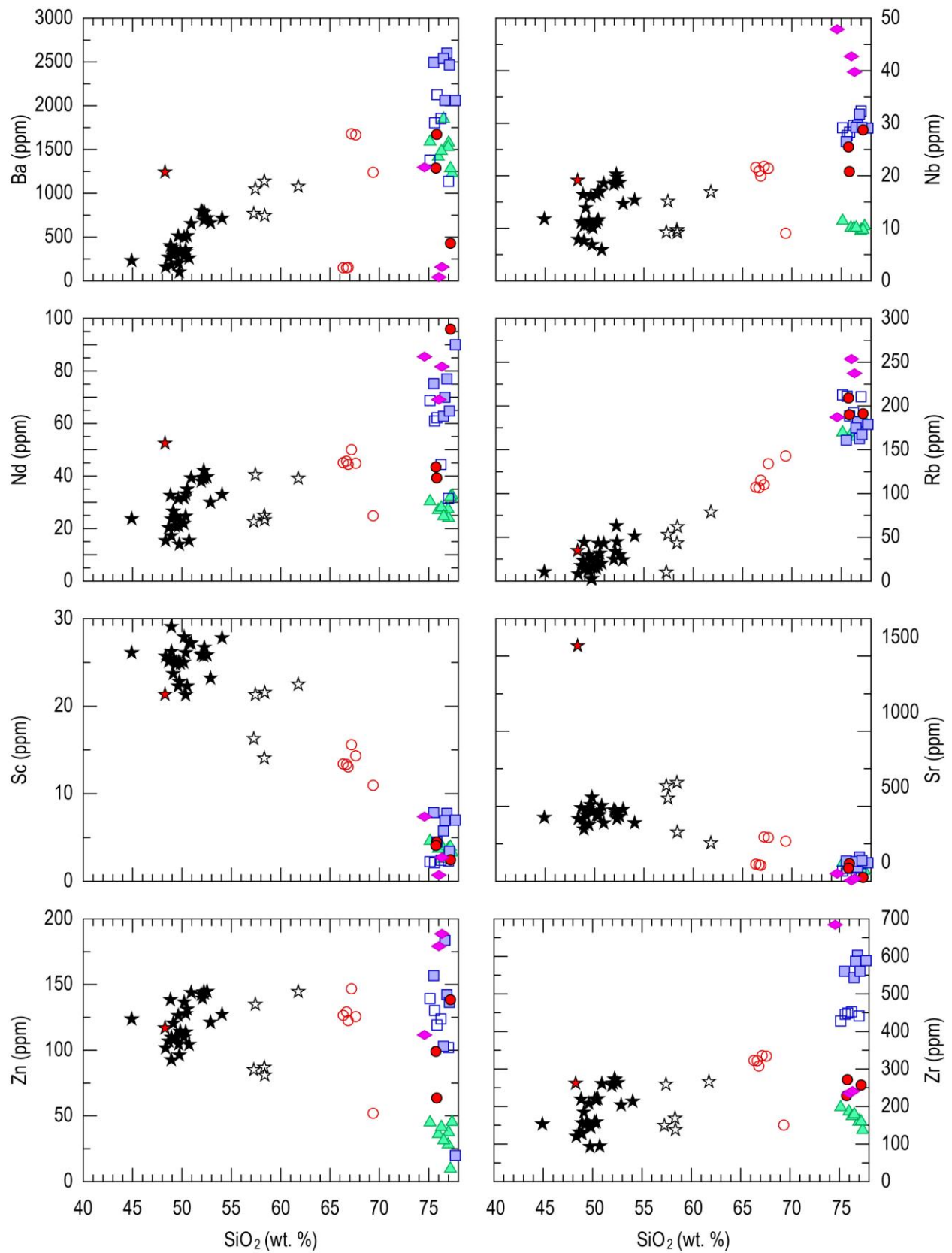
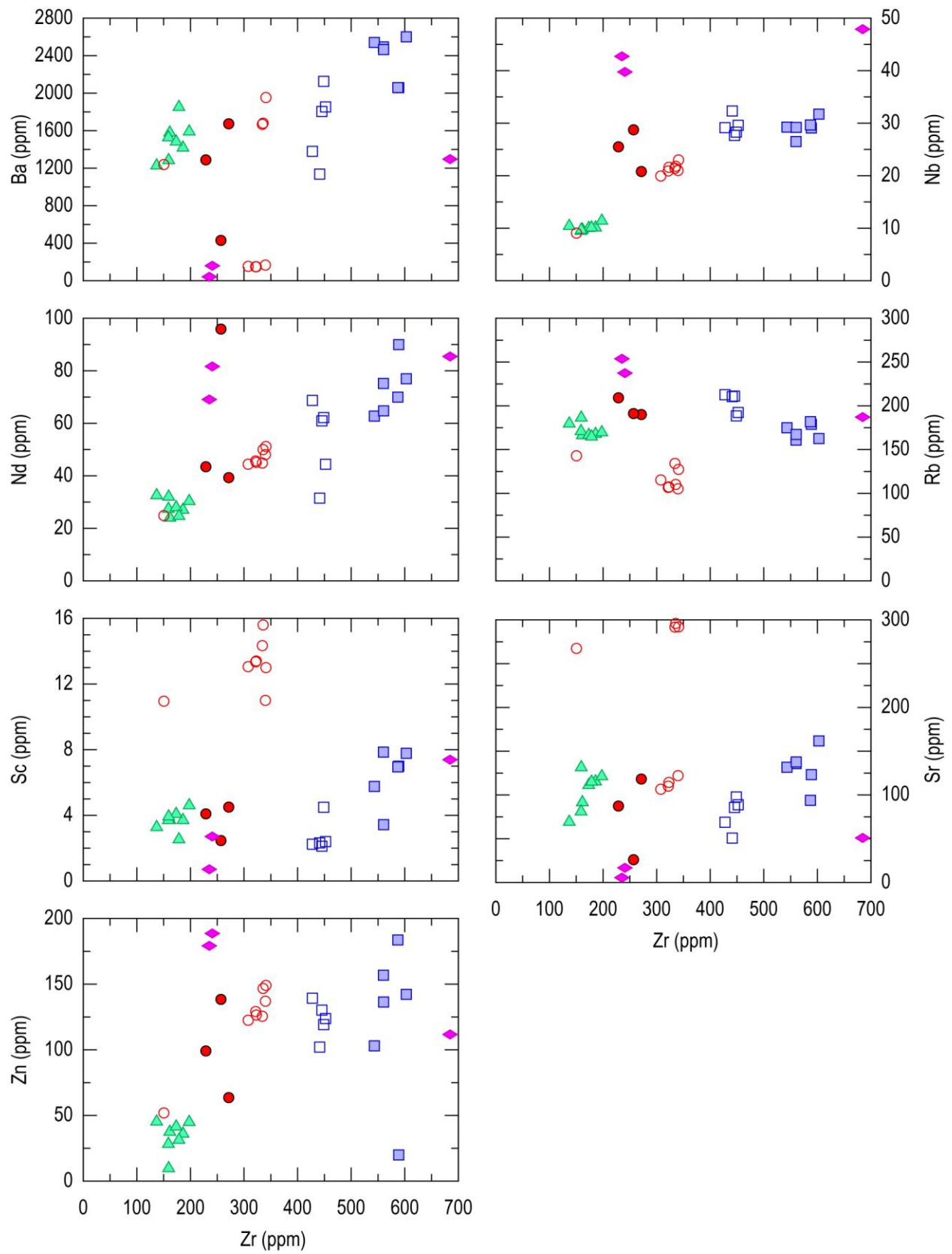


Figure 5.13: Zr trace element diagrams

Next page - Select trace element concentrations (ppm) plotted against Zr concentrations (ppm).

- | | | |
|---|---|--|
| <input type="checkbox"/> Hayden Peak latite | <input type="checkbox"/> Silver City rhyolite | <input type="checkbox"/> Glass Mountain dacite |
| <input type="checkbox"/> Quartz latite | <input type="checkbox"/> Tuff units | <input type="checkbox"/> Glass Mountain rhyolite |



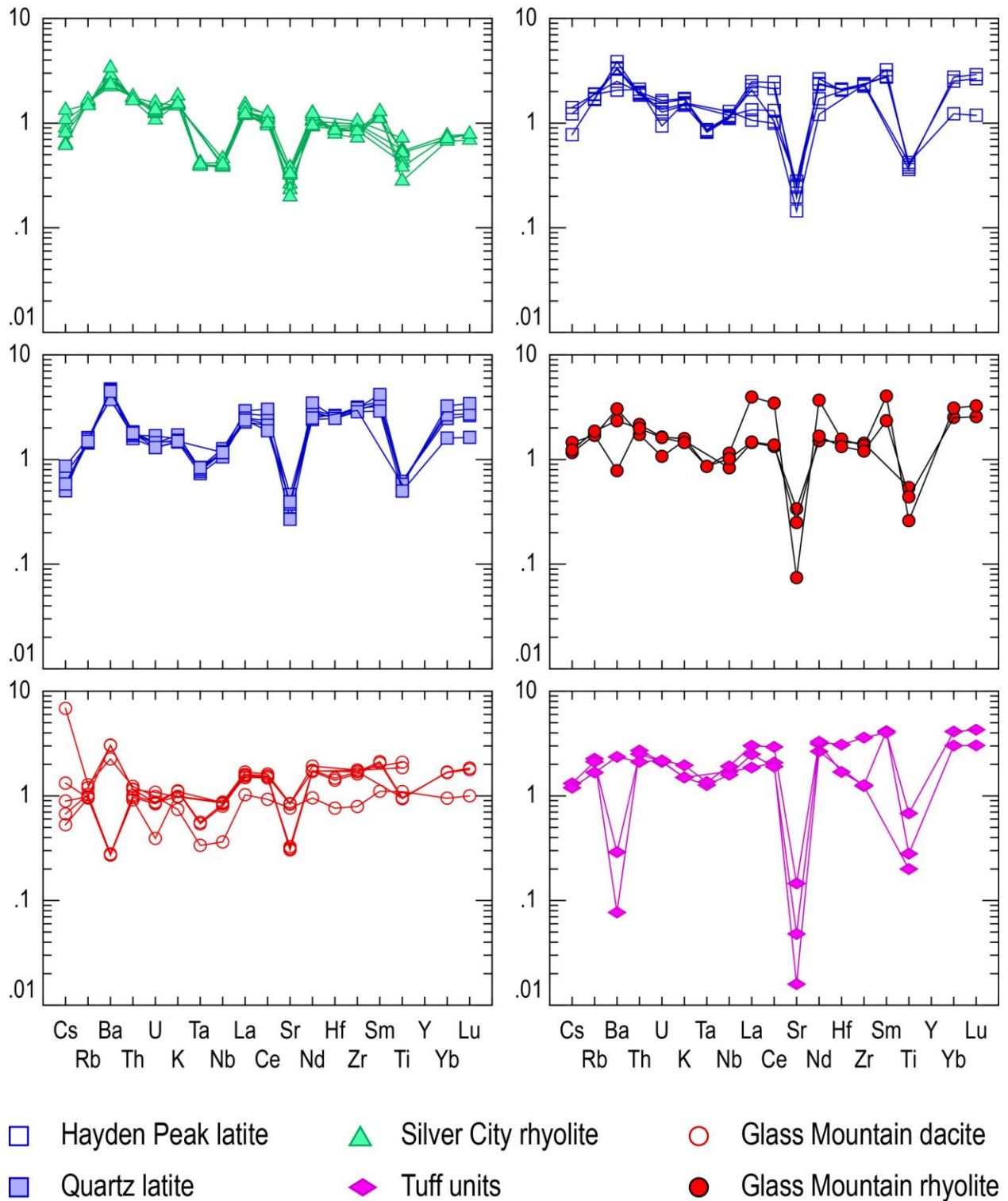


Figure 5.14: Upper continental crust normalized trace element diagrams
Silicic units normalized to upper continental crust after Taylor and McLennan (1985).

Rare Earth Element Geochemistry

Basalt and andesite

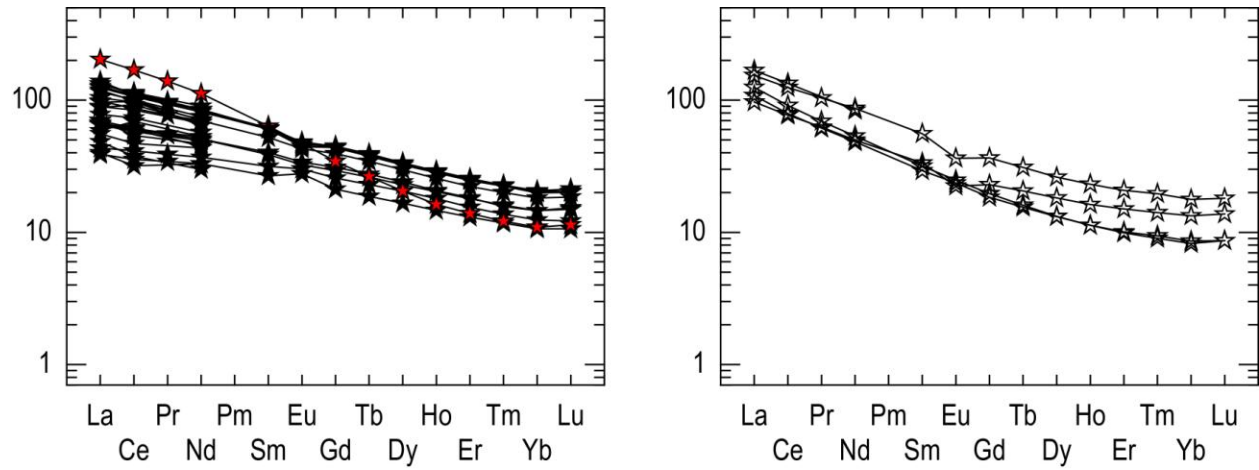
Rare earth element (REE) compositions of the mafic Silver City district samples show values that increase with increasing SiO₂ wt. % through the basalt and basaltic andesite samples and then decrease through the andesite samples. However, La and Ce show continuing increases with increasing SiO₂ wt. %. Figure 5.15 shows the Steens Basalt and andesites plotted on chondrite (Sun and McDonough, 1989) normalized spider diagrams. The samples follow a pattern of high enrichment in the light REE and less enriched in the heavy REE. The olivine rich basalt sample has a steeper decline in enrichment having the highest light REE and some of the lowest heavy REE.

Dacite and rhyolite

Rare earth element data show similar characteristics as the trace elements with the Silver City rhyolite generally having lower REE concentrations and the Hayden Peak and quartz latite, the tuff of Flint Creek and the Cold Springs tuff samples having higher concentrations, while the Glass Mountain dacite and rhyolite samples maintain intermediate REE concentrations. When plotted against Zr (Figure 5.16) similar to the trace element plots, the samples consistently show increasing REE concentrations with increasing Zr concentrations. Much like trace element data, the Zr plots of REE are useful to show the unit classifications defined in this study.

Multi-element diagrams of the REE (Figure 5.17) show consistent patterns through all of the samples. When normalized to upper continental crust of Taylor and McLennan (1985), most of the silicic samples show slight enrichment of both light and heavy rare earth elements. The Silver City rhyolite samples are only slightly enriched in the light REE and depleted in the heavy REE. All samples are highly enriched in light REE and only slightly enriched in heavy REE when normalized to chondrites (Figure 5.18) after Sun and McDonough (1989). All samples show a negative Eu anomaly in both normalized spider diagrams. The Silver City rhyolite consistently plots between very slightly depleted to very slightly enriched while the Hayden Peak

and quartz latite units are more enriched in all REEs. The Glass Mountain dacite and rhyolite plot as transitional between the other units.



★ Steens Basalt ★ Olivine rich basalt ☆ Andesite

Figure 5.15: Chondrite normalized rare earth element diagrams

Rare earth element spider diagrams normalized to chondrites (Sun and McDonough, 1989) for the mafic (<65 wt. % SiO₂) samples.

Figure 5.16: REE vs. Zr Harker diagrams

Next page - Select rare earth element concentrations (ppm) plotted against Zr concentrations (ppm).

□ Hayden Peak latite

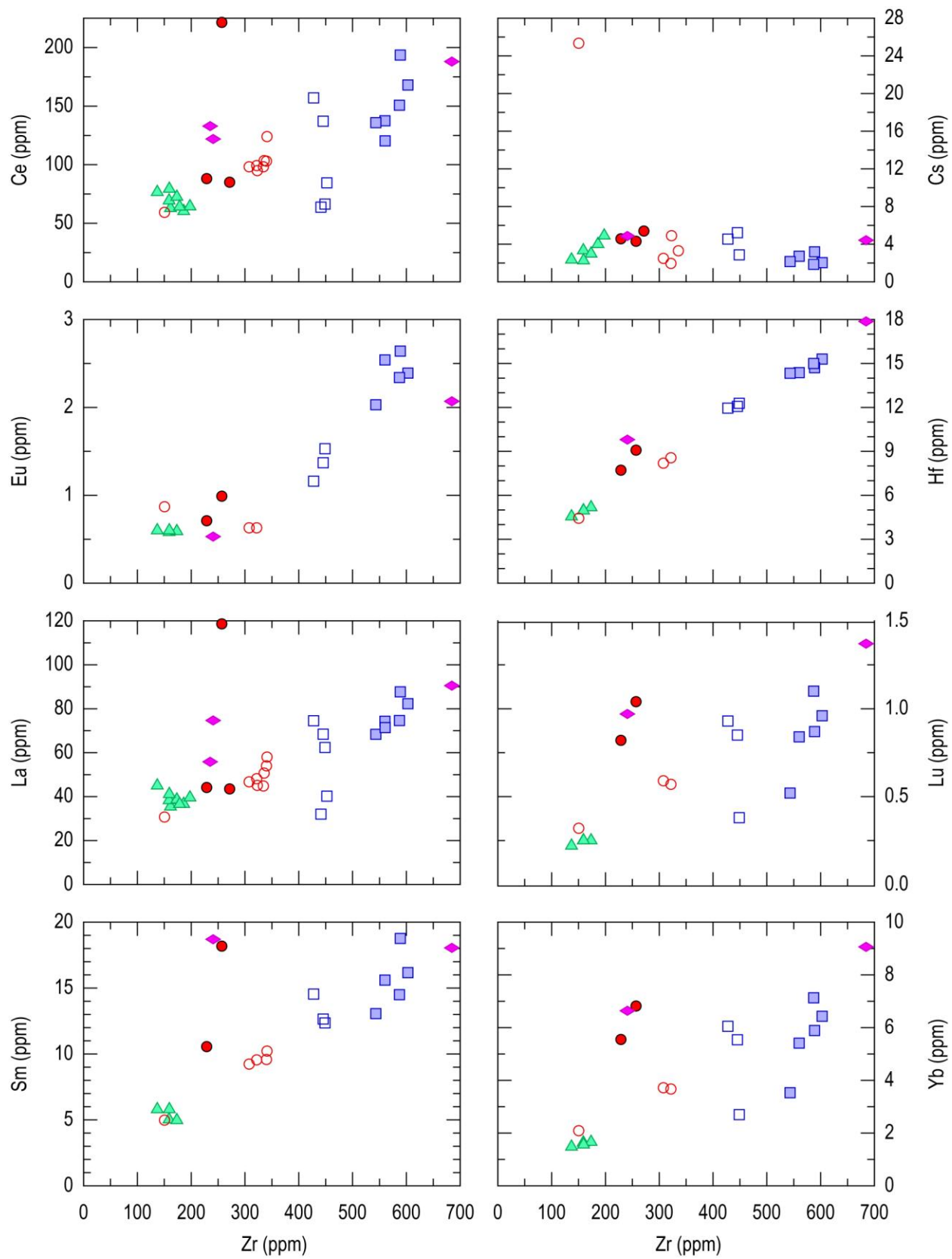
▲ Silver City rhyolite

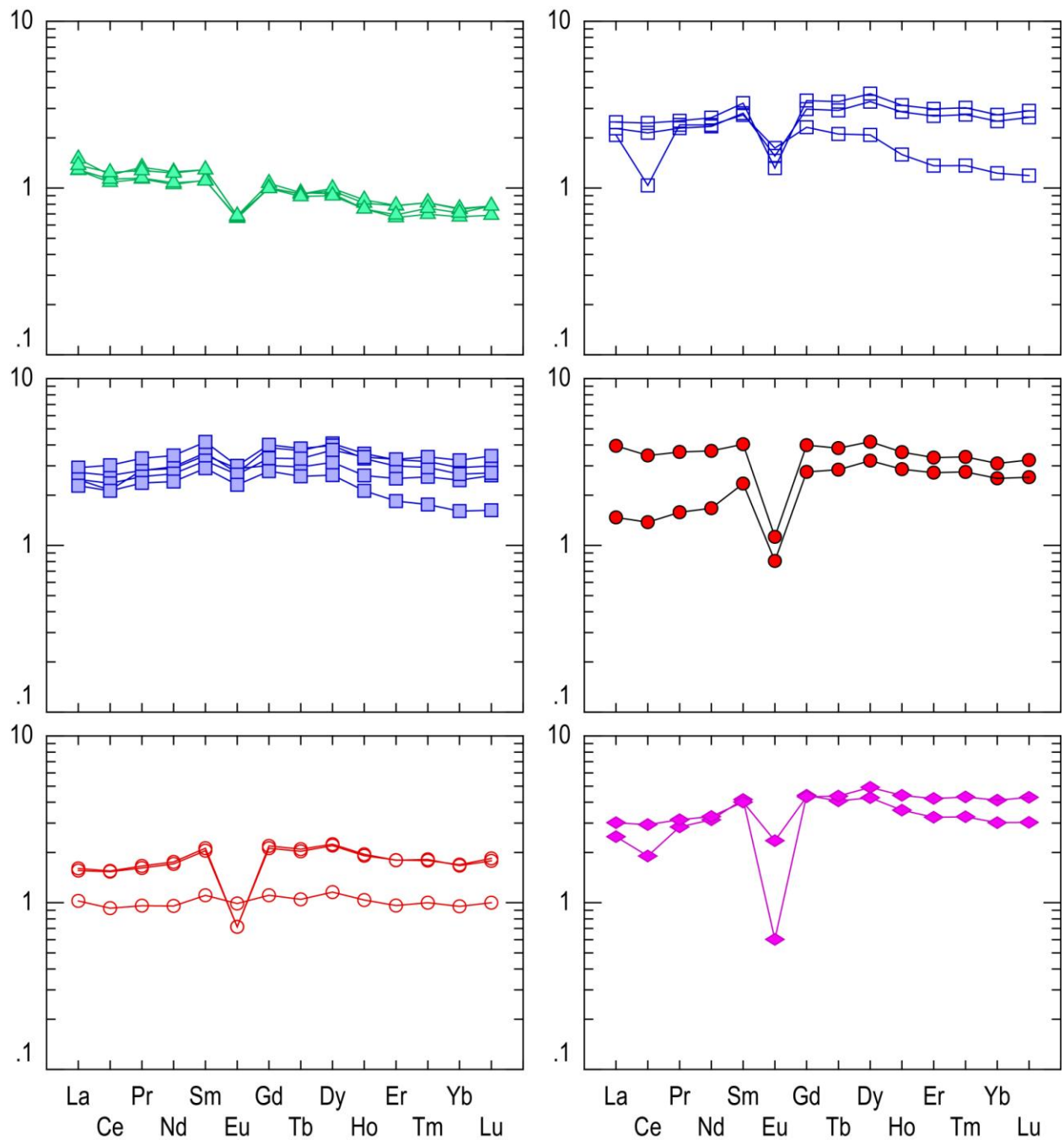
○ Glass Mountain dacite

■ Quartz latite

◆ Tuff units

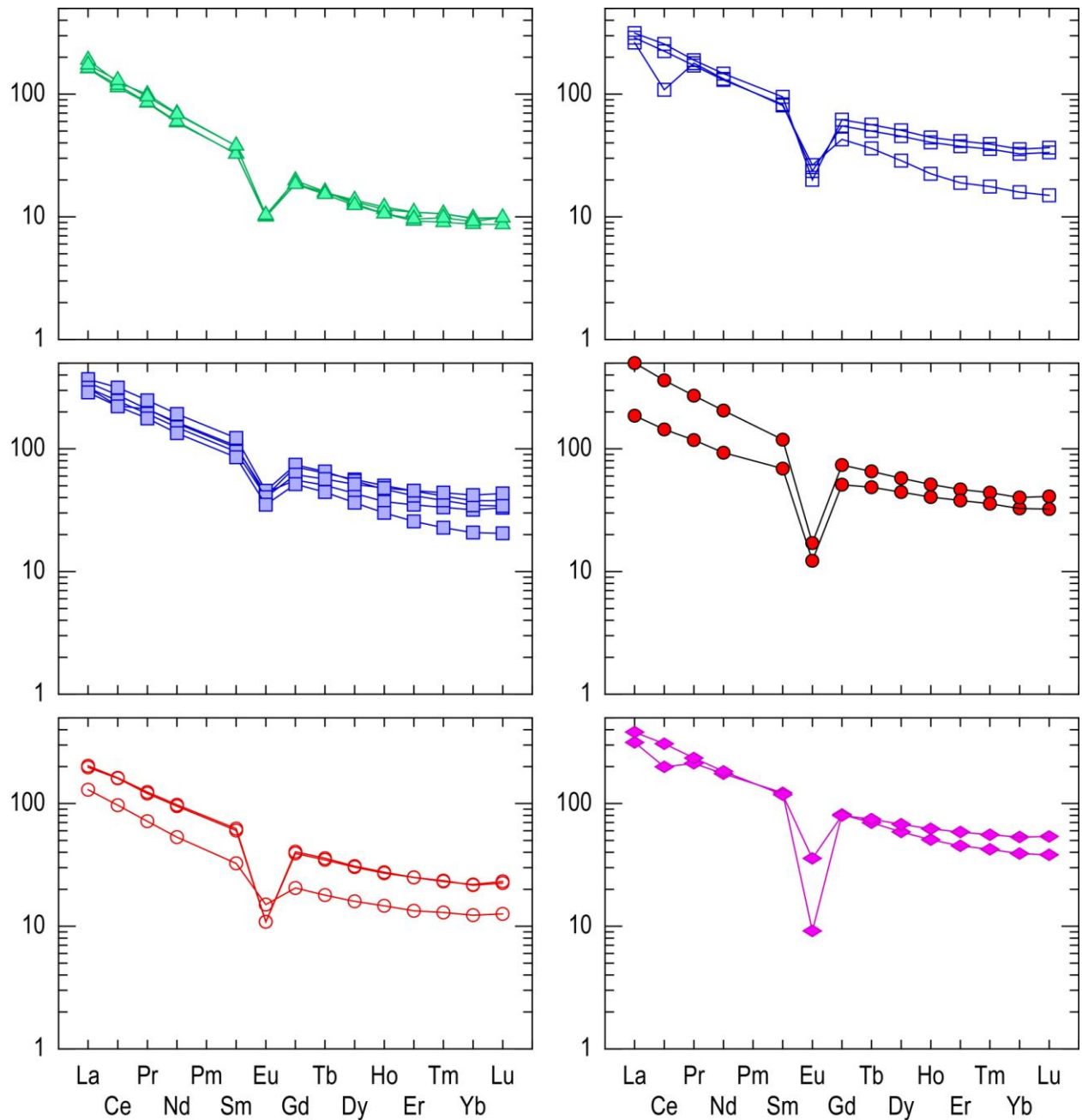
● Glass Mountain rhyolite





- Hayden Peak latite ▲ Silver City rhyolite ○ Glass Mountain dacite
- Quartz latite ◆ Tuff units ● Glass Mountain rhyolite

Figure 5.17: Upper continental crust normalized rare earth element diagrams
Rare earth element spider diagrams normalized to upper continental crust (Taylor and McLennan, 1985).



- Hayden Peak latite ▲ Silver City rhyolite ○ Glass Mountain dacite
- Quartz latite ◆ Tuff units ● Glass Mountain rhyolite

Figure 5.18: Chondrite normalized rare earth element diagrams
Rare earth element spider diagrams normalized to chondrites (Sun and McDonough, 1989).

Radiogenic Isotope Geology

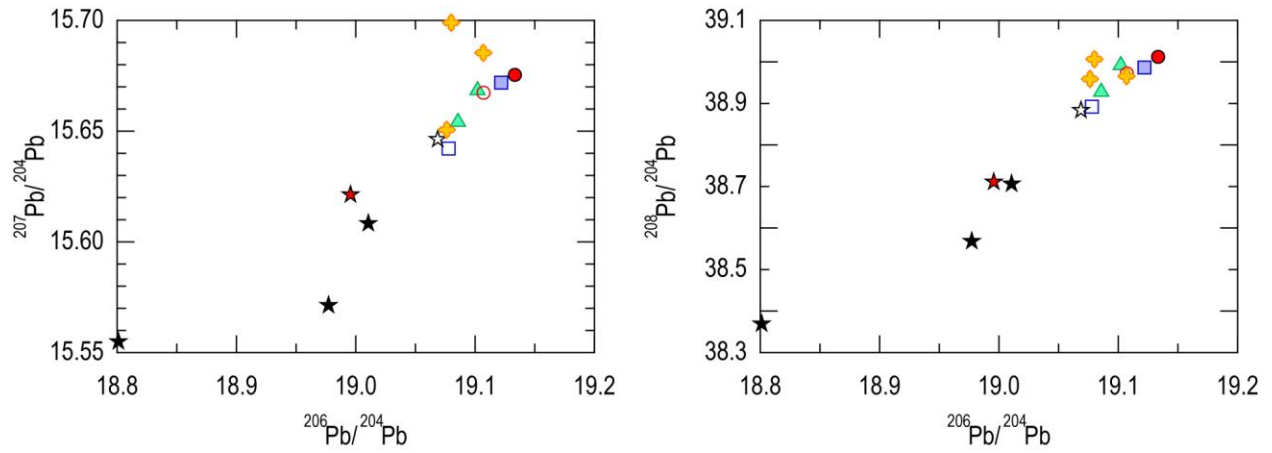
Isotopic analysis of Pb, Sr, and Nd were conducted on select samples from the Silver City district. The samples represent the complete compositional range of the volcanic and granitic rocks in the district. Care was also taken to select samples from each of the distinct silicic units to produce an accurate representation of the isotopic signature of the Silver City district volcanics. The sample suite included three basement granitoids, one olivine basalt, two basalts, one basaltic andesite, one andesite, two Silver City rhyolites, one Glass Mountain dacite, one Glass Mountain rhyolite, one Hayden Peak latite, and one quartz latite.

The analyzed samples fall in fairly linear arrays from the basalt through the granitoid samples in all of the isotope plots. $^{206}\text{Pb}/^{204}\text{Pb}$ plots (Figure 5.19) show values for the basalts range from 18.801 - 19.011 while the andesites through rhyolites/granitoids range from 19.069 - 19.133. The basalts have $^{207}\text{Pb}/^{204}\text{Pb}$ values between 15.555 - 15.621 and $^{208}\text{Pb}/^{204}\text{Pb}$ values between 38.369 - 38.711. The andesites through rhyolites/granitoids have overlapping values of Pb isotope ratios. The $^{207}\text{Pb}/^{204}\text{Pb}$ values lie between 15.642 - 15.699 and $^{208}\text{Pb}/^{204}\text{Pb}$ values between 38.884 - 39.012. Figure 5.20 shows the Pb isotopic data with mantle reservoirs as defined by Carlson (1984) and Camp and Hanan (2008) and additional Silver City district isotope data from Norman and Leeman (1989). The Norman and Leeman data have been given symbol designations based on the geochemical classifications defined previously in this study. The basalt and basaltic andesite samples fall along an array between the C1 (depleted mantle MORB) and C2 (Carlson - sediment contaminated C1; Camp and Hanan - plume derived mantle) mantle reservoirs. The andesite, dacite and rhyolite samples have overlapping values that continue to plot in a positive array at higher isotopic ratios than the C2 mantle reservoir.

The samples continue to fall into an array on a plot of $^{87}\text{Sr}/^{86}\text{Sr}_i$ vs. $^{143}\text{Nd}/^{144}\text{Nd}_i$ with the samples decreasing in $^{143}\text{Nd}/^{144}\text{Nd}_i$ with increasing $^{87}\text{Sr}/^{86}\text{Sr}_i$. The $^{87}\text{Sr}/^{86}\text{Sr}_i$ values range from 0.7034 to 0.7085 and the $^{143}\text{Nd}/^{144}\text{Nd}_i$ values range from 0.51218 - 0.51296. The plot (Figure 5.21) shows three groups within the array. The Steens Basalt, andesite, and Glass Mountain dacite samples plot below 0.7049 $^{87}\text{Sr}/^{86}\text{Sr}_i$ and above 0.51247 $^{143}\text{Nd}/^{144}\text{Nd}_i$; the rhyolites plot between 0.7062 - 0.7071 $^{87}\text{Sr}/^{86}\text{Sr}_i$ and between 0.51243 and 0.51250 $^{143}\text{Nd}/^{144}\text{Nd}_i$; the age-

corrected granitoids lie above $0.7075 \text{ }^{87}\text{Sr}/^{86}\text{Sr}_i$ and below $0.51218 \text{ }^{143}\text{Nd}/^{144}\text{Nd}_i$. Samples from Norman and Leeman (1989) are included on the plot in Figure 5.22.

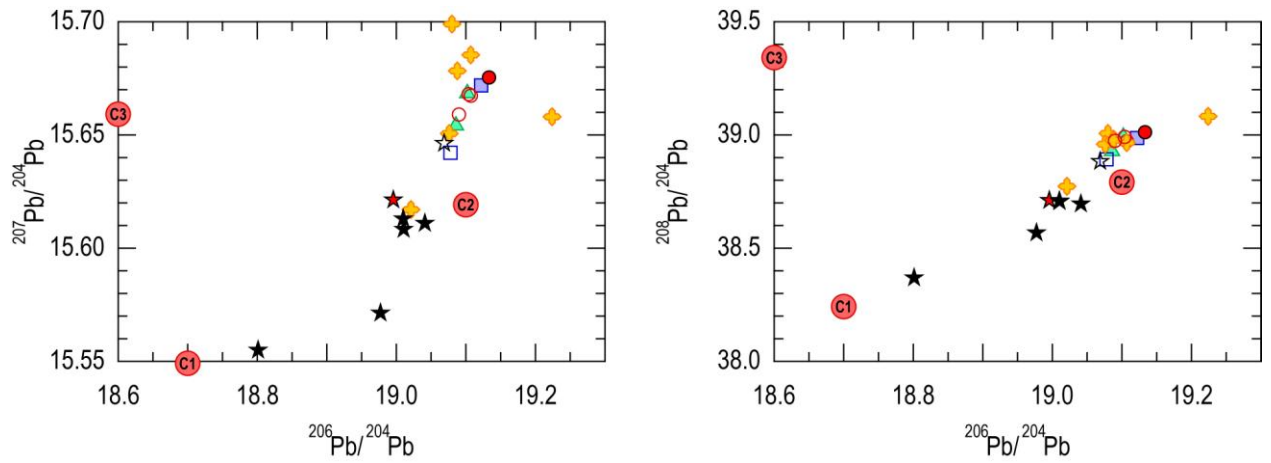
DePaolo et al. (1992) defined the Neodymium crustal index (NCI) as a measure of crustal contribution in silicic igneous rocks. NCI is calculated using the equation $\text{NCI} = (\epsilon\text{Nd}_{\text{ROCK}} - \epsilon\text{Nd}_{\text{MC}})/(\epsilon\text{Nd}_{\text{CC}} - \epsilon\text{Nd}_{\text{MC}})$ where MC is mantle component and CC is the crustal component. NCI values presented below were calculated using a MC value from the Steens Basalt sample MB09-13 and a CC value from the average granitoid samples analyzed in this study. A plot of ϵNd vs. NCI in Figure 5.21 shows unit groupings similar to those seen in other plots. The Steens Basalt and andesite samples plot above $-0.4 \text{ } \epsilon\text{Nd}$ and below 0.5 NCI ; the dacite and rhyolite samples plot between -2.3 and $-3.7 \text{ } \epsilon\text{Nd}$ and between $0.5 - 0.7 \text{ NCI}$; while the granitoids plot below $-6.5 \text{ } \epsilon\text{Nd}$ and above 0.8 NCI . Norman and Leeman (1989) samples are also shown in Figure 5.22.



- | | | |
|-----------------------|------------------------|---------------------------|
| ★ Steens Basalt | □ Hayden Peak latite | ○ Glass Mountain dacite |
| ★ Olivine rich basalt | □ Quartz latite | ● Glass Mountain rhyolite |
| ☆ Andesite | ▲ Silver City rhyolite | ✦ Granitoid |

Figure 5.19: Pb isotope diagrams

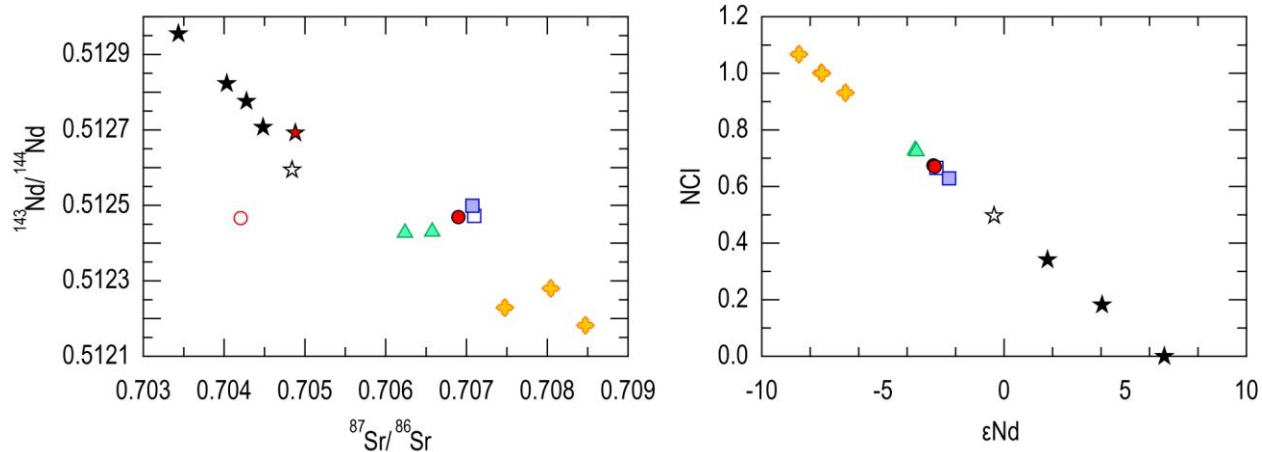
$^{206}\text{Pb}/^{204}\text{Pb}$ vs $^{207}\text{Pb}/^{204}\text{Pb}$ (left) and $^{206}\text{Pb}/^{204}\text{Pb}$ vs $^{208}\text{Pb}/^{204}\text{Pb}$ (right).



- ★ Steens Basalt
- ★ Olivine rich basalt
- ☆ Andesite
- Hayden Peak latite
- Quartz latite
- △ Silver City rhyolite
- Glass Mountain dacite
- Glass Mountain rhyolite
- ◆ Granitoid

Figure 5.20: Pb isotope diagrams

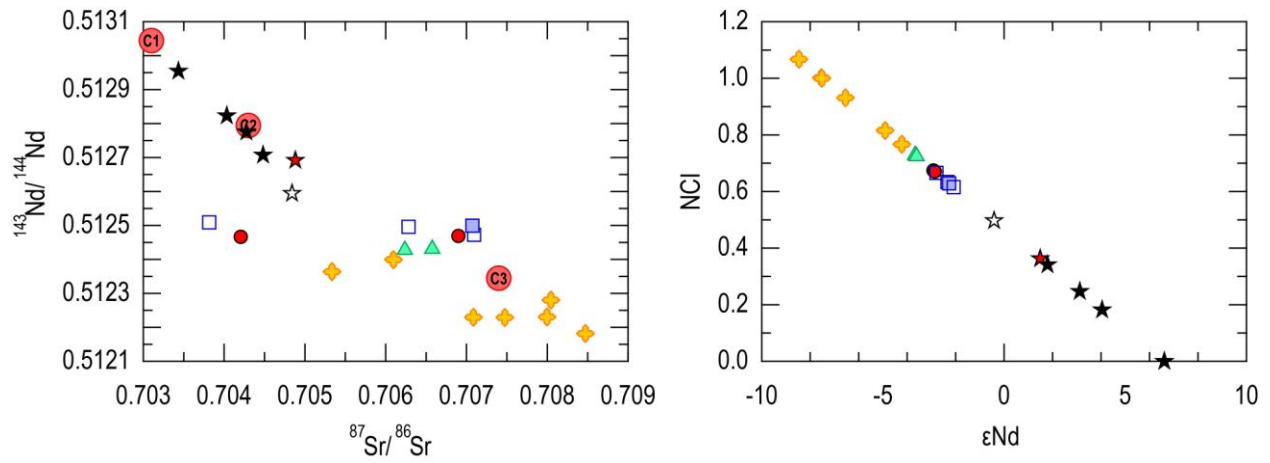
$^{206}\text{Pb}/^{204}\text{Pb}$ vs $^{207}\text{Pb}/^{204}\text{Pb}$ (left) and $^{206}\text{Pb}/^{204}\text{Pb}$ vs $^{208}\text{Pb}/^{204}\text{Pb}$ (right). The Carlson (1984) mantle reservoirs are included.



- | | | |
|-----------------------|------------------------|---------------------------|
| ★ Steens Basalt | □ Hayden Peak latite | ○ Glass Mountain dacite |
| ★ Olivine rich basalt | □ Quartz latite | ● Glass Mountain rhyolite |
| ☆ Andesite | ▲ Silver City rhyolite | ◆ Granitoid |

Figure 5.21: Sr and Nd isotope diagrams

Plot of $^{87}\text{Sr}/^{86}\text{Sr}_i$ vs $^{143}\text{Nd}/^{144}\text{Nd}_i$ showing the samples plotting into three groups including the granitoid samples. The three groups can also be seen in the ϵNd vs NCI plot with all of the samples plotting in a linear array.



- ★ Steens Basalt
- ★ Olivine rich basalt
- ☆ Andesite
- Hayden Peak latite
- Quartz latite
- △ Silver City rhyolite
- Glass Mountain dacite
- Glass Mountain rhyolite
- ◆ Granitoid

Figure 5.22: Silver City district Sr and Nd diagrams

Plot of $^{87}\text{Sr}/^{86}\text{Sr}_i$ vs $^{143}\text{Nd}/^{144}\text{Nd}_i$ and ϵNd vs NCI showing the samples collected as part of this study as well as the Silver City district samples from Norman and Leeman (1989).

Chapter 6 - Oxygen Isotopes

Fifteen samples from the silicic volcanic units and granitic basement rock were analyzed for oxygen isotopes. The analyzed samples included five granitoids; five Silver City rhyolites; two Glass Mountain rhyolites; two Hayden Peak latites; and one quartz latite.

It has been noted that samples with $\delta^{18}\text{O}_{\text{feldspar}} < \delta^{18}\text{O}_{\text{quartz}}$ and $\Delta_{\text{quartz} - \text{feldspar}}$ values less than 2‰ can be inferred to contain minerals that were in isotopic equilibrium with the magma and have not undergone post emplacement alteration events (Taylor, 1968; and Borouhgs et al., 2005). Two of the granitoid and six of the silicic samples have $\delta^{18}\text{O}$ values that fall into these parameters, with $\Delta_{\text{quartz} - \text{feldspar}}$ values ranging from 0.38 - 1.94‰ (Fig 6.1). These samples were in isotopic equilibrium prior to eruption and thus the $\delta^{18}\text{O}_{\text{feldspar}}$ values can be used as a proxy for the magmatic $\delta^{18}\text{O}$ value (Taylor, 1979; and Borouhgs et al., 2005). The equilibrium samples have $\delta^{18}\text{O}_{\text{feldspar}}$ values between 7.48 - 10.01‰. While the $\delta^{18}\text{O}_{\text{feldspar}}$ values of rhyolitic melts can be 0.2 - 0.4‰ lower than the parent material, these $\delta^{18}\text{O}_{\text{feldspar}}$ values are within the 6 - 10‰ values for unaltered igneous rock (Taylor, 1978).

The lone Silver City rhyolite sample with a higher $\delta^{18}\text{O}_{\text{feldspar}}$ value is indicative of alteration from a low temperature hydrothermal event (Taylor, 1978). The remaining samples with a negative trend and $\Delta_{\text{quartz} - \text{feldspar}}$ values larger than 2‰ have undergone abundant post emplacement depletion of $\delta^{18}\text{O}_{\text{feldspar}}$ (Taylor, 1978). This depletion can be attributed to alteration related to the hydrothermal system that was responsible for the local ore mineralization. Interaction with hydrothermal fluid with $\delta^{18}\text{O}$ values between -6.5 and -9.7‰ likely resulted in some samples containing low feldspar values (Cupp, 1989).

Analysis of the unaltered silicic volcanic units indicate that the $\delta^{18}\text{O}_{\text{feldspar}}$ values align with the $\delta^{18}\text{O}_{\text{feldspar}}$ values of the unaltered granitoid basement rock. Note that at least one sample from all of the different silicic units is in isotopic equilibrium with the granitoid and have nearly the same $\delta^{18}\text{O}$ values.

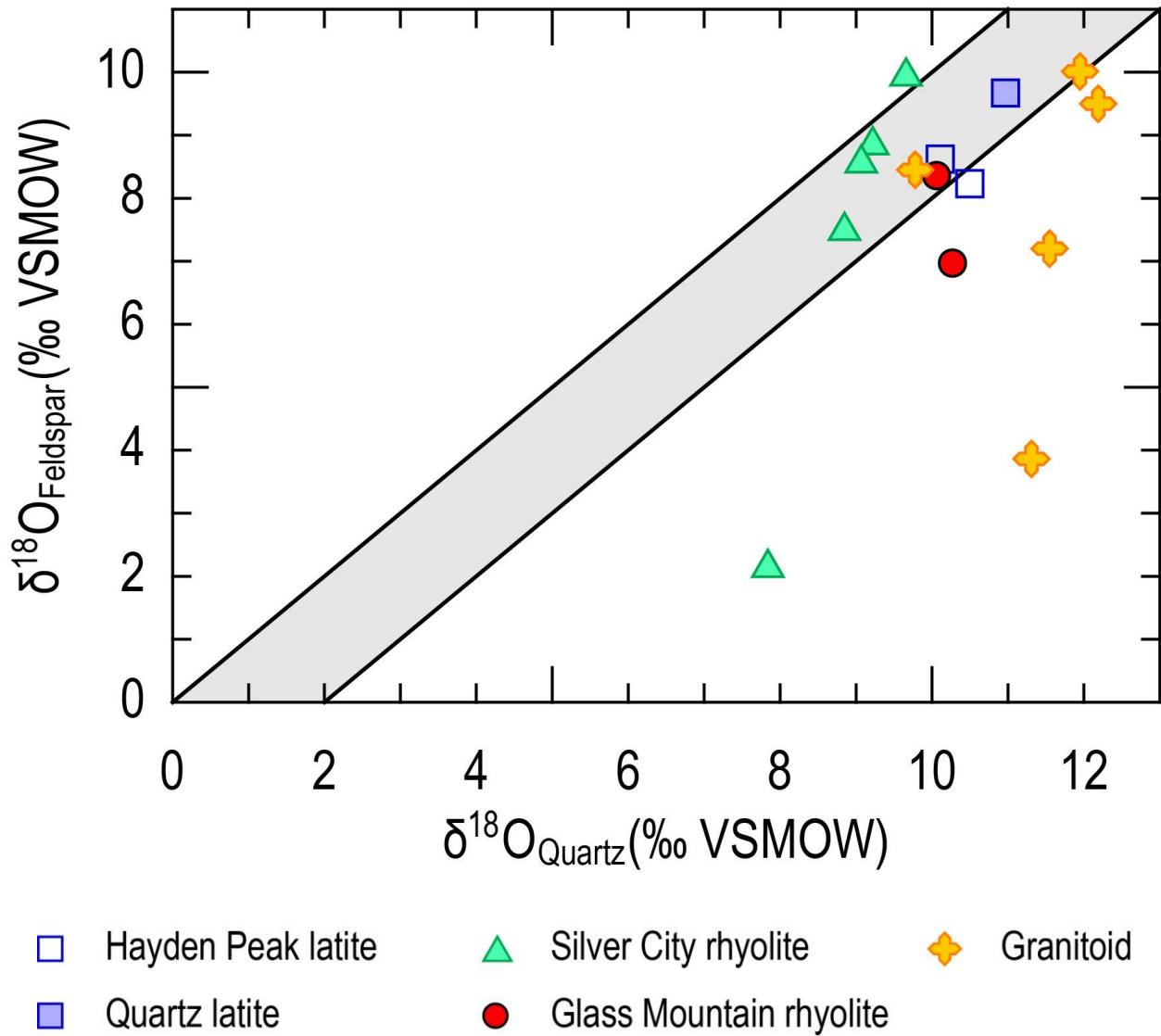


Figure 6.1: Oxygen isotopes

Plot of $\delta^{18}\text{O}_{\text{quartz}}$ vs. $\delta^{18}\text{O}_{\text{feldspar}}$. Samples in isotopic equilibrium fall within the shaded region.

Chapter 7 - Geochronology

Twenty-eight samples were chosen for $^{40}\text{Ar}/^{39}\text{Ar}$ geochronology. Multiple samples were chosen from each volcanic unit to provide adequate geochronological constraints. At this time, final geochronological data is not yet available. While there is confidence in the relative eruption timing, based on field relationships, the ages produced by $^{40}\text{Ar}/^{39}\text{Ar}$ geochronology will provide more distinct timing constraints on the Silver City district volcanic history. The samples included seven basalts, one adularia deposit, five quartz latites, three Hayden Peak latites, three Glass Mountain dacites, three Glass Mountain rhyolites, and six Silver City rhyolites. Previous work has indicated that the silicic volcanism was approximately 16.6 - 14 Ma (Bonnichsen and Godchaux, 2006). However, two previously obtained age dates from a basalt and a rhyolite sample in the Silver City district as part of the companion study indicate a formational age of 16.08 ± 0.18 (basalt) - 15.94 ± 0.10 (rhyolite) Ma (Aseto, 2012). Additionally, geochronology of the precious metal epithermal mineralization veins in Silver City district produced ages of 16.1 - 15.4 Ma with the majority of the mineralization occurring around 15.7 Ma (Aseto et al., 2011; Aseto, 2012). The fact that the epithermal mineralization is present in nearly all of the volcanic units indicates that the Silver City district eruptive history was contained to a short amount of time (less than 1 million years) with the majority of the volcanic units being deposited by 15.5 Ma.

Chapter 8 - Geochemical and Isotopic Constraints on Magma Production

Trace Element Modeling

While the stratigraphy and petrography provide some information on the petrogenetic history of the Silver City district, the geochemical analysis allows for a more complete understanding of the mid-Miocene volcanic history.

Geochemical analysis indicates that there are distinct volcanic units that can be defined by major, trace, rare earth element, and isotopic analysis. Trace elements plotted against Zr show three mafic and intermediate units (Steens Basalt, andesite type 1 and type 2) and six locally erupted silicic units (Hayden Peak latite, quartz latite, Glass Mountain dacite, Glass Mountain rhyolite, Silver City rhyolite and the tuff of Flint Creek).

A plot of Sr and Nd isotope data (Figure 5.21) shows that the intermediate and silicic samples plot transitional between basaltic and granitic reservoirs indicating a petrogenesis that includes interaction between mafic and silicic components. Additionally NCI values (Figure 5.21) show varying degrees of mafic input with the Silver City rhyolite containing the least amount of mafic component with more mafic interaction occurring for the latites and andesites (DePaolo et al., 1992). These relationships were incorporated into geochemical modeling (fractional crystallization, assimilation, and magma mixing) using representative samples from the volcanic units. Geochemical data for the samples used in the modeling are presented in Table 8.1.

Table 8.1: Representative Unit Geochemistry

Next page - Major element oxide (wt. %), select trace and rare earth element (ppm) concentrations and radiogenic isotope ratios for the volcanic samples used in the petrogenetic modeling.

Sample	MB09-13	ZH10-40	ZH11-2	ZH10-15	ZH10-24	ZH11-6	ZH10-22	ZH10-43
Rock Unit	Tsb	Ta1	Thpl	Tsc	Tql	Ta2	Tlgd	Tlgr
SiO ₂ (wt. %)	48.92	58.39	75.59	76.28	77.69	57.44	66.84	75.72
TiO ₂ (wt. %)	1.91	1.02	0.20	0.27	0.31	1.61	0.47	0.22
Al ₂ O ₃ (wt. %)	15.21	15.23	12.60	12.96	13.22	15.08	14.01	12.93
FeO* (wt. %)	11.10	7.25	2.27	1.25	0.37	8.30	4.96	1.76
MnO (wt. %)	0.18	0.13	0.03	0.01	0.00	0.00	0.08	0.03
MgO (wt. %)	7.77	4.94	0.00	0.25	0.01	3.80	2.95	0.21
CaO (wt. %)	10.23	7.11	0.80	0.98	0.51	7.21	4.26	1.11
Na ₂ O (wt. %)	2.60	2.87	2.57	2.76	2.52	2.77	2.09	2.90
K ₂ O (wt. %)	0.63	2.01	5.67	5.06	5.29	2.32	3.73	4.89
P ₂ O ₅ (wt. %)	0.21	0.24	0.01	0.04	0.04	0.55	0.06	0.03
Ba (ppm)	180.42	743.93	1,804.63	1,481.99	2,058.81	1,049.46	153.45	1,288.08
Cr (ppm)	197.60	71.30	2.83	4.80	2.70	38.89	34.20	4.60
Nb (ppm)	7.61	9.24	27.66	10.01	29.08	15.12	19.94	25.50
Nd (ppm)	17.27	23.32	60.93	27.96	89.97	40.52	44.41	43.43
Ni (ppm)	177.30	48.20	0.61	3.50	4.10	16.97	37.10	2.30
Rb (ppm)	13.43	61.99	211.05	166.49	178.88	53.07	115.28	209.06
Sc (ppm)	29.09	21.57	2.12	4.07	6.99	21.32	13.06	4.09
Sr (ppm)	348.27	328.30	85.63	111.15	123.24	553.89	106.47	87.34
Zn (ppm)	92.80	81.00	130.19	41.40	19.90	134.84	122.50	99.10
Zr (ppm)	127.68	138.07	445.41	173.45	588.76	259.08	307.76	228.88
La (ppm)	10.32	22.98	68.39	38.59	87.70	36.47	46.71	44.14
Ce (ppm)	25.32	47.17	137.11	72.47	193.51	76.48	98.20	88.13
Cs (ppm)	0.58	1.58	5.22	2.98	3.19	0.92	2.49	4.57
Hf (ppm)	3.40	3.88	12.07	5.17	14.71	6.42	8.19	7.71
Sm (ppm)	4.83	5.13	12.65	4.97	18.76	8.54	9.23	10.56
Eu (ppm)	1.75	1.30	1.37	0.59	2.64	2.11	0.63	0.71
Yb (ppm)	2.11	2.27	5.54	1.66	5.89	3.02	3.72	5.55
Lu (ppm)	0.31	0.35	0.85	0.25	0.87	0.46	0.59	0.82
⁸⁷ Sr/ ⁸⁶ Sr _i	0.703435	0.704842	0.707096	0.706577	0.707074	---	0.704206	0.706900
¹⁴³ Nd/ ¹⁴⁴ Nd _i	0.512955	0.512594	0.512472	0.512430	0.512499	---	0.512466	0.512469
epsilon Nd	6.615746	-0.408301	-2.791614	-3.611458	-2.266222	---	-2.908941	-2.856759
²⁰⁶ Pb/ ²⁰⁴ Pb	18.801188	19.068790	19.077900	19.102097	19.121947	---	19.107133	19.133378
²⁰⁷ Pb/ ²⁰⁴ Pb	15.554989	15.646342	15.642112	15.668357	15.671847	---	15.667332	15.675390
²⁰⁸ Pb/ ²⁰⁴ Pb	38.369343	38.883678	38.892011	38.991452	38.986439	---	38.972380	39.012091

Using these datasets, a series of petrogenetic models were created to address the petrogenesis of Silver City district magmas. These models are based on the premises discussed above, including that there were at least two separate silicic magmatic systems (Hayden Peak latite and Silver City rhyolite) present beneath the Silver City district and that varying degrees of interaction between these magmatic bodies and with Steens Basalt magmas produced multiple intermediate and silicic units. The calculated major and trace element geochemistries from the proposed models are summarized in Tables 8.2 and 8.3

In order to further understand the history of the magma generation in the Silver City district, modeling is used to address the potential for partial melting of granitic basement by mafic input, assimilation and fractional crystallization of granitoid, granitoid melt and intermediate magma, and magma mixing between both mafic and silicic magma bodies and also mixing between separate silicic bodies as the dominant petrogenetic process that formed the Silver City district magmas in this study. Basalts and basaltic andesites of the Silver City district have similar geochemistry to the regional Steens Basalt and are tholeiitic in nature. The basalts and basaltic andesites have K/P ratios falling below 8.1 and the andesites show higher K/P ratios ranging from 6.9 up to 33.9. These ratios indicate that the more mafic samples underwent limited amounts of crustal contamination during prior to their eruption while the andesite samples contain more input from crustal sources (e.g. more upper crustal contamination). Steens Basalt magmas have been interpreted as being melts of depleted mantle (Carlson and Hart, 1988; Camp et al., 2003). The ascension and eruption of the basaltic magma also provided heat and mass fluxes into the upper crust under the Owyhee Mountains which led to the initiation of crustal melting.

Assimilation and fractional crystallization modeling shows the andesite type 1 unit (ZH10-40) can be formed through the fractional crystallization of basaltic magma (MB09-13) and assimilation of granitoid basement (AvgKg) with results and AFC trends shown in Table 8.2 and Figure 8.1. The modeling results in F values (% liquid remaining) of 0.962 and a sum of the residuals squared value of 0.134. This andesite also serves as a key component in forming the Silver City rhyolite and Hayden Peak latite. Modeling for the andesite was performed using a fractional crystallization mineral assemblage of 5.7% titanomagnetite (Ti10), 61.5% plagioclase (An63), and 32.9% clinopyroxene (Wo30:Mg48:Fe21). Figure 8.2 shows multi-element

diagrams with the andesite used for modeling (ZH10-40) and the calculated AFC modeled results. When normalized to chondrites (Sun, 1980) the two samples follow similar trends with positive anomalies in Ba and K and negative anomalies in Nb and Ti. MORB normalized diagrams after Pearce (1983) show high enrichment of large ion lithophile elements and slight enrichment to slight depletion of the high field strength elements. Rare earth elements normalized to chondrites (Sun and McDonough, 1989) show highly enriched light rare earths and moderately enriched heavy rare earths with the modeled sample plotting slightly below the actual sample. Both samples show similar negative anomalies in Nb and positive anomalies in Ce.

Mafic magma upwelling likely stimulated partial melting of the Silver City granite. The Hayden Peak latite samples have high Zr concentrations (ppm) while the Silver City granite typically contains less than 100 ppm Zr. A high Zr liquid, which can be modeled by low degrees (5 - 25%) of partial melting of granitoid (Figure 8.3) is needed to form the Hayden Peak latites. The Hayden Peak latite (ZH11-2) can be modeled with 24.7% fractional crystallization of this initial 5 - 25% partial melt liquid (Avg5% and Avg25%), with a mineral assemblage of 77.7% plagioclase (An63) and 22.3% titanomagnetite (Ti10), and assimilation of the previously formed andesite type 1 (ZH10-40). The results (presented in Table 8.2) for both 5% and 25% partial granite melts both have an F value of 0.753. Two AFC trend lines on trace element diagrams are seen in Figure 8.3. Figure 8.4 shows the Hayden Peak latite plotted with both of the modeled assimilation and fractional crystallization results (5% and 20% melt) on multi-element diagrams normalized to chondrites (Sun, 1980) and upper continental crust (Taylor and McLennan, 1985). There are large negative Nb, Sr, and Ti anomalies when normalized to chondrites. The upper continental crust plots show similar patterns with positive Ba anomalies and negative Nb, Sr, and Ti anomalies. Sun and McDonough (1989) chondrite normalized rare earth patterns have highly enriched (>100) light rare earths with negative Eu anomalies and moderately enriched heavy rare earths.

The physically similar quartz latite unit is also chemically similar to the Hayden Peak latite. Fractional crystallization modeling shows that the quartz latite unit can be formed via fractional crystallization of the Hayden Peak latite. Modeling of a hypothetical parent magma (Hayden Peak latite) that underwent 2.1% fractional crystallization of 100% plagioclase to produce a quartz latite daughter magma (ZH10-24) yields a parent magma similar to the observed Hayden Peak latite samples (ZH11-2). A sum of the residuals squared value of 4.374

was observed. The fairly large value is in part due to the large difference in observed and calculated FeO wt. % values as seen in Table 8.3. The actual parental Hayden Peak latite (ZH11-2) sample is plotted with the hypothetical parental magma on the same multi-element diagrams in Figure 8.5. The plots are nearly identical patterns with the modeled parent plotting as slightly more enriched in chondrite normalized rare earth elements and follow the same enrichment and depletion patterns with consistent anomalies.

Contemporaneous with the formation of the Hayden Peak and quartz latite magmas, Silver City rhyolite magmas were also forming under the study area. The major, trace, and isotopic characteristics of Silver City rhyolite indicate that like the Hayden Peak latite, it formed via melting of Silver City granite, followed by fractional crystallization and assimilation of less evolved melts. However, it is important to recall that unlike the other silicic units, the Silver City rhyolite plots along with the Silver City Granitoid on discrimination diagrams in the I-type granite field (Figure 8.6) and also has a NCI value closest to the Kg (Figure 5.21). Its Sr-Nd-Pb-O isotope values also partially overlap with Kg, again suggesting that both units are related and that the Silver City rhyolite did not form via melting of underplated basalt or mafic cumulates. Thus, the petrogenesis of the Silver City rhyolite (ZH10-15) is best modeled using 24.9% fractionation of a liquid formed by 60% partial melting of granitoid (Avg60%) and assimilation of the previously formed andesite type 1 (ZH10-40). Similar large percent melting have been reported from previous studies (Vielzeuf and Holloway, 1988; Patino Douce and Johnston, 1991; Patino Douce and Beard, 1995; Patino Douce and Beard, 1996; Otamendi and Patino Douce, 2001; and Petcovic and Grunder, 2003). Fractional crystallization of a similar mineral assemblage of 75.5% plagioclase (An63) and 24.5 titanomagnetite (Ti10) was used for modeling purposes with a resultant F value of 0.751 as seen in Table 8.2. Figure 8.7 contains trace element plots with the AFC trends. Chondrite and upper continental crust normalized multi-element diagrams of the Silver City rhyolite and modeled AFC samples follow similar patterns with negative Nb, Sr, and Ti anomalies (Figure 8.8). The chondrite normalized rare earth element patterns show nearly identical light rare earths (La, Ce and Nd), however the heavy rare earths are slightly more enriched in the modeled samples.

With the presence of three prominent magmatic bodies (Steens Basalt, Hayden Peak latite and Silver City rhyolite) beneath the Silver City district, the other units (Glass Mountain dacite, Glass Mountain rhyolite, and the andesite type 2) can be formed through simple magma mixing.

The andesite type 2 unit can be modeled via the mixing of Steens Basalt with Hayden Peak latite magmas. Magma mixing models show the andesite can be formed with roughly 65% basaltic component and 35% rhyolite component, using samples MB09-13 (Steens Basalt) and ZH11-2 (Hayden Peak latite) as the mixing endmembers. Calculated results can be seen in Table 8.3 and mixing trends can be seen in Figure 8.9. Figure 8.10 also show the andesite type 2 (ZH11-6) and modeled mixing samples have consistent patterns on chondrite and MORB normalized multi-element diagrams.

Both the Glass Mountain dacite and rhyolite members of the have the Hayden Peak latite (ZH11-2) as one mixing endmember (Table 8.3). The mixing formation of the type 1 member is similar to the formation of the andesite type 2. These dacitic lavas are modeled by magma mixing of Hayden Peak latite (ZH11-2) and Steens Basalt (MB09-13), and includes more of the silicic Hayden Peak latite component (65%) and less of a basaltic component (35%) as seen in Figure 8.11. The Glass Mountain rhyolite can be modeled through the mixing of two silicic magma bodies, the Hayden Peak latite (ZH11-2) and the Silver City rhyolite (ZH10-15). The modeled magma is more closely related to the Silver City rhyolite and consists of nearly 74% input from the Silver City rhyolite source and 26% from the Hayden Peak latite source (Figure 8.11). Chondrite and upper continental crust normalized multi-element diagrams of the Glass Mountain dacite and rhyolite units and associated modeled magmas show nearly identical patterns (Figures 8.12 and Figure 8.13). Similar to the other silicic units, the Glass Mountain samples have strong negative Nb, Sr, and Ti anomalies. The only deviations are in the dacite unit (Figure 8.12) where the actual Glass Mountain dacite samples have a large negative Ba anomaly that was not seen in the modeled magma. This can be attributed to the presence of feldspar fractionation that was not accounted for in the mixing-only modeling. And in the rhyolite unit (Figure 8.13) the actual sample has higher enrichment of chondrite normalized heavy rare earth elements.

Table 8.2: AFC modeling results

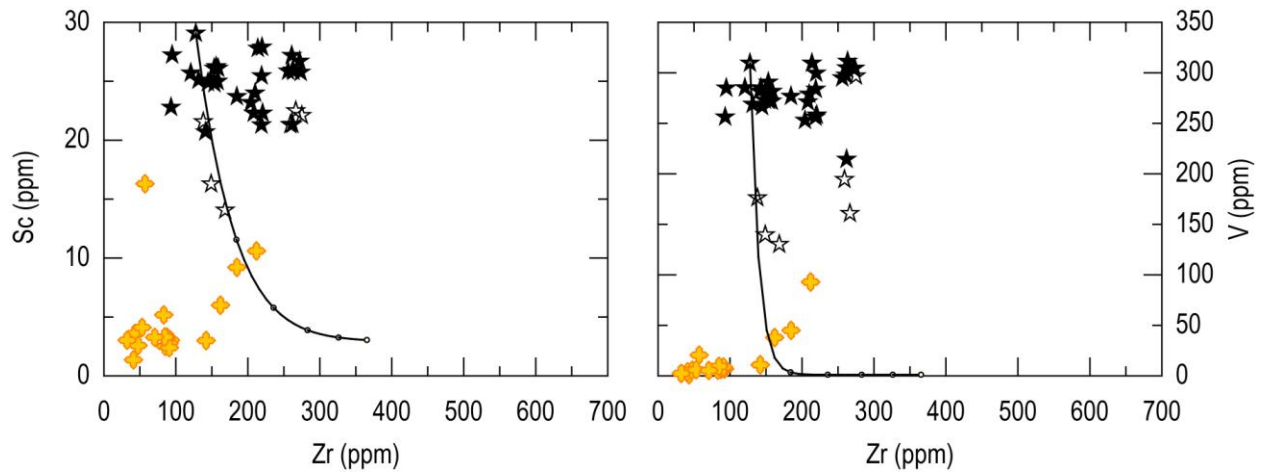
Next page - Major and trace element compositions are presented for modeled and observed magmas to demonstrate the modeling used for petrogenetic analysis. The modeled magmas are presented with the sum of the squared residuals. R = ratio of calculated daughter to observed daughter values and F = % liquid remaining after AFC. The samples used for calculations are: Kg - Average; Tsb - MB09-13; Ta₁ - ZH10-40; Thpl - ZH11-2; Tsc - ZH10-15, and a 5% and 60% melt of Average Kg (labeled as Avg5% and Avg60%). The modeled magmas calculated using the Avg5% and Avg60% are only calculated for trace elements. The Ta₁ was modeled with a mineral assemblage of 61.5% plagioclase, 32.9% clinopyroxene. The Hayden Peak latite was modeled with a mineral assemblage of 77.7% plagioclase and 22.3% titanomagnetite. The Tsc was modeled with a mineral assemblage of 75.5% plagioclase and 24.5% titanomagnetite. AFC and mixing calculations were performed using the MIXING module in IgPet 2010.

Assimilation and Fractional Crystallization																
Endmember A	Tsb	MB09-13	F = 0.962	Ta1	ZH10-40	F = 0.753	Ta1	ZH10-40	F = 0.753	Ta1	ZH10-40	F = 0.753	Ta1	ZH10-40	F = 0.751	
Endmember B	Kg	Avg Kg		Kg Melt	Avg5%		Kg Melt	Avg25%		Kg Melt	Avg60%		Kg Melt	Avg60%		
Hybrid Mixture	Ta1	ZH10-40		Thpl	ZH11-2		Thpl	ZH11-2		Tsc	ZH10-15		Tsc	ZH10-15		
	Observed	Calculated	R													
SiO ₂ (wt. %)	58.39	59.09	1.01	---	---	---	---	---	---	---	---	---	---	---	---	---
TiO ₂ (wt. %)	1.02	1.23	1.20	---	---	---	---	---	---	---	---	---	---	---	---	---
Al ₂ O ₃ (wt. %)	15.23	15.31	1.01	---	---	---	---	---	---	---	---	---	---	---	---	---
Fe ₂ O ₃ (wt. %)	7.25	7.31	1.01	---	---	---	---	---	---	---	---	---	---	---	---	---
MnO (wt. %)	0.13	0.12	0.95	---	---	---	---	---	---	---	---	---	---	---	---	---
MgO (wt. %)	4.94	4.95	1.00	---	---	---	---	---	---	---	---	---	---	---	---	---
CaO (wt. %)	7.11	7.17	1.01	---	---	---	---	---	---	---	---	---	---	---	---	---
Na ₂ O (wt. %)	2.87	2.90	1.01	---	---	---	---	---	---	---	---	---	---	---	---	---
K ₂ O (wt. %)	2.01	1.75	0.87	---	---	---	---	---	---	---	---	---	---	---	---	---
P ₂ O ₅ (wt. %)	0.24	0.14	0.58	---	---	---	---	---	---	---	---	---	---	---	---	---
ΣR^2			0.134													
Ni (ppm)	48.20	112.76	2.34	0.61	55.32	91.29	0.61	55.33	91.30	0.61	55.64	91.30	0.61	55.64	91.30	15.90
Cr (ppm)	71.30	146.17	2.05	2.83	95.80	33.88	2.83	95.72	33.85	2.83	95.75	33.85	2.83	95.75	33.85	19.95
Sc (ppm)	21.57	19.58	0.91	2.12	31.40	14.83	2.12	30.78	14.54	2.12	29.82	14.54	2.12	29.82	14.54	7.32
Ba (ppm)	743.93	787.73	1.06	1804.63	1210.99	0.67	1804.63	1268.17	0.70	1804.63	1264.58	0.70	1804.63	1264.58	0.85	0.85
Rb (ppm)	61.99	43.24	0.70	211.05	150.96	0.72	211.05	143.46	0.68	211.05	120.01	0.68	211.05	120.01	0.72	0.72
Sr (ppm)	328.30	368.21	1.12	85.63	107.90	1.26	85.63	110.39	1.29	85.63	115.99	1.29	85.63	115.99	1.04	1.04
Zr (ppm)	138.07	103.14	0.75	445.41	438.31	0.98	445.41	281.14	0.63	445.41	218.97	0.63	445.41	218.97	1.26	1.26
Y (ppm)	23.79	18.44	0.78	59.49	49.19	0.83	59.49	40.99	0.69	59.49	35.49	0.69	59.49	35.49	1.98	1.98
Nb (ppm)	9.24	6.49	0.70	27.66	21.80	0.79	27.66	17.22	0.62	27.66	14.04	0.62	27.66	14.04	1.40	1.40
La (ppm)	22.98	13.46	0.59	68.39	62.14	0.91	68.39	48.68	0.71	68.39	37.64	0.71	68.39	37.64	0.98	0.98
Ce (ppm)	47.17	28.81	0.61	137.11	103.77	0.76	137.11	91.52	0.67	137.11	76.06	0.67	137.11	76.06	1.05	1.05
Nd (ppm)	23.32	16.19	0.69	60.93	43.02	0.71	60.93	40.90	0.67	60.93	36.43	0.67	60.93	36.43	1.30	1.30
Sm (ppm)	5.13	4.07	0.79	12.65	11.70	0.93	12.65	9.77	0.77	12.65	8.09	0.77	12.65	8.09	1.63	1.63
Eu (ppm)	1.30	1.33	1.03	1.37	1.29	0.94	1.37	1.30	0.95	1.37	1.28	0.95	1.37	1.28	2.15	2.15
Gd (ppm)	4.72	4.00	0.85	11.31	10.44	0.92	11.31	8.67	0.77	11.31	7.33	0.77	11.31	7.33	1.92	1.92
Dy (ppm)	4.63	3.75	0.81	11.54	9.83	0.85	11.54	8.07	0.70	11.54	6.95	0.70	11.54	6.95	2.00	2.00
Er (ppm)	2.49	1.83	0.74	6.22	4.91	0.79	6.22	4.18	0.67	6.22	3.68	0.67	6.22	3.68	2.03	2.03
Yb (ppm)	2.27	1.55	0.68	5.54	4.51	0.81	5.54	3.79	0.68	5.54	3.32	0.68	5.54	3.32	2.00	2.00

Table 8.3: Fractional crystallization and mixing modeling results

Next page - Major and trace element compositions are presented for calculated and observed hybrid magmas to demonstrate the modeling used for petrogenetic analysis. The hybrid magmas are presented with the sum of the squared residuals. R = ratio of calculated daughter to observed daughter values and endmember mixing percentages. The samples used for mixing are: Tsb - MB09-13; Thpl - ZH11-2; Tsc - ZH10-15. AFC and mixing calculations were performed using the MIXING module in IgPet 2010.

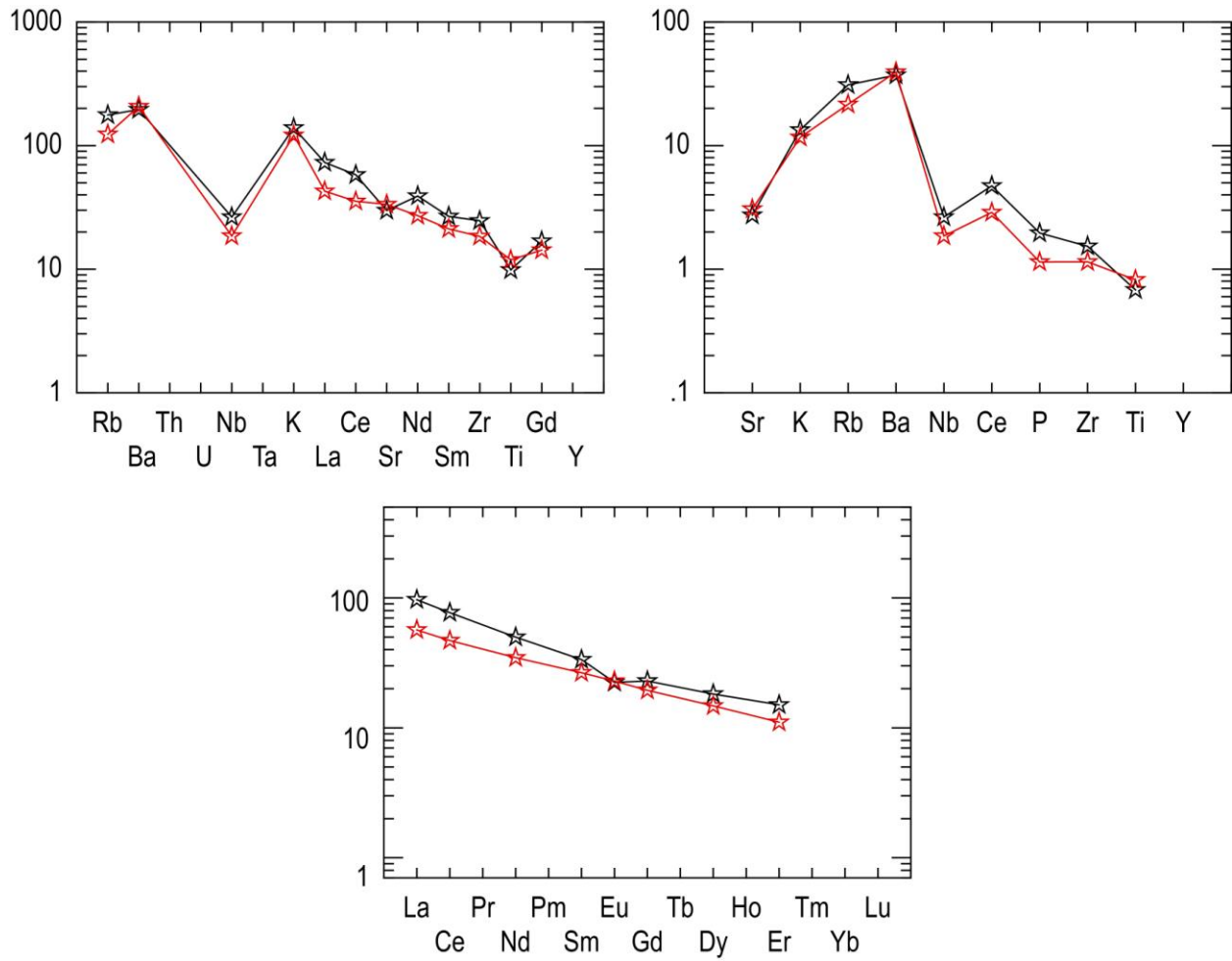
	Fractional Crystallization			Magma Mixing								
	Thpl	ZH11-2	F = 979	Tsb	MB09-13	64.9%	Tsb	MB09-13	34.3%	Thpl	ZH11-2	26.3%
Endmember A	---	---	---	Thpl	ZH11-2	35.1%	Thpl	ZH11-2	65.7%	Tsc	ZH10-15	73.7%
Endmember B	Tql	ZH10-24		Taz	ZH11-6		Tgml1	ZH10-22		Tgml2	ZH10-43	
Hybrid Mixture	Observed	Calculated	R	Observed	Calculated	R	Observed	Calculated	R	Observed	Calculated	R
SiO ₂ (wt. %)	75.59	77.11	1.02	57.44	58.73	1.02	66.84	66.81	1.00	75.72	76.20	1.01
TiO ₂ (wt. %)	0.20	0.31	1.51	1.61	1.32	0.82	0.47	0.79	1.67	0.22	0.25	1.16
Al ₂ O ₃ (wt. %)	12.60	13.53	1.07	15.08	14.42	0.96	14.01	13.59	0.97	12.93	12.88	1.00
Fe ₂ O ₃ (wt. %)	2.27	0.37	0.16	8.30	8.09	0.97	4.96	5.35	1.08	1.76	1.52	0.86
MnO (wt. %)	0.03	0.00	0.00	0.00	0.13	66.55	0.08	0.08	1.05	0.03	0.02	0.78
MgO (wt. %)	0.00	0.01	0.00	3.80	5.10	1.34	2.95	2.70	0.91	0.21	0.18	0.85
CaO (wt. %)	0.80	0.75	0.94	7.21	7.00	0.97	4.26	4.08	0.96	1.11	0.93	0.83
Na ₂ O (wt. %)	2.57	2.55	0.99	2.77	2.61	0.94	2.09	2.60	1.24	2.90	2.71	0.93
K ₂ O (wt. %)	5.67	5.19	0.92	2.32	2.41	1.04	3.73	3.96	1.06	4.89	5.23	1.07
P ₂ O ₅ (wt. %)	0.01	0.04	3.38	0.55	0.14	0.25	0.06	0.08	1.32	0.03	0.03	0.92
ΣR^2			4.374			2.331			0.726			0.255
Ni (ppm)	0.61	4.08	6.73	16.97	116.60	6.87	37.10	61.90	1.67	2.30	2.70	1.17
Cr (ppm)	2.83	2.65	0.94	38.89	130.70	3.36	34.20	70.40	2.06	4.60	4.30	0.93
Sc (ppm)	2.12	6.85	3.24	21.32	19.80	0.93	13.06	11.50	0.88	4.09	3.60	0.88
Ba (ppm)	1804.63	2040.52	1.13	1049.46	753.80	0.72	153.45	1252.50	8.16	1288.08	1568.90	1.22
Rb (ppm)	211.05	175.42	0.83	53.07	83.10	1.57	115.28	143.80	1.25	209.06	178.40	0.85
Sr (ppm)	85.63	139.41	1.63	553.89	258.80	0.47	106.47	177.30	1.67	87.34	104.60	1.20
Zr (ppm)	445.41	577.14	1.30	259.08	240.60	0.93	307.76	338.00	1.10	228.88	245.30	1.07
Y (ppm)	59.49	64.57	1.09	33.26	37.40	1.12	39.43	47.90	1.21	62.96	28.90	0.46
Nb (ppm)	27.66	28.64	1.04	15.12	14.70	0.97	19.94	20.90	1.05	25.50	14.70	0.58
La (ppm)	68.39	86.44	1.26	36.47	30.90	0.85	46.71	48.70	1.04	44.14	46.50	1.05
Ce (ppm)	137.11	190.37	1.39	76.48	64.90	0.85	98.20	99.20	1.01	88.13	89.60	1.02
Nd (ppm)	60.93	88.38	1.45	40.52	32.80	0.81	44.41	46.20	1.04	43.43	36.70	0.85
Sm (ppm)	12.65	18.42	1.46	8.54	7.60	0.89	9.23	10.00	1.08	10.56	7.00	0.66
Eu (ppm)	1.37	2.70	1.97	2.11	1.60	0.76	0.63	1.50	2.39	0.71	0.80	1.13
Gd (ppm)	11.31	14.93	1.32	7.52	7.50	1.00	8.06	9.30	1.15	10.48	5.80	0.55
Dy (ppm)	11.54	13.63	1.18	6.65	7.50	1.13	7.70	9.40	1.22	11.28	5.60	0.50
Er (ppm)	6.22	6.73	1.08	3.44	3.90	1.14	4.14	5.00	1.21	6.28	3.00	0.48
Yb (ppm)	5.54	5.78	1.04	3.02	3.30	1.09	3.72	4.40	1.18	5.55	2.70	0.49



★ Steens Basalt ☆ Andesite ♦ Granitoid

Figure 8.1: Andesite type 1 AFC trends

Trace element diagrams plotted with AFC trends. The small dots along the trend line indicate incremental increases in the ratio (from 1 to 5) of the mass of assimilated to the total mass of magma. The calculated trends use MB09-13 and average granite as the AFC endmembers. The trends were plotted using the “model” function in IgPet 2010.



☆ andesite

☆ Calculated andesite

Figure 8.2: Andesite type 1 AFC comparison

Spider diagrams normalized to chondrites (Sun, 1980) on the left, to MORB (Pearce, 1983) on the right, and to chondrites (Sun and McDonough, 1989). The open red star represents the calculated AFC results.

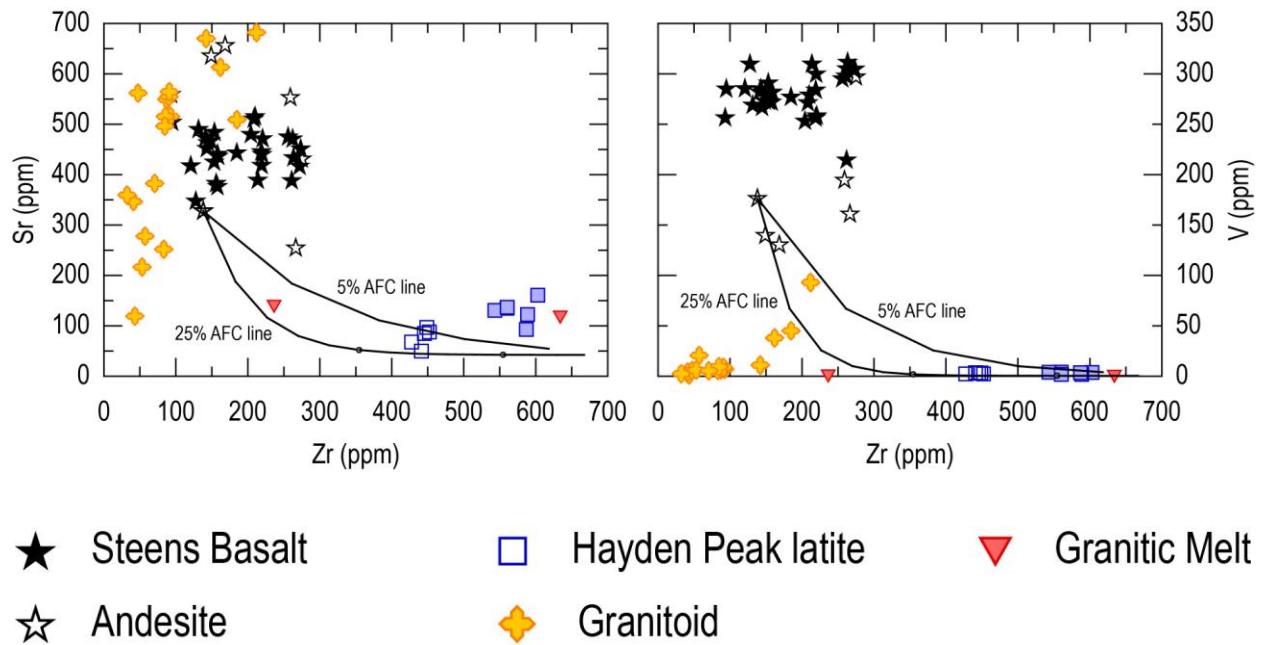
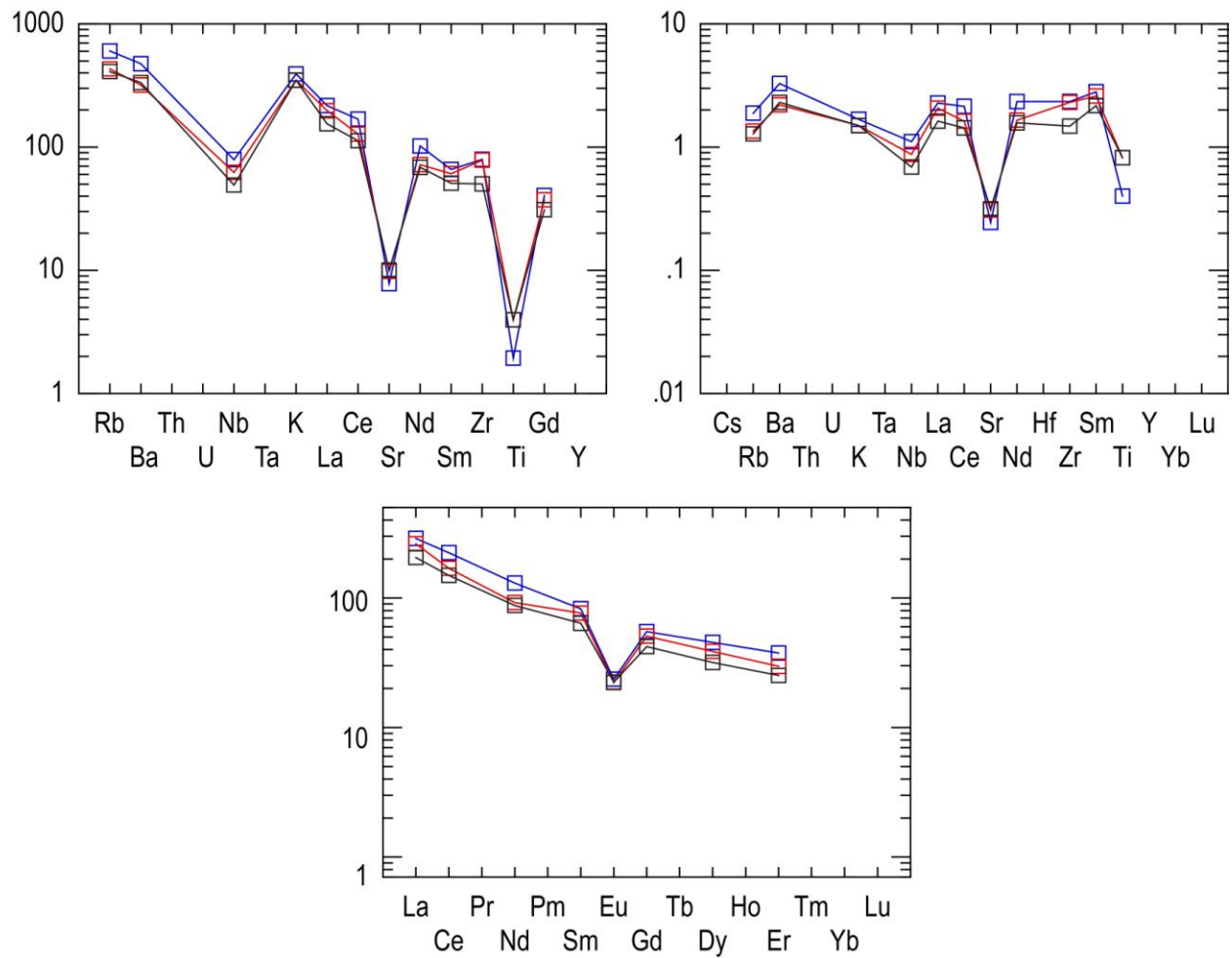


Figure 8.3: Hayden Peak latite AFC trends

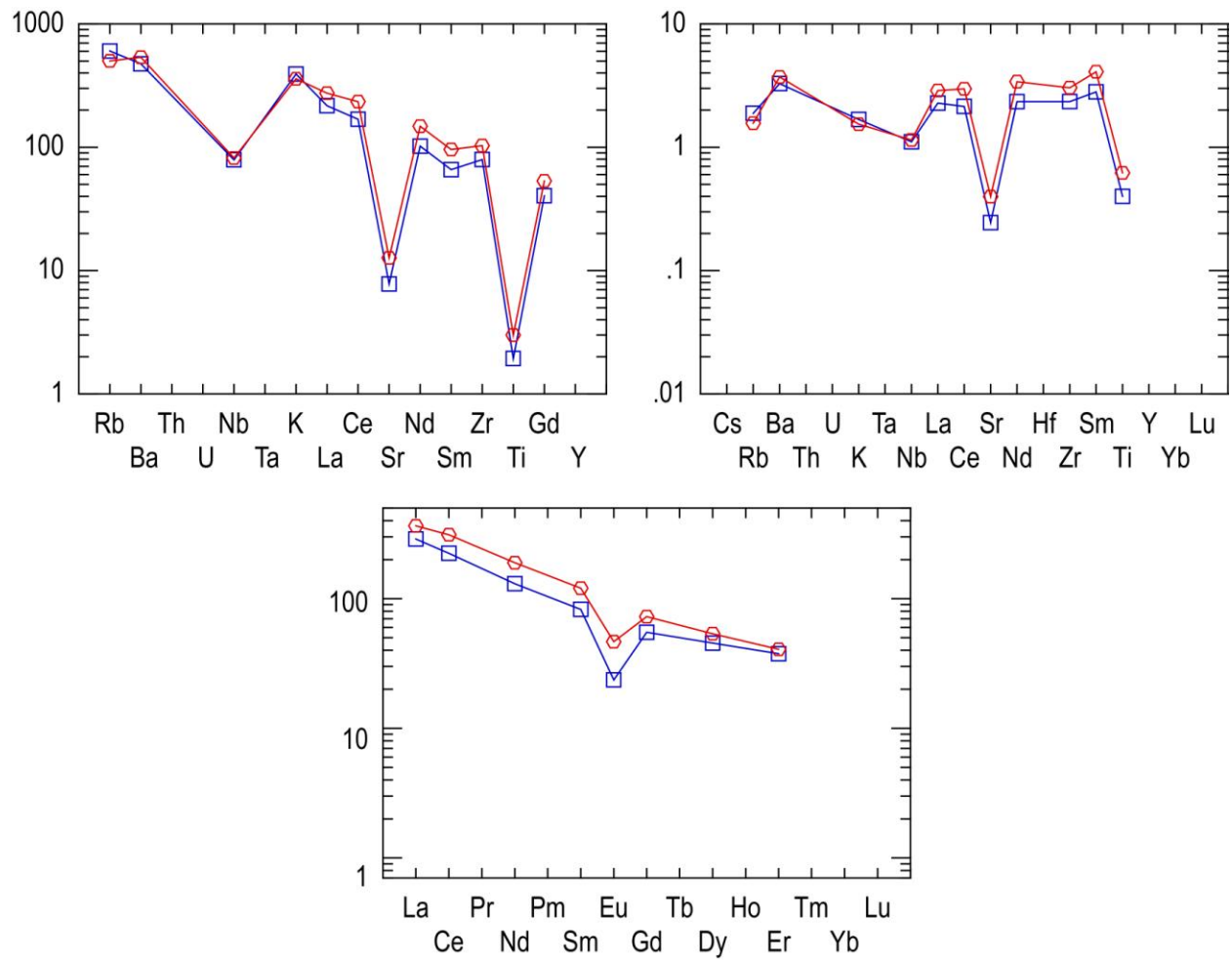
Trace element diagrams plotted with AFC trends. The calculated trends use ZH10-40 and 5 and 25% melt of average granite as the AFC endmembers. The red triangles represent the 5% (~640 ppm Zr) and 20% (~240 ppm Zr) granitoid melt compositions. The trends were plotted using the “model” function in IgPet 2010.



□ Hayden Peak latite
 □ Calculated Hayden Peak latite (5%)
 □ Calculated Hayden Peak latite (25%)

Figure 8.4: Hayden Peak latite AFC comparison

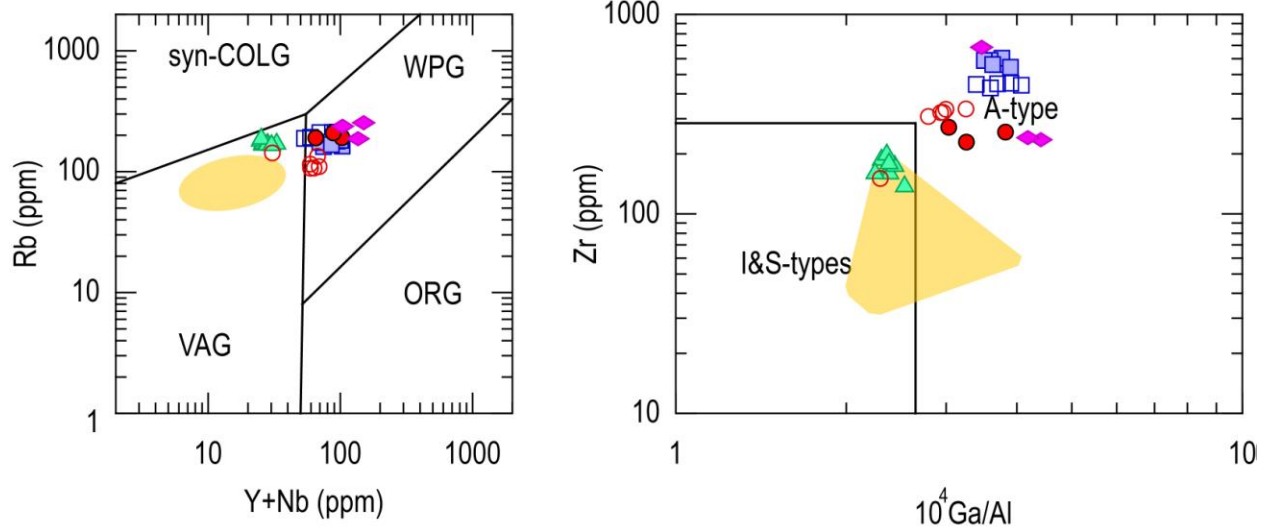
Spider diagrams normalized to chondrites (Sun, 1980) on the left, to upper continental crust (Taylor and McLennan, 1985) on the right, and to chondrites (Sun and McDonough, 1989). The open red (5%) and black (25%) squares represent the calculated AFC results.



□ Hayden Peak latite ◊ Calculated quartz latite parent

Figure 8.5: Quartz latite FC comparison

Spider diagrams normalized to chondrites (Sun, 1980) on the left, to upper continental crust (Taylor and McLennan, 1985) on the right, and to chondrites (Sun and McDonough, 1989). The open red hexagons represent the calculated FC results.



- ★ Steens Basalt
- ★ Olivine rich basalt
- ☆ Andesite
- Hayden Peak latite
- Quartz latite
- △ Silver City rhyolite
- Glass Mountain latite type 1
- Glass Mountain latite type 2
- ◇ Tuff units

Figure 8.6: Granite classification diagrams

Granitoid classification scheme after Pearce et al. (1984) and Whalen et al. (1987). Yellow fields are included that represent the Silver City granite basement material. The Silver City rhyolite falls in the volcanic arc and I/S type granite fields. The Hayden Peak, quartz, and Glass Mountain dacites and rhyolites plot as within plate and A type granite fields. One tuffaceous Tgml latite deposit also plots near the Tsc samples.

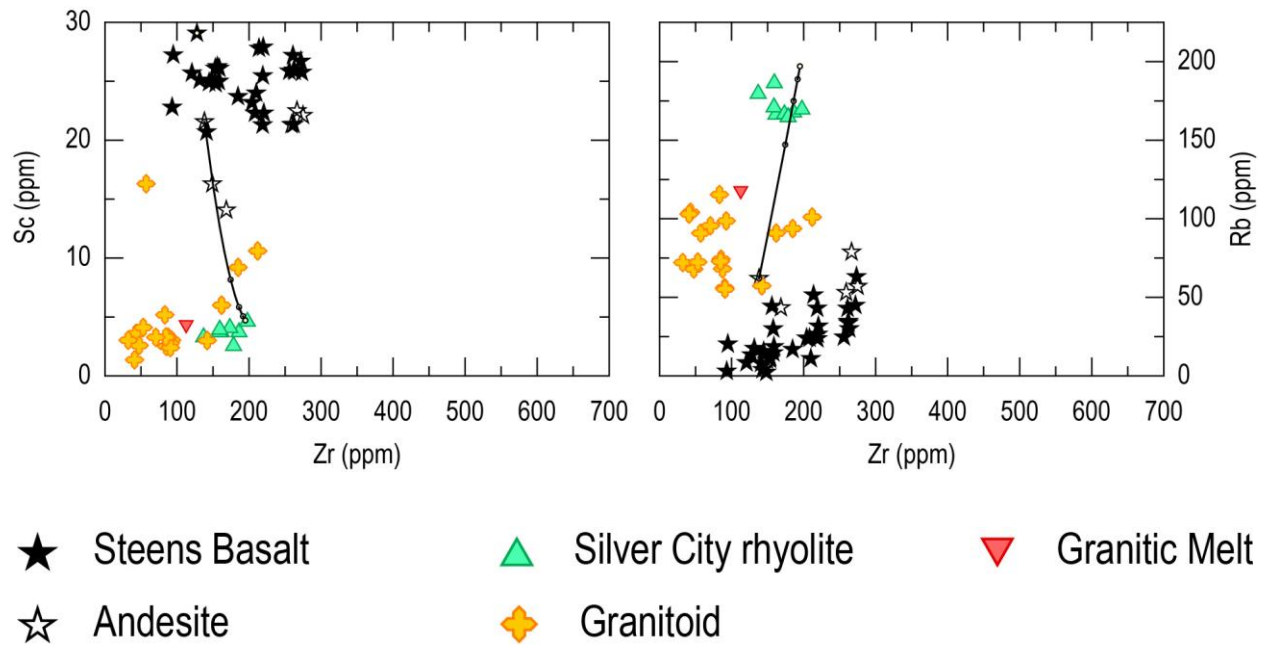
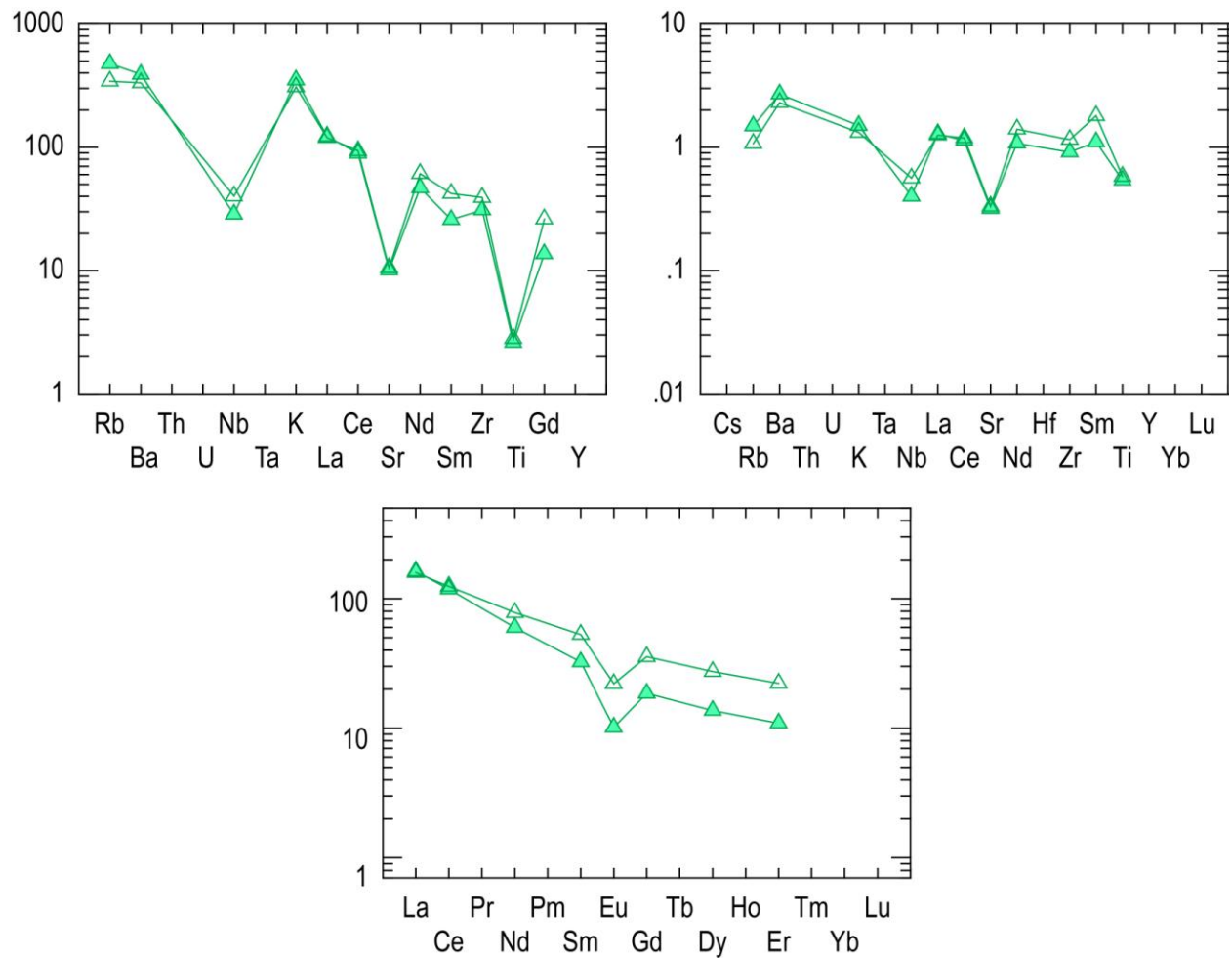


Figure 8.7: Silver City rhyolite AFC trends

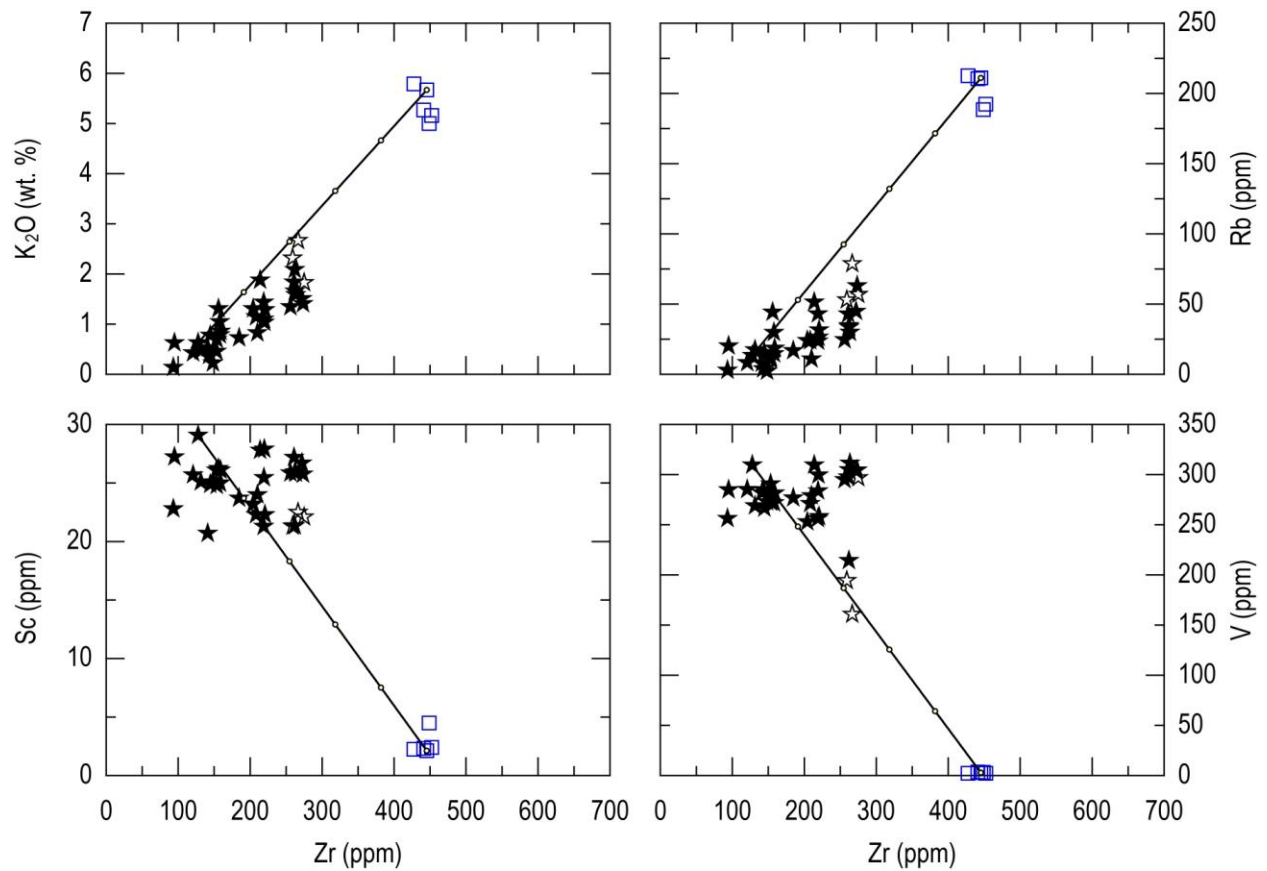
Trace element diagrams plotted with AFC trends. The calculated trends use ZH10-40 and 60% melt of average granite as the AFC endmembers. The small dots along the trend line indicate incremental increases in the ratio (from 1 to 5) of the mass of assimilant to the total mass of magma. The red triangle represents the 60% granitoid melt compositions. The trends were plotted using the “model” function in IgPet 2010.



▲ Silver City rhyolite △ Calculated Silver City rhyolite

Figure 8.8: Silver City rhyolite AFC comparison

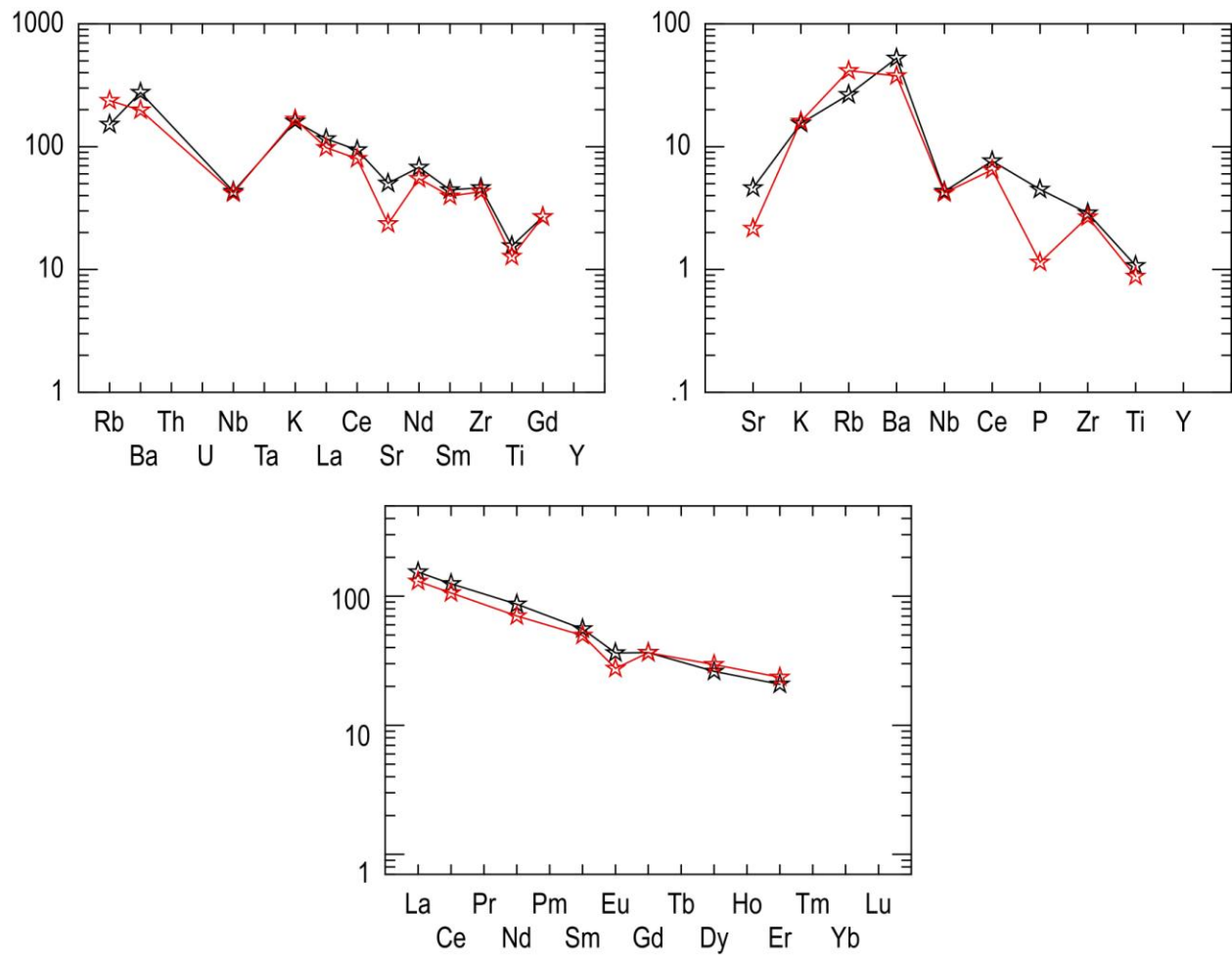
Spider diagrams normalized to chondrites (Sun, 1980) on the left, to upper continental crust (Taylor and McLennan, 1985) on the right, and to chondrites (Sun and McDonough, 1989). The open green triangles represent the calculated AFC results.



★ Steens Basalt ☆ Andesite □ Hayden Peak latite

Figure 8.9: Andesite type 2 mixing trends

Select major and trace element diagrams plotted with the mixing trends to form the andesite type 2 unit (ZH11-6). The endmembers used were ZH11-2 and MB09-13. The small dots along the trend line indicate incremental (20%) increases in the mixing percentages between endmembers. The trends were plotted using the “model” function in IgPet 2010.

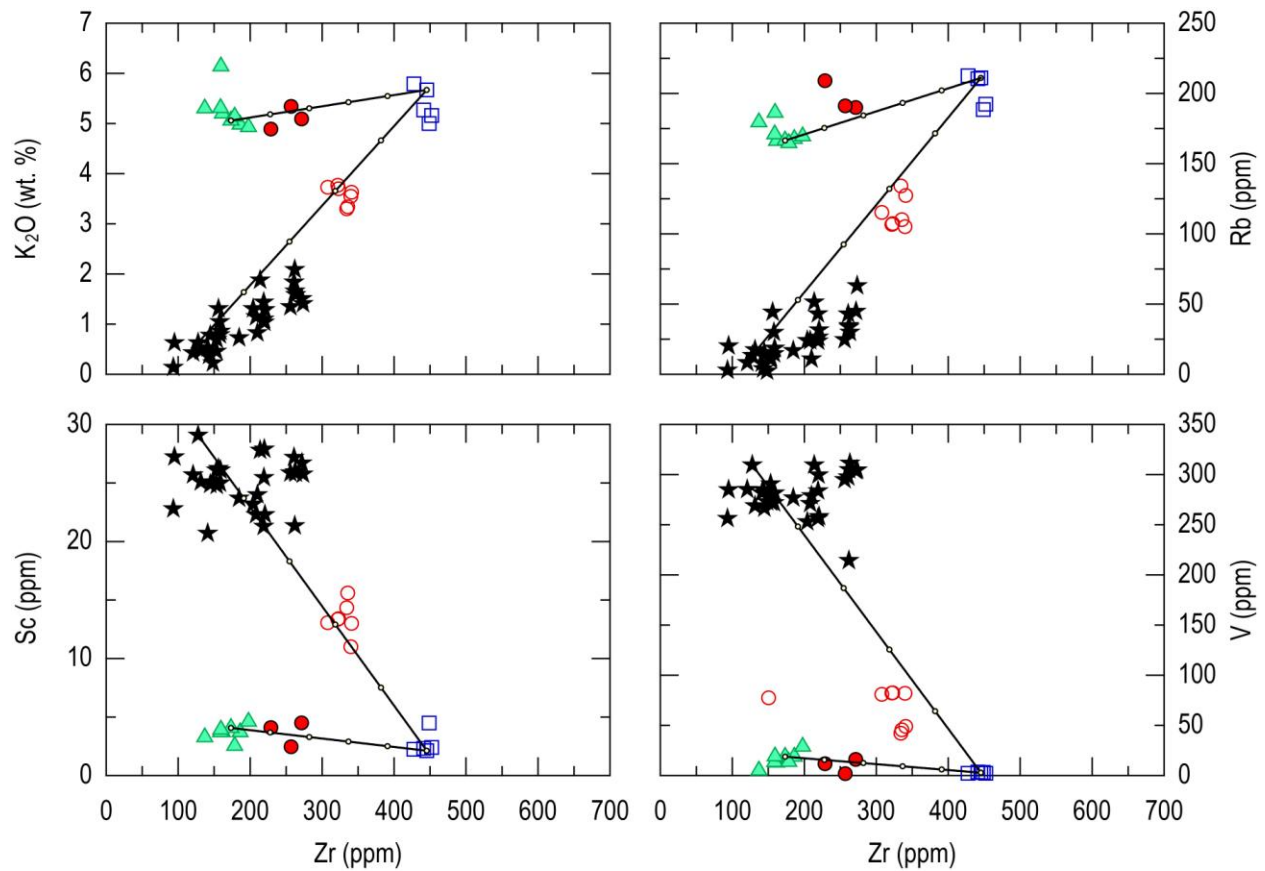


☆ andesite

☆ Calculated andesite

Figure 8.10: Andesite type 2 mixing comparison

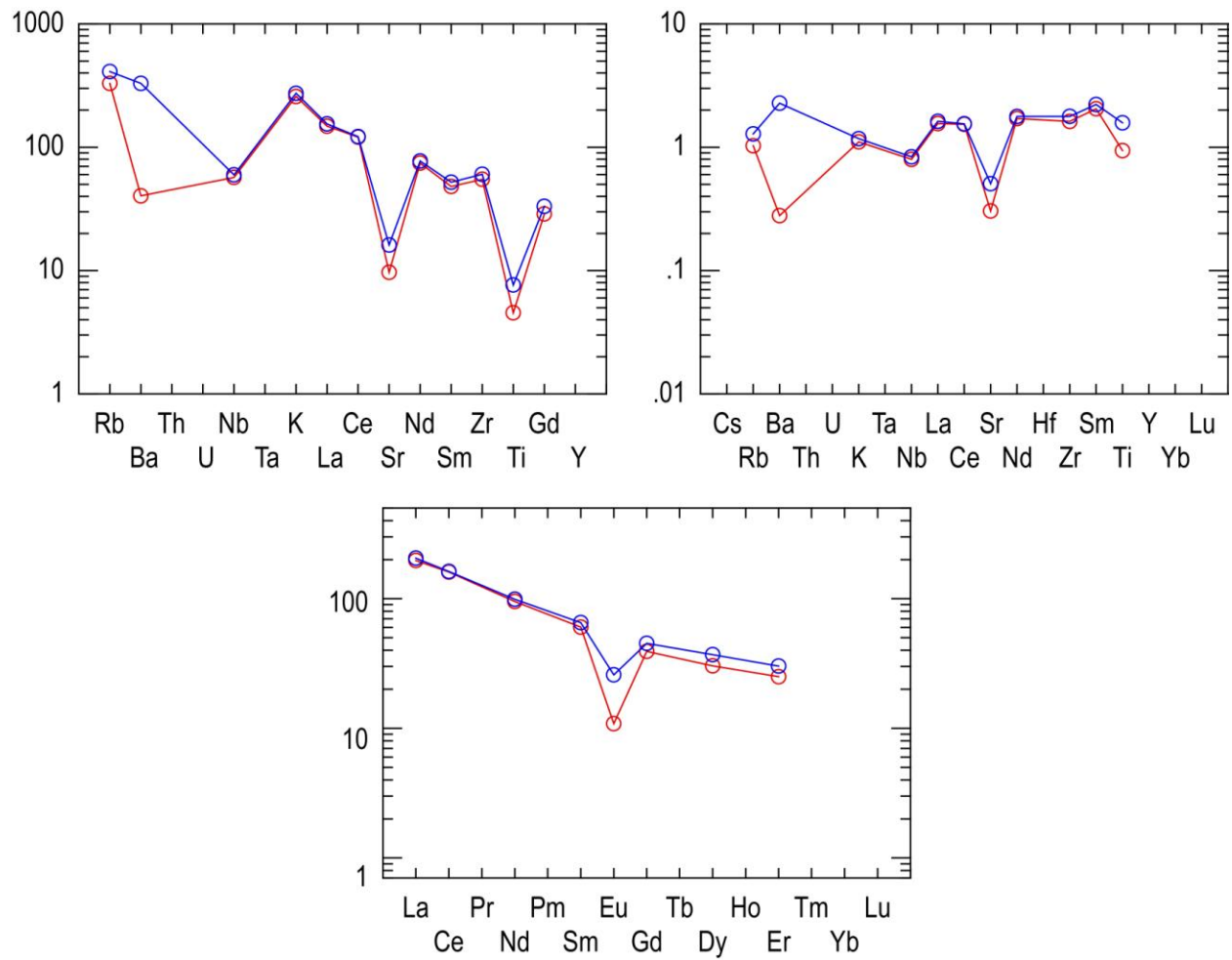
Spider diagrams normalized to chondrites (Sun, 1980) on the left, to MORB (Pearce, 1983) on the right, and to chondrites (Sun and McDonough, 1989). The open red stars represents the calculated mixing results.



- ★ Steens Basalt ▲ Silver City rhyolite ● Glass Mountain rhyolite
- Hayden Peak latite ○ Glass Mountain dacite

Figure 8.11: Glass Mountain dacite and rhyolite mixing trends

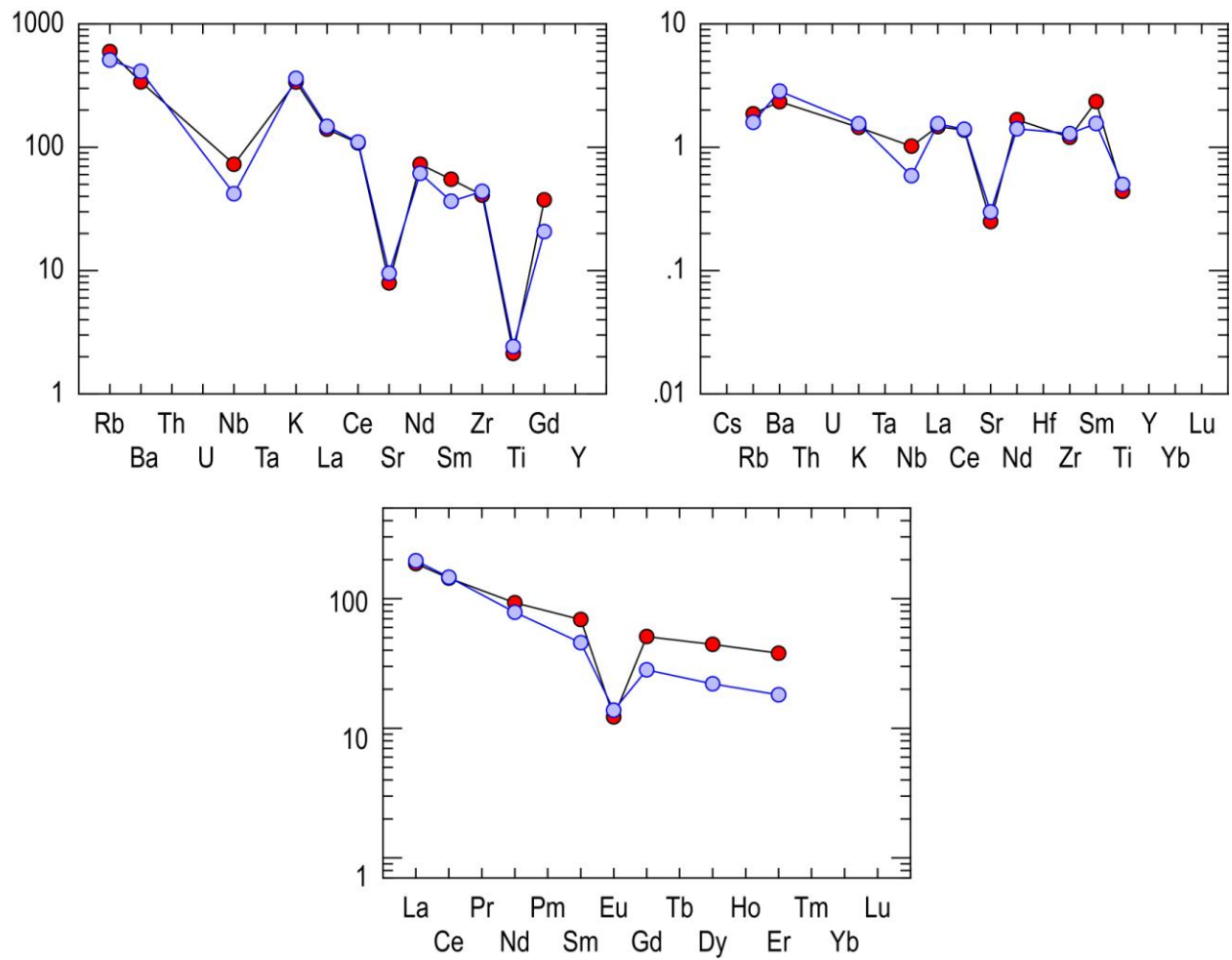
Select major and trace element diagrams plotted with the mixing trends to form the Glass Mountain units. The endmembers used for the dacite samples (open red circles) were ZH11-2 and MB09-13. The endmembers used for the rhyolite samples (solid red circles) were ZH11-2 and ZH10-15. The small dots along the trend line indicate incremental (20%) increases in the mixing percentages between endmembers. The trends were plotted using the “model” function in IgPet 2010.



○ Glass Mountain dacite ○ Calculated Glass Mountain dacite

Figure 8.12: Glass Mountain dacite mixing comparison

Spider diagrams normalized to chondrites (Sun, 1980) on the left, to upper continental crust (Taylor and McLennan, 1985) on the right, and to chondrites (Sun and McDonough, 1989). The open blue circles represent the calculated mixing results.



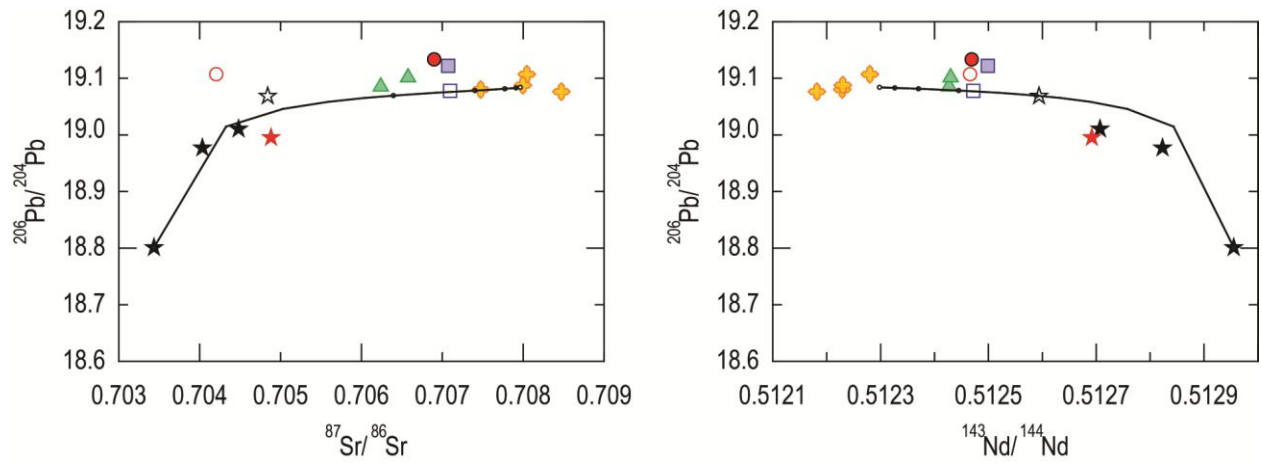
● Glass Mountain rhyolite ● Calculated Glass Mountain rhyolite

Figure 8.13: Glass Mountain rhyolite mixing comparison

Spider diagrams normalized to chondrites (Sun, 1980) on the left, to upper continental crust (Taylor and McLennan, 1985) on the right, and to chondrites (Sun and McDonough, 1989). The solid blue circles represent the calculated mixing results.

Isotope Modeling

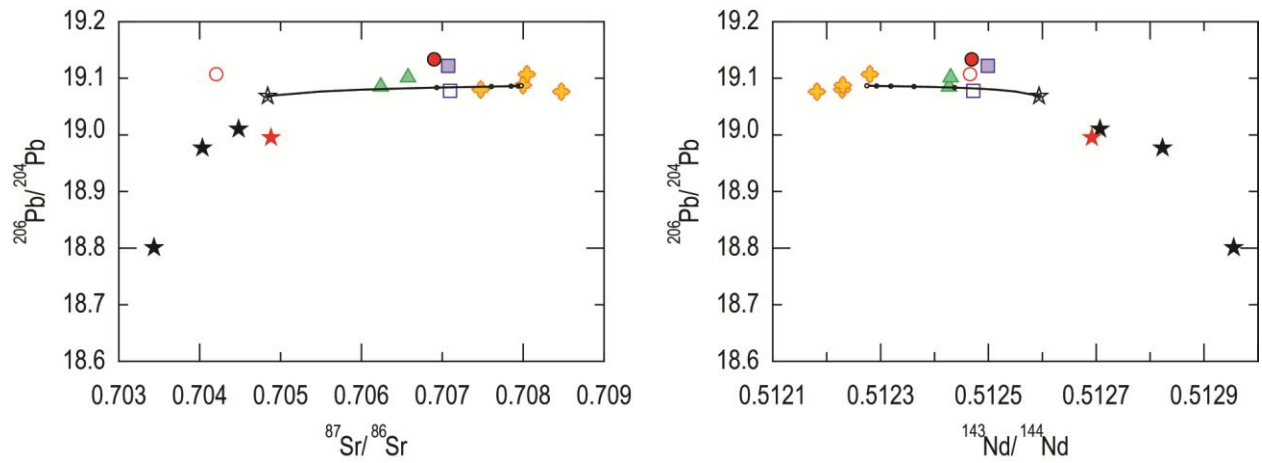
In addition to trace element modeling, the AFC trends associated with the petrogenesis of the andesite type 1, Hayden Peak latite and Silver City rhyolite were plotted on Sr, Nd, and Pb diagrams to help constrain their accuracy. Figure 8.14 shows the AFC trends for the andesite type 1 (ZH10-40) sample on plots of $^{87}\text{Sr}/^{86}\text{Sr}$ vs $^{206}\text{Pb}/^{204}\text{Pb}$ and $^{143}\text{Nd}/^{144}\text{Nd}$ vs $^{206}\text{Pb}/^{204}\text{Pb}$. Like the trace element modeling the trend line indicates the fractional crystallization of a Steens Basalt sample (MB09-13) and assimilation of the average granitoid crust (AvgKg). The trend line falls in close proximity to the actual value of the andesite type 1. Figure 8.15 shows the AFC trend lines for both the Hayden Peak latite and Silver City rhyolite. The AFC trend with andesite type 1 and Silver City granite partial melt endmembers are consistent with the isotopic values of the Hayden Peak latite and Silver City rhyolite samples. The average granitoid 5% and 25% partial melt liquids are represented by the average granite isotopic values in the diagrams. While radiogenic isotopes from the Silver City district confirm the trace element modeling results presented in the previous chapter, the overlap in isotopic values of the intermediate and silicic units makes the trace elements easier to use for modeling purposes.



- | | | |
|-----------------------|------------------------|---------------------------|
| ★ Steens Basalt | □ Hayden Peak latite | ○ Glass Mountain dacite |
| ★ Olivine rich basalt | □ Quartz latite | ● Glass Mountain rhyolite |
| ☆ Andesite | ▲ Silver City rhyolite | ◆ Granitoid |

Figure 8.14: Andesite type 1 isotope modeling

$^{87}\text{Sr}/^{86}\text{Sr}$ vs $^{206}\text{Pb}/^{204}\text{Pb}$ and $^{143}\text{Nd}/^{144}\text{Nd}$ vs $^{206}\text{Pb}/^{204}\text{Pb}$ plots showing the AFC trend line for the andesite type 1 modeling.



- ★ Steens Basalt
- ★ Olivine rich basalt
- ☆ Andesite
- Hayden Peak latite
- Quartz latite
- ▲ Silver City rhyolite
- Glass Mountain dacite
- Glass Mountain rhyolite
- ◆ Granitoid

Figure 8.15: Hayden Peak latite and Silver City rhyolite isotope modeling

$^{87}\text{Sr}/^{86}\text{Sr}$ vs $^{206}\text{Pb}/^{204}\text{Pb}$ and $^{143}\text{Nd}/^{144}\text{Nd}$ vs $^{206}\text{Pb}/^{204}\text{Pb}$ plots showing the AFC trend line for both the Hayden Peak latite and Silver City rhyolite modeling. Note that both samples fall along the single trend line included.

Chapter 9 - Regional Comparison

Previous studies of the Steens Basalt unit in the Silver City district have come to multiple conclusions with regards to the relationship to the Columbia River Basalt (CRB) group. Lindgren (1900), Asher (1968), Bennett and Galbraith (1975), Pansze (1975) determined that while the basalt was temporally similar to the CRB, it was not similar enough chemically or physically to be included in the CRB. Later work by Bonnicksen (1983) speculated that the Steens Basalt could be a southern extension of the CRB Innaha basalt. However, more recent work (Carlson and Hart, 1987; Cupp, 1989; Camp and Ross, 2009) and this study has concluded that the Silver City district basalts are locally erupted Steens Basalt. The Silver City district samples overlap regional Steens Basalt samples in these classifications as well as in normalized chondrite and MORB spider diagrams of Sun (1980) and Pearce (1980) as also seen in Figure 9.1. The fact that the Silver City district mafic samples are similar to and consistently plot with the Steens Basalt, except for the olivine basalt, is evidence to support the interpretation that these lava flows (except the olivine basalt) should be considered Steens Basalt.

In order to better understand the petrogenesis of the Silver City district silicic volcanism and their tectonomagmatic affinity, they have been compared to other regional mid-Miocene silicic volcanic systems. Included in the comparison are the ~16.7 Ma Santa Rosa-Calico volcanic field (Brueseke and Hart, 2009) and the 16.7 – 15.8 Ma Jarbidge Rhyolite (Calliccoat, 2010) from the northern Great Basin as well as the 12.7 – 10.5 Ma central Snake River Plain volcanics (Cathey and Nash, 2004). The peraluminous and A-type nature of the Hayden Peak latite, quartz latite and Glass Mountain rhyolite and dacite units is similar to all three of the regional silicics. However, geochemical differences can be seen between the central Snake River Plain and the Silver City district, Jarbidge Rhyolite, and Santa Rosa-Calico volcanic systems. As seen in Figure 9.2 the central Snake River Plain have higher MgO concentrations than the other three volcanic systems. Trace elements are also useful for comparison as the Silver City district often overlaps with the Jarbidge Rhyolite. Figure 9.2 also shows the lower Nb concentrations for the Silver City district that overlap the Santa Rosa-Calico and Jarbidge Rhyolite and are markedly different from the central Snake River Plain. An important petrogenetic comparison is the Rb/Nb ratio, which provides insight into basaltic and crustal material inputs with samples

derived from crustal material having higher Rb/Nb ratios (Pearce et al., 1984; Ayalew and Yirgu, 2003). The central Snake River Plain rhyolites have low ratios and indicate a source dominated by basaltic material whereas the Silver City district and Jarbidge Rhyolite have higher ratios and are proposed to have been formed via mid to upper crustal melting of quartzofeldspathic crustal with limited basaltic input (Brueseke and Hart, 2008; Calliccoat, 2010). Silver City district rhyolite's Rb/Nb ratios range from 4.97 - 19.24, which are higher than the central Snake River Plain and similar to the Jarbidge Rhyolite and Santa Rosa-Calico as seen in Figure 9.2. These intermediate values are consistent with the petrogenetic models that show upper crustal melting associated with some basaltic components involved. The major and trace element analysis indicates that the petrogenesis of the Silver City district are more closely related to the petrogenesis of the Jarbidge Rhyolite and Santa Rosa-Calico and were formed via mid to upper crustal melting of the granitic crust beneath Silver City along with varying degrees of mafic input.

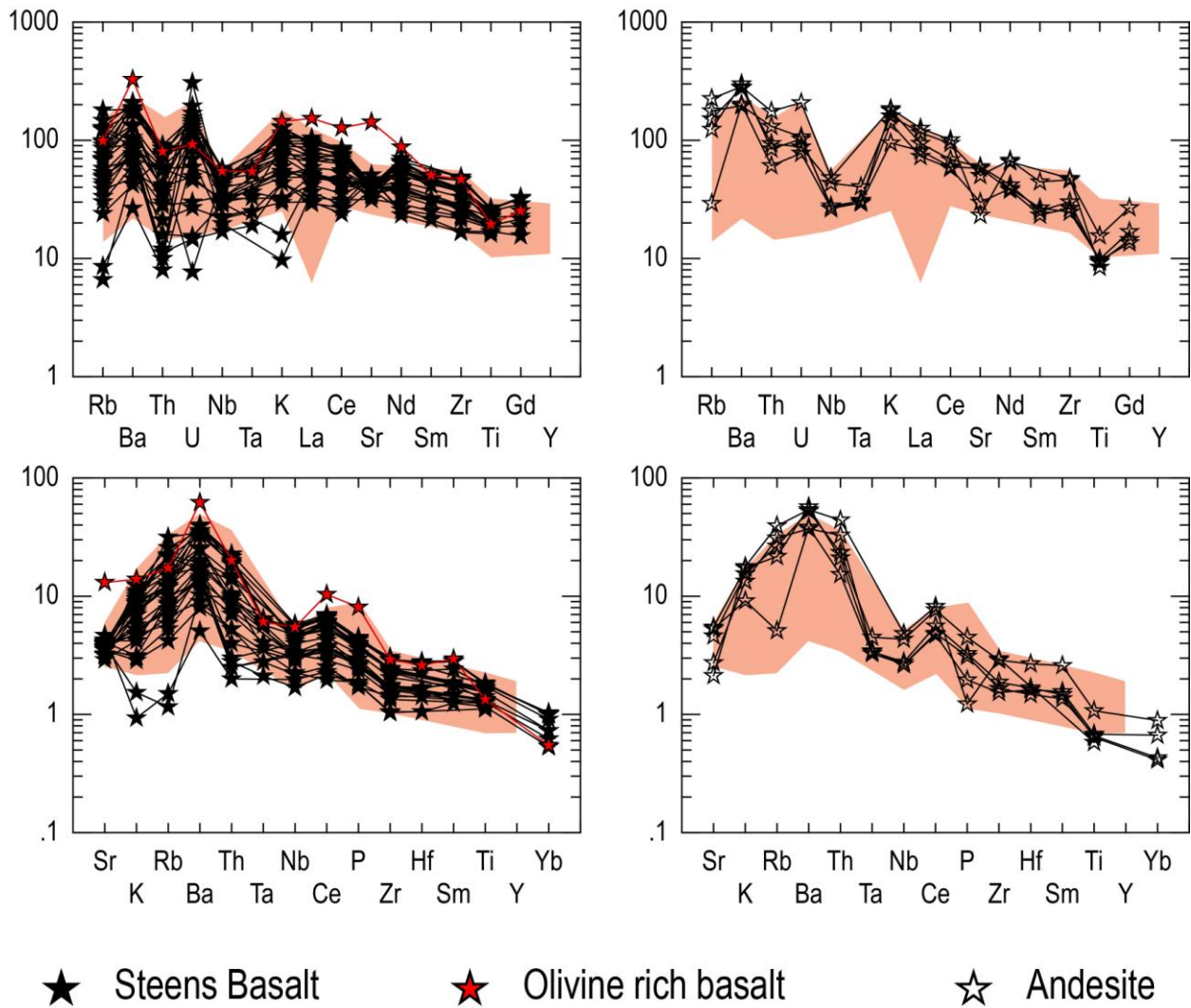


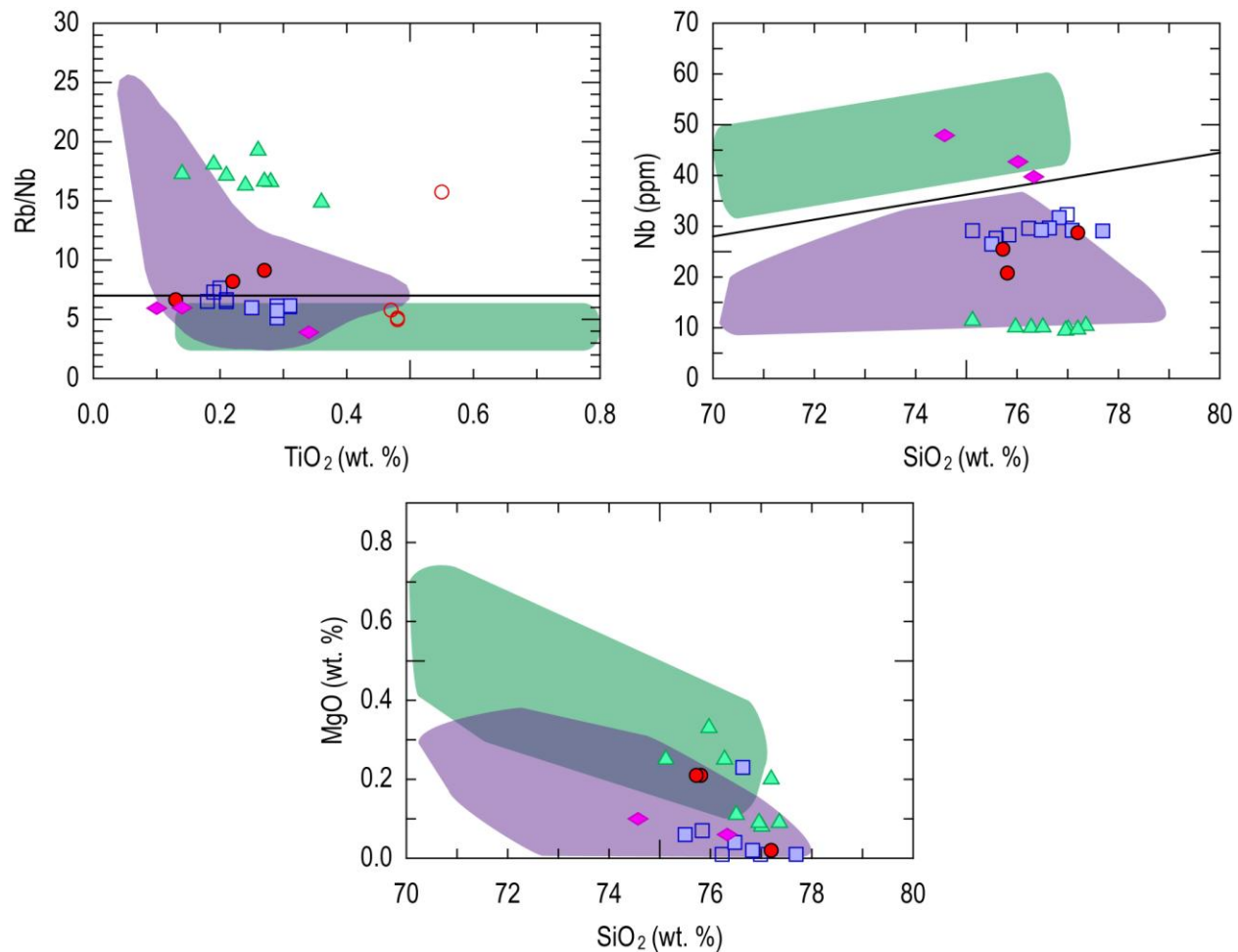
Figure 9.1: Steens Basalt comparison

Top - Spider diagrams normalized to chondrites (Sun, 1980) with basalt and basaltic andesites on the left and andesites on the right.

Bottom - Spider diagrams normalized to MORB (Pearce, 1983) with basalt and basaltic andesites on the left and andesites on the right. The Silver City district basalts follow similar enrichment patterns as the regional Steens Basalt.

Figure 9.2: Regional silicic comparison

Next page - SiO_2 vs Rb/Nb, SiO_2 vs Nb, and SiO_2 vs MgO showing the regional comparison to the central Snake River Plain after Cathey and Nash (2004) in the green field and the Santa Rosa-Calico volcanic field after Brueseke and Hart (2009) and Jarbidge Rhyolite after Calliccoat (2010) in the purple field. The Silver City district volcanic samples overlap with the Santa Rosa-Calico and Jarbidge Rhyolite consistently and showing lower MgO and Nb and higher Rb/Nb ratios than the central Snake River Plain volcanics. The range of Rb/Nb ratio seen in the Silver City district is a measure of the amount of basaltic input involved in the magma formation. Plots such as these suggest that the Silver City district volcanics were formed by mid to upper crustal melting of quartzofeldspathic basement, similar to what has been proposed for the Santa Rosa-Calico and Jarbidge Rhyolite.



- Hayden Peak latite
 - Quartz latite
- ▲ Silver City rhyolite
 - ◆ Tuff units
- Glass Mountain dacite
 - Glass Mountain rhyolite

Chapter 10 - Results

Physical Characteristics

The Silver City district volcanic complex shows evidence that the volcanic units were derived and erupted from within the district. The majority of the mafic volcanic deposits in the Silver City district are the locally erupted Steens Basalt that overlies the granitoid basement and are found throughout the Silver City district. The basalt flows were erupted as fissure eruptions from local dikes and small vent eruptions. Some basaltic feeder dikes have been traced into overlying flow layers (Piper and Laney, 1926; and Bennett and Galbraith, 1975). In addition to the fissure eruptions, local vents have been identified at Black Warrior near Flint, south of the Silver City district (Piper and Laney, 1926; Bennett and Galbraith, 1975; W.K. Hart, personal communication).

The intermediate and silicic samples that overlie the Steens Basalt are similarly erupted from local vents in the Silver City district. The majority of intermediate and silicic units were deposited as lava flows with some ash flow tuffs found in the area. The area has numerous vents including Hayden Peak (Hayden Peak latite), Sawpit Peak (Silver City rhyolite), and Glass Mountain (Glass Mountain dacite). Shallow intrusive deposits are also found near Slacks Mountain, near the former site of Ruby City and throughout the district as dike exposures. The intermediate and silicic units are often found overlapping each other in varying sequences.

Petrography

The basalt to basaltic andesite Steens Basalt have abundant laths of plagioclase with olivine and Fe-oxide phenocrysts. Some the samples also contain larger plagioclase crystals with disequilibrium textures such as sieve and resorbition textures. One flow of olivine rich basalt contains abundant olivine phenocrysts in a matrix of felty plagioclase microcrysts. The olivine phenocrysts have undergone resorbition and secondary alteration along fractures in individual grains (Figure 4.3 D & E). The andesite samples have more disequilibria plagioclase phenocrysts. The presence of these textures is likely evidence magma of interaction with the Silver City granite basement.

The Silver City rhyolite, Hayden Peak latite and quartz latite samples all contain a very fine grained to aphanitic groundmass with disequilibria quartz and plagioclase phenocrysts. The quartz phenocrysts are often embayed and contain spherulite rims around phenocrysts grains and the plagioclase are resorbed and sieved. The Silver City rhyolite also contains altered and resorbed clinopyroxene phenocrysts that are not present in the Hayden Peak latite and quartz latite. The disequilibrium textures found in thin section indicate a role for open-system processes (e.g. crustal assimilation, magma mixing/hybridization) in the generation of these magmas (Stimac and Pearce, 1992; Johnson and Grunder, 2000; Seaman, 2000; Streck, 2008).

The Glass Mountain dacite unit has abundant glomeroporphyritic pyroxene clots, embayed quartz, skeletal and resorbed plagioclase and entrapped xenolith material that shows evidence of mixing between mafic and silicic magmas (Seaman, 2000). Xenoliths, plagioclase overgrowth and clinopyroxene coronas around plagioclase grains are all present in the Glass Mountain dacite and are common in intermediate rocks formed through mixing of mafic and silicic magma bodies (Johnson and Grunder, 2000; Brueseke and Hart, 2009). The dacite matrix is commonly aphanitic with micro laths of plagioclase and mafic xenoliths which contain larger skeletal plagioclase phenocrysts. The Glass Mountain rhyolite samples do not include the same mafic magma mixing textures that are seen in the dacite samples. The rhyolite has aphanitic groundmass with coarse plagioclase phenocrysts with only slight resorbtion, myrmekitic texture and secondary alteration to muscovite. The plagioclase textures point to an open system formation of the rhyolitic magma (Streck, 2008).

Trace Element and Radiogenic Isotope Modeling

The range of NCI values (Figure 5.21) seen in the Silver City district samples indicate that the silicic units underwent varying degrees of crustal and mafic interaction in their petrogenesis. The Silver City rhyolite has the highest NCI values which indicates a greater input of crustal material with the andesite type 1 and Hayden Peak latite having lower NCI values indicating less crustal interaction and more mafic input. Trace element modeling agrees with what is indicated by the NCI values with the andesite type 1 forming through fractional crystallization of basaltic magma and assimilation of small amounts of granitic crust. The

Hayden Peak latite and Silver City rhyolite have been modeled using similar assimilation and fractional crystallization formation with the Silver City rhyolite having more crustal input.

After formation of two silicic magma bodies the rest of the intermediate and silicic units in the Silver City district can be modeled through simple magma mixing with two endmembers. The andesite type 2 and Glass Mountain dacite have basaltic and silicic endmembers (Hayden Peak latite) while the Glass Mountain Rhyolite has the two silicic (Hayden Peak latite and Silver City rhyolite) as the mixing endmembers. Normalized multi-element diagrams show consistent patterns and enrichment levels for all of the Silver City district samples and their modeled magmas.

Oxygen Isotope

The silicic units in the Silver City district have normal $\delta^{18}\text{O}$ values (7‰ - 10‰) values for silicic igneous rocks (Taylor, 1968). The majority of the Silver City district silicic volcanism samples also show that the volcanics fall within the normal range ($\delta^{18}\text{O}_{\text{feldspar}} < \delta^{18}\text{O}_{\text{quartz}}$ and $\Delta_{\text{quartz} - \text{feldspar}} < 2\%$) for unaltered rocks (Taylor, 1979). The samples with normal value ranges indicate a lack of interaction with hydrothermally altered crust or sedimentary material. The silicic and granitoid samples that fall outside of the normal values have lower $\delta^{18}\text{O}_{\text{feldspar}}$ values that indicate the samples have undergone post emplacement alteration by locally active hydrothermal fluid. The precious metal mineralization that is present in the Silver City district, confirms the existence of a post-volcanic epithermal mineralization system. One sample that has slightly higher $\delta^{18}\text{O}_{\text{feldspar}}$ appears to have experienced a low temperature hydrothermal event (Taylor, 1978). Like younger (<12 Ma) rhyolites from the western Snake River plain (Boroughs et al., 2005), all Silver City district rhyolites have oxygen isotope values ($\delta^{18}\text{O}_{\text{quartz}} > 8.9\%$ and $\delta^{18}\text{O}_{\text{feldspar}} > 7.0\%$). This lack of low oxygen samples indicates that local crust (e.g. Silver City granite) was not hydrothermally altered prior to magma generation and the general overlap between Silver City granite and Silver City district rhyolites supports the trace element and radiogenic isotope constraints that melting of Silver City granite lead to local rhyolite production.

Geochronology

Previous work has dated the Silver City district volcanism to between 16.6 and 14 Ma (Bonnichsen and Godchaux, 2006). While new geochronological data of the volcanic rocks from this project is still pending, two new $^{40}\text{Ar}/^{39}\text{Ar}$ age dates have been analyzed as part of a companion research project. In addition to analyzing the Silver City district mineralization, Aseto (2012) has analyzed one basalt and one rhyolite sample from the Silver City district. Plagioclase grains from the basalt were analyzed and produced $^{40}\text{Ar}/^{39}\text{Ar}$ ages of 16.08 ± 0.18 Ma, and sanidine grains from the rhyolite produced ages of 15.94 ± 0.10 Ma. Analysis of adularia grains from the mineralization that is hosted in the Silver City district volcanic units produced ages between 16.08 ± 0.08 and 15.37 ± 0.06 Ma (Aseto, 2012). These age dates provide some constraints into the volcanic temporal history of the district. While Bonnichsen and Godchaux (2006) provided a date range that extended to 14 Ma, the presence of the youngest epithermal mineralization at 15.37 Ma is evidence that Silver City district volcanism ended prior to 15.4 Ma.

Regional Comparison

The Silver City district volcanic systems includes local eruptions of Steens Basalt that are chemically similar and were effusively erupted contemporaneous to the regional Steens Basalt. The basalt samples from the Silver City district overlap in major, trace and rare earth element geochemistry and maintain similar enrichment patterns in normalized multi-element diagrams.

When compared to other silicic volcanic systems in the region the Silver City district samples are closely related to the Santa Rosa-Calico volcanic field and the Jarbidge Rhyolite. The Silver City district samples have lower Nb and MgO concentrations and slightly higher Rb/Nb ratios similar to the Santa Rosa-Calico volcanics and Jarbidge Rhyolite. These systems have both been recently studied in depth and have a probable petrogenesis associated with mid to upper crustal melting of quartzofeldspathic rocks that is similar to the proposed petrogenesis of the Silver City rhyolite district (Brueseke and Hart, 2009; and Calliccoat, 2010). Trace element modeling of the intermediate and silicic units in Silver City indicates a formation through melting and assimilation of upper crustal silicic material and not melting of underplated basalt that can be seen in the central Snake River Plain.

Chapter 11 - Summary

The emergence of the Yellowstone hotspot coupled with widespread extensional tectonism in the mid-Miocene, initiated a period of widespread dominantly bimodal basalt-rhyolite volcanism across the northern Great Basin and Oregon Plateau. The Owyhee Mountains of southwestern Idaho provide a good area to observe the effects of the volcanism in the region. The region in and around the Silver City mining district contains a volcanic suite that spans a continuous compositional range from basalts to rhyolites.

New $^{40}\text{Ar}/^{39}\text{Ar}$ age data suggests that volcanism in the Silver City district occurred over a brief period of time (less than 1.2 Ma) and was accompanied by a period of epithermal precious metal mineralization. The volcanism began with fissure-fed local eruptions of Steens Basalt that was deposited on top of exposed Cretaceous granitoid. Overlaying the basalt is a thick package (up to 550 m) of intermediate and rhyolitic eruptive products that were also erupted from local vents. The silicic package (above 65 wt. % SiO_2), previously identified as the Silver City rhyolite, has been separated into five distinct units: Silver City rhyolite, Hayden Peak latite, quartz latite, and Glass Mountain dacite, Glass Mountain rhyolite, that are characterized by different evolutionary histories.

Petrographic analysis shows evidence of disequilibrium textures in olivine, feldspar, and quartz phenocrysts including skeletal plagioclase with overgrowth rims in andesite type 1, altered clinopyroxene in the Silver City rhyolite. Additionally, thin sections of the Glass Mountain dacite samples contain entrapped xenoliths that are typical of mixing between distinct magmatic bodies. The thin section textures are evidence of open system processes such as assimilation and magma mixing.

Petrogenesis of the local Steens Basalt is consistent with previous petrogenetic determinations of melting of depleted mantle with limited subduction and crustal contamination signatures (Norman and Leeman, 1989).

Trace element and radiogenic isotope geochemistry can be used to differentiate the distinct silicic units that are found in the Silver City district. Particularly Zr concentrations that show minimal overlap between the silicic units. Trace element modeling is most consistent with the intermediate and silicic units forming by mid to upper crustal melting and assimilation of

granitoid basement, as well as subsequent mixing between mafic and silicic magma bodies. The partial melting and assimilation in the petrogenesis of the intermediate and silicic units is also consistent with the crustal component findings of Norman and Leeman (1989). Trace element modeling results are supported by Sr-Nd-Pb data and modeling, as well as O isotope constraints.

Bulk geochemistry and petrogenetic modeling show that the Silver City district silicic volcanism is petrogenetically similar to the mid-Miocene Santa Rosa Calico volcanic field and the Jarbidge Rhyolite. Both of those volcanic systems have been suggested to form via mid to upper crustal melting of quartzofeldspathic rocks, which trace element modeling indicates is likely the probable petrogenetic conditions for the formation of the Silver City district volcanic system.

Chapter 12 - Suggested Future Work

A better understanding of the mid-Miocene volcanic system in the Owyhee Mountains can be improved upon by the continuation of new $^{40}\text{Ar}/^{39}\text{Ar}$ geochronology that is currently underway. The timing of volcanism is broadly constrained and can be improved by obtaining new age dates.

Detailed field mapping can also benefit the understanding of the volcanic system. Previous workers have created geologic maps that address the local vents and potential eruptive centers. However, with the differentiation of multiple silicic units an updated geologic map would be beneficial.

This region can benefit from a more in depth geochemical study of the Cretaceous granitoid basement, metamorphic exposures and the tuff of Flint Creek deposits. This study only addressed a small sample set of the granitoid. Further geochemical and isotopic analysis would be beneficial to understanding the complete relationship between the Silver City granitoid and the southern extension of the Idaho batholith. Additionally, further study of the metamorphic basement exposures found south of Silver City district near Flint and South Mountain could allow for new geochronology and geochemistry to better understand the role of the metamorphic basement in the development of volcanic systems in the Owyhee Mountains, ID. The tuff of Flint Creek was not address in the petrogenetic modeling and provides the opportunity for further analysis to identify if the tuff is locally or regionally derived and what role the tuff plays in the volcanic history of the Silver City district.

References

- Aseto, C.O., 2012, Geology, Geochemistry and Geochronology of the mid-Miocene, Low-Sulfidation Epithermal Gold-Silver Ores on War Eagle Mountain, Silver City District, Idaho [Master Thesis]: Auburn University.
- Aseto, C.O., Saunders, J.A., Hames, W.E., and Brueseke, M.E., 2011, Geochronology of gold-silver epithermal mineralization on War Eagle Mountain and contiguous mines in the Silver City district, Idaho: Abstracts with Programs - Geological Society of America, v. 43, no. 2, p. 28.
- Asher, R.R., 1968, Geology and mineral resources of a portion of the Silver City region, Owyhee County, Idaho: Pamphlet - Idaho Bureau of Mines and Geology, v. P-138.
- Ayalew, D., and Yirgu, G., 2003, Crustal contribution to the genesis of Ethiopian Plateau rhyolitic ignimbrites; basalt and rhyolite geochemical provinciality: Journal of the Geological Society of London, v. 160, Part 1, p. 47-56.
- Bachmann, O., Dungan, M.A., and Lipman, P.W., 2002, The Fish Canyon magma body, San Juan volcanic field, Colorado; rejuvenation and eruption of an upper-crustal batholith: Journal of Petrology, v. 43, no. 8, p. 1469-1503.
- Benford, B., Crowley, J., Schmitz, M., Northrup, C.J., and Tikoff, B., 2010, Mesozoic magmatism and deformation in the northern Owyhee Mountains, Idaho; implications for along-zone variations for the western Idaho shear zone: Lithosphere, v. 2, no. 2, p. 93-118.
- Bennett, E.H.,II, 1976, Reconnaissance geology and geochemistry of the South Mountain - Juniper Mountain region, Owyhee County, Idaho: Pamphlet - Idaho Bureau of Mines and Geology, v. P-166.
- Bennett, E.H.,II, and Galbraith, J.H., 1975, Reconnaissance geology and geochemistry of the Silver City-South Mountain region, Owyhee County, Idaho: Pamphlet - Idaho Bureau of Mines and Geology, v. P-162.
- Bonnichsen, B., 1983, Epithermal gold and silver deposits, Silver City-De Lamar District, Idaho: Technical Report – Idaho Bureau of Mines and Geology, Department of Lands, v. 83-4.
- Bonnichsen, B., and Godchaux, M.M., 2006, Geologic map of the Murphy 30 X 60 Quadrangle, Ada, Canyon, Elmore, and Owyhee Counties, Idaho: United States, Idaho Geological Survey: Moscow, ID, United States.
- Bonnichsen, B., Leeman, W.P., Honjo, N., McIntosh, W.C., and Godchaux, M.M., 2008, Miocene silicic volcanism in southwestern Idaho; geochronology, geochemistry, and

- evolution of the central Snake River Plain: *Bulletin of Volcanology*, v. 70, no. 3, p. 315-342.
- Boroughs, S., Wolff, J., Bonnicksen, B., Godchaux, M., and Larson, P., 2005, Large-volume, low- $\delta^{18}\text{O}$ rhyolites of the central Snake River plain, Idaho, USA: *Geology*, v. 33, no. 10, p. 821-824.
- Brueseke, M.E., and Hart, W.K., 2008, Geology and petrology of the mid-Miocene Santa Rosa-Calico volcanic field, northern Nevada, Nevada Bureau of Mines and Geology, Bulletin 113.
- Brueseke, M.E., and Hart, W.K., 2009, Intermediate composition magma production in an intracontinental setting; unusual andesites and dacites of the mid-Miocene Santa Rosa-Calico volcanic field, northern Nevada: *Journal of Volcanology and Geothermal Research*, v. 188, no. 1-3, p. 197-213.
- Brueseke, M.E., Heizler, M.T., Hart, W.K., and Mertzman, S.A., 2007, Distribution and geochronology of Oregon Plateau (U.S.A.) flood basalt volcanism; the Steens Basalt revisited: *Journal of Volcanology and Geothermal Research*, v. 161, no. 3, p. 187-214.
- Callicoat, J., 2010, Significance of Mid-Miocene Volcanism in Northeast Nevada: Petrographic, Chemical, Isotopic, and Temporal Importance of the Jarbidge Rhyolite [Master Thesis]: Kansas State University.
- Callicoat, J., and Brueseke, M.E., 2009, Mid-Miocene volcanism in northeast Nevada; spatial, chemical, and chronologic significance of the Jarbidge Rhyolite: Abstracts with Programs - Geological Society of America, v. 41, no. 7, p. 298.
- Camp, V.E., and Ross, M.E., 2004, Mantle dynamics and genesis of mafic magmatism in the intermontane Pacific Northwest: *Journal of Geophysical Research*, v. 109, no. B08204 DOI:10.1029/2003JB002838.
- Camp, V.E., and Ross, M.E., 2009, Regional synthesis of Steens Basalt, Columbia River Basalt Group: Abstracts with Programs - Geological Society of America, v. 41, no. 7, p. 225.
- Camp, V.E., Ross, M.E., and Hanson, W.E., 2003, Genesis of flood basalts and Basin and Range volcanic rocks from Steens Mountain to the Malheur River gorge, Oregon: *Geological Society of America Bulletin*, v. 115, no. 1, p. 105-128.
- Camp, V.E., Ross, M.E., Duncan, R.A., Jarboe, N.A., Coe, R.S., and Johnson, J.A., in press, The Steens Basalt: Earliest lavas of the Columbian River Basalt Group: Special Paper – Geological Society of America
- Carlson, R.W., and Hart, W.K., 1987, Crustal genesis on the Oregon Plateau: *Journal of Geophysical Research*, v. 92, p. 6191-6206.

- Christiansen, R.L., Foulger, G.R., and Evans, J.R., 2002, Upper-mantle origin of the Yellowstone Hotspot: *Geological Society of America Bulletin*, v. 114, no. 10, p. 1245-1256.
- Coble, M.A., and Mahood, G.A., 2012, Initial impingement of the Yellowstone plume located by widespread silicic volcanism contemporaneous with Columbia River flood basalts: *Geology*, v. 40, no. 7, p. 655-658.
- Cupp, B.L., 1989, Mineralization and volcanism at the DeLamar Silver Mine, Owyhee County, Idaho [Master]: Miami University.
- DePaolo, D.J., Perry, F.V., and Baldrige, W.S., 1992, Crustal versus mantle sources of granitic magmas; a two-parameter model based on Nd isotopic studies: *Special Paper - Geological Society of America*, v. 272, p. 439-446.
- Ekren, E.B., McIntyre, D.H., Bennett, E.H., and Malde, H.E., 1981, Geologic map of Owyhee County, Idaho, west of longitude 116 degrees: United States, U. S. Geological Survey.
- Ekren, E.B., McIntyre, D.H., Bennett, E.H., and Marvin, R.F., 1982, Cenozoic stratigraphy of western Owyhee County, Idaho: *Bulletin - Idaho Bureau of Mines and Geology*, v. 26, p. 215-235.
- Frost, C.D., and Frost, R., 2011, On ferroran (A-type) granitoids; their compositional variability and modes of origin: *Journal of Petrology*, v. 52, no. 1, p. 39-53.
- Gaschnig, R.M., Vervoort, J.D., Lewis, R.S., and Tikoff, B., 2011, Isotopic evolution of the Idaho Batholith and Challis intrusive province, northern US Cordillera: *Journal of Petrology*, v. 52, no. 12, p. 2397-2429.
- Halsor, S.P., Bornhorst, T.J., Beebe, M., Richardson, K., and Stowd, W., 1988, Geology of the DeLamar silver mine, Idaho; a volcanic dome complex and genetically associated hydrothermal system: *Economic Geology*, v. 83, no. 6, p. 1159-1169.
- Hames, W., Unger, D., Saunders, J., and Kamenov, G., 2009, Early Yellowstone hotspot magmatism and gold metallogeny: *Journal of Volcanology and Geothermal Research*, v. 188, no. 1-3, p. 214-224.
- Hasten, Z.E.L., Brueseke, M.E., Hames, W.E., and Saunders, J.A., 2011, Petrology and magmatic evolution of the Silver City District, Owyhee Mountains (ID): *Abstracts with Programs - Geological Society of America*, v. 43, no. 4, p. 14.
- Hibbard, M.J., 1981, The magma mixing origin of mantled feldspars: *Contributions to Mineralogy and Petrology*, v. 76, no. 2, p. 158-170.
- Irvine, T.N., and Baragar, W.R.A., 1971, A guide to the chemical classification of the common volcanic rocks: *Canadian Journal of Earth*, v. 8, no. 5, p. 523-548.

- John, D.A., 2001, Miocene and early Pliocene epithermal gold-silver deposits in the northern Great Basin, Western United States; characteristics, distribution, and relationship to magmatism: *Economic Geology*, v. 96, no. 8, p. 1827-1853.
- Johnson, J.A., C.J. Hawkesworth, C.J., Hooper, P.R., and Binger, G.B., 1998, Major- and trace element analyses of Steens Basalt, Southeastern Oregon: United States Geological Survey Open File Report 98-482, 30 p.
- Johnson, D.M., Hooper, P.R., and Conrey, R.M., 1999, XRF Analysis of Rocks and Minerals for Major and Trace Elements on a Single Low Dilution Li-tetraborate Fused Bead: *Advances in X-ray Analysis*, v. 41, p. 843-867.
- Johnson, J.A., and Grunder, A.L., 2000, The making of intermediate composition magma in a bimodal suite; Duck Butte eruptive center, Oregon, USA: *Journal of Volcanology and Geothermal Research*, v. 95, no. 1-4, p. 175-195.
- Jordan, B.T., Grunder, A.L., and Duncan, R.A., 2004, Geochronology of age-progressive volcanism of the Oregon High Lava Plains; implications for the plume interpretation of Yellowstone: *Journal of Geophysical Research*, v. 109, B10202 DOI:10.1029/2003JB002776.
- Kamenov, G.D., Saunders, J.A., Hames, W.E., and Unger, D.L., 2007, Mafic magmas as sources for gold in middle Miocene epithermal deposits of the northern Great Basin, United States; evidence from Pb isotope compositions of native gold: *Economic Geology*, v. 102, no. 7, p. 1191-1195.
- Knight, J.E., Brueseke, M.E., and Hart, W.K., 2004, Physical, petrographic, and geochemical characterization of ash flow volcanism; the mid-Miocene Cold Springs Tuff of the Santa Rosa-Calico volcanic field, Nevada: *Abstracts with Programs - Geological Society of America*, v. 36, no. 5, p. 77-78.
- Kolb, J., Whiting, E., Brueseke, M.E., and Hasten, Z.E.L., 2011, Petrographic and geochemical characterization of granitoid and metamorphic basement rocks, Owyhee Mountains, ID: *Abstracts with Programs - Geological Society of America*, v. 43, no. 4, p. 66.
- Le Bas, M.J., Le Maitre, R.W., Streckeisen, A., and Zanettin, B.A., 1986, Chemical classification of volcanic rocks based on the total alkali-silica diagram: *Journal of Petrology*, v. 27, no. 3, p. 745-750.
- Le Bas, M.J., and Streckeisen, A.L., 1991, The IUGS systematics of igneous rocks: *Journal of the Geological Society of London*, v. 148, Part 5, p. 825-833.
- Le Maitre, R.W., 1976, Some problems of the projection of chemical data into mineralogical classifications: *Contributions to Mineralogy and Petrology*, v. 56, no. 2, p. 181-189.
- Lindgren, W., 1900, Part 3; The gold and silver veins of Silver City, De Lamar, and other mining districts in Idaho: 20, Part 3, 65 p.

- Ludwig, K., 2003, User's manual for Isoplot 3.0: A geochronological tool kit for Microsoft excel: Berkley geochronology center, v. Special Publication No. 4.
- Miyashiro, A., 1974, Volcanic rock series in island arcs and active continental margins: *American Journal of Science*, v. 274, no. 4, p. 321-355.
- Norman, M.D., 1987, Geology, geochemistry, and tectonic implications of the Salmon Creek volcanic sequence, Owyhee Mountains, Idaho [Pd. D. Thesis]: Rice University.
- Norman, M.D., and Mertzman, S.A., 1991, Petrogenesis of Challis Volcanics from central and southwestern Idaho; trace element and Pb isotopic evidence: *Journal of Geophysical Research*, v. 96, B8, p. 13,279–13,293, DOI:10.1029/91JB00285.
- Otamendi, J.E., and Patino Douce, A.E., 2001, Partial melting of aluminous metagreywackes in the northern Sierra de Comechingones, central Argentina: *Journal of Petrology*, v. 42, no. 9, p. 1751-1772.
- Pansze, A.J., 1975, Geology and ore deposits of the Silver City - De Lamar - Flint region, Owyhee County, Idaho: Pamphlet - Idaho Bureau of Mines and Geology, v. P-161.
- Patino Douce, A.E., and Beard, J.S., 1995, Dehydration-melting of biotite gneiss and quartz amphibolite from 3 to 15 kbar: *Journal of Petrology*, v. 36, no. 3, p. 707-738.
- Patino Douce, A.E., and Beard, J.S., 1996, Effects of P, fO_2 and Mg/Fe ratio on dehydration melting of model metagreywackes: *Journal of Petrology*, v. 37, no. 5, p. 999-1024.
- Patino Douce, A.E., and Johnston, A.D., 1991, Phase equilibria and melt productivity in the pelitic system; implications for the origin of peraluminous granitoids and aluminous granulites: *Contributions to Mineralogy and Petrology*, v. 107, no. 2, p. 202-218.
- Pearce, J.A., 1983, Role of the sub-continental lithosphere in magma genesis at active continental margins *in: Continental basalts and mantle xenoliths*, Shiva Publ.: Nantwich, United Kingdom, p.230-249.
- Pearce, J.A., Harris, N.B.W., and Tindle, A.G., 1984, Trace element discrimination diagrams for the tectonic interpretation of granitic rocks: *Journal of Petrology*, v. 25, no. 4, p. 956-983.
- Petcovic, H.L., and Grunder, A.L., 2003, Textural and thermal history of partial melting in tonalitic wallrock at the margin of a basalt dike, Wallowa Mountains, Oregon: *Journal of Petrology*, v. 44, no. 12, p. 2287-2312.
- Pin, C., and Zalduegui, J.F.S., 1997, Sequential separation of light rare-earth elements, thorium and uranium by miniaturized extraction chromatography: application to isotopic analyses of silicate rocks: *Analytica Chimica Acta* v. 339, p. 79-89.
- Piper, A.M., and Laney, F.B., 1926, Geology and metalliferous resources of the region about Silver City, Idaho: Bulletin - Idaho Bureau of Mines and Geology, v. 11.

- Saunders, J.A., and Crowe, D.E., 1996, Retardation of boiling and the genesis of shallow Bonanza epithermal gold deposits; evidence from the Sleeper Deposit, Nevada: Abstracts with Programs - Geological Society of America, v. 28, no. 7, p. 94.
- Saunders, J.A., Unger, D.L., Kamenov, G.D., Fayek, M., Hames, W.E., and Utterback, W.C., 2008, Genesis of middle Miocene Yellowstone Hot Spot-related bonanza epithermal Au-Ag deposits, northern Great Basin, USA: *Mineralium Deposita*, v. 43, no. 7, p. 715-734.
- Seaman, S.J., 2000, Crystal clusters, feldspar glomerocrysts, and magma envelopes in the Atascosa Lookout lava flow, southern Arizona, USA; recorders of magmatic events: *Journal of Petrology*, v. 41, no. 5, p. 693-716.
- Shand, S.J., 1943, Eruptive rocks, their genesis, composition, classification, and their relation to ore deposits, with a chapter on meteorites (revised second edition), Thomas Murby & Co.: London, United Kingdom.
- Sharp, Z.D., 1990, A laser-based microanalytical method for the in situ determination of oxygen isotope ratios of silicates and oxides: *Geochimica et Cosmochimica Acta*, v. 54, no. 5, p. 1353-1357.
- Starkel, W.A., Wolff, J., Henry, C.D., and Castor, S., 2009, Geologic evolution and initial constraints on the petrogenesis of the McDermitt volcanic center, northern NV and southern OR: Abstracts with Programs - Geological Society of America, v. 41, no. 7, p. 369.
- Stimac, J.A., and Pearce, T.H., 1992, Textural evidence of mafic-felsic magma interaction in dacite lavas, Clear Lake, California: *American Mineralogist*, v. 77, no. 7-8, p. 795-809.
- Streck, M.J., 2008, Mineral textures and zoning as evidence for open system processes: *Reviews in Mineralogy and Geochemistry*, v. 69, no. 1, p. 595-622.
- Sun, S.S., 1980, Lead isotopic study of young volcanic rocks from mid-ocean ridges, ocean islands and island arcs: *Philosophical Transactions of the Royal Society of London, Series A: Mathematical and Physical Sciences*, v. 297, no. 1431, p. 409-445.
- Sun, S.S., and McDonough, W.F., 1989, Chemical and isotopic systematics of oceanic basalts; implications for mantle composition and processes: *Special Publication - Geological Society of London*, v. 42, p. 313-345.
- Taubeneck, W.H., 1971, Idaho batholith and its southern extension: *Geological Society of America Bulletin*, v. 82, no. 7, p. 1899-1928.
- Taylor, H.P., Jr., 1968, The oxygen isotope geochemistry of igneous rocks: *Contributions to Mineralogy and Petrology*, v. 19, no. 1, p. 1-71.
- Taylor, H.P., J., 1978, Oxygen and hydrogen isotope studies of plutonic granitic rocks: *Earth and Planetary Science Letters*, v. 38, no. 1, p. 177-210.

- Taylor, H.P., J., 1979, Oxygen and hydrogen isotope relationships in hydrothermal mineral deposits *in*: Geochemistry of hydrothermal ore deposits, John Wiley & Sons: New York, NY, United States, p.236-277.
- Taylor, S.R., and McClennan, S.M., 1985, The continental crust; its composition and evolution; an examination of the geochemical record preserved in sedimentary rocks, Geoscience texts: United Kingdom, Blackwell Scientific Publ.: Oxford, United Kingdom.
- Technical Notes, 2012, Washington State University, School of Earth and Environmental Sciences Geoanalytical Lab, < www.sees.wsu.edu/Geolab/note.html >
- Vielzeuf, D., and Holloway, J.R., 1988, Experimental determination of the fluid-absent melting relations in the pelitic system; consequences for crustal differentiation: Contributions to Mineralogy and Petrology, v. 98, no. 3, p. 257-276.
- Walker, R.J., Carlson, R.W., Shirey, S.B., and Boyd, F.R., 1989, Os, Sr, Nd, and Pb isotope systematics of Southern African peridotite xenoliths; implications for the chemical evolution of subcontinental mantle: Geochimica et Cosmochimica Acta, v. 53, no. 7, p. 1583-1595.
- Wallace, A.R., 2003, Geology of the Ivanhoe Hg-Au district, northern Nevada; influence of Miocene volcanism, lakes, and active faulting on epithermal mineralization: Economic, v. 98, no. 2, p. 409-424.
- Whalen, J.B., Currie, K.L., and Chappell, B.W., 1987, A-type granites; geochemical characteristics, discrimination and petrogenesis: Contributions to Mineralogy and Petrology, v. 95, no. 4, p. 407-419.
- Zoback, M.L., McKee, E.H., Blakely, R.J., and Thompson, G.A., 1994, The northern Nevada rift; regional tectono-magmatic relations and middle Miocene stress direction: Geological Society of America Bulletin, v. 106, no. 3, p. 371-382.

Appendix A - Sample Locations and Petrographic Descriptions

All samples collected as part of this project are listed below in alpha-numeric order. The locations are presented in UTM coordinates based on the NAD27 CONUS datum with all samples located in UTM Zone 11. Rock types are based geochemistry using the total alkali silica (TAS) diagram of LeBas et al.(1986) or modal abundances using the IUGS classification of igneous rocks of LeBas and Streckeisen (1991). Samples that were not analyzed for chemistry are only estimations and an asterisk follows the designation. Rock/mineral types are abbreviated with the following: Gr - Granite, Gd - Granodiorite, Tb - Trachybasalt, B - Basalt, Ba - Basaltic andesite, A - Andesite, D - Dacite, Td - Trachydacite, R - Rhyolite, Ad - Adularia, Br - Breccia, Tu - Tuff. Rock units are based on classifications discussed previously in this paper. Descriptions contain field and hand sample appearance. For point counted samples, detailed thin section petrography is included in the descriptions and mineral modes, in order of abundance, are listed under the petrography heading.

Sample ID: MB07-13A

Rock Type: Gr Rock Unit: Kg

Northing: 0520766

Easting: 4764395

Description: Muscovite and biotite rich granite with quartz and feldspar. Slight alteration. Very coarse grained. Up to 5 mm crystals.

Petrography: Quartz 34.52%, plagioclase 24.61%, orthoclase 24.15%, microcline 8.98%, garnet 5.11%, and biotite 2.63%.

Sample ID: MB07-13B

Rock Type: Gr Rock Unit: Kg

Northing: 0520766

Easting: 4764395

Description: Fine grained biotite and muscovite rich granite. Approximately 3 mm quartz and feldspar. Biotite forms slight fabric.

Petrography: Quartz 46.27%, orthoclase 25.16%, plagioclase 22.98%, biotite 4.04%, and microcline 1.55%.

Sample ID: MB07-14

Rock Type: Gr Rock Unit: Kg

Northing: 0522606

Easting: 4763682

Description: Feldspar and quartz bearing muscovite and biotite granite. Medium grained with less than 3 mm crystals. Slightly altered but still relatively fresh. Some low temperature garnet inclusions.

Petrography: Quartz 39.91%, plagioclase 24.19%, orthoclase 13.25%, microcline 12.94%, muscovite 7.55%, biotite 1.54%, and garnet 0.62%

Sample ID: MB07-16

Rock Type: Gr Rock Unit: Kg

Northing: 0524530

Easting: 4762057

Description: Very fine grained biotite granite. Abundant 1 - 2 mm plagioclase and k-feldspar. Slight green color due to alteration. Some chloritized hornblende up to 3 mm.

Sample ID: MB07-17A

Rock Type: Gd Rock Unit: Kg

Northing: 0524612

Easting: 4761881

Description: Biotite and muscovite rich granodiorite. Abundant 2 - 4 mm books of micas. Slight green tint from alteration to feldspars. Overall, relatively fresh.

Petrography: Plagioclase 46.11%, quartz 32.49%, orthoclase 13.77%, biotite 4.64%, muscovite 2.54%, and microcline 0.45%

Sample ID: MB07-17B

Rock Type: D Rock Unit: N/A

Northing: 0524612

Easting: 4761881

Description: Biotite-hornblende porphyry. Abundant white feldspar and mafics in green to gray matrix. Some resorption to the feldspars. With 3 mm mafic minerals.

Sample ID: MB07-18

Rock Type: Gr Rock Unit: Kg

Northing: 0525012

Easting: 4761454

Description: Coarse grained muscovite and biotite rich granite. Abundant 2 - 4 mm books of micas. Quartz, plagioclase and k-feldspar in equal proportions. Fairly fresh.

Petrography: Quartz 32.23%, orthoclase 28.77%, plagioclase 26.05%, biotite 9.19%, muscovite 2.11%, microcline 1.51%, and zircon 0.15%

Sample ID: MB07-19

Rock Type: Gr Rock Unit: Kg

Northing: 0524745

Easting: 4765167

Description: Coarse grained biotite and muscovite granite. Abundant 1 - 3 mm micas with visible oxidation. 2 - 3 mm fresh quartz and feldspars.

Petrography: Plagioclase 39.58%, quartz 34.29%, orthoclase 14.50%, microcline 6.95%, muscovite 2.72%, and biotite 1.96%

Sample ID: MB07-20

Rock Type: Gr Rock Unit: Kg

Northing: 0529331

Easting: 4767072

Description: Medium to coarse grained, biotite-muscovite granite. 3 - 4 mm micas with 6 - 7 mm quartz and feldspar. Some iron oxidation staining. Relatively fresh sample.

Petrography: Quartz 39.73%, plagioclase 30.59%, orthoclase 17.35%, microcline 6.39%, biotite 4.41%, and muscovite 1.52%

Sample ID: MB09-1

Rock Type: R Rock Unit: Tql

Northing: 0519344

Easting: 4762548

Description: Sampled from blocky rhyolite outcrop. Very fine grained white matrix with 10 - 20% 1 mm quartz crystals. Slightly altered.

Sample ID: MB09-2

Rock Type: Ba Rock Unit: Tsb

Northing: 0519389

Easting: 0519389

Description: Dense, aphanitic black matrix. Fine grained 0.5 mm plagioclase crystals. Some vesiculation. Fresh.

Sample ID: MB09-3

Rock Type: Ba Rock Unit: Tsb

Northing: 0519175

Easting: 4764491

Description: Very fine grained to aphanitic. Similar to MB09-2 although more altered.

Sample ID: MB09-4

Rock Type: Ba Rock Unit: Tsb

Northing: 0518929

Easting: 4764941

Description: Very fine grained dark matrix. More silicic. Abundant large, up to 1 cm, feldspars.

Sample ID: MB09-5

Rock Type: Ba Rock Unit: Tsb

Northing: 0518742

Easting: 4765166

Description: Very fresh sample with very fine grained to aphanitic matrix. Large plagioclase phenocrysts up to 3 cm.

Petrography: Matrix 61.78%, oxide 23.04%, plagioclase 14.80%, and vesicle fill 0.39%

Hypocrystalline sample with aphanitic matrix. Abundant iron oxide microphenocrysts. Fine grained, 0.15 mm, plagioclase with some evidence of resorbition and muscovite replacement.

Sample ID: MB09-11

Rock Type: R Rock Unit: Tsc

Northing: 0522238

Easting: 4757106

Description: Rhyolite with very fine grained matrix and abundant 1 mm quartz. Some frothy texture with compaction features. Outcrop appears to be a float like zone. Possible ash flow or fall.

Sample ID: MB09-12

Rock Type: R Rock Unit: Tsc

Northing: 0523054

Easting: 4757955

Description: Flow banded rhyolite with light pink to pink matrix. Abundant 1 mm quartz and 1 - 2 mm feldspars and 1 mm mafics, possibly pyroxene.

Petrography: Matrix 90.60%, quartz 7.34%, and altered xenolith 2.06%

Aphanitic, flow banded groundmass. Medium grained, 1 mm, embayed subhedral quartz and rare zoned 1 mm resorbed plagioclase phenocrysts. Rare zircon and altered biotite.

Sample ID: MB09-13

Rock Type: B Rock Unit: Tsb

Northing: 0517148

Easting: 4752833

Description: Medium to coarse grained basalt with aphanitic matrix. Abundant 1 mm plagioclase, rare 5 - 7 mm plagioclase phenocrysts. No obvious mafics. Very fresh.

Petrography: Plagioclase 46.98%, clinopyroxene 28.44%, olivine 16.47%, and oxide 8.11%

Fine grained felty plagioclase matrix with laths up to 0.25 mm. Some 1 mm plagioclase occurs in glomeroporphyritic clots. Matrix plagioclase have composition of An₉₀₋₉₈ while phenocrystic plagioclase have composition of An₅₄. Additional 1 mm subhedral olivine and clinopyroxene. Some olivine altered to iddingsite. Scattered iron oxide.

Sample ID: MB09-19

Rock Type: B Rock Unit: Tsb

Northing: 0516074

Easting: 4748997

Description: Plagioclase phyric basalt. Dark gray to black matrix. Some rare altered 1 - 2 feldspars. Relatively fresh overall.

Sample ID: MB09-20A

Rock Type: Tu Rock Unit: Tcst

Northing: 0515303

Easting: 4748947

Description: Very fine grained, gray slightly welded air fall tuff. Abundant 0.5 to 1 mm black glassy fragments with 1 mm feldspars.

Sample ID: MB09-20B

Rock Type: Tu Rock Unit: Tcst

Northing: 0515303

Easting: 4748947

Description: Similar to MB09-20A although more welded.

Sample ID: MB09-21

Rock Type: B Rock Unit: Tsb

Northing: 0514158

Easting: 4748585

Description: Very fine grained basalt. Platy jointing with grey matrix. Some alteration in zones. No visible phenocrysts.

Sample ID: MB09-22

Rock Type: R Rock Unit: Tsc

Northing: 0516576

Easting: 4760833

Description: Flow banded rhyolite. Very fine grained white to pink matrix. Abundant bands that are 1 - 4 cm thick. 2 mm quartz and 1 mm feldspar phenocrysts.

Petrography: Matrix 97.67%, xenolith 1.43%, myrmikitic quartz and plagioclase 0.39%, and altered 0.26%

Aphanitic groundmass with 0.05 mm microcrysts of quartz. 1 mm quartz and plagioclase phenocrysts and rare 0.1 mm oxides.

Sample ID: MB09-23

Rock Type: B Rock Unit: Tsb

Northing: 0517810

Easting: 4760740

Description: Basalt with fairly fresh interior but oxidized exterior. Coarse grained.

Sample ID: MB09-24A

Rock Type: R* Rock Unit: N/A

Northing: 0520945

Easting: 4762953

Description: Punky flow banded rhyolite with large quartz veins. Possible mineralization of naumenite.

Sample ID: MB09-24B

Rock Type: Ad Rock Unit: N/A

Northing: 0520945

Easting: 4762953

Description: Adularia samples from outcrop area.

Sample ID: MB09-25

Rock Type: B Rock Unit: Tsb

Northing: 0521320

Easting: 4762301

Description: Very fine grained, aphanitic basalt with gray matrix. Weathers from blocky to platy to shards. Dark brown weathering rind.

Sample ID: MB09-26

Rock Type: B Rock Unit: Tsb

Northing: 0521406

Easting: 4762248

Description: Fine grained basalt with gray to green matrix. Abundant plagioclase laths up to 1 cm. Some radiating and possible clinopyroxene.

Sample ID: MB09-27

Rock Type: B Rock Unit: Tsb

Northing: 0521446

Easting: 4762237

Description: Very fine grained basalt. Blue gray matrix, with vesicles and plagioclase phenocrysts.

Petrography: Matrix 81.47%, pyroxene 11.20%, oxide 5.66%, vesicle fill 1.16%, and plagioclase 0.51%

Hypocrystalline sample with aphanitic matrix. Scattered iron oxide microphenocrysts. Interstitial clinopyroxene scattered throughout. Areas of chlorite/epidote/calcite alteration. Amygdaloidal vesicle fill with oxide and chlorite/epidote/calcite fill. Rare plagioclase phenocrysts with sieve texture and oxide replacement.

Sample ID: MB09-29

Rock Type: B Rock Unit: Tsb

Northing: 0521619

Easting: 4762312

Description: Black to dark gray plagioclase phyric basalt. Up to 1 cm long phenocrysts. Possible 1 mm pyroxenes. Fairly fresh.

Sample ID: JK10-1

Rock Type: Gr Rock Unit: Kg

Northing: 0517728

Easting: 4752009

Description: White quartz, feldspar and muscovite rich granite with <1mm garnet phenocrysts.

Petrography: Quartz 42.62%, plagioclase 24.85%, microcline 15.66%, orthoclase 10.69%, muscovite 5.57%, garnet 0.45% and biotite 0.15%

Sample ID: JK10-2A

Rock Type: Gr Rock Unit: Kg

Northing: 0521066

Easting: 4763112

Description: White fine grained, quartz, feldspar and muscovite rich apalite. Mostly fresh with minor iron oxidation. Some <1 mm garnet phenocrysts.

Petrography: Quartz 42.55%, plagioclase 21.89%, microcline 18.94%, orthoclase 10.56%, muscovite 5.75%, and biotite 0.31%

Sample ID: JK10-2B

Rock Type: Gd Rock Unit: Kg

Northing: 0521066

Easting: 4763112

Description: White coarse grained, quartz, feldspar and mica rich granodiorite. Mostly fresh with minor iron oxidation. Thin weathering rind but minerals appear fresh.

Petrography: Plagioclase 39.31%, quartz 37.16%, microcline 10.33%, orthoclase 10.04%, biotite 1.87%, and muscovite 1.29%

Sample ID: JK10-3

Rock Type: Gr Rock Unit: Kg

Northing: 0523586

Easting: 4761853

Description: Light gray very coarse granite. Contains very coarse feldspar crystals. Abundant muscovite and scattered biotite. No chemical analysis because of highly altered material.

Petrography: Plagioclase 34.15%, quartz 31.98%, microcline 13.31%, muscovite 9.70%, orthoclase 6.66%, and biotite 4.20%

Sample ID: JK10-4

Rock Type: Gr Rock Unit: Kg

Northing: 0523192

Easting: 4762024

Description: White coarse grained quartz, feldspar, muscovite and biotite rich granite. Mostly fresh with slight greening of biotite present. Very coarse feldspar crystals.

Petrography: Quartz 38.96%, plagioclase 31.49%, microcline 10.15%, orthoclase 9.40%, biotite 6.27%, and muscovite 3.73%

Sample ID: JK10-5

Rock Type: Gr Rock Unit: Kg

Northing: 052448

Easting: 4761802

Description: White very coarse grained, quartz, feldspar, and muscovite rich granite with rare biotite. Large smoky quartz and feldspar up phenocrysts. Very fresh sample with only thin weathering rind.

Petrography: Quartz 33.68%, plagioclase 31.74%, microcline 13.41%, orthoclase 10.73%, biotite 6.11%, and muscovite 4.32%

Sample ID: JK10-6

Rock Type: Gr Rock Unit: Kg

Northing: 0521970

Easting: 4762075

Description: White coarse grained quartz, feldspar, muscovite and biotite rich granite similar to JK10-4. Mostly fresh with slight alteration of biotite present.

Petrography: Quartz 38.54%, plagioclase 30.06%, orthoclase 14.29%, microcline 9.23%, muscovite 4.17%, and biotite 3.72%

Sample ID: JK10-7

Rock Type: Gr Rock Unit: Kg

Northing: 0521202

Easting: 4767827

Description: Orangish, fine to medium coarse grained quartz and feldspar granite with abundant muscovite and biotite. Oxidation weathering present. Not completely fresh.

Petrography: Quartz 34.09%, plagioclase 23.44%, orthoclase 18.72%, microcline 16.59%, biotite 3.81%, and muscovite 3.35%

Sample ID: JK10-8

Rock Type: Gd Rock Unit: Kg

Northing: 0521600

Easting: 4767412

Description: White to pinkish, coarse grained quartz and feldspar granodiorite with scattered muscovite and biotite. Pinkish color possibly caused by k-feldspar or slight alteration. Relatively fresh sample.

Petrography: Plagioclase 40.09%, quartz 34.79%, microcline 10.76%, orthoclase 10.14%, muscovite 2.81%, and biotite 1.40%

Sample ID: JK10-9

Rock Type: Gr Rock Unit: Kg

Northing: 0520831

Easting: 4764393

Description: White, coarse grained quartz and feldspar granite with abundant muscovite and biotite. Small 1 mm garnet phenocrysts present.

Petrography: Quartz 32.51%, plagioclase 27.89, orthoclase 16.64%, microcline 15.41%, biotite 5.08%, and muscovite 2.47%

Sample ID: JK10-10

Rock Type: Gd Rock Unit: Kg

Northing: 0521792

Easting: 4762429

Description: Biotite and muscovite granitoid. Abundant 2 - 3 mm muscovite that seem to be in zones. Biotite is subordinate to muscovite and slightly oxidized. Larger quartz than feldspar and up to 4 mm with feldspars up to 1 mm. Seems slightly different than previous samples.

Petrography: Plagioclase 40.99%, quartz 36.18%, orthoclase 11.96%, biotite 4.97%, microcline 3.26%, and muscovite 2.64%

Sample ID: MB10-3

Rock Type: Gr Rock Unit: Kg

Northing: 0521854

Easting: 4759868

Description: Dike material. Clear to white quartz rim with golden color quartz, plagioclase and altered muscovite and possibly altered biotite. Color appears to be from muscovite alteration.

Petrography: Quartz and plagioclase dominated granitoid with medium grained 0.75 - 1 mm subhedral quartz grains. Smaller subhedral plagioclase and microcline with evident twinning. Some areas of myrmekitic textures associated with plagioclase grains. Thin bands of muscovite throughout with rarer altered biotite grains.

Sample ID: MB10-4

Rock Type: Gd Rock Unit: Kg

Northing: 0521904

Easting: 4759860

Description: Quartz and feldspar granitoid with some large biotite and thick muscovite crystals. Relatively fresh with some iron oxide staining. Just below dike material.

Petrography: Quartz 42.11%, plagioclase 35.62%, K-feldspar 10.56%, muscovite 6.87%, biotite 4.07%, and chlorite 0.76%.

Coarse grained up to 5 mm quartz with finer grained plagioclase and K-feldspar. Some altered plagioclase filled with muscovite and quartz. Rare poikilitic zoned plagioclase that has been filled with plagioclase and muscovite. Up to 6 mm muscovite and 1 mm biotite. Some biotite altered to chlorite. Some myrmekitic textures and skeletal alteration.

Sample ID: MB10-5A

Rock Type: N/A Rock Unit: Jms

Northing: 0517728

Easting: 4752009

Description: Foliated granitoid with alternating white and black, coarse grained layers. Composed of quartz, feldspar, biotite and muscovite. Weak to slight layering or foliation.

Sample ID: MB10-5B

Rock Type: N/A Rock Unit: Jms

Northing: 0517728

Easting: 4752009

Description: Black and white foliated schist. Fine to medium grained with quartz, feldspar, biotite and muscovite. Slight schistosity with beginning evidence of platy mineral alignment and foliating.

Sample ID: MB10-5C

Rock Type: N/A Rock Unit: Jms

Northing: 0517728

Easting: 4752009

Description: Schist. Definitive schistosity with well defined bands of foliation and biotite alignment. Some iron oxide staining with bands of granitoid that are unaltered to slightly altered.

Sample ID: ZH10-1

Rock Type: B* Rock Unit: Tsb*

Northing: 0521300

Easting: 4762308

Description: Yellowish tan, fine grained with black, gray and white phenocrysts. Possible tuff deposit. Weathered and slightly altered. Collected from bench.

Sample ID: ZH10-2

Rock Type: B Rock Unit: Tsb

Northing: 0521197

Easting: 4762334

Description: Light gray, very fine grained matrix. Abundant white plagioclase phenocrysts up to 1 cm with scattered red possible pyroxene phenocrysts. Small epidote veins. Fractures into small platy pieces. Appears relatively fresh below surface.

Sample ID: ZH10-3

Rock Type: B Rock Unit: Tsb

Northing: 0521091

Easting: 4762354

Description: Dark gray, very fine grained to aphanitic basalt. Few large plagioclase phenocrysts. Epidote alteration including greenish gray rind. Core appears to be relatively fresh.

Sample ID: ZH10-4

Rock Type: B Rock Unit: Tsb

Northing: 0521024

Easting: 4762411

Description: Light greenish gray and pink fine grained basalt. Some ophio mottling and small epidote alteration rind.

Sample ID: ZH10-5

Rock Type: R Rock Unit: Tsc

Northing: 0520793

Easting: 4762524

Description: Very pale pink to white, very fine grained rhyolite, quartz and feldspar phenocrysts. Hydrothermally bleached. Relatively fresher sample. Still some pink color that is noted in portions of sample.

Sample ID: ZH10-6

Rock Type: R Rock Unit: Tsc

Northing: 0521575

Easting: 4761792

Description: White, very fine grained rhyolite with quartz phenocrysts and epidote growths and some linear quartz veins. Slight iron oxide staining.

Sample ID: ZH10-7

Rock Type: R Rock Unit: Tql

Northing: 0521528

Easting: 4761698

Description: Olive gray tuff with few smoky quartz phenocrysts and pumice clasts. Increasing alteration upwards. Some pumice altered or replaced towards top of sample. Pumice at bottom of outcrop compressed and elongated and decreasing upwards.

Sample ID: ZH10-8

Rock Type: R Rock Unit: Tsc

Northing: 0521528

Easting: 4761698

Description: White to light gray rhyolite with fine grained, crystal rich, silicified matrix. Flow banding present alternating clear and milky layers. Some epidote alteration.

Sample ID: ZH10-9

Rock Type: Ad Rock Unit: N/A

Northing: 0521528

Easting: 4761698

Description: Adularia patch with abundant crystal growth on tuffaceous unit. Off white diamond shaped angular crystals.

Sample ID: ZH10-10

Rock Type: N/A Rock Unit: N/A

Northing: 0521528

Easting: 4761698

Description: Possible sinter deposit. exterior has sinter texture while interior has white, silicified rhyolite texture.

Sample ID: ZH10-11

Rock Type: R Rock Unit: Tgml

Northing: 0520917

Easting: 4761016

Description: Very pale light greenish gray rhyolite. Abundant 5 mm quartz phenocrysts in very fine grained mafic minerals. Fairly fresh to fresh sample. Small pinkish rind.

Sample ID: ZH10-12

Rock Type: R Rock Unit: Tsc

Northing: 0520451

Easting: 4760016

Description: Purplish gray, very fine grained matrix with 1 cm feldspar phenocrysts with possible reaction rims. Some sanidine, quartz and rare biotite crystals. Platy jointing with thin flow banding present.

Sample ID: ZH10-13

Rock Type: R Rock Unit: Tgml

Northing: 0520335

Easting: 4759638

Description: Black glassy vitrophyre with abundant feldspar, sanidine and quartz phenocrysts. Very fresh.

Sample ID: ZH10-14

Rock Type: B Rock Unit: Tsb

Northing: 0521106

Easting: 4760424

Description: Greenish gray, very fine grained basalt from tailings pile. Few small plagioclase phenocrysts. Relatively fresh sample collected. Pile was mixed with basalts of varying degrees of alteration and white altered rhyolite. Rhyolite had massive flow banding present and quartz veins. No rhyolite sample was taken.

Sample ID: ZH10-15

Rock Type: R Rock Unit: Tsc

Northing: 0521481

Easting: 4759643

Description: Pinkish purple, very fine grained matrix. Abundant phenocrysts of sanidine, quartz, plagioclase and mafics. Relatively fresh. Majority of crystals seem fresh. Some alteration along and near fractures. Sample and outcrop have widespread platy jointing.

Petrography: Matrix 86.77%, plagioclase 5.84%, quartz 4.28%, biotite 1.69%, orthopyroxene 1.17%, and oxide 0.26%

Flow banded, aphanitic to very fine grained groundmass. Rare 0.5 mm biotite and 0.1 mm zircons. Medium grained, 1 mm subhedral, zoned plagioclase phenocrysts. Quartz phenocrysts with corona reaction rims.

Sample ID: ZH10-16

Rock Type: R Rock Unit: Tsc

Northing: 0521700

Easting: 4759747

Description: Dark purplish gray and light gray flow banded rhyolite. Very fine grained with mafic phenocrysts that appear fresh. Plagioclase, sanidine and quartz phenocrysts are slightly altered. Possible large granitoid xenolith present.

Sample ID: ZH10-17

Rock Type: R Rock Unit: Tql

Northing: 0523754

Easting: 4758210

Description: Purplish gray, very fine grained latite. Predominately matrix with few phenocrysts of pyroxene, plagioclase, sanidine, quartz and rare biotite. Relatively fresh with thin alteration rim.

Sample ID: ZH10-18

Rock Type: Br Rock Unit: N/A

Northing: 0523754

Easting: 4758210

Description: Grayish purple breccia with very fine grained matrix with latite and other volcanic clasts. Matrix supported with possible flow top breccia. Possible clasts of breccia included.

Sample ID: ZH10-19

Rock Type: Tu Rock Unit: N/A

Northing: 0524055

Easting: 4760166

Description: Light gray and light pink tuffaceous unit. Compressed layering or flow banding. Small quartz and sanidine crystals. Weathered or silicified.

Sample ID: ZH10-20

Rock Type: A Rock Unit: Ta

Northing: 0524293

Easting: 4760942

Description: Dark gray very fine grained to aphanitic andesite. Fresh, very thin alteration rim. Very small plagioclase laths.

Sample ID: ZH10-21

Rock Type: R Rock Unit: Tql

Northing: 0514789

Easting: 4748721

Description: Pinkish purple latite. Very fine grained matrix with feldspar banding and quartz phenocrysts and rare mafic phenocrysts. Some larger feldspar phenocrysts. Very fresh.

Sample ID: ZH10-22

Rock Type: D Rock Unit: Tgml

Northing: 0518384

Easting: 4768353

Description: Black, aphanitic vitrophyre. Possible granitoid and basaltic xenoliths or possibly vesicle fill. Few crystal inclusions, some weathered out pore spaces. Some slight epidote alteration.

Petrography: Matrix 56.11%, plagioclase 27.06%, vesicle fill 5.78%, orthopyroxene 5.61%, and clinopyroxene 5.45%

Aphanitic to fine grained matrix with equigranular felty plagioclase. Fine grained 0.1 mm plagioclase and pyroxene microcrysts. Glomeroporphyritic clots of plagioclase and pyroxene. Some xenolithic very fine grained matrix. Xenolithic plagioclase with sieve and resorbtion textures.

Sample ID: ZH10-23

Rock Type: D Rock Unit: Tgml

Northing: 0518281

Easting: 4768398

Description: Dark gray dacite. Slight ophio texture. 5 mm feldspar phenocrysts in a very fine grained matrix. Slight weathering rind outside. Appears to have similar texture as vitrophyre unit below.

Sample ID: ZH10-24

Rock Type: R Rock Unit: Tql

Northing: 0517117

Easting: 4767708

Description: White, very fine grained rhyolite with quartz and feldspar phenocrysts throughout. Fresh with 1 cm thick weathering rind.

Petrography: Matrix 96.53%, quartz 2.32%, and plagioclase 1.16%

Feathery, very fine grained matrix. Medium grained 0.5 mm embayed, subhedral quartz and 0.5 mm altered and replaced plagioclase. Rare 0.25 zircon.

Sample ID: ZH10-25

Rock Type: A Rock Unit: Ta

Northing: 0517776

Easting: 4766073

Description: Black, very dense latite. Very fine grained to aphanitic with some quartz and feldspar phenocrysts. Very fresh sample.

Sample ID: ZH10-26

Rock Type: D Rock Unit: Tgml

Northing: 0518038

Easting: 4765566

Description: Greenish gray dacite. Very fine grained matrix with 1 cm feldspar phenocrysts. Some quartz and mafic crystals with reaction rims and potential vesicle fill or alteration.

Sample ID: ZH10-27

Rock Type: R Rock Unit: Tsc

Northing: 0518303

Easting: 4765003

Description: White rhyolite with very fine grained matrix. Quartz and feldspar phenocrysts throughout. Fresh core but majority of the outcrop too weathered to sample. Possible feeder dike for above units.

Sample ID: ZH10-28

Rock Type: B Rock Unit: Tsb

Northing: 0511976

Easting: 4763961

Description: Black, very fine grained basalt with feldspar and quartz phenocrysts. Possible vesicle fill responsible for larger crystals. Larger crystals appear to be slightly altered with groundmass relatively fresh. Small oxidized rind.

Sample ID: ZH10-29

Rock Type: R Rock Unit: Tql

Northing: 0512121

Easting: 4764655

Description: Rhyolite with pale pink to white matrix. Very fine grained with small 1 mm vesicles throughout. Some vesicles have alteration and secondary fill. Matrix is relatively fresh. Some very fresh quartz and feldspar phenocrysts.

Petrography: Matrix 97.55%, quartz 2.06%, plagioclase 0.39%

Very fine grained with some iddingsite alteration. Medium grained, subhedral and slightly embayed quartz phenocrysts. Rare altered and replaced plagioclase up to 0.1 mm and 0.025 mm zircons.

Sample ID: ZH10-30

Rock Type: B Rock Unit: Tsb

Northing: 0512379

Easting: 4765110

Description: Basalt with black, very fine grained matrix and some 1 mm feldspar and quartz phenocrysts. Some large vesicles filled with chalcedony and quartz. Very fresh with a small oxidized rim.

Sample ID: ZH10-31

Rock Type: R Rock Unit: Tsc

Northing: 0511908

Easting: 4765626

Description: Light gray to white flow banded rhyolite. Very fine grained matrix. 1 mm quartz and feldspar phenocrysts. Platy fracturing with thin weathered rinds. Fresh matrix with fresh crystals.

Petrography: Matrix 99.15%, quartz 0.43%, and biotite 0.42%

Flow banded, aphanitic to very fine grained matrix. Felty plagioclase in some matrix bands. Medium grained 0.5 mm embayed quartz phenocrysts. Rare oxides and 0.05 mm zircons.

Sample ID: ZH10-32

Rock Type: R Rock Unit: Tsc

Northing: 0511307

Easting: 4765808

Description: Rhyolite with light gray to white, very fine grained matrix. Some flow banding and quartz veins. Scattered quartz and feldspar phenocrysts. Very fresh with small weathering rind only on the surface.

Sample ID: ZH10-33

Rock Type: D Rock Unit: Tgml

Northing: 0511277

Easting: 4765524

Description: Black, very fine grained dacite with quartz and feldspar phenocrysts. Small weathering rind. Relatively fresh sample with fresh crystals. Platy fracturing with large 2 cm inclusions.

Petrography: Matrix 86.23%, xenolith 10.42%, clinopyroxene 2.19%, orthopyroxene 0.39%, quartz 0.39%, plagioclase 0.26%, and altered 0.13%

Aphanitic to fine grained matrix with equigranular felty plagioclase. Fine grained 0.1 - 0.5 mm plagioclase and pyroxene microcrysts. Glomeroporphyritic clots of plagioclase and pyroxene. Some xenolithic very fine grained matrix. Xenolithic plagioclase with sieve and resorption textures.

Sample ID: ZH10-34

Rock Type: Tu Rock Unit: N/A

Northing: 0517846

Easting: 4750420

Description: Light gray tuffaceous unit. Well defined glass shards. Some possible feldspar fragments and mafic or glassy shards.

Sample ID: ZH10-35

Rock Type: R Rock Unit: Thpl

Northing: 0537153

Easting: 4750072

Description: Latite with light purplish gray, very fine grained matrix. Relatively fresh with small weathering rind. Weathering leaches inward in a few places. Few quartz and feldspar phenocrysts. Most very fresh with rare altered crystals.

Petrography: Matrix 97.13%, quartz 2.38%, and plagioclase 0.50%

Very fine grained plagioclase rich matrix. Few 0.25 - 0.5 mm resorbed plagioclase and quartz phenocrysts. Rare zircons.

Sample ID: ZH10-36

Rock Type: R Rock Unit: Tql

Northing: 0530532

Easting: 4768276

Description: Light gray, flow banded rhyolite with fine grained matrix. Relatively fresh feldspar and quartz phenocrysts. Some possible vesicle fill.

Sample ID: ZH10-37

Rock Type: Td Rock Unit: N/A

Northing: 0521063

Easting: 4763099

Description: Extremely altered material with very fine grained matrix. Visibly altered phenocrysts.

Sample ID: ZH10-38

Rock Type: R Rock Unit: Tsc

Northing: 0522483

Easting: 4761834

Description: White, fine grained rhyolite with very small quartz and feldspar phenocrysts. Abundant altered and filled vesicles. Relatively fresh except for areas immediately contacting vesicle fill. Some evidence of flow banding.

Sample ID: ZH10-39A

Rock Type: B Rock Unit: Tsb

Northing: 0520509

Easting: 4761270

Description: Basalt with very fine grained matrix. Appears relatively fresh. Some small feldspar phenocrysts with some secondary pyrite mineralization.

Sample ID: ZH10-39B

Rock Type: B Rock Unit: Tsb

Northing: 0520509

Easting: 4761270

Description: Similar to previous sample. 2 cm amygdule. Inclusion is fine grained with quartz, feldspar, muscovite and biotite present.

Sample ID: ZH10-40

Rock Type: A Rock Unit: Ta

Northing: 0520636

Easting: 4768263

Description: Black, andesitic sample with very fine grained matrix and rare 1 mm feldspar phenocrysts. Some large 5 mm glassy phenocrysts. Very fresh inside but abundant weathering rind along many fractures. Pseudo-columnar jointing present in the outcrop.

Petrography: Matrix 98.07%, and plagioclase 1.93%

Aphanitic groundmass with 0.40 mm microphenocrysts of plagioclase. Pyroxene and oxides also present in the matrix. Medium grained 0.5 - 0.75 mm plagioclase in glomerocrysts with sieve and resorbition textures.

Sample ID: ZH10-41

Rock Type: D Rock Unit: Tgml

Northing: 0520842

Easting: 4767808

Description: Black to dark green with olive green banding. Possible dacite flow or fall deposit. Some altered plagioclase and relatively fresh quartz phenocrysts. Very altered, very fine grained groundmass.

Petrography: Matrix 83.64%, xenolith 13.25%, and plagioclase 3.12%

Aphanitic to fine grained matrix with equigranular felty plagioclase. Glomeroporphyritic clots of plagioclase with additional 0.5 - 1 mm plagioclase with resorption and sieved textures. Rare 0.1 mm pyroxenes. Some xenolithic very fine grained matrix.

Sample ID: ZH10-42

Rock Type: R Rock Unit: Tsc

Northing: 0522700

Easting: 4764649

Description: Possible tuffaceous unit. White, very fine grained rhyolite. Very fresh with quartz and feldspar phenocrysts. Very rare biotite. Outside texture indicates possible horizontal layering with possible condensed fiamme structures.

Petrography: Matrix 96.27%, plagioclase 2.45%, and quartz 1.29%

Aphanitic groundmass with coarse grained 3 mm subhedral plagioclase with alteration rims. Scattered subhedral and embayed 0.25 mm quartz. Rare oxides, biotite and zircons.

Sample ID: ZH10-43

Rock Type: R Rock Unit: Tgml

Northing: 0521053

Easting: 4764090

Description: Bluish gray, very fine grained rhyolite. Very fresh quartz and feldspar phenocrysts. Matrix appears relatively fresh.

Petrography: Matrix 85.07%, plagioclase 8.37%, quartz 5.02%, altered 0.77%, oxide 0.51%, and zircon 0.26%

Aphanitic groundmass. Medium grained, 0.5 - 1 mm embayed quartz phenocrysts. Plagioclase phenocrysts with zoning and sieve and alteration textures. Some myrmekitic textures. Rare zircon and oxides. Biotite altered to chlorite. Some additional epidote and calcite alteration.

Sample ID: ZH11-1

Rock Type: R Rock Unit: Thpl

Northing: 0526157

Easting: 4759308

Description: Light gray latite similar to ZH10-17. 1 mm plagioclase and quartz. Possible biotite or brown lathy and blocky altered pyroxene phenocrysts. Possible sericite present.

Sample ID: ZH11-2

Rock Type: R Rock Unit: Thpl

Northing: 0527998

Easting: 4758515

Description: Black vitrophyre. Slightly waxy but relatively fresh phenocrysts. Abundant spheruloids present indicating upper area of flow. Small 1 - 2 mm plagioclase and quartz phenocrysts.

Petrography: Matrix 79.11%, altered 14.81%, quartz 3.54%, K-feldspar 2.15%, and oxide 0.38%

Vitrophyric matrix. Fine to medium grained embayed quartz and feldspar phenocrysts. Scattered alteration throughout. Rare oxide.

Sample ID: ZH11-3

Rock Type: R Rock Unit: Thpl

Northing: 0524884

Easting: 4759030

Description: Light grayish purple fine grained latite. 1 Mm plagioclase and quartz. Fresh not much weathering rind. Some ramping or flow evidence is present in the outcrop.

Sample ID: ZH11-4

Rock Type: Tb Rock Unit: N/A

Northing: 0520668

Easting: 4756681

Description: Outcrop of basaltic unit overlying granitoid. Very fresh, some weathering rind. Abundant 1 - 2 mm olivine phenocrysts. Very fine grained to aphanitic groundmass.

Petrography: Matrix 88.16%, olivine 8.49%, and brown interstitial 3.35%

Aphanitic groundmass with abundant 0.15 mm felty aligned plagioclase. Abundant euhedral to subhedral olivine phenocrysts with iddingsite altered rims.

Sample ID: ZH11-5

Rock Type: R Rock Unit: Thpl

Northing: 0520733

Easting: 4756988

Description: Vitrophyre from base of rhyolite. Relatively fresh 1 - 2 mm plagioclase and quartz phenocrysts. Some waxy appearance but crystals appear fresh. Multiple samples collected because of weathering.

Petrography: Matrix 95.50%, quartz 3.35%, altered 0.77%, and plagioclase 0.39%

Vitrophyric, flow banded matrix with some perlitic texture. Rare micro laths of plagioclase in matrix. Flow textures around 0.5 mm plagioclase and subhedral and embayed quartz phenocrysts. Some chloritized altered grains.

Sample ID: ZH11-6

Rock Type: A Rock Unit: Ta

Northing: 0521830

Easting: 4756960

Description: Black aphanitic andesite with glassy matrix. Fresh. Most likely upper vitrophyre. Grades into platy weathering with some vesiculated areas. Sampled blocky portion with no weathering inside. Some alteration rind and in fractures.

Sample ID: ZH11-7

Rock Type: R Rock Unit: Tsc

Northing: 0522832

Easting: 4757695

Description: Purplish flow banded rhyolite. Fine grained matrix with abundant well formed 1 - 2 mm plagioclase and quartz. Relatively fresh samples with small weathering rind. Some altered vesicle fill.

Sample ID: ZH11-8

Rock Type: R Rock Unit: Tql

Northing: 0519171

Easting: 4760098

Description: Light gray, latite similar to ZH10-17. Very fine grained matrix. Pretty fresh. Fine grained plagioclase and quartz and scattered rare biotite.

Sample ID: ZH11-9

Rock Type: B Rock Unit: Tsb

Northing: 0518334

Easting: 4764571

Description: Black very fine grained to aphanitic basalt. Some areas of extremely fresh but abundant fractures allow for seams of alteration. Some pyrite found near alteration bands. Potential 0.5 mm quartz and plagioclase.

Sample ID: ZH11-13

Rock Type: Ba Rock Unit: Tsb

Northing: 0512206

Easting: 4763644

Description: Black basalt with very fine grained matrix. Aphanitic, fresh 1 mm plagioclase and quartz scattered throughout. Possible dike material. Horizontal columnar jointing.

Sample ID: ZH11-14

Rock Type: R Rock Unit: Tsc

Northing: 0518303

Easting: 4765003

Description: Rhyolite dike material. Same outcrop as ZH10-27. White, fine grained, and slightly altered. Best available massive sample was collected.

Sample ID: ZH11-15

Rock Type: R Rock Unit: Tsc

Northing: 0516085

Easting: 4766186

Description: Purplish gray latite. Relatively fresh with 1 mm quartz and plagioclase phenocrysts. Some biotite as well. Crystals fresh with some banding of minerals present.

Sample ID: ZH11-16

Rock Type: D Rock Unit: Tgml

Northing: 0516227

Easting: 4765651

Description: Latite with vitrophyric black groundmass. Relatively fresh in the core. Lots of alteration rind in fracture zones. 1 - 2 mm plagioclase and quartz. Possible mafics and vesicle fill.

Sample ID: ZH11-17

Rock Type: R Rock Unit: Tsc

Northing: 0516182

Easting: 4765491

Description: Relatively fresh rhyolite dike material. White very fine grained. 1 - 2 mm quartz, plagioclase and biotite. Some feldspar alteration but majority of phenocrysts are relatively fresh.

Sample ID: ZH11-18

Rock Type: Ba Rock Unit: Tsb

Northing: 0516038

Easting: 4765239

Description: Very fine grained basaltic andesite that was relatively fresh. Possible sericite veins throughout. Fine grained 0.5 mm quartz and plagioclase phenocrysts. Upper most flow of basaltic unit. Slight weathering rind and alteration in fractures.

Appendix B - Geochemistry

Major, trace and rare earth element geochemical results were all obtained at Washington State University. Major and trace elements for all samples were analyzed by XRF. More detailed trace element and rare earth elements were determined for select subset of samples using inductively coupled plasma mass spectrometer (ICP-MS). All samples used XRF analysis for the trace elements Ni, Cr, V, Ga, Cu, Zn and As. The trace elements La, Ce, Nd, Ba, Th, Nb, Y, U, Pb, Rb, Cs, Sr, Sc, and Zr were analyzed with ICP-MS for the select subset samples and XRF for the remainder of the samples. Elements that were not analyzed for a given sample are denoted in the table with a “---” symbol. The raw major element geochemistry results are summarized in the table below. The following samples were not analyzed for geochemistry and are not included in the appendix.

Samples not analyzed:

MB07-13A	MB07-13B	MB07-14	MB07-18	MB07-19	MB07-20	MB09-8A
MB09-8B	MB09-8C	MB09-24	JK10-3	JK10-7	ZH10-1	ZH10-9
ZH10-18	ZH10-19	ZH10-27	ZH10-34	ZH11-10B		

Major Element Data (wt. %)

Table B.1: Raw major element geochemistry

Sample	Unit	SiO ₂	TiO ₂	Al ₂ O ₃	FeO*	MnO	MgO	CaO	Na ₂ O	K ₂ O	P ₂ O ₅	Total	LOI
MB07-16	Kg	63.83	0.64	15.98	4.16	0.08	1.83	4.38	2.54	3.14	0.18	96.75	3.36
MB07-17A	Kg	72.49	0.16	15.46	1.15	0.04	0.38	2.62	3.89	2.39	0.05	98.63	1.04
MB07-17B	N?A	67.00	0.46	15.29	2.73	0.06	1.42	3.18	3.07	3.78	0.18	97.16	2.13
MB07-17C	N?A	74.45	0.97	10.47	2.01	0.01	0.08	0.89	0.12	7.93	0.14	97.06	1.51
MB09-1	Tql	77.38	0.27	12.70	0.62	0.01	0.01	0.07	0.12	5.28	0.02	96.48	2.10
MB09-2	Tsb	50.07	2.60	13.89	11.95	0.22	3.52	8.73	2.24	1.30	0.50	95.02	4.50
MB09-3	Tsb	50.93	2.63	13.69	12.02	0.17	3.87	8.39	2.38	1.47	0.52	96.06	3.31
MB09-4	Tsb	50.80	2.03	14.79	11.12	0.17	3.54	8.38	2.23	1.26	0.47	94.79	4.61
MB09-5	Tsb	48.95	2.60	13.15	12.48	0.17	2.58	8.59	2.00	1.56	0.52	92.58	6.06
MB09-6	Tsb	48.38	2.33	15.14	11.85	0.18	4.71	8.62	3.35	1.13	0.46	96.15	3.82
MB09-7	Tsb	49.53	2.26	15.30	11.32	0.15	5.51	7.67	3.25	1.27	0.46	96.73	2.03
MB09-9	Ta ₁	56.87	0.93	16.41	6.50	0.12	3.31	6.75	2.92	2.53	0.39	96.73	3.09
MB09-10	Kg	72.60	0.17	15.41	1.23	0.03	0.40	2.60	3.84	2.48	0.06	98.82	0.88
MB09-11	Tsc	75.60	0.20	12.21	1.25	0.01	0.08	0.75	2.80	5.10	0.02	98.03	0.94
MB09-12	Tsc	76.20	0.19	12.54	1.10	0.02	0.09	0.67	2.80	5.25	0.02	98.88	0.76
MB09-13	Tsb	48.30	1.89	15.02	10.92	0.17	7.68	10.10	2.57	0.63	0.21	97.49	1.55
MB09-15	Ttfc	75.24	0.09	12.50	1.54	0.02	0.00	0.68	3.70	5.02	0.01	98.80	0.61
MB09-16	Ttfc	75.59	0.14	12.57	1.44	0.01	0.06	0.51	3.53	5.00	0.02	98.88	0.53
MB09-17	Tsb	52.82	2.41	13.79	11.15	0.17	3.60	7.35	2.88	1.83	0.43	96.44	2.74
MB09-18	Tsb	49.79	1.94	15.79	10.91	0.17	5.96	8.73	3.14	0.85	0.33	97.62	1.90
MB09-19	Tsb	48.41	2.57	14.81	13.23	0.18	5.43	8.28	3.22	1.09	0.43	97.65	1.54
MB09-20	Tcst	70.84	0.32	11.96	2.55	0.04	0.10	0.84	1.75	6.28	0.03	94.71	4.04
MB09-21	Tsb	48.08	1.85	15.90	11.47	0.18	7.59	9.61	2.81	0.43	0.23	98.15	1.82
MB09-22	Tsc	76.33	0.13	12.28	0.99	0.01	0.09	0.60	2.88	5.23	0.01	98.55	0.70
MB09-23	Tsb	48.80	1.82	15.87	10.89	0.17	5.86	9.11	3.10	0.77	0.30	96.69	2.73

Major Element Data (wt. %)

Sample	Unit	SiO ₂	TiO ₂	Al ₂ O ₃	FeO*	MnO	MgO	CaO	Na ₂ O	K ₂ O	P ₂ O ₅	Total	LOI
MB09-25	Tsb	49.35	2.60	13.99	12.62	0.20	3.84	8.50	2.06	1.78	0.50	95.46	3.46
MB09-26	Tsb	49.49	2.25	15.51	11.87	0.17	4.62	8.87	2.26	1.42	0.45	96.91	2.94
MB09-27	Tsb	42.27	2.19	16.21	13.20	0.22	4.67	11.19	1.91	0.43	0.34	92.63	7.03
MB09-29	Tsb	47.19	2.30	16.40	11.76	0.18	4.08	9.54	2.21	0.70	0.39	94.74	3.73
JK10-1	Kg	76.60	0.01	14.51	0.27	0.02	0.10	0.63	3.65	3.98	0.03	99.80	1.08
JK10-2A	Kg	76.21	0.05	13.66	0.18	0.00	0.02	1.01	3.34	3.72	0.02	98.21	1.03
JK10-2B	Kg	74.30	0.11	14.83	0.90	0.02	0.23	1.61	3.69	3.50	0.04	99.23	0.86
JK10-4	Kg	72.96	0.17	14.84	1.21	0.03	0.42	2.14	3.31	3.26	0.07	98.41	1.79
JK10-5	Kg	73.24	0.13	15.44	1.15	0.03	0.34	2.15	3.63	3.20	0.07	99.38	0.89
JK10-6	Kg	73.95	0.15	14.94	1.28	0.04	0.33	2.08	3.71	2.97	0.04	99.49	0.88
JK10-8	Kg	76.33	0.09	13.59	0.55	0.01	0.17	1.28	3.15	3.83	0.04	99.04	0.71
JK10-9	Kg	74.60	0.15	14.37	0.90	0.03	0.22	1.03	3.02	4.15	0.07	98.54	0.97
JK10-10	Kg	73.50	0.22	15.60	0.80	0.02	0.31	1.20	2.02	3.76	0.06	97.50	1.55
MB10-3	Kg	71.76	0.15	15.45	1.46	0.02	0.36	1.05	3.52	3.73	0.09	97.59	1.30
MB10-4	Kg	73.31	0.14	15.24	1.06	0.03	0.34	2.06	3.58	2.86	0.07	98.69	1.12
MB10-5A	Jms	73.19	0.24	14.38	1.20	0.01	0.46	1.48	2.69	4.73	0.06	98.44	0.96
MB10-5B	Jms	68.60	0.58	16.04	2.24	0.02	0.90	2.96	3.92	2.36	0.18	97.80	1.07
MB10-5C	Jms	39.28	1.94	32.84	8.69	0.06	3.77	0.51	0.46	8.28	0.07	95.90	4.21
ZH10-2	Tsb	48.97	1.69	17.04	11.00	0.19	4.00	9.37	2.23	0.61	0.21	95.30	4.34
ZH10-3	Tsb	48.36	1.96	15.96	12.22	0.23	4.70	9.64	2.04	1.02	0.32	96.47	4.10
ZH10-4	Tsb	48.11	1.94	16.00	11.76	0.22	5.48	9.45	2.43	1.29	0.32	96.98	2.32
ZH10-5A	Tsc	78.46	0.12	11.20	0.15	0.00	0.04	0.08	0.79	7.43	0.01	98.29	0.92
ZH10-6	Tsc	80.41	0.10	10.55	1.00	0.03	0.05	1.25	3.30	1.64	0.01	98.34	1.16
ZH10-7	Tql	79.29	0.22	9.37	2.77	0.02	0.21	0.23	0.17	4.97	0.01	97.27	1.94
ZH10-8	Tsc	80.87	0.08	10.47	0.79	0.02	0.05	1.17	5.19	0.46	0.01	99.12	0.68

Major Element Data (wt. %)

Sample	Unit	SiO ₂	TiO ₂	Al ₂ O ₃	FeO*	MnO	MgO	CaO	Na ₂ O	K ₂ O	P ₂ O ₅	Total	LOI
ZH10-10	N/A	87.11	0.08	7.72	0.21	0.00	0.02	0.05	0.09	2.95	0.01	98.24	1.17
ZH10-11	Tgmr	74.14	0.27	13.03	1.66	0.03	0.20	1.08	2.17	4.98	0.04	97.61	1.50
ZH10-12	Tsc	74.31	0.27	12.66	1.46	0.01	0.33	0.95	2.74	4.87	0.04	97.64	1.33
ZH10-13	Tgmr	74.37	0.13	11.39	1.60	0.02	0.02	0.67	2.80	5.15	0.01	96.16	3.10
ZH10-14	Tsb	46.39	1.56	17.09	10.84	0.16	4.12	9.53	2.05	0.13	0.20	92.06	6.80
ZH10-15	Tsc	74.69	0.27	12.69	1.22	0.01	0.25	0.96	2.70	4.95	0.04	97.77	1.47
ZH10-16	Tsc	72.84	0.35	13.36	1.86	0.04	0.24	0.86	2.38	4.78	0.05	96.76	1.99
ZH10-17	Tql	73.81	0.30	12.24	3.19	0.00	0.06	0.52	2.40	4.84	0.03	97.39	1.78
ZH10-20	Ta ₁	55.51	0.96	16.23	7.05	0.12	3.45	8.05	3.04	1.33	0.37	96.10	4.05
ZH10-21	Tql	75.70	0.28	12.51	0.83	0.00	0.02	0.78	3.34	4.92	0.04	98.44	0.41
ZH10-22	Tgmd	64.36	0.46	13.49	4.76	0.07	2.84	4.10	2.01	3.59	0.06	95.76	3.85
ZH10-23	Tgmd	66.18	0.48	13.84	5.55	0.12	2.48	3.72	3.02	3.69	0.06	99.13	1.31
ZH10-24	Tql	75.85	0.30	12.91	0.36	0.00	0.01	0.50	2.46	5.17	0.03	97.60	1.51
ZH10-25	Ta ₂	60.12	0.85	13.44	8.04	0.26	2.71	5.90	2.34	2.60	0.15	96.40	3.22
ZH10-26	Tgmd	65.39	1.02	13.01	7.47	0.18	0.81	2.03	2.97	3.25	0.35	96.49	2.80
ZH10-28	Tsb	49.54	2.47	14.34	12.36	0.19	4.70	8.96	3.22	1.03	0.43	97.24	2.14
ZH10-29	Tql	75.56	0.28	12.44	1.21	0.00	0.22	0.53	2.46	5.71	0.04	98.46	1.56
ZH10-30	Tsb	47.60	1.87	14.74	11.02	0.17	6.77	11.02	2.67	0.46	0.28	96.60	3.22
ZH10-31	Tsc	78.40	0.14	11.46	0.38	0.00	0.24	0.41	2.07	5.17	0.02	98.28	1.72
ZH10-32	Tsc	79.98	0.15	11.31	0.11	0.00	0.17	0.33	1.41	5.24	0.02	98.72	1.65
ZH10-33	Tgmd	66.00	0.48	13.71	4.88	0.07	2.62	3.96	2.94	3.74	0.06	98.45	1.18
ZH10-35	Thpl	74.48	0.20	12.19	2.10	0.01	0.07	0.63	3.38	4.91	0.02	97.98	1.29
ZH10-36	Tql	76.11	0.25	12.79	0.87	0.00	0.04	0.79	3.40	5.13	0.03	99.41	0.47
ZH10-37	N/A	63.46	1.49	13.28	5.90	0.08	0.82	2.10	0.34	8.30	1.13	96.90	2.93
ZH10-38	Tsc	80.95	0.23	11.47	0.80	0.01	0.14	0.13	0.20	4.60	0.03	98.55	1.76

Major Element Data (wt. %)

Sample	Unit	SiO ₂	TiO ₂	Al ₂ O ₃	FeO*	MnO	MgO	CaO	Na ₂ O	K ₂ O	P ₂ O ₅	Total	LOI
ZH10-39A	Tsb	46.93	1.89	15.66	11.27	0.20	3.12	11.41	2.40	0.67	0.31	93.86	5.47
ZH10-39B	Tsb	49.53	1.93	15.97	11.16	0.16	5.29	9.75	2.53	0.78	0.33	97.42	2.98
ZH10-40	Ta ₁	57.54	1.01	15.01	7.12	0.12	4.87	7.01	2.83	1.98	0.24	97.74	2.18
ZH10-41	Tgmd	66.52	0.53	13.25	3.57	0.06	2.11	4.17	2.75	2.40	0.12	95.48	4.41
ZH10-42	Tsc	75.54	0.26	12.83	0.24	0.00	0.20	0.56	2.14	6.01	0.05	97.81	1.71
ZH10-43	Tgmr	74.51	0.21	12.72	1.73	0.03	0.21	1.10	2.86	4.82	0.03	98.21	1.20
ZH11-1	Thpl	75.71	0.21	12.64	1.35	0.01	0.01	0.48	3.61	5.12	0.03	99.17	0.26
ZH11-2	Thpl	71.97	0.20	12.00	2.16	0.03	0.00	0.76	2.45	5.39	0.01	94.94	3.61
ZH11-3	Thpl	75.82	0.18	12.59	0.85	0.00	0.01	0.42	3.30	5.19	0.01	98.38	0.87
ZH11-4	N/A	47.76	1.99	15.77	9.03	0.15	8.25	8.72	3.34	2.07	0.98	98.06	1.81
ZH11-5	Thpl	72.44	0.18	12.04	2.29	0.03	0.00	0.83	2.78	5.59	0.01	96.20	3.39
ZH11-6	Ta ₂	57.02	1.60	14.97	8.21	0.16	3.77	7.15	2.75	2.30	0.55	98.49	1.24
ZH11-7	Tsc	75.79	0.24	12.71	1.08	0.02	0.11	0.91	3.00	5.09	0.02	98.96	0.64
ZH11-8	Tql	75.74	0.28	12.87	0.87	0.01	0.00	0.55	2.86	4.95	0.02	98.15	1.26
ZH11-9	Tsb	47.01	1.86	16.17	10.40	0.17	3.72	11.31	2.48	0.22	0.31	93.67	5.42
ZH11-10a	Tql	75.69	0.25	13.10	0.67	0.00	0.00	0.09	0.50	5.66	0.04	96.00	2.70
ZH11-11	Tsc	78.32	0.14	11.14	0.73	0.01	0.03	0.64	2.77	4.72	0.01	98.50	1.23
ZH11-12	Ttfc	79.81	0.09	9.94	0.49	0.00	0.00	0.13	1.17	6.77	0.03	98.42	1.06
ZH11-13	Tsb	51.73	2.67	14.06	12.05	0.19	4.13	8.00	3.17	1.39	0.52	97.90	1.70
ZH11-14	Tsc	81.71	0.08	10.21	0.39	0.01	0.34	0.18	0.06	3.75	0.01	96.73	2.94
ZH11-15	Tsc	76.22	0.14	12.06	0.69	0.00	0.03	0.45	2.18	5.36	0.02	97.14	1.66
ZH11-16	Tgmd	65.87	0.91	12.96	6.31	0.09	0.71	3.32	3.21	3.21	0.21	96.80	3.10
ZH11-17	Tsc	75.50	0.16	11.93	0.93	0.01	0.21	0.42	1.59	5.10	0.02	95.87	3.12
ZH11-18	Tsb	51.59	2.66	13.56	12.44	0.21	3.35	7.87	3.22	1.57	0.53	97.00	2.72

Trace Element Data (ppm)

Table B.2: Trace element geochemistry

Sample	Ni	Cr	V	Ga	Cu	Zn	As	Sc	Ba	Rb	Sr
MB07-16	3	25	45	20	10	80	11	9	1111	94	510
MB07-17A	0	5	8	20	1	53	6	3	1694	56	556
MB07-17B	3	20	46	21	3	56	13	5	1510	128	620
MB07-17C	4	16	40	7	984	108	34	13	354	362	129
MB09-1	2	4	1	24	5	10	33	4	2596	196	73
MB09-2	24	30	295	24	36	142	0	26	798	25	476
MB09-3	21	22	304	23	39	143	4	27	783	45	418
MB09-4	56	48	253	22	79	121	3	23	664	24	481
MB09-5	30	16	305	22	40	140	0	26	789	34	472
MB09-6	80	48	271	21	70	126	7	22	513	24	511
MB09-7	83	42	258	22	61	131	0	22	515	32	472
MB09-9	45	69	130	19	57	87	14	14	1138	43	657
MB09-10	3	5	9	18	1	39	1	2	1743	55	566
MB09-11	3	5	13	16	3	37	2	4	1578	166	91
MB09-12	2	3	14	16	2	28	1	4	1527	171	81
MB09-13	177	198	310	19	168	93	6	29	180	13	348
MB09-15	0	4	2	29	6	179	0	1	42	254	6
MB09-16	4	5	6	28	13	189	3	3	159	237	17
MB09-17	7	4	310	23	11	127	2	28	715	52	390
MB09-18	60	83	282	20	47	114	3	26	355	19	437
MB09-19	116	73	284	23	104	138	0	25	403	24	419
MB09-20	3	3	17	23	6	112	1	7	1297	187	51
MB09-21	129	79	285	21	67	102	2	26	160	8	418
MB09-22	3	3	5	17	1	45	0	3	1227	179	69
MB09-23	62	81	267	21	70	114	4	25	342	16	464

Trace Element Data (ppm)

Sample	Ni	Cr	V	Ga	Cu	Zn	As	Sc	Ba	Rb	Sr
MB09-25	27	30	298	23	40	144	1	27	653	43	389
MB09-26	92	45	256	22	57	128	4	21	334	43	446
MB09-27	123	91	291	21	80	124	3	26.1	232	11	426
MB09-29	67	47	277	23	63	121	5	23.7	293	17	444
JK10-1	4	4	1	18	1	10	---	3.6	639	104	120
JK10-2A	1	3	4	15	0	20	---	1.4	1986	103	348
JK10-2B	4	4	6	19	1	67	---	2.6	3048	68	563
JK10-4	4	6	7	19	1	52	---	3.0	1647	99	516
JK10-5	3	4	7	19	28	66	---	3.3	2512	68	550
JK10-6	3	7	7	19	0	52	---	2.5	1743	74	516
JK10-8	3	3	2	16	0	32	---	3.0	1863	72	360
JK10-9	2	3	6	22	0	34	---	5.2	1016	115	253
JK10-10	1	3	21	34	0	30	---	16.3	1290	91	279
MB10-3	3	2	6	23	0	71	---	4.1	2088	72	218
MB10-4	4	5	10	18	0	51	---	3.3	1824	73	497
MB10-5A	7	9	13	15	2	38	---	3.6	3319	95	493
MB10-5B	6	5	45	23	1	79	---	4.4	1468	81	611
MB10-5C	33	221	269	68	19	288	---	23.3	2343	281	112
ZH10-2	138	53	285	20	84	104	---	27.2	261	20	505
ZH10-3	59	85	281	22	21	110	---	25.0	352	30	377
ZH10-4	62	88	282	22	41	110	---	26.2	381	44	384
ZH10-5A	4	4	3	8	1	6	---	2.4	689	290	75
ZH10-6	4	4	6	15	3	35	---	3.8	877	62	211
ZH10-7	4	3	10	12	11	139	---	2.5	447	218	175
ZH10-8	3	4	4	13	1	14	---	2.4	193	17	201

Trace Element Data (ppm)

Sample	Ni	Cr	V	Ga	Cu	Zn	As	Sc	Ba	Rb	Sr
ZH10-10	3	4	3	11	1	11	---	2.1	88	120	14
ZH10-11	4	5	16	21	3	64	---	4.5	1674	190	118
ZH10-12	4	6	19	16	2	36	---	3.7	1417	168	115
ZH10-13	3	3	2	24	4	138	---	2.5	430	191	26
ZH10-14	153	51	256	20	133	96	---	22.8	101	3	560
ZH10-15	4	5	19	17	1	41	---	4.1	1482	166	111
ZH10-16	4	5	29	17	5	45	---	4.6	1589	170	121
ZH10-17	2	2	4	24	1	157	---	7.8	2493	161	136
ZH10-20	64	99	140	19	58	85	---	16.3	767	10	636
ZH10-21	4	2	4	25	2	142	---	7.8	2601	163	162
ZH10-22	37	34	81	21	22	123	---	13.1	153	115	106
ZH10-23	47	35	83	22	24	127	---	13.4	150	107	114
ZH10-24	4	3	2	25	1	20	---	7.0	2059	179	123
ZH10-25	18	36	161	20	30	145	---	22.5	1079	79	255
ZH10-26	6	2	46	23	13	147	---	15.6	1680	110	296
ZH10-28	48	48	300	22	48	137	---	27.9	500	27	441
ZH10-29	4	3	4	23	2	184	---	7.0	2060	182	94
ZH10-30	107	150	269	19	32	107	---	25.1	271	18	491
ZH10-31	3	5	7	16	1	6	---	3.1	1670	171	63
ZH10-32	4	3	7	15	1	3	---	3.4	1546	175	68
ZH10-33	44	33	82	22	25	129	---	13.3	149	107	110
ZH10-35	3	4	3	24	5	119	---	4.5	2126	188	98
ZH10-36	4	2	4	27	1	103	---	5.8	2541	175	132
ZH10-37	70	424	127	14	21	210	---	20.9	2514	345	406
ZH10-38	4	5	21	16	1	16	---	2.9	1602	157	55

Trace Element Data (ppm)

Sample	Ni	Cr	V	Ga	Cu	Zn	As	Sc	Ba	Rb	Sr
ZH10-39A	63	80	273	21	37	109	---	24.8	315	12	485
ZH10-39B	62	82	272	21	44	110	---	25.0	282	15	441
ZH10-40	48	71	176	18	29	81	---	21.6	744	62	328
ZH10-41	21	30	78	17	12	52	---	10.9	1239	143	267
ZH10-42	2	6	19	16	2	10	---	3.9	1284	186	131
ZH10-43	2	5	12	22	3	99	---	4.1	1288	209	87
ZH11-1	2	4	2	26	6	124	0	2.4	1853	192	89
ZH11-2	1	3	3	23	4	130	1	2.1	1805	211	86
ZH11-3	1	1	3	28	2	102	0	2.3	1136	210	51
ZH11-4	142	205	214	21	47	117	0	21.4	1242	35	1568
ZH11-5	3	4	2	24	6	139	0	2.2	1380	213	69
ZH11-6	17	39	194	21	14	135	2	21.3	1049	53	554
ZH11-7	0	5	14	16	2	31	0	2.5	1851	165	115
ZH11-8	2	2	2	25	3	136	0	3.4	2465	167	138
ZH11-9	60	88	273	21	30	105	4	25.0	205	2	468
ZH11-10a	2	3	2	25	2	78	0	3.1	2564	215	151
ZH11-11	0	2	9	16	3	15	0	2.9	1545	156	77
ZH11-12	1	4	5	17	2	7	94	1.9	248	273	28
ZH11-13	22	23	305	24	41	144	7	25.8	692	63	452
ZH11-14	1	3	9	11	1	3	0	1.6	287	176	66
ZH11-15	1	2	7	16	2	10	2	3.4	1472	175	54
ZH11-16	3	2	42	21	9	126	4	14.3	1668	134	292
ZH11-17	2	2	10	16	1	22	0	2.4	1171	174	53
ZH11-18	31	20	311	23	97	145	2	25.9	719	30	434

Trace Element Data (ppm)

Table B.3: Trace element geochemistry (continued)

Sample	Zr	Y	Nb	Pb	La	Ce	Th	Nd	U	Cs
MB07-16	185	17	13	16	37.2	63.4	10.5	27.3	4.0	---
MB07-17A	90	8	5	19	25.2	46.7	7.0	19.6	0.9	1.43
MB07-17B	163	12	15	20	40.7	75.2	13.5	29.9	2.9	---
MB07-17C	288	36	20	143	39.7	76.7	13.6	35.4	3.2	---
MB09-1	560	56	31	16	33.6	74.1	19.2	36.1	4.9	---
MB09-2	256	40	18	6	29.4	65.1	4.2	38.0	1.1	0.50
MB09-3	272	41	20	6	32.9	67.2	3.9	39.5	1.9	---
MB09-4	204	33	15	7	22.9	59.8	3.8	30.0	1.2	---
MB09-5	262	40	19	8	31.4	68.4	4.5	39.2	1.1	2.68
MB09-6	208	34	16	5	21.2	51.5	2.1	31.4	1.7	---
MB09-7	221	36	17	5	27.4	61.6	1.8	35.0	1.4	---
MB09-9	168	16	10	9	29.6	55.9	4.2	25.0	1.3	1.32
MB09-10	91	8	7	20	27.2	42.4	7.6	15.7	0.2	---
MB09-11	162	16	10	23	35.4	62.8	17.6	24.0	3.0	---
MB09-12	159	17	9	22	38.3	69.3	18.9	27.3	3.4	3.33
MB09-13	128	25	8	2	10.3	25.3	1.1	17.3	0.3	0.58
MB09-15	235	108	43	47	55.9	132.9	29.0	69.1	6.0	---
MB09-16	241	64	40	41	74.6	121.9	26.9	81.6	5.9	4.87
MB09-17	214	37	15	9	28.2	60.5	3.7	33.0	2.2	---
MB09-18	159	29	12	4	13.9	42.3	0.5	24.7	4.0	---
MB09-19	219	37	16	4	23.3	53.1	2.9	32.6	0.8	0.22
MB09-20	684	88	48	28	90.5	188.0	22.6	85.4	6.1	4.42
MB09-21	121	23	8	1	9.5	19.5	0.0	15.4	1.6	---
MB09-22	137	14	10	24	45.0	76.5	19.1	32.5	3.5	2.35
MB09-23	145	27	10	3	15.4	35.4	0.8	23.0	0.2	---

Trace Element Data (ppm)

Sample	Zr	Y	Nb	Pb	La	Ce	Th	Nd	U	Cs
MB09-25	261	42	19	6	30.1	66.8	4.3	39.3	1.1	0.82
MB09-26	219	34	17	3	24.7	59.1	2.8	33.2	0.1	---
MB09-27	153	30	12	2	15.7	36.8	1.4	23.7	0.4	0.89
MB09-29	185	31	14	3	18.5	44.9	0.6	26.6	1.5	---
JK10-1	43	9	5	28	13.8	20.8	4.1	8.9	1.3	1.40
JK10-2A	41	9	3	22	13.3	23.9	4.9	9.6	0.8	0.72
JK10-2B	48	5	2	38	27.1	51.6	8.5	22.7	0.6	0.77
JK10-4	93	8	6	18	24.5	45.1	6.9	18.8	1.3	1.85
JK10-5	87	7	6	46	21.8	39.6	6.1	16.4	0.7	0.75
JK10-6	85	7	7	21	23.6	39.8	5.9	14.7	0.0	0.00
JK10-8	32	21	4	28	18.7	35.7	7.0	15.3	0.7	0.27
JK10-9	83	9	7	25	23.2	45.5	8.2	19.9	1.4	0.81
JK10-10	57	5	13	11	13.9	24.6	4.3	10.2	0.0	2.60
MB10-3	53	6	4	21	21.2	39.8	6.1	18.2	0.1	0.30
MB10-4	85	8	7	22	21.8	38.0	6.2	16.1	1.2	0.00
MB10-5A	125	9	5	41	47.9	87.7	18.1	35.8	3.6	1.50
MB10-5B	174	9	9	23	27.9	57.2	10.3	25.9	1.8	1.20
MB10-5C	406	37	34	9	178.6	353.9	52.4	157.8	9.5	3.74
ZH10-2	95	21	6	2	9.2	21.8	0.6	15.4	0.2	0.48
ZH10-3	158	29	12	3	15.9	37.2	2.0	24.6	1.9	0.00
ZH10-4	156	29	11	3	16.5	37.7	2.0	23.7	0.6	0.56
ZH10-5A	125	14	7	9	28.7	56.3	19.6	21.0	3.1	1.58
ZH10-6	110	22	9	14	30.5	49.9	17.9	20.5	3.7	3.10
ZH10-7	561	72	28	13	28.8	35.7	15.7	31.3	6.4	1.90
ZH10-8	93	21	9	25	33.3	63.4	18.2	25.1	2.8	0.00

Trace Element Data (ppm)

Sample	Zr	Y	Nb	Pb	La	Ce	Th	Nd	U	Cs
ZH10-10	69	11	7	5	7.4	20.4	13.8	8.9	2.7	0.00
ZH10-11	272	44	21	23	43.5	85.0	18.5	39.3	3.0	5.40
ZH10-12	186	18	10	22	36.6	60.3	18.7	27.0	3.5	4.00
ZH10-13	257	74	29	34	118.6	221.4	23.1	95.9	4.6	4.31
ZH10-14	93	20	7	1	11.5	23.0	0.4	14.0	0.9	2.90
ZH10-15	173	18	10	21	38.6	72.5	18.6	28.0	3.6	2.98
ZH10-16	198	22	11	23	39.5	64.3	18.8	30.3	4.4	4.90
ZH10-17	560	48	27	30	74.3	137.4	17.0	75.2	3.6	2.72
ZH10-20	149	17	9	8	25.7	48.5	3.1	22.6	1.0	0.50
ZH10-21	603	72	32	33	82.3	168.0	18.8	76.9	4.1	2.04
ZH10-22	308	39	20	20	46.7	98.2	10.3	44.4	2.3	2.49
ZH10-23	323	42	22	20	45.1	94.9	9.8	45.1	1.1	4.90
ZH10-24	589	66	29	27	87.7	193.5	18.1	90.0	4.7	3.19
ZH10-25	267	46	17	17	39.8	82.0	8.8	39.2	2.7	1.30
ZH10-26	336	47	22	22	50.7	103.5	12.4	50.0	2.4	3.30
ZH10-28	220	37	16	4	20.9	56.3	3.0	31.7	1.3	3.20
ZH10-29	587	71	30	28	74.6	150.7	18.7	70.0	4.0	1.86
ZH10-30	132	26	11	3	13.2	28.8	0.0	20.3	0.6	1.40
ZH10-31	147	14	10	21	38.9	71.6	18.4	25.3	3.1	5.69
ZH10-32	188	22	11	20	41.3	73.6	18.9	29.7	4.1	0.40
ZH10-33	322	39	21	20	48.1	99.2	10.8	45.6	2.4	1.96
ZH10-35	449	25	28	33	62.4	66.4	20.4	62.2	3.6	2.87
ZH10-36	543	41	29	34	68.4	135.8	19.7	62.7	4.1	2.16
ZH10-37	249	23	18	14	57.3	115.2	6.8	58.8	1.9	3.40
ZH10-38	165	15	9	16	24.7	40.9	15.7	16.1	3.6	3.70

Trace Element Data (ppm)

Sample	Zr	Y	Nb	Pb	La	Ce	Th	Nd	U	Cs
ZH10-39A	154	28	11	3	15.4	36.7	1.5	20.9	1.3	2.30
ZH10-39B	158	28	11	4	16.7	33.1	0.5	21.9	1.8	7.40
ZH10-40	138	24	9	9	23.0	47.2	6.6	23.3	1.4	1.58
ZH10-41	150	22	9	16	30.7	59.3	13.2	24.8	2.8	25.34
ZH10-42	159	16	10	22	41.1	79.3	19.1	32.0	3.8	2.26
ZH10-43	229	63	26	31	44.1	88.1	21.2	43.4	4.5	4.57
ZH11-1	452	30	30	37	40.2	84.5	20.7	44.4	3.8	---
ZH11-2	445	59	28	35	68.4	137.1	19.8	60.9	4.4	5.22
ZH11-3	441	38	32	38	32.0	63.7	22.5	31.5	2.6	---
ZH11-4	262	24	19	9	48.2	103.6	4.0	52.4	1.2	6.53
ZH11-5	428	66	29	37	74.5	157.0	21.2	68.7	4.6	4.54
ZH11-6	259	33	15	10	36.5	76.5	4.7	40.5	1.1	0.92
ZH11-7	179	20	10	23	36.6	64.0	17.6	24.6	3.7	---
ZH11-8	560	56	29	29	71.4	120.3	19.1	64.7	3.6	---
ZH11-9	148	27	10	5	15.5	36.9	1.9	21.0	2.5	---
ZH11-10a	534	80	29	18	124.5	216.0	20.2	108.6	3.9	---
ZH11-11	176	22	10	21	42.2	77.8	17.2	29.6	3.4	3.10
ZH11-12	218	71	35	26	68.8	105.3	18.4	71.4	6.5	---
ZH11-13	274	42	20	7	31.3	69.9	4.5	42.1	2.0	---
ZH11-14	94	15	10	2	13.1	24.7	18.7	9.9	5.2	---
ZH11-15	135	18	9	23	46.1	69.6	19.0	33.1	3.4	---
ZH11-16	334	46	21	23	44.8	98.2	12.3	44.8	3.0	---
ZH11-17	145	16	8	16	37.5	70.0	19.4	26.4	3.5	3.34
ZH11-18	263	41	19	7	31.3	69.1	4.5	39.7	1.2	2.06

Rare Earth Element Data (ppm)

Table B.4: Rare earth element geochemistry

Sample	Hf	Ta	Pr	Sm	Eu	Gd	Tb	Dy	Ho	Er	Tm	Yb	Lu
MB07-17A	2.57	0.33	5.38	3.57	1.04	2.28	0.28	1.43	0.27	0.71	0.11	0.69	0.11
MB09-2	6.56	1.14	8.83	9.24	2.58	9.02	1.44	8.35	1.63	4.20	0.58	3.43	0.52
MB09-5	6.63	1.16	9.17	9.29	2.78	8.97	1.41	8.20	1.60	4.08	0.57	3.38	0.51
MB09-9	4.02	0.61	6.58	4.85	1.44	4.04	0.60	3.36	0.64	1.64	0.23	1.40	0.22
MB09-12	4.95	0.87	8.05	5.02	0.58	3.80	0.59	3.37	0.65	1.80	0.27	1.64	0.25
MB09-13	3.40	0.50	3.70	4.83	1.75	5.29	0.86	5.21	1.02	2.56	0.35	2.11	0.31
MB09-16	9.80	2.79	20.20	18.70	0.53	16.73	2.61	14.91	2.87	7.48	1.08	6.64	0.97
MB09-19	5.63	1.03	7.33	7.99	2.49	8.10	1.29	7.55	1.45	3.68	0.51	3.09	0.47
MB09-20	17.87	2.98	22.33	18.05	2.07	16.40	2.79	17.21	3.52	9.69	1.42	9.06	1.37
MB09-22	4.55	0.92	9.47	5.80	0.60	4.06	0.60	3.24	0.60	1.53	0.23	1.48	0.22
MB09-25	6.71	1.15	9.03	9.43	2.80	9.18	1.47	8.52	1.65	4.23	0.58	3.51	0.54
MB09-27	3.94	0.73	5.20	6.16	1.97	6.38	1.03	6.11	1.17	3.02	0.40	2.48	0.39
JK10-2A	1.34	0.21	2.74	1.74	0.56	1.32	0.21	1.34	0.28	0.82	0.13	0.82	0.13
JK10-2B	1.40	0.06	6.15	4.32	1.69	2.68	0.28	1.10	0.17	0.38	0.05	0.29	0.05
JK10-4	2.57	0.33	5.19	3.49	1.04	2.43	0.33	1.67	0.31	0.76	0.11	0.65	0.11
JK10-5	2.38	0.27	4.55	3.08	1.03	2.10	0.27	1.38	0.25	0.65	0.09	0.58	0.09
JK10-8	1.04	0.14	4.27	3.54	0.71	3.28	0.55	3.47	0.74	2.03	0.29	1.64	0.24
JK10-9	2.74	0.47	5.50	4.18	0.59	3.07	0.42	2.13	0.35	0.82	0.12	0.69	0.11
MB10-5C	11.32	1.50	42.37	31.62	1.50	23.32	2.95	12.31	1.60	2.76	0.30	1.60	0.25
ZH10-2	2.53	0.38	3.27	4.10	1.61	4.36	0.70	4.22	0.83	2.16	0.30	1.81	0.27
ZH10-4	4.04	0.66	5.28	5.93	1.88	6.02	0.98	5.82	1.15	2.97	0.41	2.48	0.38
ZH10-5A	4.21	0.67	6.35	3.78	0.25	2.70	0.43	2.60	0.53	1.48	0.23	1.45	0.22
ZH10-13	9.08	1.89	25.78	18.18	0.99	15.16	2.45	14.64	2.90	7.73	1.12	6.82	1.04
ZH10-15	5.17	0.85	8.15	4.97	0.59	3.82	0.59	3.48	0.68	1.81	0.27	1.66	0.25
ZH10-17	14.37	1.61	20.05	15.60	2.54	11.45	1.89	11.02	2.10	5.79	0.85	5.41	0.84

Rare Earth Element Data (ppm)

Sample	Hf	Ta	Pr	Sm	Eu	Gd	Tb	Dy	Ho	Er	Tm	Yb	Lu
ZH10-20	3.54	0.59	5.84	4.48	1.37	3.79	0.58	3.34	0.64	1.67	0.24	1.46	0.22
ZH10-21	15.30	1.85	19.97	16.17	2.39	14.63	2.37	14.29	2.84	7.50	1.05	6.43	0.96
ZH10-22	8.19	1.19	11.46	9.23	0.63	8.06	1.30	7.70	1.53	4.14	0.59	3.72	0.59
ZH10-24	14.71	1.70	23.63	18.76	2.64	15.24	2.44	13.91	2.65	6.87	0.97	5.89	0.87
ZH10-29	15.00	1.77	18.35	14.50	2.34	12.66	2.12	13.07	2.71	7.55	1.12	7.13	1.10
ZH10-31	4.74	0.83	7.77	4.24	0.52	2.94	0.46	2.78	0.56	1.58	0.24	1.61	0.24
ZH10-33	8.56	1.23	11.79	9.55	0.63	8.32	1.34	7.85	1.56	4.13	0.60	3.67	0.57
ZH10-35	12.28	1.85	16.99	12.36	1.53	8.80	1.35	7.29	1.27	3.13	0.45	2.70	0.38
ZH10-36	14.33	1.84	16.81	13.06	2.03	10.59	1.66	9.24	1.70	4.24	0.58	3.53	0.52
ZH10-40	3.88	0.62	5.94	5.13	1.30	4.72	0.77	4.63	0.92	2.49	0.36	2.27	0.35
ZH10-41	4.43	0.74	6.81	4.98	0.87	4.21	0.67	4.05	0.83	2.21	0.33	2.09	0.32
ZH10-42	4.95	0.89	9.05	5.80	0.60	3.78	0.57	3.15	0.60	1.59	0.25	1.56	0.25
ZH10-43	7.71	1.89	11.21	10.56	0.71	10.48	1.82	11.28	2.29	6.28	0.91	5.55	0.82
ZH11-2	12.07	1.80	16.24	12.65	1.37	11.31	1.87	11.54	2.29	6.22	0.91	5.54	0.85
ZH11-4	6.25	1.09	13.23	9.73	2.73	7.08	0.99	5.21	0.92	2.30	0.31	1.86	0.29
ZH11-5	11.95	1.91	17.97	14.54	1.16	12.72	2.11	12.88	2.51	6.86	1.00	6.05	0.93
ZH11-6	6.42	0.81	9.87	8.54	2.11	7.52	1.16	6.65	1.31	3.44	0.50	3.02	0.46
ZH11-11	5.37	0.82	8.71	5.47	0.58	4.14	0.69	4.16	0.81	2.20	0.33	2.09	0.31
ZH11-17	4.67	0.81	7.76	4.79	0.45	3.61	0.58	3.27	0.63	1.69	0.26	1.62	0.25
ZH11-18	6.64	1.15	9.29	9.33	2.66	9.21	1.46	8.49	1.64	4.17	0.58	3.47	0.52

Appendix C - Radiogenic Isotope Data

Radiogenic isotopes of strontium, neodymium and lead were analyzed at MU. Fourteen samples and one replicate were analyzed using a TIMS. The radiogenic isotope values are summarized in the table below. The 2σ values listed for the isotope ratios are based on MU's internal reproducibility of a known standard sample. MU uses the standards NBS981 (Pb), NBS987 (Sr), and NBSXXX (Nd). The 2σ values for the fourteen samples are not reported but are well below (typically three magnitudes lower) than the standards error values. The Sr and Nd ratios have been corrected for Rb and Sm interferences respectively. Additionally, the ratio values were corrected during analysis for fractionation with the exponential law using $^{86}\text{Sr}/^{88}\text{Sr} = 0.1194$ and $^{143}\text{Nd}/^{146}\text{Nd} = 0.7219$. The samples were processed in the clean lab at MU using the following guidelines.

Sample Dissolution:

Weigh out 50 - 200 μg of rock powder based on ppm Pb data from XRF.

Dissolve powder in 0.5 mL concentrated HNO_3 (per 50 μg powder) and 1.0 mL concentrated HF (per 50 μg powder) and cook overnight on hotplate.

Completely dry sample.

Dissolve sample in 0.5 mL concentrated HNO_3 and completely dry.

Repeat previous step.

Dissolve in 1 mL 0.5N HBr and completely dry.

Repeat previous step.

Dissolve in 3 mL 0.5N HBr.

Pb Separations:

Load columns with resin and clean with 12 mL 8N HNO_3 , then 6 mL 0.5 HNO_3 , and then 0.5 mL E-Pure water.

Charge resin with 0.5 mL 0.5N HBr.

Load samples in HBr onto columns and collect solution in teflon vial.

Rinse with 0.3 mL 0.5N HBr and collect solution in teflon vial.

Rinse with 0.5 mL 0.5N HBr and collect solution in teflon vial.

Repeat previous step.

Save solution for Sr separation.

Rinse with 1 mL 0.5N HNO₃ and collect Pb solution in teflon vial.

Completely dry Pb solution, re-dissolve in 1.0 mL 0.5 HBr.

Clean columns with 12 mL 6N HNO₃, and then 0.5 mL E-Pure water.

Charge resin with 0.5 mL 0.5N HBr.

Reload columns with Pb solution in HBr.

Rinse with 0.5 mL 0.5N HBr.

Repeat previous step.

Rinse with a mL 0.5N HNO₃ and collect Pb solution in teflon vial.

Discard resin.

Add 1 µL 0.1N H₃PO₄ to Pb solution and dry on hotplate and save for analysis.

Sr Separations:

Completely dry solution set aside for Sr separation, re-dissolve in small amount of E-Pure water and concentrated HNO₃ and completely dry.

Dissolve in 1.25 mL of 2N HNO₃ and heat on hotplate for 1 hour and centrifuge.

Load columns with resin and clean with 8 mL of 6N HCl twice and then 2 mL of 0.05 HNO₃.

Charge resin with 0.3 mL of 2N HNO₃.

Load samples in HNO₃ onto the columns and collect solution in teflon vial.

Rinse with 0.4 mL 2N HNO₃ and collect solution in teflon vial.

Save solution for REE separation.

Rinse columns with 1 mL 7N HNO₃.

Rinse with 0.2 mL 2N HNO₃.

Rinse with 1 mL 0.05N HNO₃ and collect Sr solution in teflon vial.

Complete dry solution, re-dissolve in 0.5 mL 2N HNO₃.

Clean columns with 0.5 mL E-Pure water twice.

Charge resin with 0.3 mL 2N HNO₃.

Load samples in HNO₃.

Rinse columns with 0.4 mL 2N HNO₃.

Rinse with 1 mL 7N HNO₃.

Rinse with 0.2 mL 2N HNO₃.

Rinse with 1 mL 0.05N HNO₃ and collect Sr solution in teflon vial.

Discard resin.

Completely dry Sr solution, re-dissolve with 1 drop of concentrated HNO₃, completely dry again and save for analysis.

REE Separations:

Completely dry solution set aside for REE separation, re-dissolve in 1 mL 4N HCl and heat on hotplate for 1 hour and centrifuge.

Clean columns with pre-loaded resin with 20 mL 6N HCl.

Charge resin with 5 mL 4N HCl.

Load sample in HCl.

Rinse with 1 mL 4N HCl.

Rinse with 3 mL 4N HCl.

Rinse with 5 mL 4N HCl and collect REE solution in teflon vial.

Repeat previous step.

Clean resin with 60 mL 6N HCl and 5 mL E-Pure water and store in XXX bath.

Nd Separations:

Completely dry REE solution and re-dissolve in 0.25 mL 0.25N HCl.

Clean columns with pre-loaded resin with 20 mL 6N HCl and then 20 mL E-Pure water.

Charge resin with 5 mL 0.25N HCl.

Load sample in HCl.

Rinse with 0.25 mL 0.25N HCl and collect in REE solution vial.

Reload REE solution onto columns.

Rinse with 0.25 mL 0.25N HCl.

Rinse with 5 mL 0.25N HCl.

Rinse with 3 mL 0.25N HCl.

Rinse with 6 mL 0.25N HCl and collect Nd solution in teflon vial.

Clean resin with 40 mL 6N HCl and 5 mL 1N HCl and store in 1N HCl bath.

Completely dry Nd solution, re-dissolve with 1 drop of concentrated HNO₃, completely dry again and save for analysis.

Radiogenic Isotope Results

Table C.1: Radiogenic isotope geochemistry

Sample	$^{206}\text{Pb}/^{204}\text{Pb}$	$^{207}\text{Pb}/^{204}\text{Pb}$	$^{208}\text{Pb}/^{204}\text{Pb}$	$^{87}\text{Sr}/^{86}\text{Sr}$ Measured	$^{87}\text{Sr}/^{86}\text{Sr}$ Corrected	$^{143}\text{Nd}/^{144}\text{Nd}$ Measured	$^{143}\text{Nd}/^{144}\text{Nd}$ Corrected
2σ	0.0145	0.0195	0.0621	0.00002	0.00002	0.000007	0.000007
JK10-2A	19.080	15.699	39.006	0.707663	0.707475	0.512241	0.512229
JK10-5	19.076	15.651	38.959	0.708552	0.708473	0.512194	0.512182
JK10-9	19.107	15.685	38.966	0.708336	0.708045	0.512294	0.512280
MB09-5	19.011	15.608	38.707	0.704528	0.704482	0.512723	0.512707
MB09-13	18.801	15.555	38.369	0.703459	0.703435	0.512973	0.512955
MB09-22	19.086	15.654	38.928	0.707890	0.706239	0.512439	0.512427
MB09-27	18.977	15.571	38.568	0.704049	0.704034	0.512840	0.512823
ZH10-15	19.102	15.668	38.991	0.707529	0.706577	0.512442	0.512430
ZH10-22	19.107	15.667	38.972	0.704892	0.704206	0.512480	0.512466
ZH10-22R	19.097	15.655	38.930	0.704905	0.704220	0.512503	0.512489
ZH10-24	19.122	15.672	38.986	0.707997	0.707074	0.512513	0.512499
ZH10-40	19.069	15.646	38.884	0.704961	0.704842	0.512609	0.512594
ZH10-43	19.133	15.675	39.012	0.708423	0.706900	0.512485	0.512469
ZH11-2	19.078	15.642	38.892	0.708664	0.707096	0.512486	0.512472
ZH11-4	18.996	15.621	38.711	0.704897	0.704882	0.512704	0.512692

Appendix D - Oxygen Isotope Results

Oxygen Isotopes for select samples were analyzed at WSU. The samples were run with the UWG-2 standard. The standard was used to normalize the data to a value of 5.8‰ on the VSMOW scale. The oxygen isotope values are summarized in the table below.

Table D.1: Oxygen isotope data

Sample	$\delta^{18}\text{O}_{\text{quartz}}$	$\delta^{18}\text{O}_{\text{feldspar}}$	$\Delta_{\text{quartz} - \text{feldspar}}$
MB07-17A	11.55	7.20	4.35
MB09-12	9.22	8.84	0.38
MB09-22	9.66	9.93	-0.27
JK10-2A	11.31	3.86	7.45
JK10-5	9.78	8.45	1.33
JK10-8	11.95	10.01	1.94
JK10-9	12.19	9.50	2.69
ZH10-5A	7.84	2.13	5.71
ZH10-13	10.06	8.36	1.70
ZH10-15	8.85	7.48	1.37
ZH10-24	10.97	9.67	1.30
ZH10-31	9.07	8.55	0.52
ZH10-35	10.50	8.23	2.27
ZH10-43	10.27	6.97	3.30
ZH11-2	10.11	8.62	1.49

Appendix E - Geochronology

Twenty-eight samples were analyzed for $^{40}\text{Ar}/^{39}\text{Ar}$ geochronology at ANIMAL. Individual plagioclase (mafic samples) and sanidine (silicic samples) minerals were run as single crystal analyses. At this time, the Ar data for the samples is not available.